DOT/FAA/AR-05/56

Office of Aviation Research
and Development
Washington, DC 20591

Vertical Drop Test of an ATR 42-300 Airplane

Allan Abramowitz
Timothy G. Smith
Dr. Tong Vu
John Zvanya

March 2006

Final Report

This document is available to the U.S. public through the National Technical Information Service (NTIS), Springfield, Virginia 22161.

U.S. Department of Transportation
Federal Aviation Administration

NOTICE

This document is disseminated under the sponsorship of the U.S. Department of Transportation in the interest of information exchange. The United States Government assumes no liability for the contents or use thereof. The United States Government does not endorse products or manufacturers. Trade or manufacturer's names appear herein solely because they are considered essential to the objective of this report. This document does not constitute FAA certification policy. Consult your local FAA aircraft certification office as to its use.

This report is available at the Federal Aviation Administration William J. Hughes Technical Center's Full-Text Technical Reports page: actlibrary.tc.faa.gov in Adobe Acrobat portable document format (PDF).

Technical Report Documentation Page

1. Report No.	2. Government Accession No.	3. Recipient's Catalog No.
DOT/FAA/AR-05/56		

4. Title and Subtitle	5. Report Date
VERTICAL DROP TEST OF AN ATR 42-300 AIRPLANE	March 2006
	6. Performing Organization Code ATO-P R&D
7. Author(s) Allan Abramowitz, Timothy G. Smith, Dr. Tong Vu, and John R. Zvanya	8. Performing Organization Report No.
9. Performing Organization Name and Address Federal Aviation Administration William J. Hughes Technical Center Materials and Structures Branch Atlantic City International Airport, NJ 08405	10. Work Unit No. (TRAIS) 11. Contract or Grant No.
12. Sponsoring Agency Name and Address U.S. Department of Transportation Federal Aviation Administration Office of Aviation Research and Development Washington, DC 20591	13. Type of Report and Period Covered Final Report July 2003 - August 2004 14. Sponsoring Agency Code ANM-100

15. Supplementary Notes

Federal Aviation Administration Airport and Aircraft Safety R&D Division Crashworthiness Program Manager: Gary Frings, Crashworthiness Project Manager: Allan Abramowitz.

16. Abstract

On July 30, 2003, the Federal Aviation Administration conducted a vertical impact test of a large high-wing airplane. The test was conducted at the William J. Hughes Technical Center, Atlantic City International Airport, New Jersey. The objective of this test was to determine the impact response of the fuselage, fuel system, floor tracks, seats, and anthropomorphic test dummies when subjected to a severe, but survivable, simulated crash impact. An ATR 42-300 (42-passenger regional transport airplane) was dropped from a height of 14 ft (4.3 meters) that resulted in a vertical impact velocity of 30 ft/s (9.1 m/s). The airplane was configured to simulate a typical flight condition, including seats, cargo, simulated occupants, and simulated fuel. The final test weight of the airplane was 33,200 pounds (15,059 kg).

The airplane sustained major structural damage and deformation. A habitable environment for some of the passengers was not maintained due to the penetration of the wing and landing gearbox into the cabin. The service door on the right rear side of the airplane and the cockpit emergency ceiling exit were usable. The passenger and cargo doors and the two emergency window exits were unusable. The left engine impacted the concrete drop test platform and a fuel leak developed in the leading edge of the left wing near the engine. The right engine also impacted the concrete drop test platform; however, the right wing fuel tank was not ruptured.

The sidewalls experienced approximately an 19-g maximum deceleration with pulse duration of approximately 83 msec. The floor tracks experienced approximately a 26-g maximum deceleration with pulse duration of approximately 68 msec.

17. Key Words	18. Distribution Statement
Crash testing, Vertical impact, Drop test, Dynamic testing, Acceleration, Airplane, ATR	This document is available to the public through the National Technical Information Service (NTIS) Springfield, Virginia 22161.

19. Security Classif. (of this report)	20. Security Classif. (of this page)	21. No. of Pages	22. Price
Unclassified	Unclassified	224	

Form DOT F1700.7 (8-72) Reproduction of completed page authorized

ACKNOWLEDGMENTS

The authors would like to thank Mr. Stephen Soltis, the Federal Aviation Administration Chief Scientific and Technical Advisor for Crash Dynamics, for his technical direction during this test.

They would also like to thank Mr. Anthony Dang, airframe and powerplant technician, for his invaluable assistance.

TABLE OF CONTENTS

		Page
EXECUTIVE SUMMARY		xi
1.	INTRODUCTION	1
2.	BACKGROUND	1
3.	DESCRIPTION OF TEST FACILITY AND TEST ARTICLE	1
3.1	Test Facility	1
3.2	Test Article	3
3.3	Test Article Numbering Convention	4
3.4	Test Article Configuration	5
3.5	Structural Details	9
3.5.1	Floor Beams	10
3.5.2	Upper Frame Sections	11
3.5.3	Wing Fuselage Intersection	11
3.5.4	Fuselage Stringers	13
4.	MODELING OF THE ATR 42-300 AIRPLANE	13
5.	TEST INITIATION	14
6.	INSTRUMENTATION	14
6.1	Fuselage	18
6.1.1	Accelerometers	18
6.1.2	Contact Switches	18
6.1.3	Wing Fittings	18
6.1.4	Wing Fitting Calibrations	19
6.2	Wings and Engines	19
6.3	Overhead Stowage Bins	19
6.4	Anthropomorphic Test Dummies	20
6.5	Visual Imaging	20
7.	DATA ACQUISITION, COLLECTION, AND REDUCTION	22
7.1	Data Acquisition Systems	22
7.1.1	System 1—NEFF 490	22
7.1.2	System 2—EME DAS-48S	23

7.2 Data Collection 23
7.3 Data Reduction 24

8. DATA ANALYSIS 25

8.1 Time to Impact 25
8.2 Impact Velocity 25
8.3 Fuselage Static Crush Measurements 25
8.4 Posttest Airframe Acceleration Estimate 26
8.5 Sequence of Events 26
8.6 Airframe Accelerations 27

8.6.1 Sidewall Accelerations 27
8.6.2 Cabin Floor Track Accelerations 29
8.6.3 Additional Accelerations 31

8.7 Overhead Stowage Bin Analysis 32
8.8 Anthropomorphic Test Dummies 34
8.9 Wing Fittings 34

9. RESULTS AND DISCUSSION 35

9.1 Fuselage Structure 35
9.2 Fuselage Response 35
9.3 Exterior 35
9.4 Cabin Subfloor Area 36
9.5 Upper Cabin Interior 36
9.6 Exits 37
9.7 Cockpit 37
9.8 Overhead Stowage Bins 37
9.9 Seats 37

10. SUMMARY OF RESULTS 38

11. REFERENCES 40

APPENDICES

A—Wing Fitting Calibration Data
B—Test Data
C—Photographic Documentation

LIST OF FIGURES

Figure		Page
1	Dynamic Drop Test Facility	2
2	Dynamic Drop Test Facility and ATR 42-300 Airplane	2
3	Aerial View of ATR 42-300 Airplane	3
4	Three-View Drawing of ATR 42-300 Airplane	4
5	Layout of Fuselage Frame Sections	5
6	Airplane Interior Configuration	8
7	Fuselage Frames 25 and 27	9
8	Landing Gear Housing, Left Side	9
9	Floor Beam Stanchions	10
10	ATR 42-300 Floor Beams, Cross-Sectional View	11
11	Center Interior Fuselage Area	12
12	Outside Wing fittings, Left Side Close-Up	12
13	Typical Stringer Cross-Sectional View	13
14	Finite Element Model of the ATR 42-300 Airplane	13
15	Fuselage Instrumentation Locations	17
16	Wing Fitting Strain Gage Bridge Locations	18
17	Wing and Engine Instrumentation	19
18	Overhead Stowage Bin Instrumentation	20
19	Camera Locations	21
20	NEFF 490 Data Acquisition System	22
21	EME DAS-48S Data Acquisition System	23
22	Typical Vertical Sidewall Acceleration	28
23	Typical Vertical Sidewall Velocity	28
24	Typical Vertical Floor Track Acceleration	30
25	Typical Vertical Floor Track Velocity	30
26	Left Bin, Average Vertical Acceleration	33
27	Left Bin, Calculated Vertical Velocity	33

LIST OF TABLES

Table		Page
1	Moment Arm of Fuselage Frames	5
2	Test Article Weights	6
3	Seat and Occupant Locations	7
4	Data Acquisition Systems Configurations and Sensor Locations	15
5	SAE-J211 Filter Class Comparisons	24
6	Impact Velocity	25
7	Fuselage Static Crush Measurements	26
8	Vertical Sidewall Accelerations	29
9	Vertical Floor Track Accelerations	31
10	Additional Vertical Accelerations	32
11	Anthropomorphic Test Dummy Data	34
12	Wing Fitting Loads	34
13	Fuselage Pulse Duration and Amplitude	35

LIST OF ACRONYMS

A/D	Analog-to-digital
ATD	Anthropomorphic test dummies
c.g.	Center of gravity
CFR	Code of Federal Regulations
FAA	Federal Aviation Administration
FEM	Finite element model
FS	Fuselage station
H/S	High speed
MGTOW	Maximum gross takeoff weight
MTS	Material Testing System
NAL	National Aerospace Laboratory
PC	Personal computer

EXECUTIVE SUMMARY

On July 30, 2003, the Federal Aviation Administration conducted a vertical impact test of a large high-wing airplane. The test was conducted at the William J. Hughes Technical Center, Atlantic City International Airport, New Jersey. The objective of this test was to determine the impact response of the fuselage, fuel system, floor tracks, seats, and anthropomorphic test dummies (ATD) when subjected to a severe, but survivable, simulated crash impact. The data collected in this test will supplement the existing basis for improved seat and restraint systems for Title 14 Code of Federal Regulations Part 23 commuter category airplanes.

This test entailed dropping an ATR 42-300, a 42-passenger regional transport airplane, from a height of 14 ft (4.3 meters) with a vertical impact velocity of 30 ft/s (9.1 m/s). The test weight of the airplane was 33,200 pounds (15,059 kg) (normal maximum gross takeoff weight was 36,600 lb (16,610 kg)). The final airplane configuration included seats, cargo, simulated occupants, and simulated fuel. The airplane was loaded with 8700 pounds (3946 kg) of simulated fuel equally divided between the two wing tanks. The airplane was instrumented with strain gages, accelerometers, and displacement transducers.

The airplane sustained major structural damage and deformation. This was attributed to (1) the loading of the wing on the fuselage and subsequent failure of the wing supporting frames, (2) the fracturing and failure of the landing gearbox section, and (3) the failure of the subfloor stanchions. A habitable environment for some of the passengers was not maintained due to the penetration of the wing and landing gearbox into the cabin. The service door on the right rear side of the airplane and the cockpit emergency ceiling exit were usable. The passenger and cargo doors and the two emergency window exits were unusable. The left engine impacted the concrete drop test platform and a fuel leak developed in the leading edge of the left wing near the engine. The right engine also impacted the concrete drop test platform; however, the right wing fuel tank was not ruptured.

The crushing of the fuselage frames below the floor absorbed much of the impact energy thereby limiting the g forces and extending the impact pulse duration transmitted to the occupants through the floor tracks and seats. The cabin sidewalls experienced approximately an 19-g maximum deceleration with a pulse duration of approximately 83 msec. The cabin floor tracks experienced approximately a 26-g maximum deceleration with a pulse duration of approximately 68 msec. The cockpit floor experienced approximately a 38-g maximum deceleration with a pulse duration of approximately 51 msec.

The cockpit seats did not sustain any structural damage. However, the spinal loads in the lumbar region of the ATDs were approximately 2500 pounds (1136 kg) (1500 lb (681 kg) certification limit). All the standard ATR cabin seats that were occupied fractured. A modified, in-service 16-g-rated seat occupied by an ATD and a mannequin sustained minimal damage. The maximum measured lumbar load of the ATD was 738 pounds (335 kg).

1. INTRODUCTION.

This report presents the results of a vertical impact test conducted on July 30, 2003, at the Federal Aviation Administration (FAA) William J. Hughes Technical Center, Atlantic City International Airport, New Jersey. The objective of this test was to determine the impact response of the fuselage, fuel system, floor tracks, seats, and anthropomorphic test dummies (ATD) of a large high-wing airplane. This test was conducted to simulate the vertical velocity component of a severe, but survivable, simulated crash impact. This test entailed dropping an ATR 42-300, a 42-passenger regional transport airplane, from a height of 14 ft (4.3 meters) that resulted in a vertical impact velocity of 30 ft/s (9.1 m/s). The airplane was configured to simulate a typical operational condition, including seats, simulated occupants, simulated fuel, and cargo. The data collected in this test will supplement the existing basis for improved seat and restraint systems for commuter category airplanes as defined in Title 14 Code of Federal Regulations (CFR) Part 23. The ATR 42-300 weighs more than 12,500 lb (5670 kg) and therefore is certified to 14 CFR Part 25, although it has been primarily operated as regional transport in a commuter role.

2. BACKGROUND.

This vertical impact test is the last in a series of four full-scale commuter airplane tests. The FAA has proposed seat dynamic performance standards for 14 CFR Part 23 commuter category airplanes. Those standards were established empirically using the results of prior airplane crash impact test programs. In the development of those standards it was noted that the full-scale airplane impact test database did not include airplanes representative in size of commuter category airplanes. To provide data for those size airplanes, the FAA initiated a full-scale vertical impact test program of 14 CFR Part 23 commuter category airplanes [1, 2, and 3]. The tests were structured to assess the impact response characteristics of the airframe structures and seats and the potential for occupant impact injury.

3. DESCRIPTION OF TEST FACILITY AND TEST ARTICLE.

3.1 TEST FACILITY.

The drop test facility consisted of two 57-ft (17.4-m) vertical steel towers connected at the top by a horizontal platform (figures 1 and 2). An electrically powered winch, mounted on the platform and attached to a reeved hoisting cable, was used to raise and lower the airplane. A sheave block assembly hanging from the free end of the reeved cable was attached to a solenoid-operated release hook. A sling and turnbuckle assembly that was bolted to the airplane at four locations connected the airplane to the release hook. The test article was dropped onto an 8-inch (0.2-m)-thick temporary concrete pad. The pad was composed of eight concrete slabs measuring 10′ long and 8′ wide (19.5 by 15.6 m). The concrete slabs sat on the concrete drop test platform. The airplane was angled under the drop tower to accommodate the airplane's wingspan.

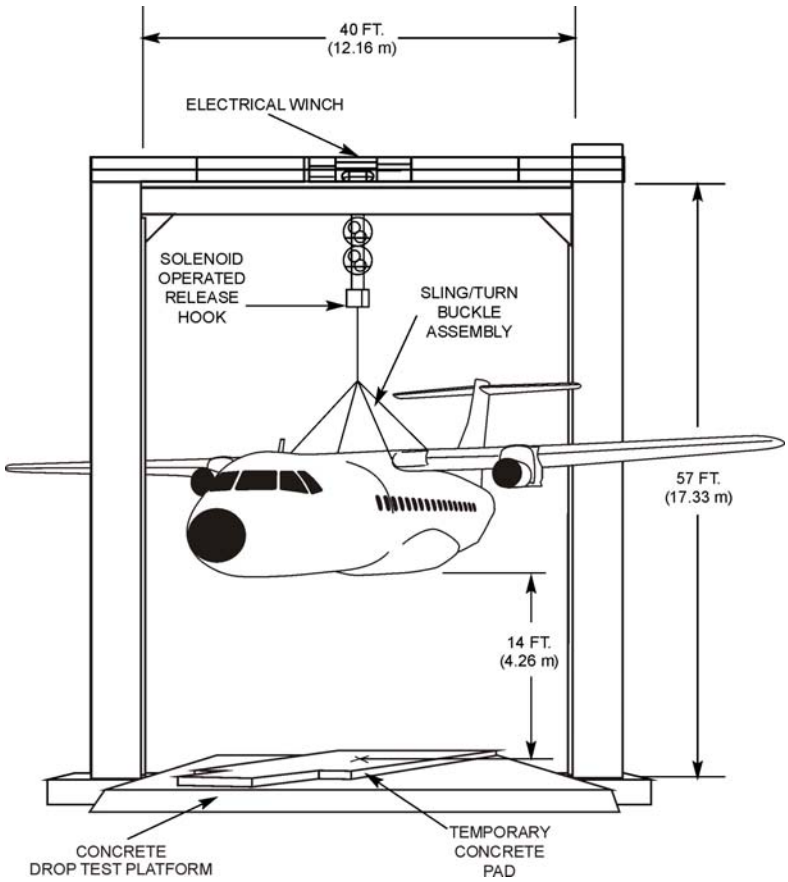

FIGURE 1. DYNAMIC DROP TEST FACILITY

FIGURE 2. DYNAMIC DROP TEST FACILITY AND ATR 42-300 AIRPLANE

3.2 TEST ARTICLE.

The test article was an ATR 42-300 (figures 2, 3, and 4), high-wing, twin-turboprop, 42-50 passenger regional transport airplane. Detailed pre- and posttest exterior and interior photographs of the airplane are shown in appendix C. At the time of manufacture, the airplane was a joint effort between Aerospatiale (France) and Aeritalia (Italy). The airplane was 74 ft (22.7 m) long, with a wingspan of 81 ft (24.6 m). The airplane was drop-tested in the following configuration:

- Engines and nacelles were simulated using partially filled concrete barrels designed and constructed to replicate the weight and the center of gravity (c.g.) of the engines and nacelles.
- Water was used to simulate fuel.
- Control surfaces (ailerons, flaps, and rudder), wing fairings, tail cone, and the radar dome were missing. Their weight and c.g. was compensated.
- The main landing gear and associated equipment were missing.
- Only two overhead stowage bins were mounted in the aircraft.
- Most nonstructural interior liners and insulation were removed.

FIGURE 3. AERIAL VIEW OF ATR 42-300 AIRPLANE

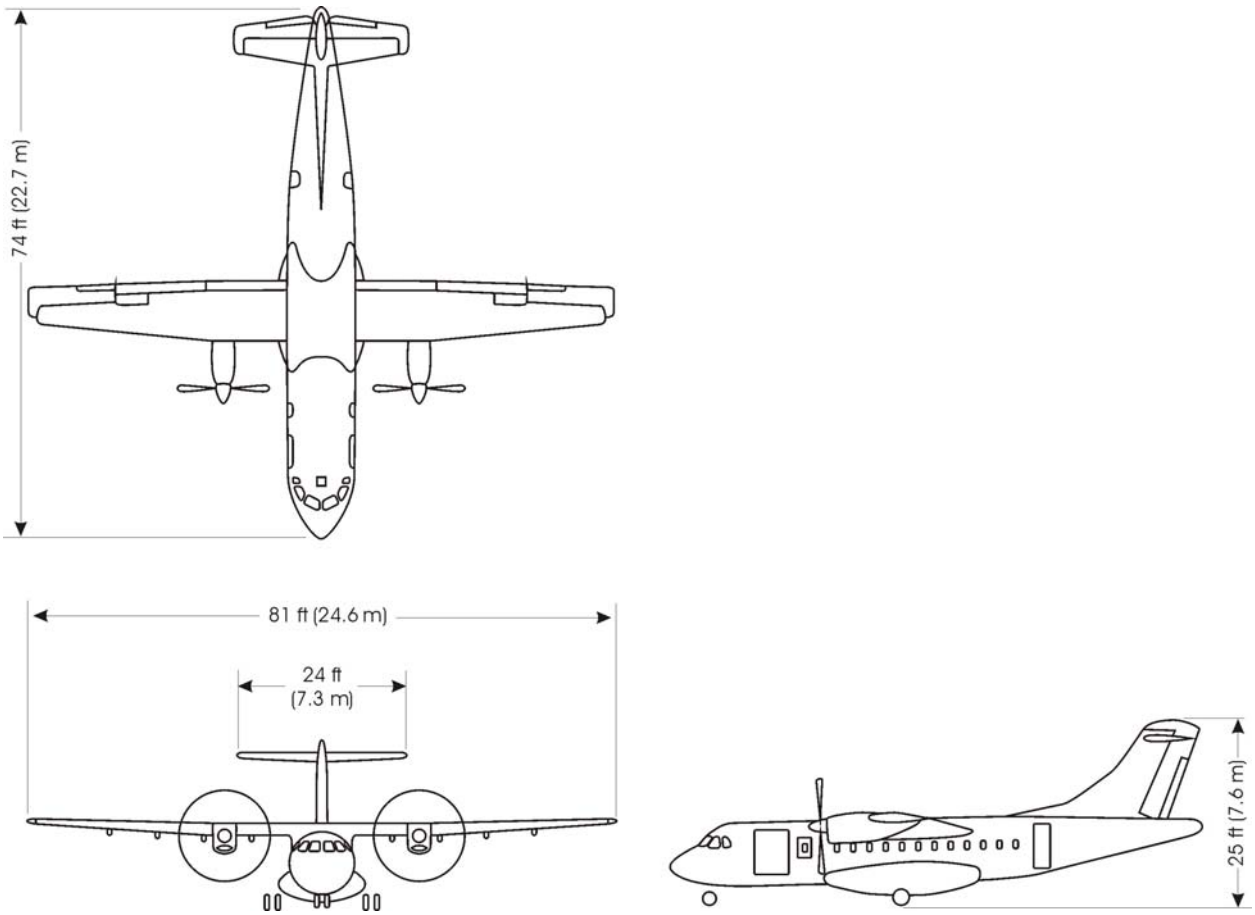

FIGURE 4. THREE-VIEW DRAWING OF ATR 42-300 AIRPLANE

3.3 TEST ARTICLE NUMBERING CONVENTION.

Fuselage location identifications were measured in three directions, longitudinal (x), lateral (y), and vertical (z). The reference point was 93 in. (236 cm) forward of the nose section (manufacturer's reference), laterally centered on the aircraft symmetry plane (longitudinal axis), and vertically centered at floor level. The moment arm (H) is the distance from the reference point to the location selected on the longitudinal axis. The moment arms for fuselage frames 1 to 47 are listed in table 1. All measurements were referenced from this point and were recorded in inches and meters. The positive directions are aft (x), right-copilot side (y), and up (z). The fuselage frame sections (F) were numbered per the manufacturer's reference, as shown in figure 5. The fuselage stations (FS) are indicated using inches and centimeters (e.g., FS 100 (254)). The fuselage frame sections will be used to approximate the locations of the ATDs, seats, and sensors. The exact locations of the frames are listed in table 1.

TABLE 1. MOMENT ARM OF FUSELAGE FRAMES

Frame Number	H-arm (in.)	H-arm (m)	Frame Number	H-arm (in.)	H-arm (m)	Frame Number	H-arm (in.)	H-arm (m)
1	116.614	2.962	17	289.291	7.348	32	607.520	15.431
2	127.913	3.249	17A	302.520	7.684	33	628.307	15.959
3	139.213	3.536	18	311.811	7.920	34	649.094	16.487
4	148.031	3.760	19	334.331	8.492	35	669.882	17.015
5	156.811	3.983	20	355.118	9.020	36	681.850	17.319
*6	165.186	4.196	21	375.906	9.548	37	687.362	17.459
7	174.252	4.426	22	396.693	10.076	38	698.189	17.734
8	182.953	4.647	23	417.480	10.604	39	714.528	18.149
9	192.795	4.897	24	438.268	11.132	40	734.213	18.649
10	202.638	5.147	25	459.055	11.660	41	753.898	19.149
11	209.961	5.333	26	481.339	12.226	42	769.961	19.557
12	217.283	5.519	27	503.583	12.791	43	787.047	19.991
13	224.685	5.707	28	524.370	13.319	44	804.134	20.425
14	234.921	5.967	29	545.157	13.847	45	821.299	20.861
15	253.031	6.427	30	565.945	14.375	46	847.087	21.516
16	271.181	6.888	31	586.732	14.903	47	872.835	22.170

*FAA measurement

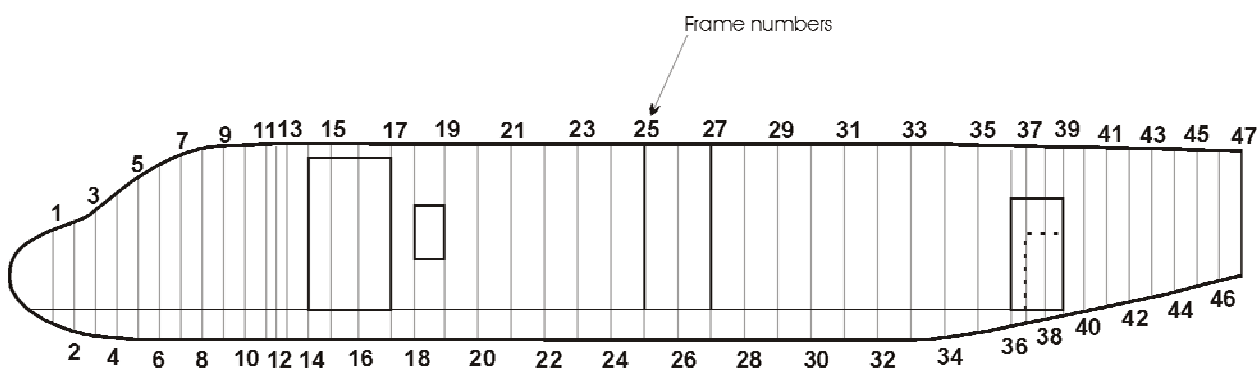

FIGURE 5. LAYOUT OF FUSELAGE FRAME SECTIONS

3.4 TEST ARTICLE CONFIGURATION.

The total test weight of the airplane was 33,200 lb (15,059 kg). This weight represents the maximum gross takeoff weight (MGTOW) of the airplane minus the removed items and a fuel load of 8700 lb (3946 kg). The airplane was loaded with 23 simulated occupants, luggage, fuel, miscellaneous-related test equipment and bags of lead shot. Lead shot was used in the cockpit, tail section, and on several seats to compensate for missing items, weight, and c.g. requirements. A list of all weights is presented in table 2. A weight and balance calculation was performed to determine the c.g. of the airplane. Three load cells were used to measure the weight of the

airplane, and the c.g. was calculated using the known moment arms of the measured locations. The luggage was distributed in the fore and aft luggage compartments to achieve a c.g. within the airplane's c.g. envelope. The c.g. was located at FS 469 (1191.3).

TABLE 2. TEST ARTICLE WEIGHTS

Item	Item Weight lb (kg)	Quantity	Total Weight lb (kg)
Fuselage	11,043 (5,009.1)	1	11,043 (5,009.1)
Engines + nacelles	1,290 (585.1)	2	2,580 (1,170.3)
Center wing section	2,400 (1,088.6)	1	2,400 (1,088.6)
Outer wing section	450 (204.1)	2	900 (408.2)
Simulated fuel (water)	8.33 lb/gal (1 kg/liter)	1044 gal (3951.5 liter)	8,700 (3,946.3)
ATD	170 (77.1)	7	1,190 (539.8)
Mannequins	167 (75.8)	16	2,672 (1,212.0)
Forward luggage	1,450 (657.7)	1	1,450 (657.7)
Aft luggage	739 (335.2)	1	739 (335.2)
Seats – lead shot	152 (68.9)	4	608 (275.8)
Seats – lead shot	135 (61.2)	2	270 (122.5)
Cameras + mounts	35 (15.9)	4	140 (63.5)
Bins loaded	55 (24.9)	2	110 (49.9)
Misc.	398 (180.5)	1	398 (180.5)
Test Weight			33,200 (15,059.4)
Deleted Items			
Main gear	503 (228.2)	2	1,006 (456.3)
Main gear wheel fairing panels + equipment	634 (287.6)	1	634 (287.6)
Ailerons, flaps	205 (93)	2	410 (186.0)
Nacelle components	75 (34)	2	150 (68.0)
Max fuel difference	8.33 lb/gal (1 kg/liter)	146.5 (599)	1,220 (599)
		Subtotal	3,420 (1,604.8)
MGTOW			36,620 (16,610.5)

The ATR-42-300 fuel system consisted of two tanks, one in each cantilever wing box. Each tank was filled to approximately 3/4 capacity with water for a total weight of 8700 lb (3946 kg). Each tank was capable of holding 4960 lb (2250 kg) of useable fuel for a total capacity of 9920 lb (4500 kg).

Seating consisted of a pilot and copilot seat, eight rows of double passenger seats (32 seats), and one flight attendant seat located in the aft section of the passenger cabin. Instrumented 50th percentile adult male Hybrid II ATD occupied seven seats; mannequins 16 seats; lead shot bags 6 seats; and 6 seats were left unoccupied. Table 3 and figure 6 give the locations of the ATD, mannequins, lead shot, and seats. A center aisle divided the cabin into left and right sides. The

ATD, mannequins, and bags of lead shot were strapped firmly into the seats with the lap belt restraint systems. The airplane was configured for 11 rows of seats; however, rows 4-6 located near the middle of the fuselage) were removed. In their place were floor-mounted cameras oriented to film the floor, ceiling, and sidewalls between fuselage frames 24 and 28.

TABLE 3. SEAT AND OCCUPANT LOCATIONS

Location	Seat Location and Occupant Description			
Cockpit	Pilot – ATD 1		Copilot – ATD 2	
	A	B	C	D
Row 1	Mannequin	Mannequin	ATD 3	Mannequin
Row 2	Lead Shot	Lead Shot	Lead shot	Lead shot
Row 3	Mannequin	Mannequin	Mannequin	Mannequin
Row 4	Removed	Removed	Removed	Removed
Row 5	Removed	Removed	Removed	Removed
Row 6	Removed	Removed	Removed	Removed
Row 7	Unoccupied	Unoccupied	ATD 4	Mannequin
Row 8	Lead Shot	Lead Shot	ATD 5	Mannequin
Row 9	Mannequin	Mannequin	Unoccupied	Unoccupied
Row 10	Mannequin	Unoccupied	Mannequin	Unoccupied
Row 11	Mannequin	Mannequin	ATD 6	Mannequin
F 39/FS 708 (1798)	Flight Attendant seat – ATD 7			

Note: Letters A, B, C, and D denote left to right seat locations.
Row 2 seats were loaded with 150 lb (68.9 kg) lead shot.
Row 8, seats A and B, were loaded with 135 lb (61.2 kg) lead shot.

The cockpit seats were standard issue and manufactured by IPECO Europe Ltd Inc. Three different cabin seats were used in the test. Current in-service seats (Simca-Aero-Seat model 73) were installed throughout the cabin. The National Aerospace Laboratory (NAL) of Japan provided an experimental stroking seat (located on the right side at FS 526) and Tenyru Industries Ltd Inc. of Japan provided a modified in-service 16-g-rated seat (located on the right side at FS 556). A nominal 31-inch (78.7-cm) seat pitch (distance between seats) was used where possible. A flight attendant seat was located in the rear of the plane at FS 708 (1798).

Two in-service overhead stowage bins were installed in the aft section of the passenger cabin, as shown in figure 6. Both bins were loaded with plywood to achieve their placarded maximum weight and approximate their centers of gravity. The bin doors were strapped closed to ensure the contents remained inside the bins during the impact.

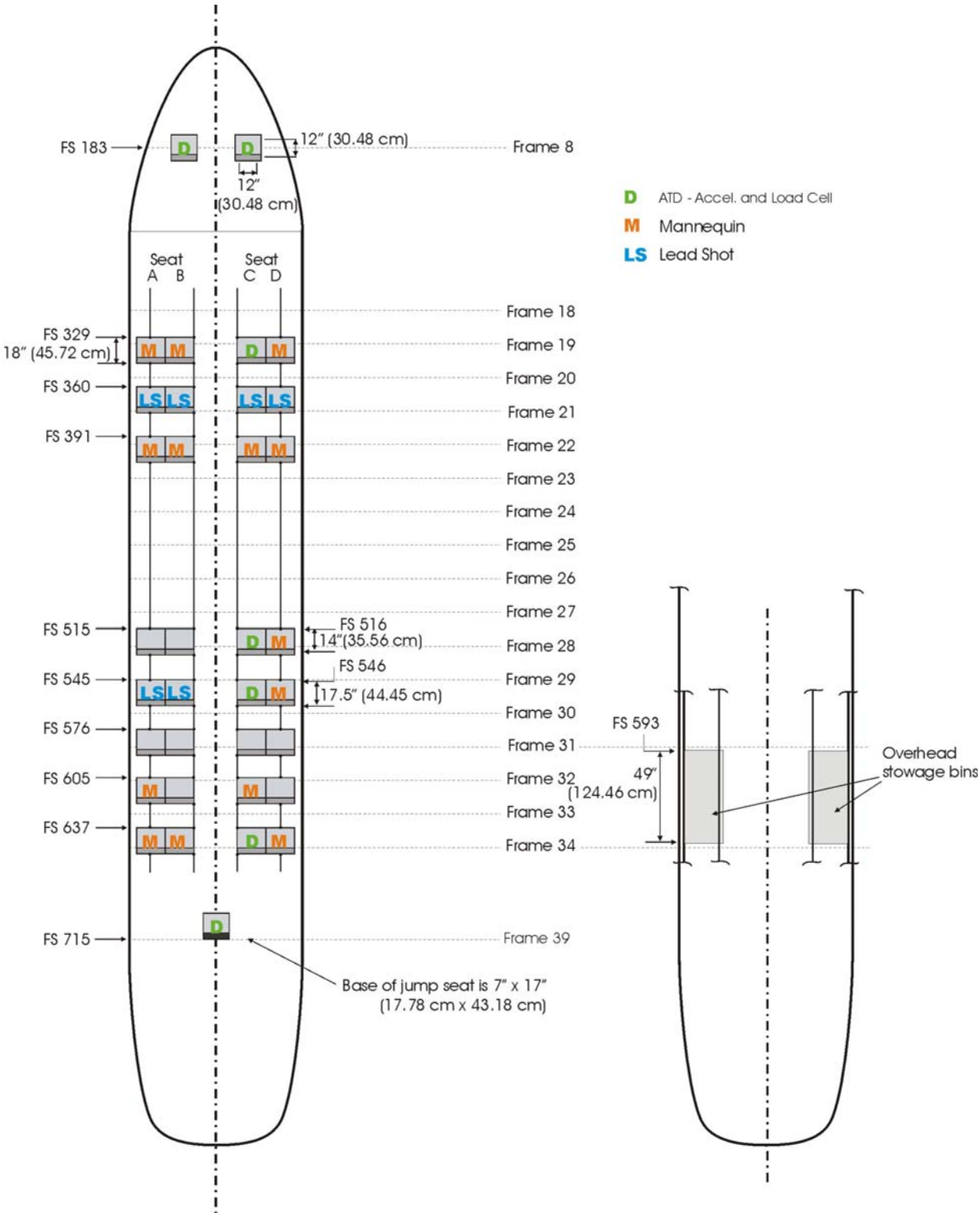

FIGURE 6. AIRPLANE INTERIOR CONFIGURATION

3.5 STRUCTURAL DETAILS.

The cabin floor beams, frames, and supports were generally similar throughout the fuselage with the exception of those located between frames 25 and 27. Frames 25 and 27 were each comprised of two half structures connected by a keel beam below floor level and acted as the frames and floor beams (see figure 7). Aluminum plates bolted between floor beams 25-26 and floor beams 26-27 were used to stiffen and reinforce the area (see figure 8).

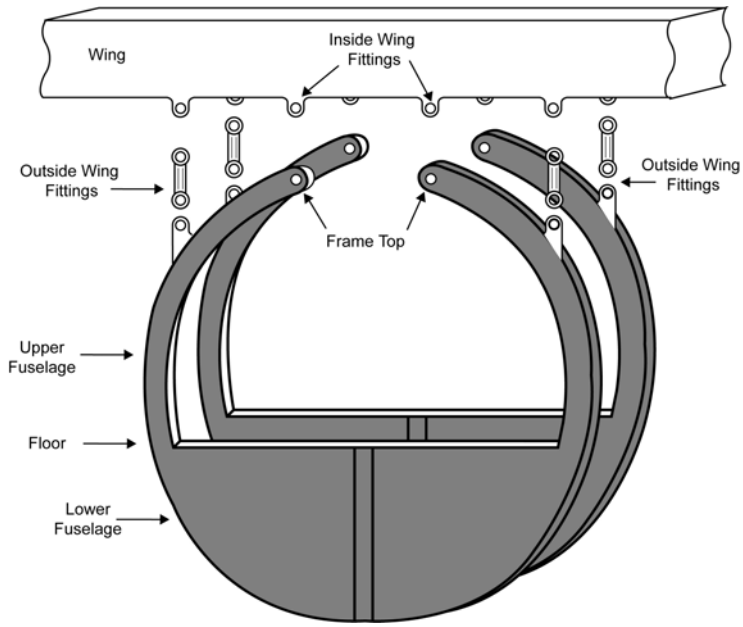

FIGURE 7. FUSELAGE FRAMES 25 AND 27

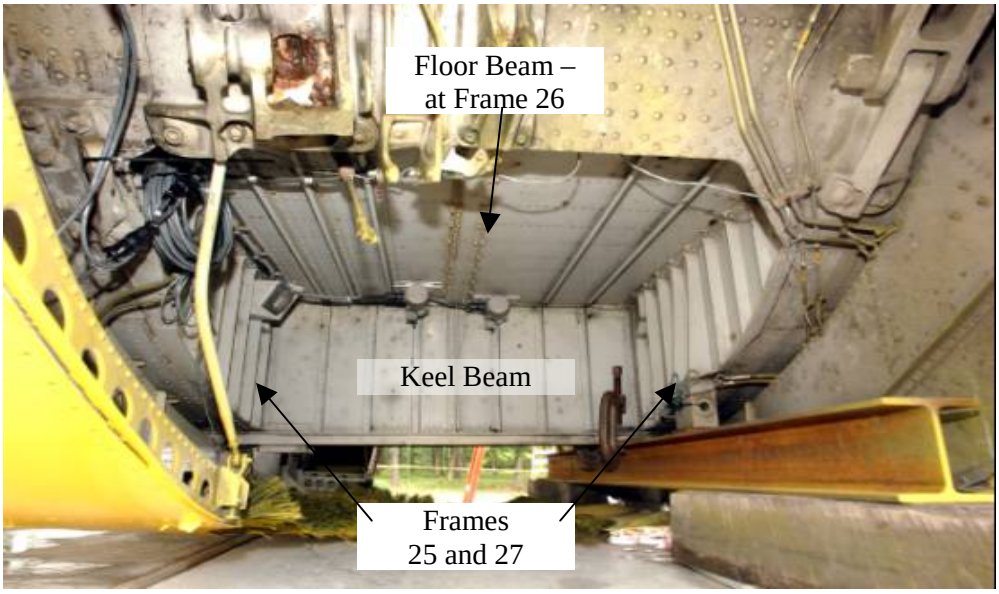

FIGURE 8. LANDING GEAR HOUSING, LEFT SIDE

3.5.1 Floor Beams.

The typical floor beam was supported by two vertical stanchions located just outboard of the inner floor track, as shown in figure 9. The stanchions were attached to the floor beams and the bottom of the fuselage frames. The length of the stanchions varied, depending upon fuselage frame location.

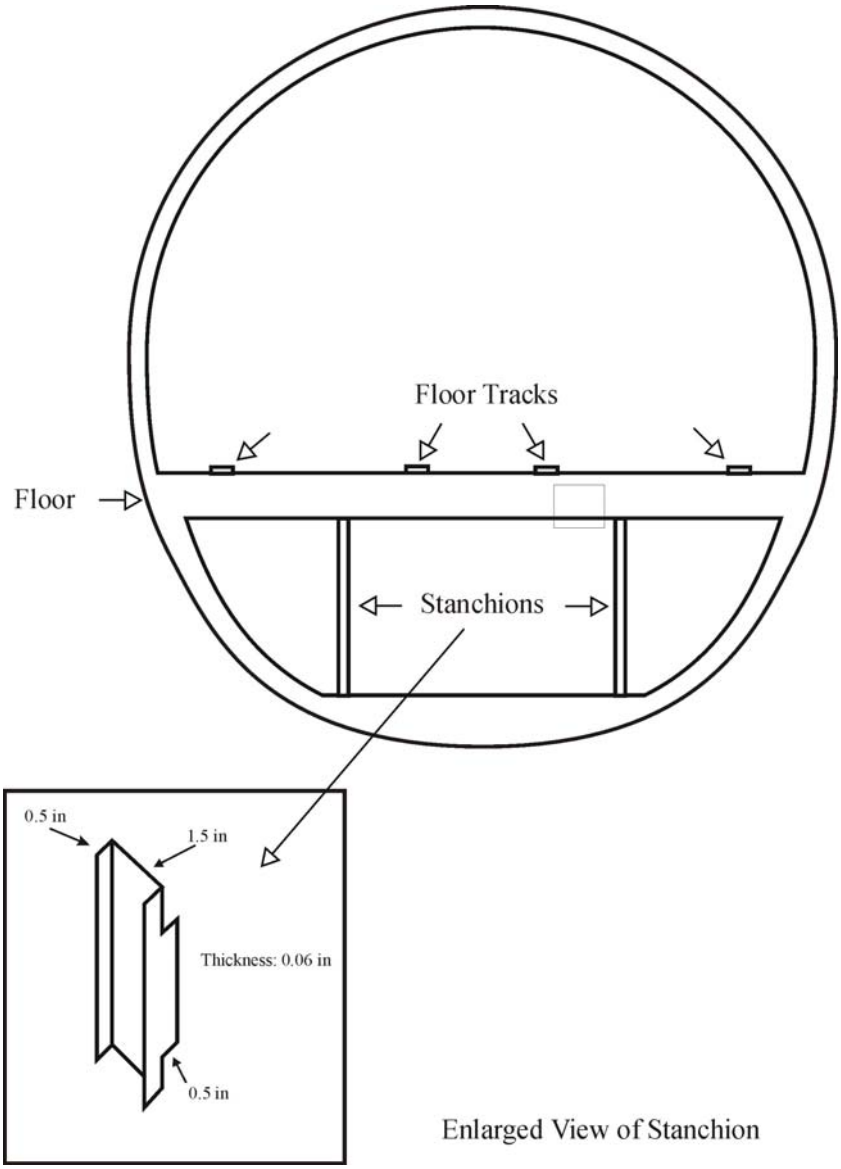

FIGURE 9. FLOOR BEAM STANCHIONS

Floor beams 25 to 27 are part of the framework for the landing gearbox housing. This area was factory-reinforced to help absorb and redistribute the landing loads, as shown in figure 8.

The three floor beam designs used in the airplane are shown in figure 10.

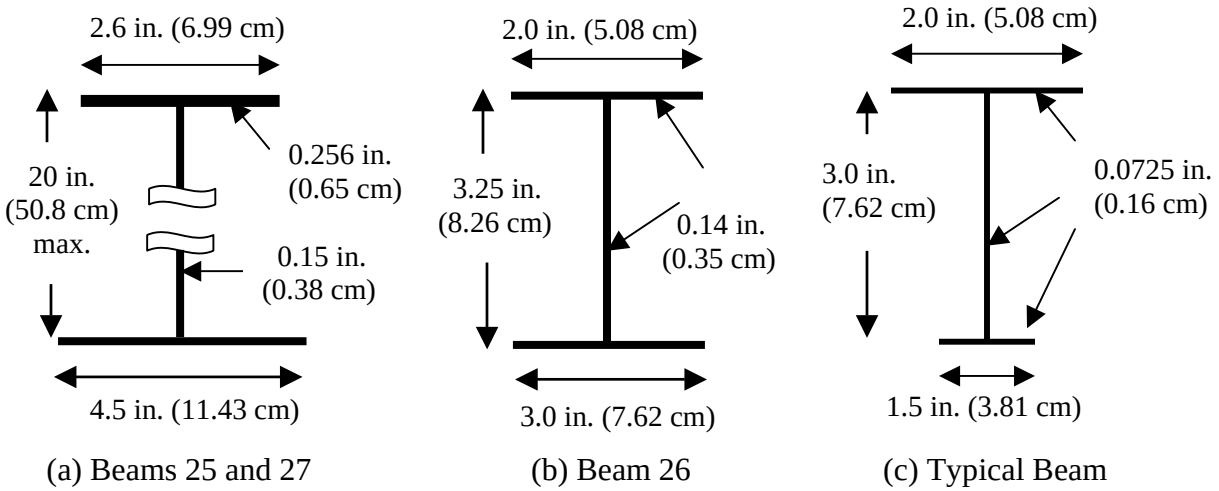

(a) Beams 25 and 27 (b) Beam 26 (c) Typical Beam

FIGURE 10. ATR 42-300 FLOOR BEAMS, CROSS-SECTIONAL VIEW

3.5.2 Upper Frame Sections.

The upper (above floor) sections of frames 25 and 27 followed the contour of the fuselage but stopped short of the crown of the airplane, as shown in figure 7. The wing attached to the tops of the frames and acted as the ceiling in this area.

Frames 25 and 27 were designed substantially stronger than the other frames to support the wing loading, as shown in figure 11. The web thickness of the upper halves of frames 25 and 27 is 0.2 in. (0.508 cm) and gradually increases to 0.627 in. (1.593 cm) toward the floor. The web width of frames 25 and 27 is 3.5 in. (8.89 cm) at the top of the frame, gradually decreases to 2.75 in. (6.99 cm) at the center, and then gradually increases to 4.62 in. (11.54 cm) at the floor. The rest of the ATR frames were not as robust, with metal thickness varying between 0.050 inch (0.13 cm) and 0.070 inch (0.18 cm).

3.5.3 Wing Fuselage Intersection.

The wing was attached to frames 25 and 27 using eight fittings. The four inside fittings attached the wing at the tops of frames 25 and 27, see figures 7 and 11. The four outside fittings connected the wing to the middle of frames 25 and 27, as shown in figures 7 and 12.

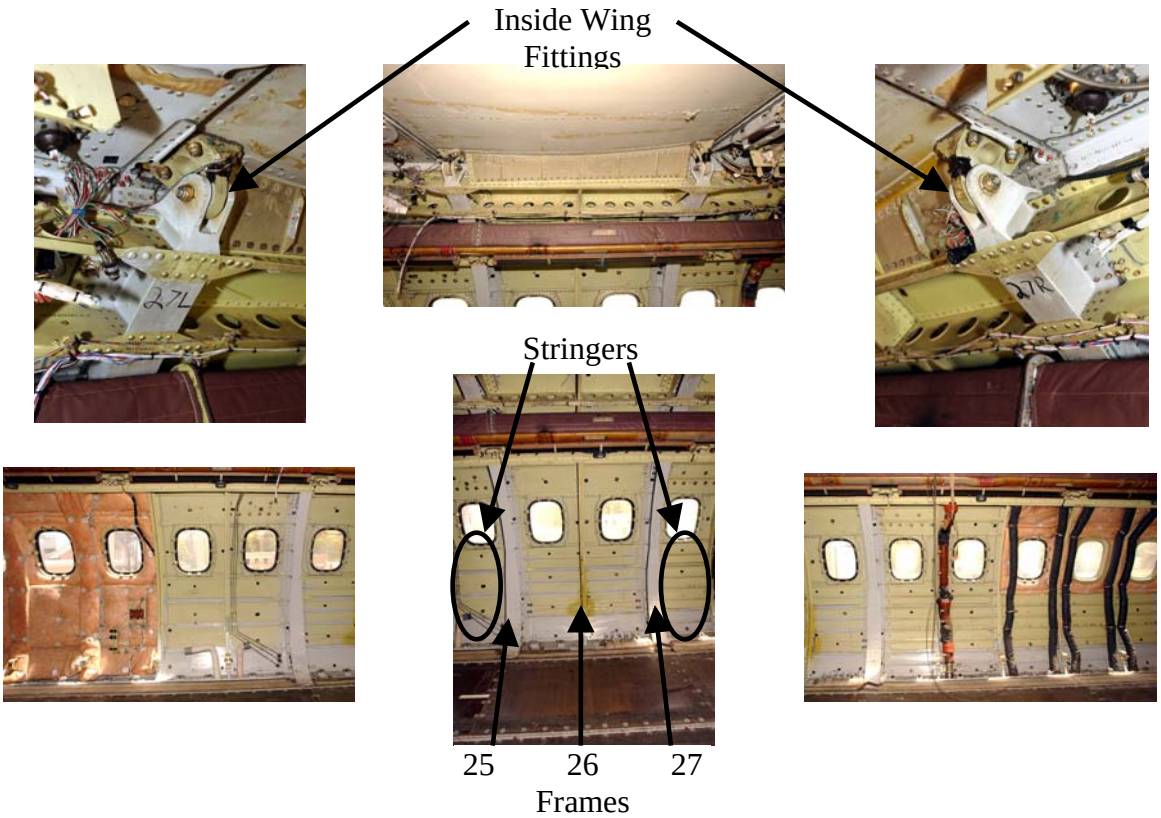

FIGURE 11. CENTER INTERIOR FUSELAGE AREA

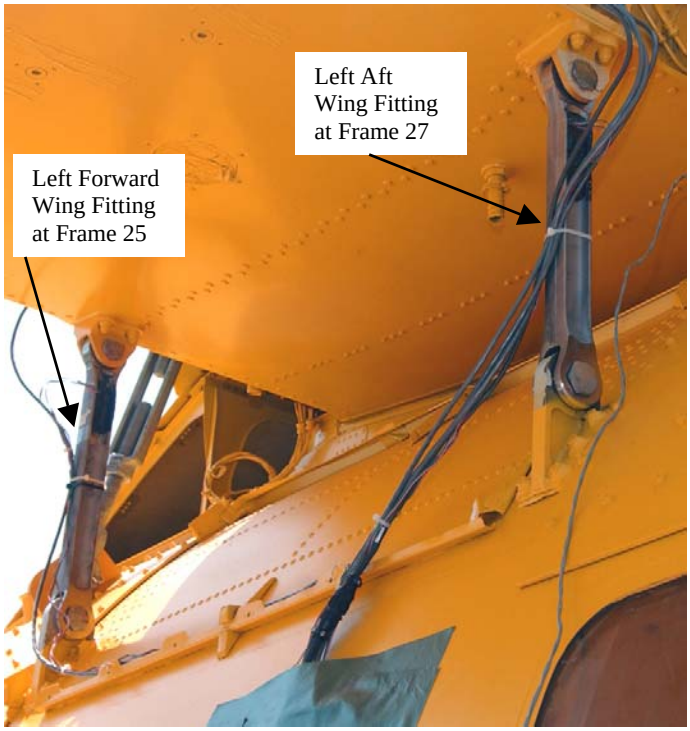

FIGURE 12. OUTSIDE WING FITTINGS, LEFT SIDE CLOSE-UP

3.5.4 Fuselage Stringers.

The number and location of stringers varied throughout the fuselage. The greatest concentration was located from frames 17 to 27, see figure 11. A typical stringer structure is shown in figure 13.

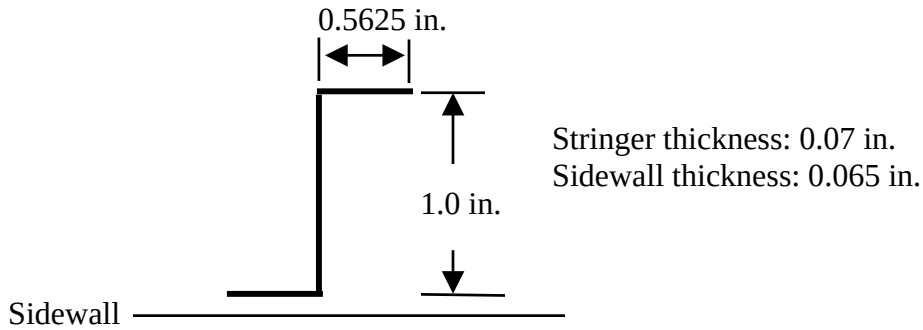

FIGURE 13. TYPICAL STRINGER CROSS-SECTIONAL VIEW

4. MODELING OF THE ATR 42-300 AIRPLANE.

An analytical model of the ATR 42-300 airplane and simulated crash impact was developed to study the airplane's structural response during impact. The model can derive detailed stresses, loads, and acceleration data at specified locations. Data from the ATR 42-300 Weight and Balance Manual and hand measurements taken of the airframe were used in developing the geometry model. The geometry model was created using MSC.Patran, which was converted to a finite element model (FEM) by meshing the geometric entities. LS-DYNA was used to execute the FEM.

The FEM contained 57,643 nodes and 62,979 elements, including 60,197 quadrilateral shell elements, 551 triangular shell elements, 526 beam elements, and 1705 point elements, which were used to assign concentrated masses to nodes in the model. The FEM is shown in figure 14.

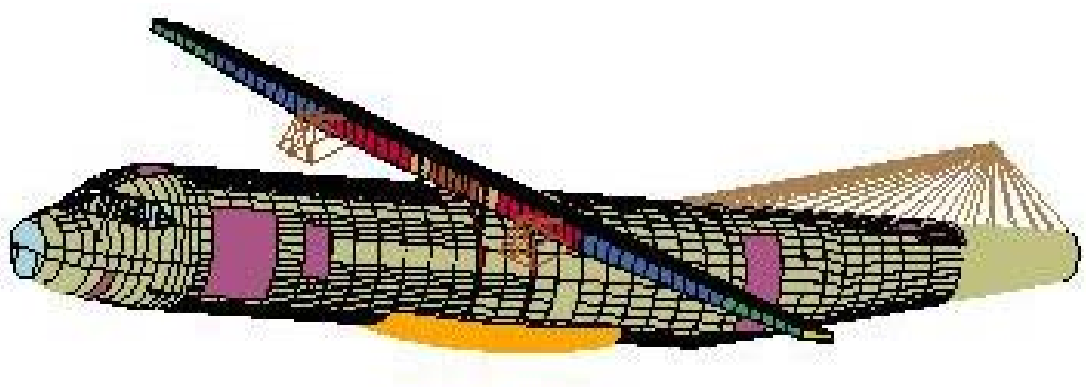

FIGURE 14. FINITE ELEMENT MODEL OF THE ATR 42-300 AIRPLANE

The following assumptions were made to simplify the FEM:

- Skin thickness was assumed to be uniform throughout the fuselage.
- The empennage, engines, seats, and dummies were represented by concentrated masses.
- Stiffened panels, to compensate for the reinforced door frames, replaced doors.
- Wing leading edges and accessories attached to the airframe (e.g., pulleys, air ducts, cables, overhead bins, and radome) were not included in the model.
- A 5-in.- (12.7-cm) -thick steel plate was used as an impact surface instead of a concrete pad.

Most of the sheet metal parts, such as the fuselage skin, were fabricated using aluminum (Al-2024-T3). The forged metal parts, such as the fuselage frames, floor tracks, floor beams, and supports, were modeled using Al-7075-T6. Frames 25 and 27 were fabricated using Al-7050-T7452. The outside wing fittings were fabricated from titanium (Ti-6Al-4V).

The total weight of the FEM, including full fuel, was 33,120 lb (15,059 kg). The FEM's longitudinal c.g. position was at FS 471.5 (1197.6).

A correlation of analysis data versus test data was performed. The FEM was executed with no fuel (0 lb), half-fuel load (4350 lb) (1977 kg), and full-fuel load (8700 lb) (3955 kg) to study the influence of fuel and wing loading. Details regarding the modeling of the airplane as well as the drop test can be found in reference 4. A report of the final FEM will be published under separate cover.

5. TEST INITIATION.

Prior to the test, the sling and turnbuckle assembly was adjusted to level the fuselage forward and aft and left and right. The data acquisition systems were started and the test article was raised 14 ft (4.3 m) above the surface of the platform (measured from the bottom of the fuselage). Four guide ropes, manned by members of the drop test team, steadied the airplane while it hung above the platform. When the test article was steady and level, the automatic timing sequence was started. The high-speed film cameras and video cameras were activated and the test article was released. Wind conditions prior to and during the test were calm (<3 mph (1.34 m/s)).

6. INSTRUMENTATION.

The airplane was instrumented to record 128 channels of data. A failure of a data acquisition subsystem resulted in the loss of 31 data channels. The descriptions and locations of the remaining 97 sensors are listed in table 4, and some are shown in figure 15. All acceleration data were measured using Endevco 7231C-750 accelerometers. All accelerometers were oriented to measure vertical reactions unless otherwise noted. All load measurements were configured to measure axial loading.

TABLE 4. DATA ACQUISITION SYSTEMS CONFIGURATIONS AND SENSOR LOCATIONS

Channel	Description	Manufacturer/ Model	Unit	Location		
				X (in.)	Y (in.)	Z (in.)
NEFF 490						
101	Left sidewall—F 18	Endevco 7231C-750T	g's	311	-52.75	11
102	Left inner floor track—F 18	Endevco 7231C-750	g's	312	-12.75	0
103	Left inner floor track—F 20	Endevco 7231C-750T	g's	357	-12.75	0
104	Left outer floor track—F 20	Endevco 7231C-750T	g's	357	-37.75	0
105	Left side cockpit floor—F 7	Endevco 7231C-750TS	g's	177	-21	12
106	ATD 20854 right side cockpit—F 9	Endevco 7231C-750T	g's	187	21	19
107	ATD 20854 right side cockpit—F 9	Denton ATD Load Cell	lbs	187	21	19
108	Right side cockpit floor—F 7	Endevco 7231C-750TS	g's	177	21	12
109	Right sidewall—F 18	Endevco 7231C-750T	g's	311	52.75	11
110	Right outer floor track—F 18	Endevco 7231C-750	g's	312	37.75	0
111	Right sidewall—F 20	Endevco 7231C-750T	g's	354	51.75	11
112	Right outer floor track—F 20	Endevco 7231C-750T	g's	357	37.75	0
113	Left inner floor track—F 27	Endevco 7231C-750	g's	504	-12.75	0
114	Left lower sidewall—F 27	Endevco 7231C-750	g's	503	-50.75	12
115	Left upper sidewall—F 27	Endevco 7231C-750	g's	505	-29.75	72
201	Right inner floor track—F 25	Endevco 7231C-750	g's	459	12.75	0
202	Right lower sidewall—F 25	Endevco 7231C-750	g's	458	50.75	11
203	ATD right side—F 28	Endevco 7231C-750TS	g's	529	19	23
204	Right middle sidewall—F 27	Endevco 7231C-750T	g's	503	47.75	52
205	Right sidewall—F 24	Endevco 7231C-750T	g's	437	51.75	11
206	ATD B91174 right side—F 20	Denton ATD Load Cell	lbs	340	19	21
208	Right upper sidewall—F 25	Endevco 7231C-750	g's	460	29.75	72
209	Front right dog bone 1 B—F 25	Measurements Group	lbs	459	48	73
210	Rear right dog bone 3 B—F 27	Measurements Group	lbs	504	48	73
213	Left inner floor track—F 29	Endevco 7231C-750	g's	540	-12.75	0
217	Left upper sidewall—F 25	Endevco 7231C-750	g's	460	-29.75	72
218	Left middle sidewall—F 25	Endevco 7231C-750	g's	458	-47.75	52
219	Left inside bracket—A—F 25	Measurements Group	lbs	459	-23	76
220	Left sidewall—F 22	Endevco 7231C-750T	g's	396	-51.75	11
221	Left outer floor track—F 25	Endevco 7231C-750T	g's	459	-37.75	0
222	Left sidewall—F 24	Endevco 7231C-750T	g's	437	-51.75	11
223	Center ceiling accel—F 26	Endevco 7231C-750T	g's	481	0	77
224	ATD right side—F 28	Denton ATD Load Cell	lbs	528	19	23
225	Right sidewall—F 28	Endevco 7231C-750T	g's	523	51.75	11
226	IRIG	True Time	volts	-	-	-
228	Right engine	Endevco 7231C-750TS	g's	428	159	67
229	Outer right wing	Endevco 7231C-750TS	g's	489	454	89
230	Right outer floor track—F 25	Endevco 7231C-750	g's	459	37.75	0
231	Right inner floor track—F 30	Endevco 7231C-750	g's	540	12.75	0
301	ATD B91175 right side—F 34	Endevco 7231C-750TS	g's	648	19	21
302	Rear equipment bay z axis	Endevco 7231C-750	g's	821	0	16
313	ATD B91175 right side—F 34	Denton ATD Load Cell	lbs	648	19	21
314	Right outer floor track—F 35	Endevco 7231C-750T	g's	661	37.75	0
315	Right inner floor track—F 35	Endevco 7231C-750T	g's	661	12.75	0

TABLE 4. DATA ACQUISITION SYSTEMS CONFIGURATIONS AND SENSOR LOCATIONS (Continued)

Channel	Description	Manufacturer/ Model	Unit	Location		
				X (in.)	Y (in.)	Z (in.)
DAS-48S						
B01	Left inner floor track—F 25	Endevco 7231C-750T	g's	459	-12.75	0
B02	Left outer floor track—F 29	Endevco 7231C-750	g's	540	-37.75	0
B03	Right upper sidewall—F 27	Endevco 7231C-750	g's	505	29.75	72
B04	Right inner floor track—F 20	Endevco 7231C-750T	g's	357	12.75	0
B05	Left middle sidewall—F 27	Endevco 7231C-750T	g's	503	-47.75	51
B06	Rear left dog bone 4 A—F 27	Measurements Group	lbs	504	-48	73
B07	Left inner floor track—F 35	Endevco 7231C-750T	g's	661	-12.75	0
B08	Right inner floor track—F 27	Endevco 7231C-750T	g's	504	12.75	0
B09	Left sidewall—F 28	Endevco 7231C-750T	g's	523	-51.75	11
B10	Left lower sidewall—F 25	Endevco 7231C-750T	g's	458	-50.75	10
B11	Right sidewall—F 22	Endevco 7231C-750T	g's	396	51.75	11
B12	Left sidewall—F 20	Endevco 7231C-750T	g's	354	-51.75	10
B13	Right sidewall—F 37	Endevco 7231C-750T	g's	686	49.75	12
B14	ATD B91201 jump seat—F 39	Endevco 7231C-750T	g's	709	0	24
B15	ATD B91201 jump seat—F 39	Denton ATD Load Cell	lbs	709	0	24
B16	ATD 694 left side cockpit—F 9	Endevco 7231C-750T	g's	187	-21	19
B17	ATD 694 left side cockpit—F 9	Denton ATD Load Cell	lbs	187	-21	19
B18	Rear tail cone—F 47	Endevco 7231C-750TS	g's	872	0	49
B19	Right middle sidewall—F 25	Endevco 7231C-750	g's	458	47.75	52
B20	Left inside bracket—B—F 25	Measurements Group	lbs	459	-23	76
B21	Right inside bracket—A—F 25	Measurements Group	lbs	459	23	76
B22	Left inside bracket—A—F 27	Measurements Group	lbs	504	-23	75
B34	Left wing—middle	Endevco 7231C-750T	g's	505	-159	75
B36	Rear left dog bone 4 B—F 27	Measurements Group	lbs	504	-48	73
B37	Left wing—inner front	Endevco 7231C-750T	g's	459	-51	89
B38	Left engine	Endevco 7231C-750TS	g's	428	-159	67
B39	Left wing—outer	Endevco 7231C-750TS	g's	489	-454	89
B40	Front left dog bone 2 B—F 25	Measurements Group	lbs	459	-48	73
B41	Left wing—inner rear	Endevco 7231C-750T	g's	504	-51	82
B42	ATD B91202 right side—F 29	Endevco 7231C-750T	g's	559	19	20
B43	ATD B91202 right side—F 29	Denton ATD Load Cell	lbs	559	19	20
B44	Left bin front—F 31	Endevco 7231C-750T	g's	593	-21	65
B45	Left bin middle—z axis—F 32	Endevco 7231C-750TS	g's	616	-21	61
B46	Left bin rear—F 34	Endevco 7231C-750	g's	641	-21	65
B47	Left bin middle—x axis—F 32	Endevco 7231C-750T	g's	616	-21	61
B48	Left bin middle—y axis—F 32	Endevco 7231C-750T	g's	616	-21	61
D1	Contact switch—hook	----	N/A	482	0	----
D2	Contact switch—F 15	----	N/A	253	0	----
D3	Contact switch—F 25	----	N/A	459	0	----
D4	Contact switch—F 27	----	N/A	505	0	----
D5	IRIG	----	N/A	----	----	----

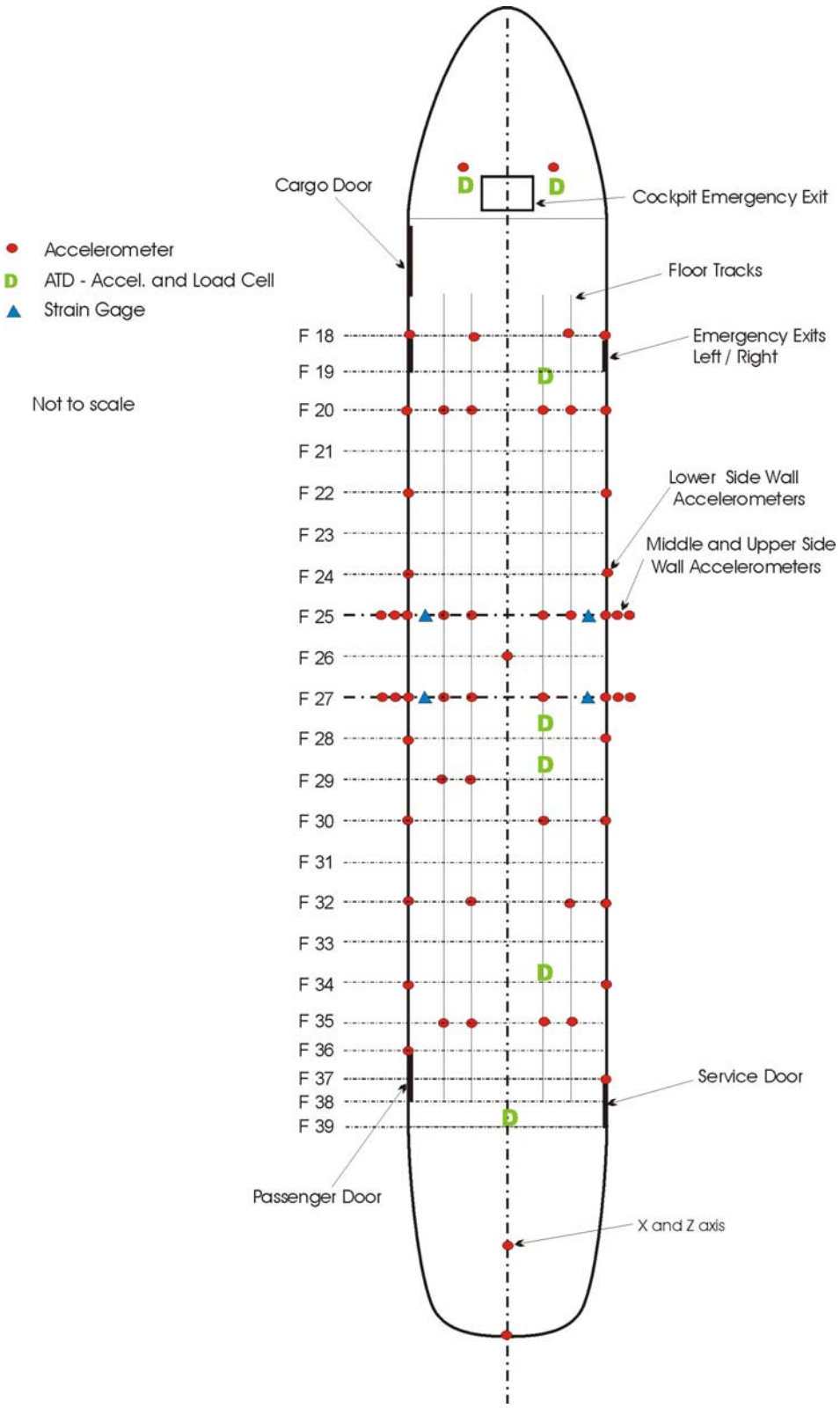

FIGURE 15. FUSELAGE INSTRUMENTATION LOCATIONS

6.1 FUSELAGE.

6.1.1 Accelerometers.

Sidewall accelerometers were mounted nominally 12 in. (30.5 cm) above the floor throughout the fuselage; additional accelerometers were mounted to the sidewall on the wing supports at frames 25 and 27. Accelerometers were mounted to floor tracks at various locations throughout the cabin.

6.1.2 Contact Switches.

Four contact switches were used to determine the elapsed time between hook release and the impact of the fuselage onto the concrete pad. One was located at the release hook and the others at the bottom of the fuselage at frames 15, 25, and 27.

6.1.3 Wing Fittings.

The eight fittings that connected the wing to the aircraft fuselage were instrumented to measure and characterize their reacted loads during the test. They were instrumented with strain gages that were configured and calibrated as load cells to measure axial loading, as shown in figure 16. Two sets of gages were mounted on each fitting for redundancy. The fittings were calibrated in both tension and compression to determine their sensitivity, linearity, and repeatability. The sensitivity coefficients were programmed into the data acquisition systems, and the results were recorded as load data.

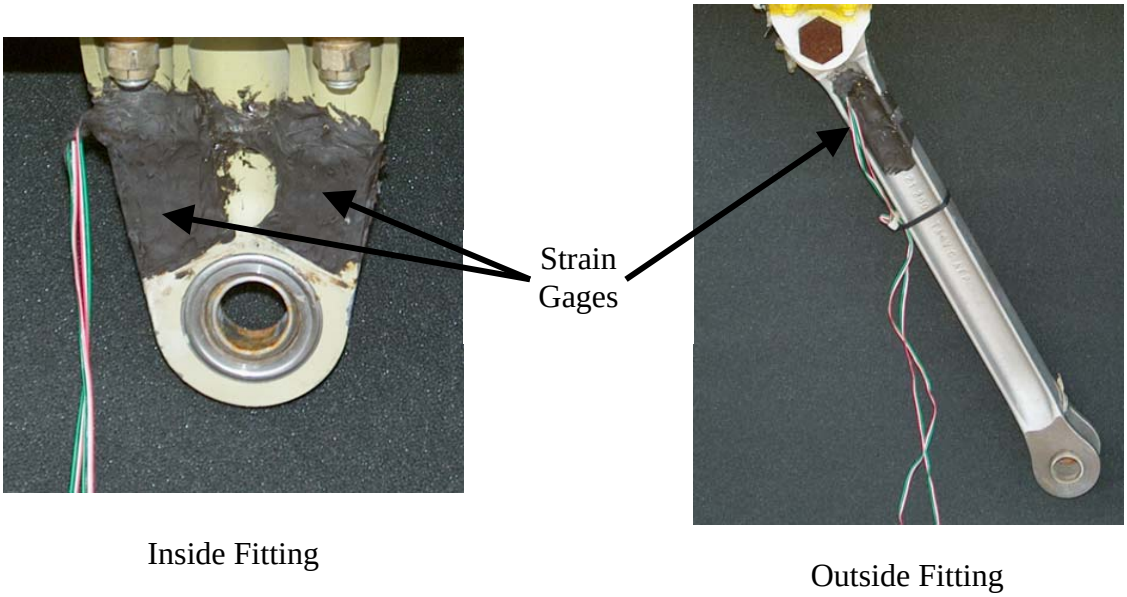

FIGURE 16. WING FITTING STRAIN GAGE BRIDGE LOCATIONS

6.1.4 Wing Fitting Calibrations.

The wing fittings were calibrated using a Material Testing System (MTS) machine. The inside and outside fittings were attached to the MTS machine (figures A-1 and A-2 in appendix A) and cycled through their calibration range, along their principal load path. The load was applied incrementally, allowed to stabilize, and then the data were collected. The fittings were unloaded, the bolts that secured the support were loosened, and the process was repeated two more times. A linear best-fit curve was used to calculate the sensitivity coefficient, linearity, hysteresis, and repeatability for each link. The results are shown in appendix A.

6.2 WINGS AND ENGINES.

Each side of the wing was instrumented with four accelerometers to measure vertical acceleration. They were located (1) at each outside wing fitting attachment point, (2) directly behind the engine on the wing trailing edge, and (3) at the wing tip (see figure 17). An accelerometer was also mounted to the bottom center of the wing. This is the area that acts as the ceiling in the passenger cabin.

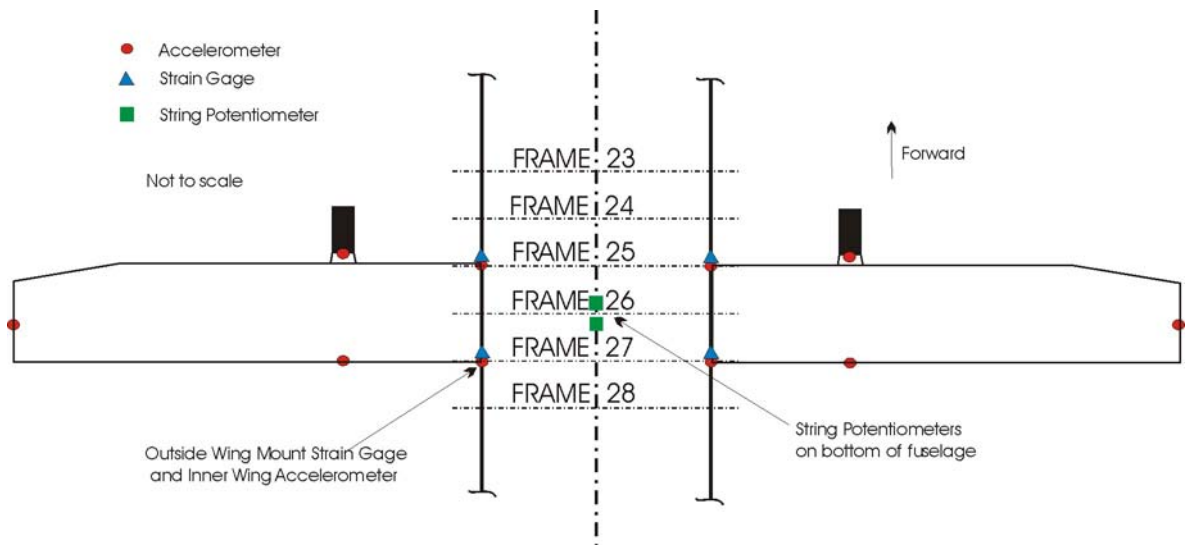

FIGURE 17. WING AND ENGINE INSTRUMENTATION

Each engine was instrumented with an accelerometer to measure vertical acceleration. The accelerometer was located at the rear of the simulated engine.

6.3 OVERHEAD STOWAGE BINS.

Although this was not an overhead stowage bin test, the overhead bins were instrumented to measure their response during the test. To characterize the dynamic response of the bins, five accelerometers were mounted on each bin to measure acceleration, as shown in figure 18. One accelerometer was attached to each end of the bin to measure acceleration in the vertical direction. Three accelerometers were mounted at the bottom center of the bin in a triaxial configuration. The data in the z direction was the average of the three z-oriented accelerometers.

The bin-mounted accelerometers were then used to determine the inertial loading in the x, y, and z directions.

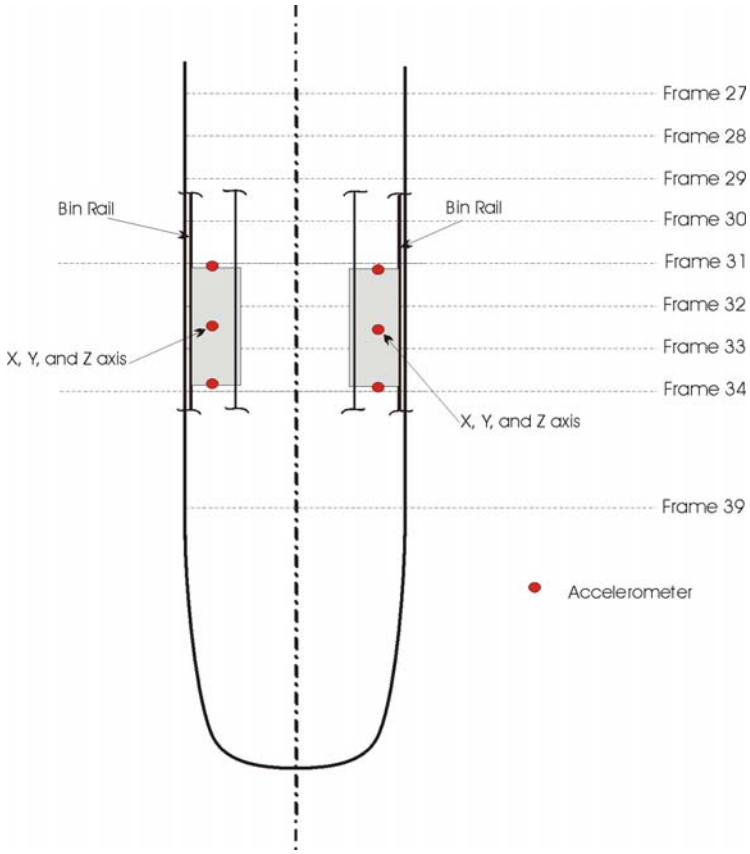

FIGURE 18. OVERHEAD STOWAGE BIN INSTRUMENTATION

6.4 ANTHROPOMORPHIC TEST DUMMIES.

Seven 50th percentile male Hybrid II ATD (49 CFR Part 572) were used in the drop test. Each ATD was instrumented with a Denton model 1708 load cell to measure spinal column axial loading in the lumbar area. An accelerometer was used to measure vertical g forces in the pelvic region. The locations of the ATD are listed in table 3 and shown in figure 6.

6.5 VISUAL IMAGING.

Twelve high-speed (H/S) film cameras were used to record the test at 500 frames per second. Four of the cameras were onboard the test article to record the reaction of the cabin interior. The remaining eight cameras were located around the exterior of the airplane to provide overall coverage of the airplane and areas of interest. All the cameras were time synchronized through a satellite-based time code receiver. This allowed for the precision time stamping of each frame of film and provided a means to synchronize the time among all cameras as well as the recorded data. Eight standard video cameras (30 frames per second) were also located around the exterior of the airplane to provide overall coverage of the test. The camera locations are shown in

figure 19. Two event bulbs were used to indicate hook release. Interior camera coverage was not obtained due to synchronization problems.

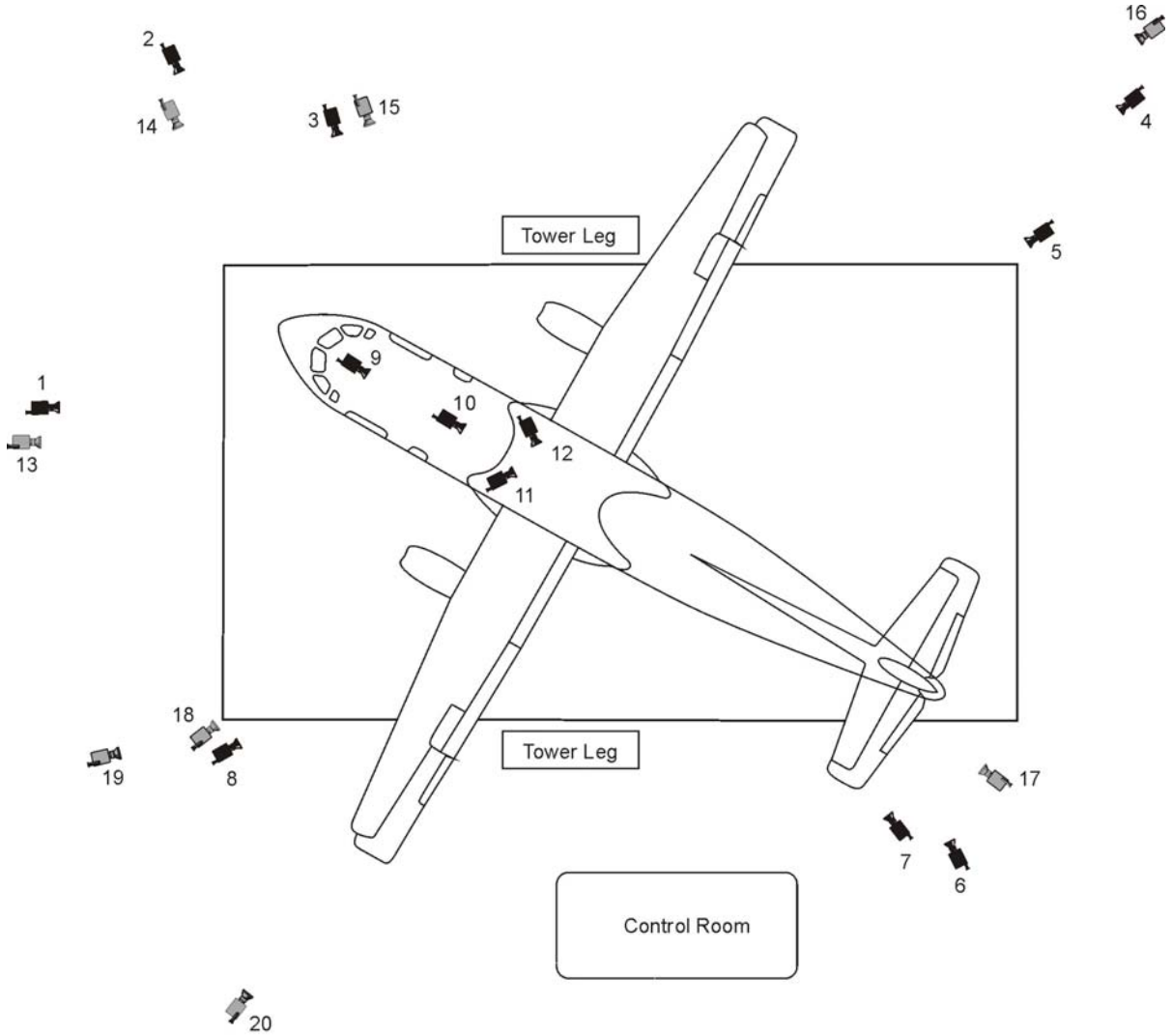

Legend
Camera Numbers

1: Overall Left Front Quarter - H/S Film
2: Overall Right Front Quarter - H/S Film
3: Right Front Quarter - H/S Film
4: Right Rear Quarter - H/S Film
5: Right Rear Quarter - Wing Fittings - H/S Film
6: Left Rear Quarter - H/S Film
7: Left Rear Quarter - Wing Fittings -H/S Film
8: Left Side - H/S Film
9: Forward Looking Aft from Cabin - H/S Film
10: Forward Looking Aft from Center -H/S Film
11: Right Inside Wing Fittings - H/S Film
12: Left Inside Wing Fittings - H/S Film
13: Front Left Quarter - Video
14: Front - Video
15: Front Right Quarter - Video
16: Right Rear Quarter - Video
17: Left Rear Quarter - Video
18: Left Side - Video
19: Left Outside Wing Fittings - Video
20: Overall from Building 287 - Video

FIGURE 19. CAMERA LOCATIONS

7. DATA ACQUISITION, COLLECTION, AND REDUCTION.

7.1 DATA ACQUISITION SYSTEMS.

Two independent data acquisition systems were used to collect test data.

7.1.1 System 1—NEFF 490.

The NEFF 490, shown in figure 20, is a H/S data acquisition system with the capability to sample and record data at rates up to 100 kHz per channel. The system consists of 92 channels distributed among four subsystems. Each channel includes a 12-bit analog-to-digital (A/D) converter, a 6-pole Bessel programmable anti-alias filter (100, 200, 1000, and 2000 Hz). Analog input is fed to a differential input amplifier with 12 programmable gain steps. Full-scale range inputs are selectable from ±5 mV to ±10.24 V.

FIGURE 20. NEFF 490 DATA ACQUISITION SYSTEM

The system was set to sample and record data simultaneously at 10 kHz per channel. All data channels were prefiltered at 1 kHz (CFC 600). The data was collected and stored in 512 Kbytes

of onboard memory. Test data was transferred to a personal computer (PC) by an IEEE-488 interface for further analysis. The full-scale range for each channel was selected based upon the expected output of the sensor.

7.1.2 System 2—EME DAS-48S.

The EME DAS-48S, shown in figure 21, is a H/S, small, flexible, ruggedized, portable data acquisition system. The system can acquire analog and digital data at rates up to 20 kHz per channel. The system consists of 48 analog channels and 24 digital channels. All channels are simultaneously sampled. The system has a 12-bit A/D converter and a 6-pole Butterworth anti-alias programmable filter (10 Hz to 20 kHz). Analog input is fed to a differential input amplifier with variable gain of 1 to 1000. The maximum input voltage is ±2.5 volts.

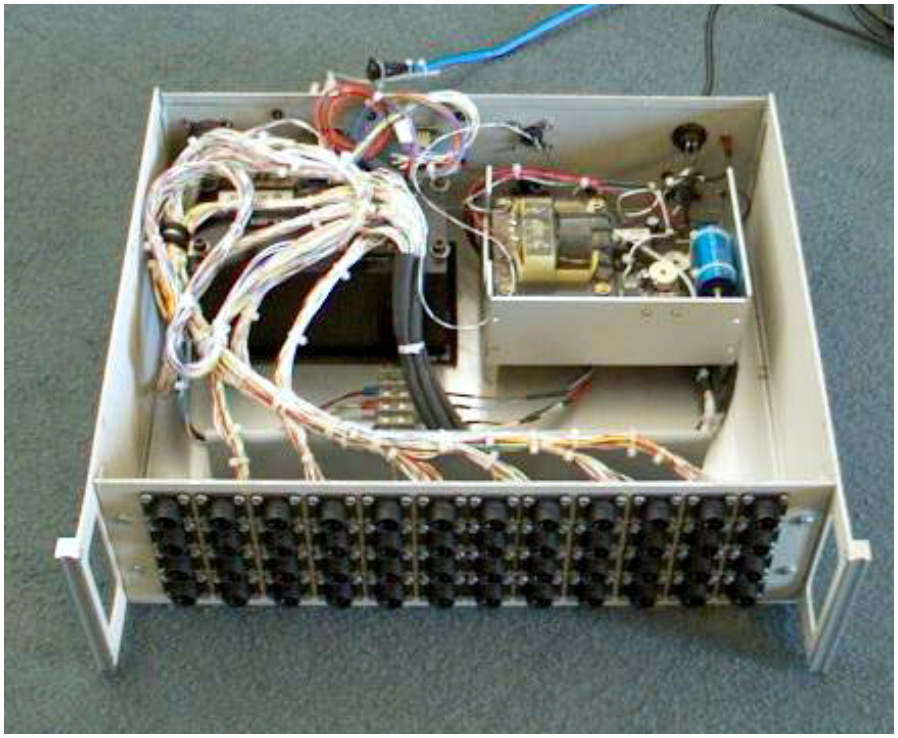

FIGURE 21. EME DAS-48S DATA ACQUISITION SYSTEM

The system was set to sample and record 48 channels of analog data and 5 channels of digital data simultaneously. A sampling rate of 10 kHz per channel was used. All data channels were prefiltered at 1.7 kHz (CFC 1000). The data was collected and stored in 32 megabytes of onboard memory. Test data was transferred to a PC by an RS-232/422 interface for further analysis. The gain value for each channel was selected based upon the expected output of the sensor.

7.2 DATA COLLECTION.

Before the test, the bridge output voltage for each channel's sensor was zero-balanced to compensate for any variation in the zero state of the sensor. The channels were then calibrated.

All phases of balancing the bridge output voltage, calibrating the channels, measuring sensitivity, and determining conversion coefficients for calculating engineering units are controlled by the data acquisition system software based upon user inputs.

The two systems were programmed to collect data in a pretrigger mode, a technique that allows the continuous sampling and storing of data into a buffer prior to the test trigger. The two data systems collected and saved data 2 seconds prior to and 8 seconds after hook release. The data acquisition systems were enabled prior to the hoisting of the ATR 42-300, thus ensuring that data would be collected in the event of an inadvertent hook release. A Bowen 10-channel sequencer was used to (1) initiate the test sequence, (2) hook release, and (3) control all the video, camera equipment, and accessories.

7.3 DATA REDUCTION.

DSP Development Corporation's DADiSP data analysis software was used to analyze the data.

For the purposes of this test, time zero, (T_0) was defined as the moment of impact as observed on the H/S film and confirmed via the recorded data. This time corresponds to an IRIG date of July 30, 2003, at 13:30:13.330 local time.

An SAE J211 CFC 600 (1000-Hz) digital filter [5] was used to filter the ATD load cell data. An SAE J211 CFC 60 (100-Hz) digital filter [5] was used to filter the strain gage data and accelerometer data. However, the use of this filter, in many cases, did not provide adequate filtering to determine the fundamental accelerometer pulse shape. Posttest analysis on the acceleration data indicated that the data exhibited large swings in value. These swings greatly influenced the pulse shape and amplitude, yet had a minimum affect on the fuselage response. A CFC 20 (33.3-Hz) digital filter, designed using SAE J211 guidelines, was therefore used to remove the unwanted signals and provide the needed pulse definition. The use of this filter was justified [6] by showing that the integrated filtered pulse yielded the same velocity value as the unfiltered and CFC 60 (100-Hz) filtered data. However, in some instances, the data was overfiltered. The results from the overfiltering did not have a significant affect on the data, and the need to simplify comparisons predicated the use of a single filtering frequency. CFC 60 (100-Hz) data was also plotted as a reference where needed. CFC 20 (33.3-Hz) filtered accelerometer data was used unless otherwise indicated. The SAE-J211 filter class and corresponding F_H frequency are listed in table 5.

TABLE 5. SAE-J211 FILTER CLASS COMPARISONS

Filter Class	F_H Frequency (Hz)
CFC 20	33.3
CFC 60	100
CFC 600	1000
CFC 1000	1667

8. DATA ANALYSIS.

8.1 TIME TO IMPACT.

The theoretical free-fall time of the airplane, 0.933 second, is calculated using the equation

$$t = \sqrt{\frac{2h}{g}} \tag{1}$$

where t is time, h is the drop test distance of 14 ft (4.3 m), and g is the acceleration due to gravity (32.2 ft/ s^2 (9.81 m/s^2)). The measured free-fall time is the elapsed time between closure of the hook contact switch and the earliest closure of the bottom-mounted contact switches. The calculated times of the three contact switches were 0.968, 0.942, and 0.940 second at the forward, center-forward, and center-aft locations respectively.

8.2 IMPACT VELOCITY.

The theoretical impact velocity was determined by the kinematic equation

$$v_t = \sqrt{2gh} \tag{2}$$

where v_t is the final theoretical velocity, g is the acceleration due to gravity, and h is the drop test distance. Using this equation, the theoretical impact velocity is 30 ft/s (9.1) m/s.

The calculated velocity is determined by the kinematic linear motion equation

$$v_b - v_0 = gt \tag{3}$$

where v_b is the final calculated velocity, v_0 is the initial velocity (0 ft/s), g is the acceleration due to gravity, and t is the measured free fall time (0.940 second).

Table 6 shows the drop test velocities obtained using the different methodologies.

TABLE 6. IMPACT VELOCITY

Methodology	Velocity ft/s (m/s)
Theoretical	30 (9.1)
Calculated	30 (9.1)

8.3 FUSELAGE STATIC CRUSH MEASUREMENTS.

The fuselage static crush measurements are listed in table 7. The bottom rear of the fuselage was deemed to be the most representative of the total crush. Therefore, an average crush of 12 in. (30.5 cm) was adopted.

TABLE 7. FUSELAGE STATIC CRUSH MEASUREMENTS

Frame	Crush Left Side		Crush Right Side	
	in.	cm	in.	cm
14	4.188	10.636	5.375	13.653
16	4.875	12.382	6.875	17.463
18	6.188	15.716	6.938	17.621
20	7.813	19.843	8.313	21.114
21	8.000	20.320	8.938	22.701
32	11.625	29.527	11.438	29.051
33	12.625	32.067	11.875	30.163
34	12.875	32.702	11.750	29.845
35	12.000	30.480	10.875	27.623
36	11.250	28.575	9.750	24.765

8.4 POSTTEST AIRFRAME ACCELERATION ESTIMATE.

An estimate of the expected g-loading (G) on the fuselage was determined using the kinematic equation for an idealized triangular pulse

$$G = (V_0^2 - V_f^2)/(gS) \tag{4}$$

where V_0 is the impact velocity, V_f is the final velocity (0), g is the acceleration due to gravity, and S is the estimated crush of the fuselage. Using the estimated crush distance of 12 in. (30.5 cm), the calculated value was 28 g's.

A corresponding pulse duration of T = 65 msec was calculated using the kinematic equation

$$T = 2(V_0 - V_f)/(gG) \tag{5}$$

In many instances, a better estimate of the expected g-loading and pulse duration could be made if a triangular wave shape with a skewed leading edge was used. This would result in a fuselage loading of 24 g's and a pulse duration of 73 msec.

8.5 SEQUENCE OF EVENTS.

The following time line was developed to denote significant events during the test.

- T_0 – Time of impact (landing gear fairing impacts temporary concrete pad).
- T_{30} – Fuselage bottom impacts temporary concrete pad (30 msec after initial impact).
- $T_{35\text{-}45}$ – Landing gearbox housing and stanchions fracture.
- T_{60} – Frames 25 and 27 fracture.
- T_{80} – Forward and aft fuselage sections are observed to begin to rebound.
- T_{250} – Leading edge of engines are observed to rotate downward.
- T_{400} – Engines impact concrete drop test platform.

8.6 AIRFRAME ACCELERATIONS.

Airframe acceleration data is given in terms of three parameters: peak acceleration (G_{peak}), pulse duration (Δt), and maximum acceleration (G_{max}). G_{max} acceleration values are used because they are better at determining the overall pulse amplitude than peak values, which show greater sensitivity to localized events. The G_{max} values were computed based on an idealized triangular pulse assumption (equation 6).

$$G_{max} = 2\frac{\Delta V}{\Delta t} \tag{6}$$

where Δt is the difference between the start and stop times of the integration interval, and ΔV is the velocity change determined by integrating the acceleration data during Δt.

All accelerations are in the z direction unless otherwise noted. The fundamental impact pulse, which is observed using 33.3-Hz filtered data, represents the overall impact response.

Airframe acceleration data are presented in three groups: (1) fuselage sidewall accelerations, (2) floor track accelerations, and (3) other accelerations. For comparison, acceleration data were filtered at 100 and 33.3 Hz. The filtered data can be found in appendix B.

Previously conducted drop tests of commuter like airplanes have shown that floor track acceleration data are good indicators of the general accelerations experienced by the test article. However, in the case of this ATR 42-300 drop test, the airplane experienced severe structural damage, particularly at the fuselage, wing, and landing gearbox interface. This resulted in secondary effect acceleration data being superimposed on the primary crash pulse, making the analysis difficult. Therefore, fuselage sidewall acceleration data was also studied to determine the overall ATR 42-300 accelerations.

Theoretically, the velocity change associated with each of the accelerometers should be 30 ft/s. In most instances, this was not the case. This can be attributed to two reasons: (1) the accelerometers were no longer vertically oriented and (2) the test article was still continuing to rebound after the pulse duration of interest.

8.6.1 Sidewall Accelerations.

The sidewall accelerations are presented in left and right lower sidewall accelerations, left and right middle sidewall accelerations, left and right upper sidewall accelerations. Typical sidewall accelerations and corresponding velocity profiles are shown in figures 22 and 23. The data are listed in table 8.

The data from the lower sidewall locations were used to determine the average fuselage G_{max} and average pulse durations. They represented a better distribution throughout the fuselage; the frame sections remained attached to the fuselage; they remained relatively vertically oriented during the impact. The average lower sidewall G_{max} acceleration value was 19 g's and the average pulse duration was 83 msec.

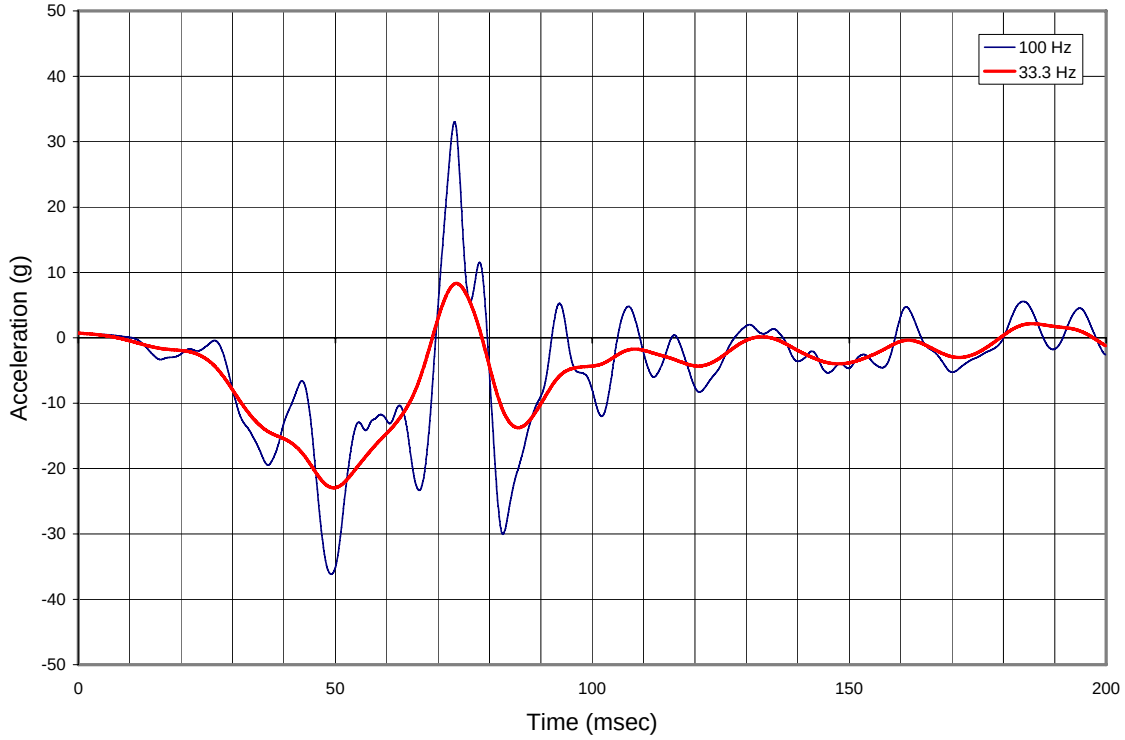

FIGURE 22. TYPICAL VERTICAL SIDEWALL ACCELERATION

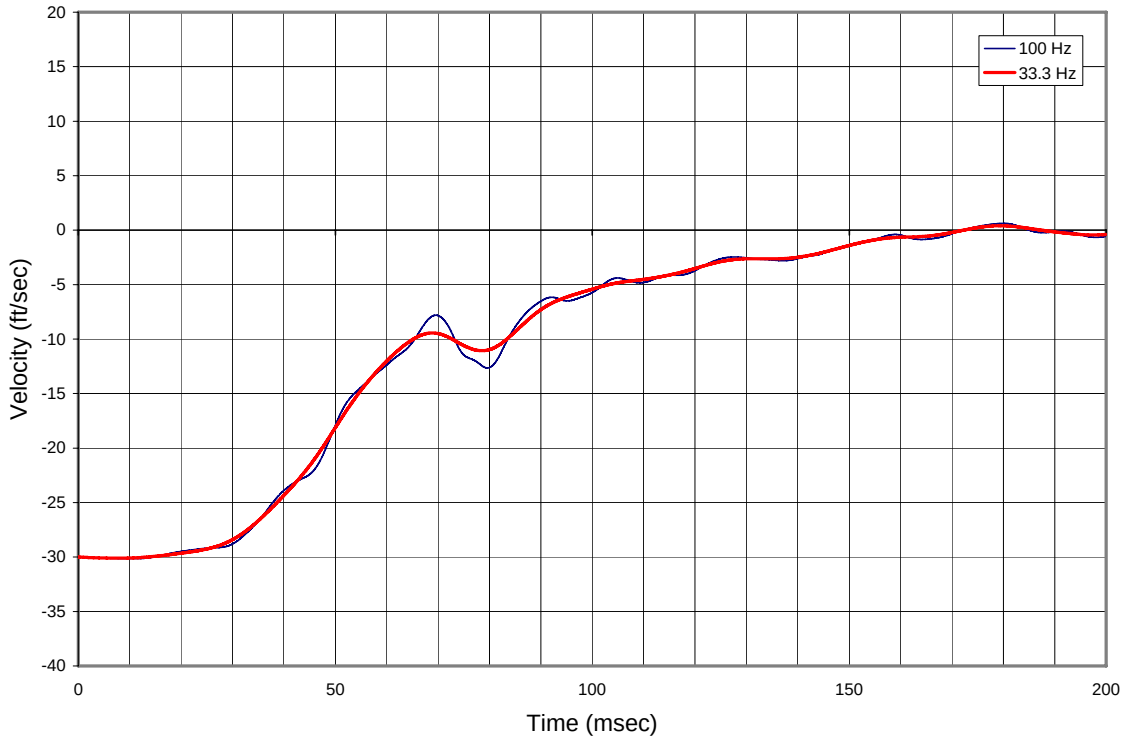

FIGURE 23. TYPICAL VERTICAL SIDEWALL VELOCITY

TABLE 8. VERTICAL SIDEWALL ACCELERATIONS

Location		G_{peak} (g)	Pulse Duration (msec)	G_{max} (g)	Velocity Change (ft/s)
Left Lower	F 18	22	72	20	28
	F 20	21	81	21	26
	F 22	21	85	19	26
	F 24	21	87	18	25
	F 25	20	85	22	29
	F 27	18	82	19	24
	F 28	15	82	19	24
Right Lower	F 18*	21	----	----	----
	F 22	23	84	19	25
	F 24	24	84	18	23
	F 25	24	85	19	25
	F 28	22	81	15	19
	F 37**	14	75	14	16

* Sensor failed at 100 msec.
** Mounted on doorframe of service door, not used in calculations.

8.6.2 Cabin Floor Track Accelerations.

The cabin floor track accelerations are presented in four groups: left outer floor track, left inner floor track, right inner floor track, and right outer floor track accelerations. Typical floor track accelerations and corresponding velocity profiles are shown in figures 24 and 25. The floor track data are listed in table 9.

Orientation of the accelerometers located near the center of the aircraft (frames 25 to 27) was unknown due to the significant structural damage in that area. Calculated values for G_{max} in the cabin area excluded accelerometers located near frames 25 and 27. The average G_{max} acceleration value for the cabin floor tracks was 26 g's and the average pulse duration was 68 msec.

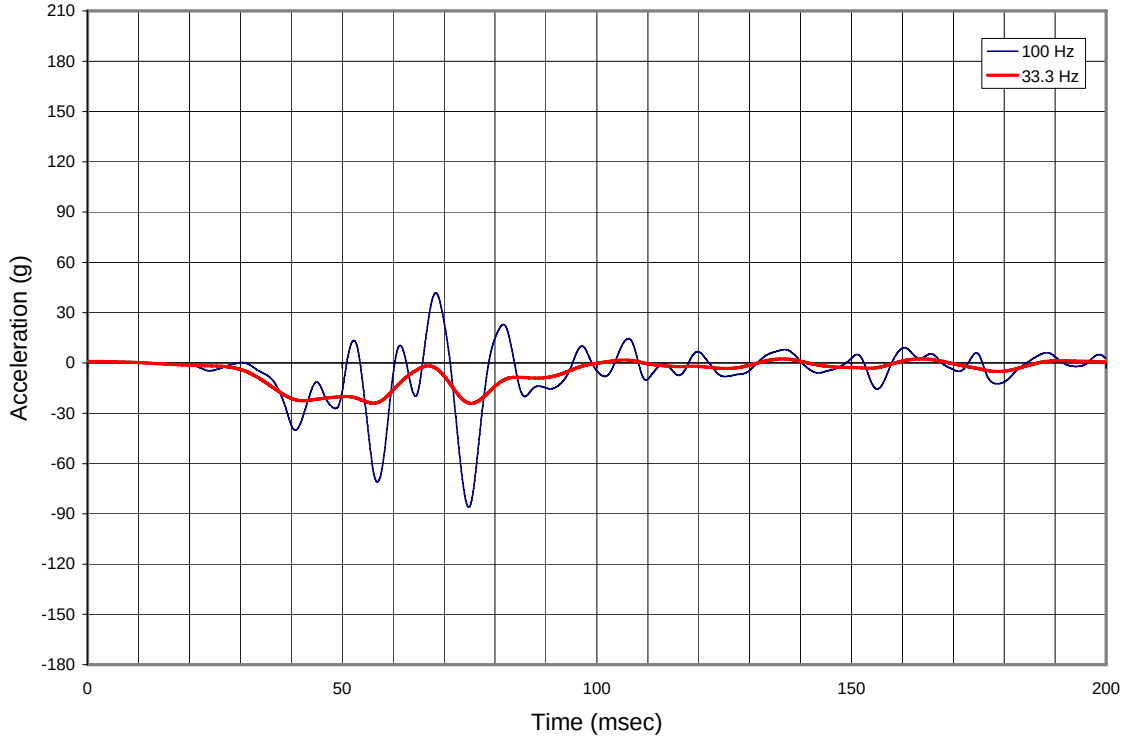

FIGURE 24. TYPICAL VERTICAL FLOOR TRACK ACCELERATION

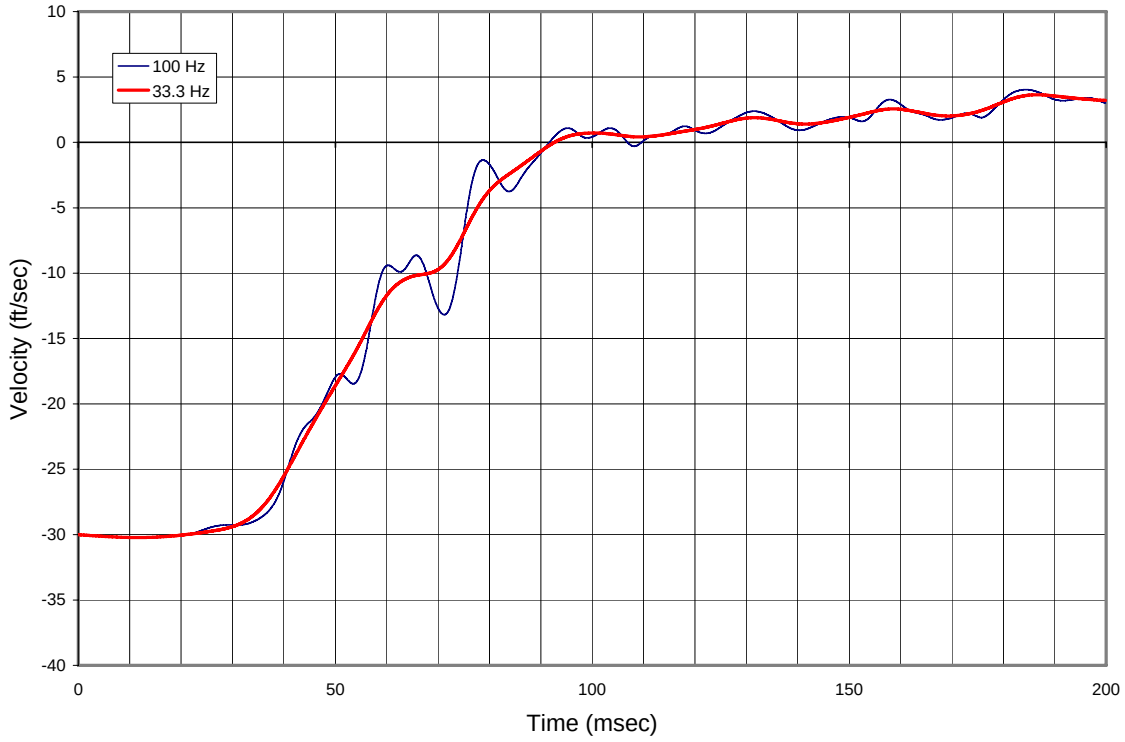

FIGURE 25. TYPICAL VERTICAL FLOOR TRACK VELOCITY

TABLE 9. VERTICAL FLOOR TRACK ACCELERATIONS

Location		G_{peak} (g)	Pulse Duration (msec)	G_{max} (g)	Velocity Change (ft/s)
Left Outside	F 20	29	52	30	25
	F 25	27	----	----	----
	F 29	23	82	21	26
Left Inside	F 18	64	64	28	28
	F 20	57	51	37	30
	F 25	57	25	59	23
	F 27	77	25	83	32
	F 29	32	79	23	28
	F 35	22	81	20	25
Right Inside	F 20*	38	----	----	24
	F 25	50	36	50	28
	F 27	57	27	60	25
	F 30**	16	----	----	----
	F 35	21	71	22	26
Right Outside	F 18	24	66	28	30
	F 20	25	72	32	36
	F 25	22	39	28	17
	F 35	17	64	17	17

*Sensor failed during test.
**Floor track failed.

8.6.3 Additional Accelerations.

Additional acceleration data can be found in table 10.

TABLE 10. ADDITIONAL VERTICAL ACCELERATIONS

Location	G_{peak} (g)	Pulse Duration (msec)	G_{max} (g)	Velocity Change (ft/s)
F 7—Left side cockpit floor**	30	----	----	----
F 7—Right side cockpit floor	34	49	41	32
F 26—Cabin ceiling	10	92	11	16
F 45—Rear equipment bay	21	75	17	21
F 47—Tail cone attachment location	12	206	12	----
Left Wing				
F 25—Inner leading edge	14	80	12	16
Engine	10	112	9	16
Wing tip*	+35/-30	----	----	----
F 27—Trailing edge behind engine	8	85	11	15
F 27—Inner trailing edge	10	106	11	19
Right Wing				
Engine	9	113	10	18
Wing tip*	+39/-34	----	----	----

* Did not maintain vertical orientation.
** Sensor failed.

8.7 OVERHEAD STOWAGE BIN ANALYSIS.

Only data for the left overhead stowage bin was obtained (appendix B). Each bin was attached to the fuselage by four brackets. Both bins and all the brackets remained intact during and after the test. A posttest inspection of both bins and their brackets showed no damage.

Vertical inertial loads (In_{bin}) for the bin are based on accelerometer data and is defined by the kinematic equation

$$In_{bin} = (w/g)(a) \tag{7}$$

Where w/g is the mass of the bin and its contents and a is the average value of the three vertical-oriented accelerometers.

The average vertical acceleration plot and corresponding velocity plot are shown in figures 26 and 27, respectively.

The peak acceleration of the left bin was 13 g's. This resulted in a maximum inertial loading of 699 lb (317.1 kg).

A failure analysis on the links was conducted prior to the test. Links B-1 and B-3 and their attachments are identical and carry the primary loads in the vertical direction. These were

identified as having the greatest probability of failure during the test. The failure load of the links and attachments was determined to be approximately 1000 lb (453.6 kg).

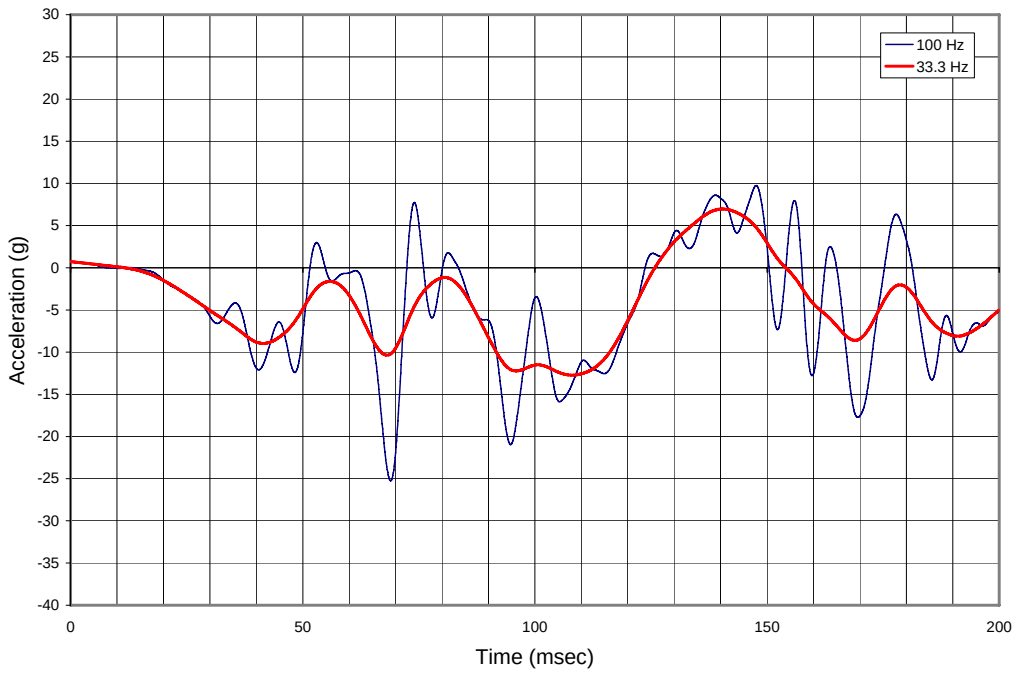

FIGURE 26. LEFT BIN, AVERAGE VERTICAL ACCELERATION

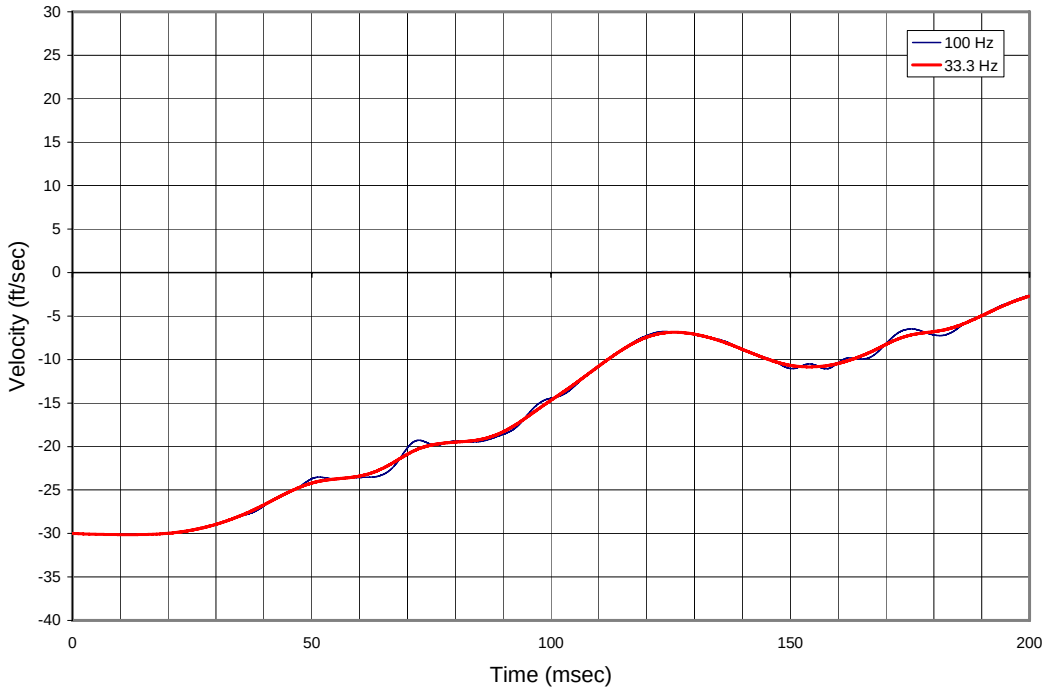

FIGURE 27. LEFT BIN, CALCULATED VERTICAL VELOCITY

8.8 ANTHROPOMORPHIC TEST DUMMIES.

Seven ATD were used to measure lumbar loads and pelvic accelerations. ATD data are presented in table 11 and appendix B. Only ATD one, two, and five occupied seats that did not fail and remained attached to the floor.

TABLE 11. ANTHROPOMORPHIC TEST DUMMY DATA

ATD No.	Location	Lumbar Load (lb (kg))	Accelerometer Data	
			G_{peak} (g)	Pulse Duration (msec)
1	F 7—Pilot seat	2403 (1090)	33	72
2	F 7—Co-pilot seat	2511 (1139)	37	52
5	F 29—Modified seat	738 (335)	50	26

Note: Seats did not fail.

A posttest inspection of ATD 7 and the flight attendant's seat at FS 708 (1798) showed that they were leaning forward. After reviewing the data, it was believed that the ATD's legs were supporting the weight of the ATD and that the load cell readings were artificially low.

8.9 WING FITTINGS.

Table 12 shows the peak loads and corresponding times of the eight instrumented wing fittings. The load profiles are shown in appendix B. As predicted, on impact, the inside fittings were initially loaded in tension and the outside fittings in compression.

TABLE 12. WING FITTING LOADS

Frame Section	Left Outside Fitting		Left Inside Fitting		Right Inside Fitting		Right Outside Fitting	
	Peak Load (1000 lb (kg))	Time (ms)	Peak Load (1000 lb (kg))	Time (ms)	Peak Load (1000 lb (kg))	Time (ms)	Peak Load (1000 lb (kg))	Time (ms)
F 25 Ch A	---- ----	----	19.9 (9.0)	57	24.3 (11.0)	57	---- ----	----
F 25 Ch B	-42.1 (-19.1)	58	19.7 (8.9)	59	---- ----	----	-44.2 (-20.0)	58
F 27 Ch A	-32.6 (-14.8)	62	50.7 (23.0)	61	---- ----	----	---- ----	----
F 27 Ch B	-31.9 (-14.2)	62	---- ----	----	----	----	-22.4 (-10.2)	62

Note: Minus (-) sign denotes compression.

9. RESULTS AND DISCUSSION.

9.1 FUSELAGE STRUCTURE.

The fuselage sustained major structural damage as shown in appendix C. This was caused by (1) the failure of the wing support structures (frames 25 and 27), thereby allowing the wing to penetrate the fuselage; (2) the fracturing of the landing gearbox section; and (3) the failure of the floor stanchions. The failure of frames 25 and 27 resulted in most of the remaining cabin frames fracturing.

At impact, a bending moment, centered near the rear cabin doors, was created by the upswept aft fuselage. This also contributed to the fracturing of the aft fuselage frames.

A review of the H/S film of the fuselage at the outside wing fittings indicated that the upper fuselage started collapsing at approximately 60 msec after impact. This was consistent with the significant load changes observed in the wing fitting data that occurred at that approximate time, see table 12.

9.2 FUSELAGE RESPONSE.

The averaged measured cabin crash pulse amplitude was approximately 23 g's maximum with a pulse duration of approximately 76 ms (see table 13). This compared favorably with the estimated crash pulse amplitude of 28 g's and a pulse duration of 65 ms (based on fuselage crush measurements). This lends support to the use of 33.3-Hz filtered data to define the fundamental pulse shape.

TABLE 13. FUSELAGE PULSE DURATION AND AMPLITUDE

Impact Pulse Source	Pulse Amplitude (g)	Pulse Duration (msec)
Estimated crush measurement—idealized triangular pulse	28	65
Estimated crush measurement—skewed triangular pulse	24	73
Average cabin sidewall data	19 (G_{max})	83 (G_{max})
Average cabin floor track data	26 (G_{max})	68 (G_{max})

9.3 EXTERIOR.

The wing penetrated the cabin area (figure C-46 in appendix C) after frames 25 and 27 fractured. The weight of the engines caused the wing leading edge to rotate downward and resulted in the engines impacting the concrete drop test platform at approximately 400 msec after T_0. The impact of the left engine resulted in the rupturing of the wing tank near the engine and allowed some of the simulated fuel to leak out. The right engine also impacted the concrete drop test platform; however, the right wing tank remained intact.

In numerous locations, the fuselage skin showed the affect of "oil canning" due to bending and flexing of the fuselage structure, see figures C-41, C-42, and C-65 in appendix C.

The outside wing fittings remained intact and showed no signs of damage. This can be attributed to the failure of the wing support structures, which are frames 25 and 27.

9.4 CABIN SUBFLOOR AREA.

The entire cabin subfloor area sustained major structural damage, see figures C-95 to C-104 in appendix C. The most significant damage occurred in the middle of the fuselage between frames 24 and 28. Floor frames 25 and 27 fractured in numerous locations and protruded into the cabin area.

The floor bulged severely into the cabin at these locations. This was attributed to the up loading from the impact of the landing gearbox and the down loading generated by the wing via frames 25 and 27. The right outer floor track at frame 22 was displaced outward and the inner right floor track at frame 22 was fractured. Floor frames 21 to 28 also fractured. Floor frames 29, 30, and 31 were twisted. Frame 29 was twisted due to the loading on the floor tracks from the landing gearbox area and the impact forces from the stanchions. The bolts securing the inner right floor track leading to frame 29 and the left inner floor track trailing from frame 29 were sheared, resulting in floor track failure.

Most of the stanchions failed at either their top or bottom attachment points. Stanchions that did not fail were attached to a floor frame or fuselage frame that did fail. Each of these failures may have resulted in at least two localized impact pulses. The first was the result of the original impact; the second may have occurred if the end of the stanchion impacted the upper portion of the floor frame or the lower fuselage frame and, in some locations, where the stanchion pierced the fuselage skin and impacted the cement pad. The locations where the floor frames fractured would have also resulted in a localized impact pulse.

A vertically oriented 6-in. (15.2-cm) -diameter fiberglass ventilation duct located beneath the aisle floorboard near FS 340 impacted the floorboard with sufficient force to dislodge the board from the floor track.

The floor track data in table 8 indicate that the inner floor tracks sustained a higher g-loading than the outer floor tracks. This was attributed to the closer proximity of the stanchions to the inner floor tracks, see figure 9.

The crushing of the fuselage frames absorbed much of the impact energy, thereby limiting the g forces transmitted to the floor tracks and extended the impact pulse duration.

9.5 UPPER CABIN INTERIOR.

Fuselage frames 25 and 27 fractured at approximately 60 msec after impact, after which the wing penetrated the cabin area. The leading edge of the wing was observed to rotate downward and into the cabin area at approximately 250 msec after impact. The sidewalls of frames 17 to 37 sustained multiple fractures. Frames 18 to 36 sustained single location fractures or other structural damage near the ceiling. The upper frame sections approaching the wing area were displaced into the cabin and would have resulted in the bins impacting the tops of the aisle seats.

9.6 EXITS.

The service door on the right rear side of the airplane and the cockpit emergency ceiling exit were usable. The passenger and cargo door as well as the two emergency window exits were unusable.

9.7 COCKPIT.

The stanchions, floor beams, lower fuselage frames, and the reinforced nose gear housing at frame 7 sustained structural damage.

9.8 OVERHEAD STOWAGE BINS.

The overhead stowage bins, their supports, and fuselage attachment points showed no signs of damage.

The peak vertical inertial loading of the left bin was 12.7 g's. This is consistent with the fuselage acceleration data. Using the integrated bin accelerometer data, the calculated impact velocity was 30 ft/s (9.81 m/s). This was equal to the fuselage impact velocity.

9.9 SEATS.

The cockpit seats remained intact and showed no signs of damage. The seats experienced approximately 38 g's vertical loading.

The cabin seats experienced an average of 22 g's vertical loading.

Posttest pictures of the ATR 42-300 seats are shown in figures C-146 to C-225 in appendix C. A postcrash inspection of the ATR 42-300 cabin seats determined the following:

- Unoccupied seats remained upright and showed no signs of structural damage.
- All the seat pans remained intact and attached to the cross tubes.
- All dual-occupied seats collapsed (except those loaded with 135 lb (61.3 kg) of lead shot).
- The rear cross tubes of all dual-occupied seats were sheared at the inboard leg (except those loaded with 135 lb (61.3 kg) of lead shot).
- All rear outboard legs on the dual-occupied seats collapsed (except those loaded with 135 lb (61.3 kg) of lead shot).
- The seatback of seat A at frame 31 was broken and the outboard end of the rear cross tube supporting the seat was bent down and back. A mannequin occupied the seat.

- The inboard end of the rear cross tube of seat C at frame 32 was almost severed. The seat remained upright.

- The rear cross tubes on the seats loaded with 150-lb lead shot were severed at both ends. The tube sheared in the center. The outboard half was pulled out of the center fitting that secured the seat frame to the rear cross tube.

- The right outboard floor track at frame 22 was slightly displaced outward. The seat leg at that position was detached from the floor track. The floor track was not damaged.

- A 6-in.- (15.2-cm) -diameter fiberglass ventilation duct located beneath the aisle floorboard near FS 340 impacted the floorboard with sufficient force to dislodge the board from the floor track.

A postcrash inspection of the NAL experimental stroking seat determined the following:

- The left inboard floor track between frames 27 and 28 was angled up toward the front of the plane, the floor track fractured just prior to the floor beam at frame 28 and dropped below floor level. The front outboard leg was detached from the floor track and the floor track was undamaged.

- The seat showed the most significant energy absorption at the forward inboard leg and the rear outboard leg.

- The seat was pitched back at approximately a 20° angle; the seat back and seat pan were not damaged.

The modified 16-g Tenryu seat remained upright, intact, and attached to the floor tracks.

The screws that secured the flight attendant seat to the floor track brackets were sheared, allowing the seat to pivot forward.

An actual crash impact imparts a longitudinal drag load on the aircraft that may significantly change the load distribution in a seat. Thus, the seat fracture modes observed in this test are not necessarily reflective of what may occur in service. Therefore, special consideration must be given when considering the results of seat test data obtained from this vertical drop test.

10. SUMMARY OF RESULTS.

On July 30, 2003, the FAA conducted a vertical impact test of a large, high-wing airplane. The test was conducted at the FAA William J. Hughes Technical Center, Atlantic City International Airport, New Jersey. The objective of this test was to determine the impact response of the fuselage, floor tracks, and seats when subjected to a severe, but survivable, simulated crash impact. The data collected in this test will supplement the existing basis for improved seat and restraint systems for Title 14 Code of Federal Regulations Part 23 commuter category airplanes. The results are as follows.

- An ATR 42-300 high-wing regional commuter airplane was dropped from a height of 14 ft (4.3 m), resulting in a vertical impact velocity of 30 ft/s (9.1 m/s). This resulted in what was considered a severe, but survivable, impact condition.

- The fuselage sustained major structural damage, which was attributed to (1) the loading of the wing and subsequent failure of the supporting frames, (2) the fracturing and failure of the landing gearbox section, and (3) the failure of the floor stanchions.

- A habitable environment for most of the passengers was not maintained due to the penetration of the wing and the landing gearbox into the cabin.

- The crushing of the fuselage frames below the floor absorbed much of the impact energy, thereby limiting the g forces and extending the impact pulse duration transmitted to the occupants through the floor tracks and seats.

- The cabin sidewalls experienced approximately 19 g's deceleration with a pulse duration of approximately 83 msec.

- The cabin floor tracks experienced approximately 26 g's maximum deceleration with a pulse duration of approximately 68 msec.

- The cockpit floor experienced approximately 38 g's maximum deceleration with a pulse duration of approximately 51 msec.

- The cockpit seats did not sustain any structural damage. Spinal loads in the ATD lumbar region were approximately 2500 pounds (1136 kg) (1500 lb (681 kg) certification limit).

- All the standard ATR 42-300 cabin seats that were occupied fractured.

- The modified in-service, 16-g-rated seat occupied by an ATD and a mannequin sustained minimal damage. The maximum measured lumbar load of the ATD was 738 lb (335 kg).

- After the left engine impacted the concrete drop test platform, a leak developed in the leading edge of the left wing near the engine. The right engine also impacted the concrete drop test platform; however, the right wing fuel tank was not ruptured.

- The service door on the right rear side of the airplane and the cockpit emergency ceiling exit were usable. The passenger and cargo doors as well as the two emergency window exits were unusable.

- The peak acceleration of the left bin was 12.7 g's. This resulted in a maximum inertial loading of 699 lb (317.1 kg).

11. REFERENCES.

1. McGuire, R., Vu, T., and Newcomb, J., "Vertical Drop Test of a Metro III Airplane," FAA report DOT/FAA/CT-93/1, June 1993.

2. McGuire, R. and Nissley, W., "Vertical Drop Test of a Beechcraft 1900C Airliner," FAA report DOT/FAA/AR-96/119, May 1998.

3. Abramowitz, A., Ingraham, P., and McGuire, R., "Vertical Drop Test of a Shorts 3-30 Airplane," FAA report DOT/FAA/AR-99/87, November 1999.

4. Jackson, Karen E. and Fasanella, Edwin L., "Test-Analysis Correlation of a Crash Simulation of a Vertical Drop Test of a Commuter-Category Aircraft," *Fourth Triennial International Aircraft Fire and Cabin Safety Conference*, Lisbon, Portugal, November 15-18, 2004.

5. SAE International, "Surface Vehicle Recommended Practice," SAE J211/1, Revised March 1995.

6. Jackson, Karen E. and Fasanella, Edwin L., "Crash Simulation of Vertical Drop Tests of Two Boeing 737 Fuselage Sections," FAA report DOT/FAA/AR-02/62, August 2002.

APPENDIX A—WING FITTING CALIBRATION DATA

A.1 WING FITTINGS AND FIXTURES.

FIGURE A-1. FIXTURE FOR THE INSIDE WING FITTING

FIGURE A-2. FIXTURE FOR THE OUTSIDE WING FITTING

A.2 WING FITTINGS—LOAD CALIBRATION CURVES.

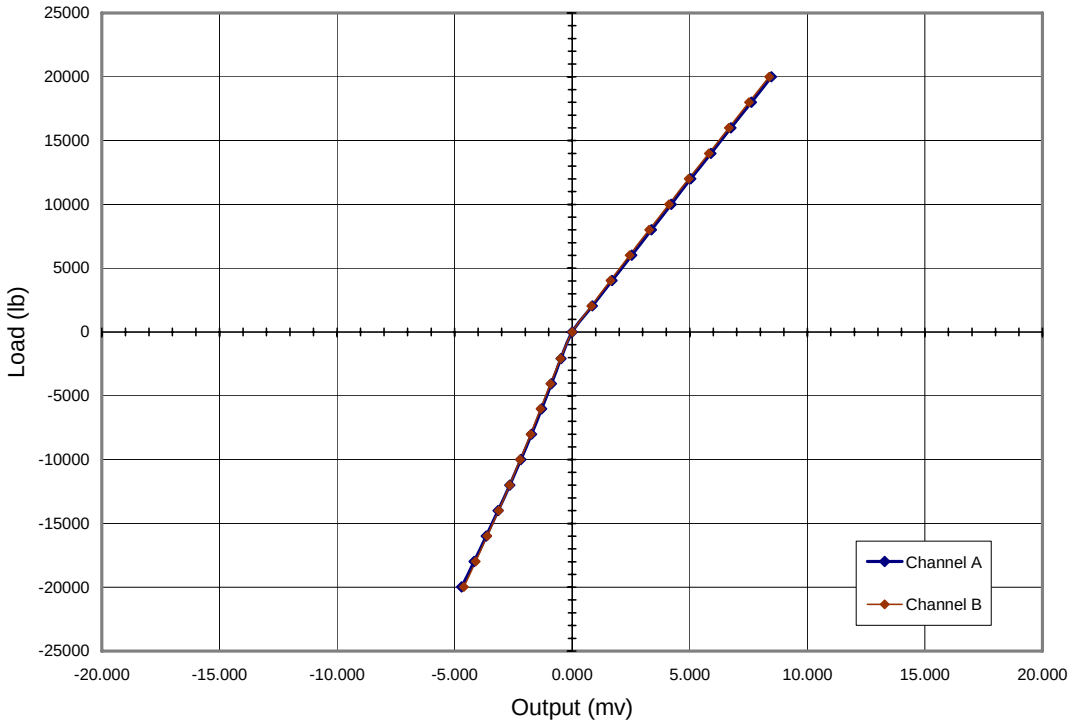

FIGURE A-3. INSIDE WING FITTING, RIGHT FRONT

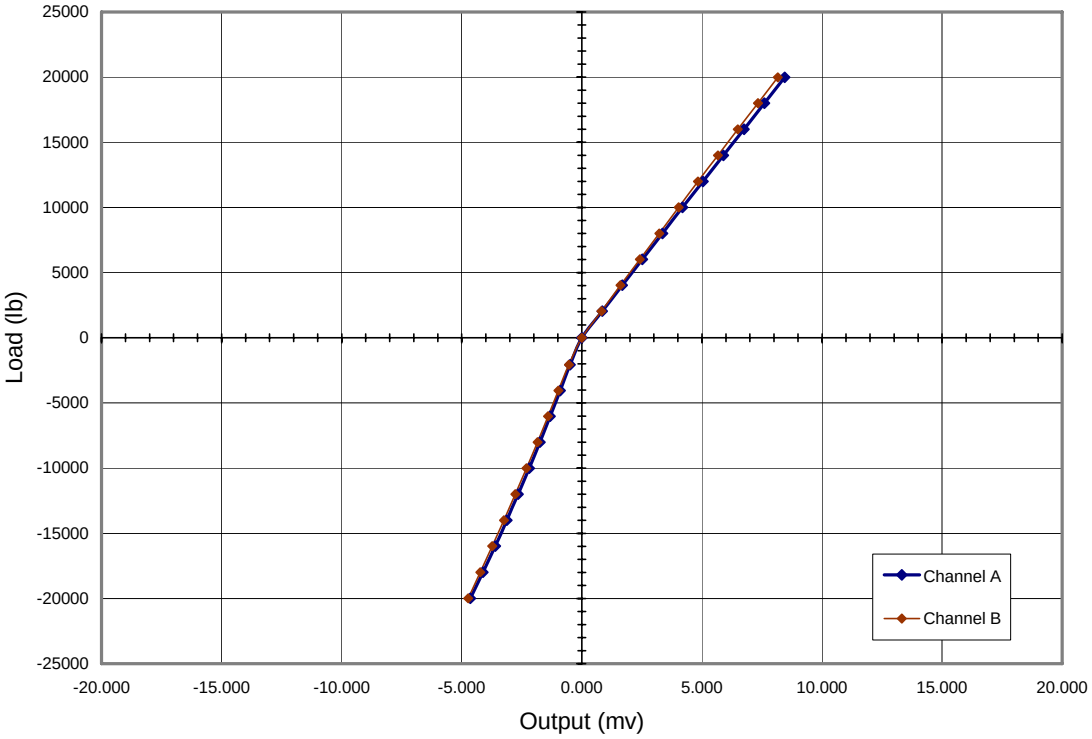

FIGURE A-4. INSIDE WING FITTING, LEFT FRONT

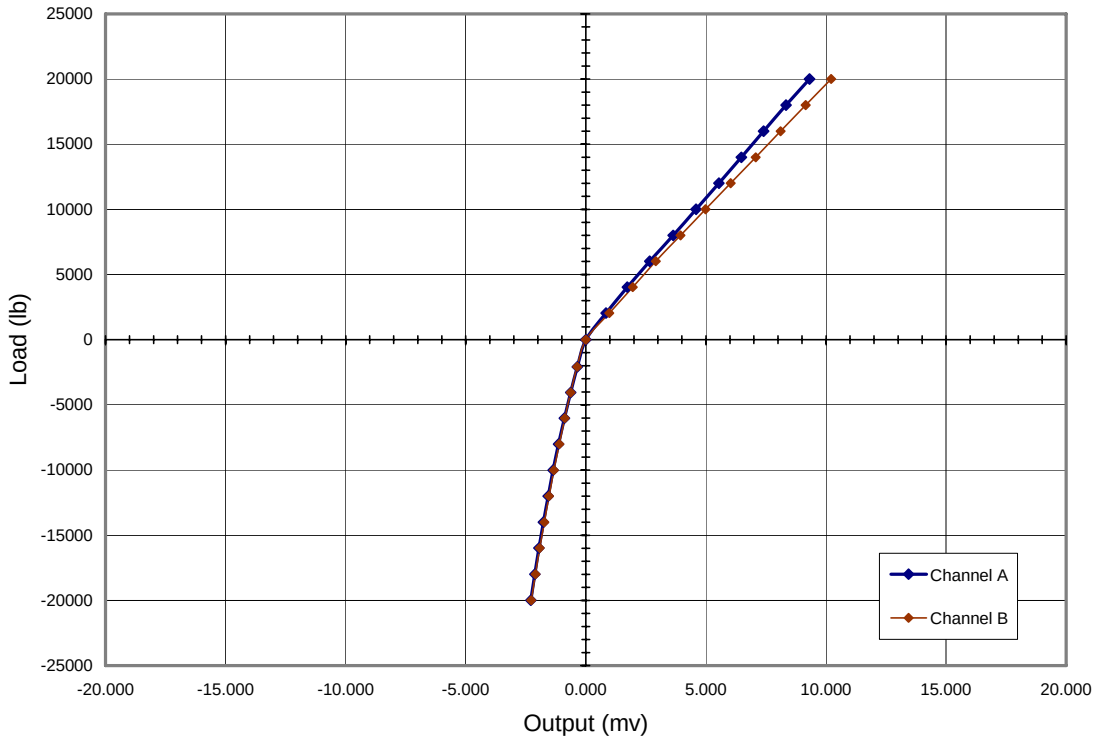

FIGURE A-5. INSIDE WING FITTING, RIGHT REAR

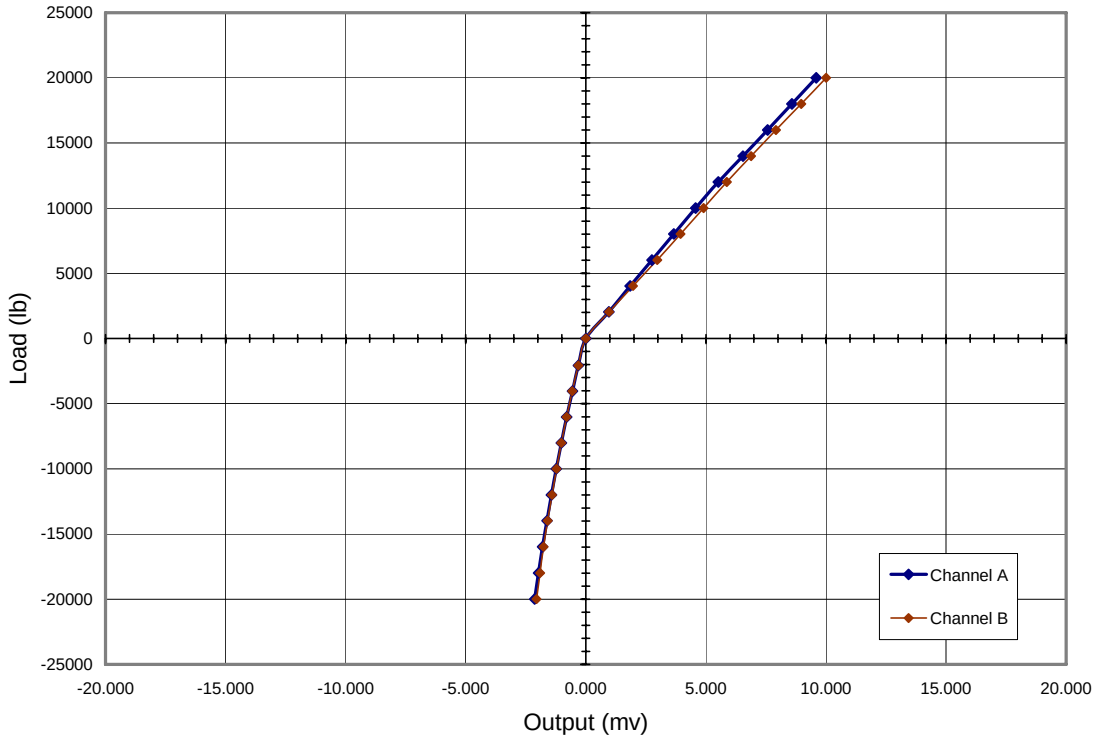

FIGURE A-6. INSIDE WING FITTING, LEFT REAR

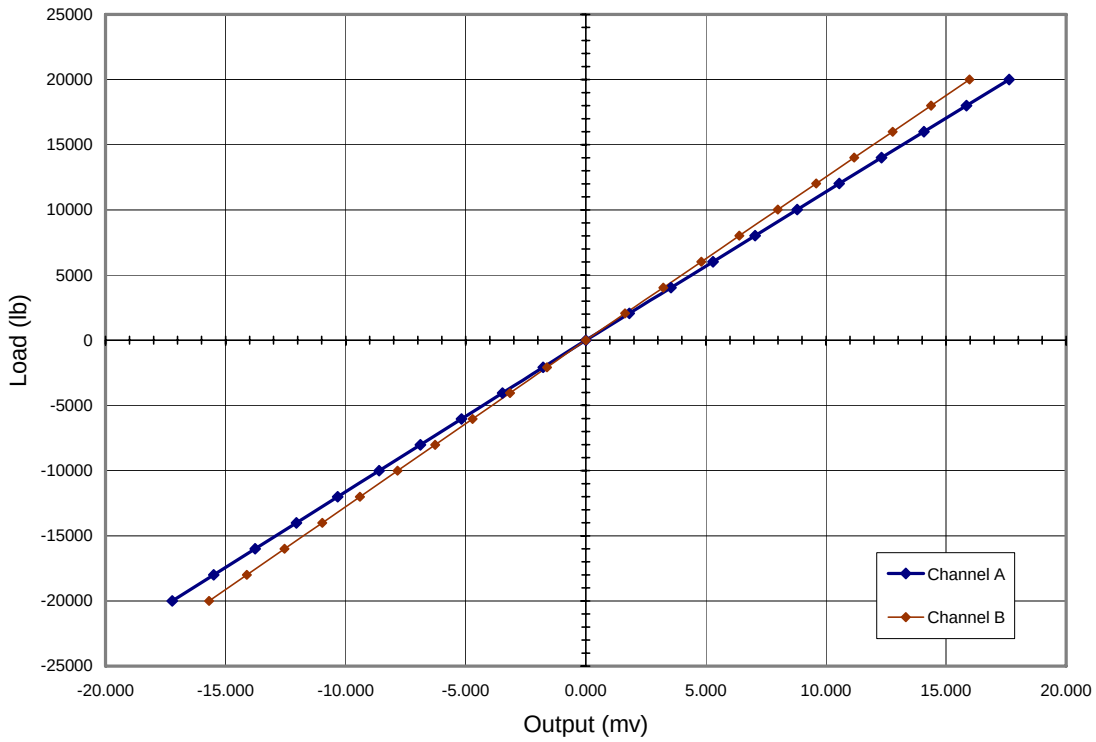

FIGURE A-7. OUTSIDE WING FITTING, RIGHT FRONT

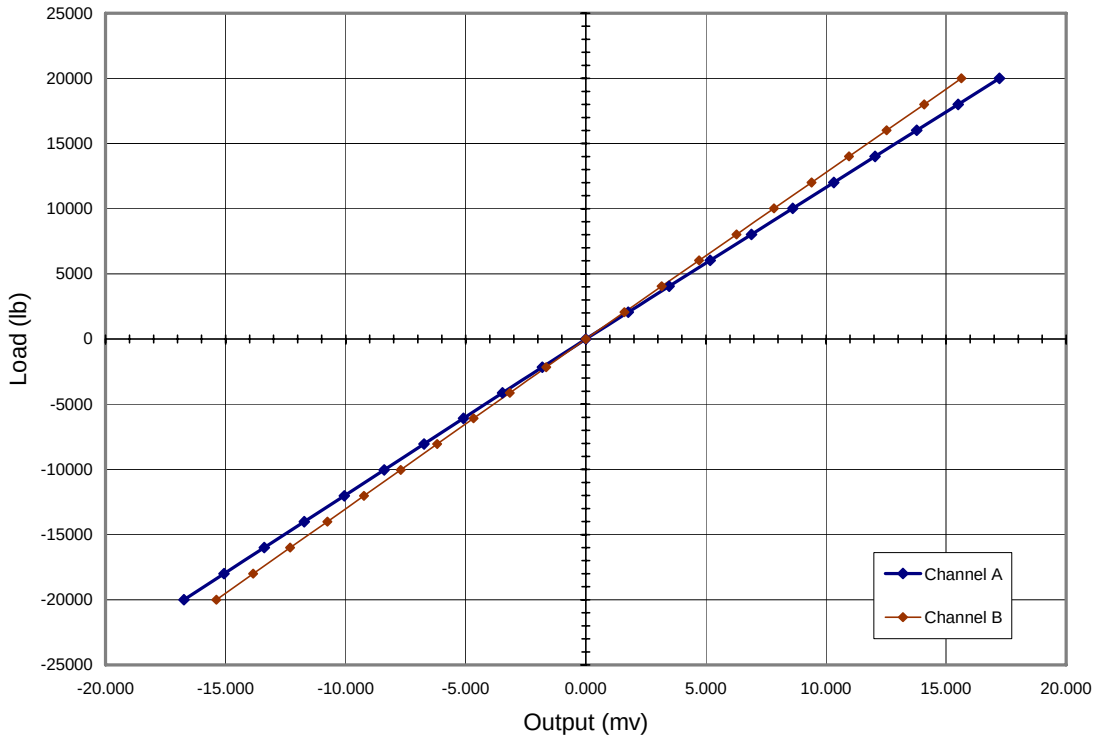

FIGURE A-8. OUTSIDE WING FITTING, LEFT FRONT

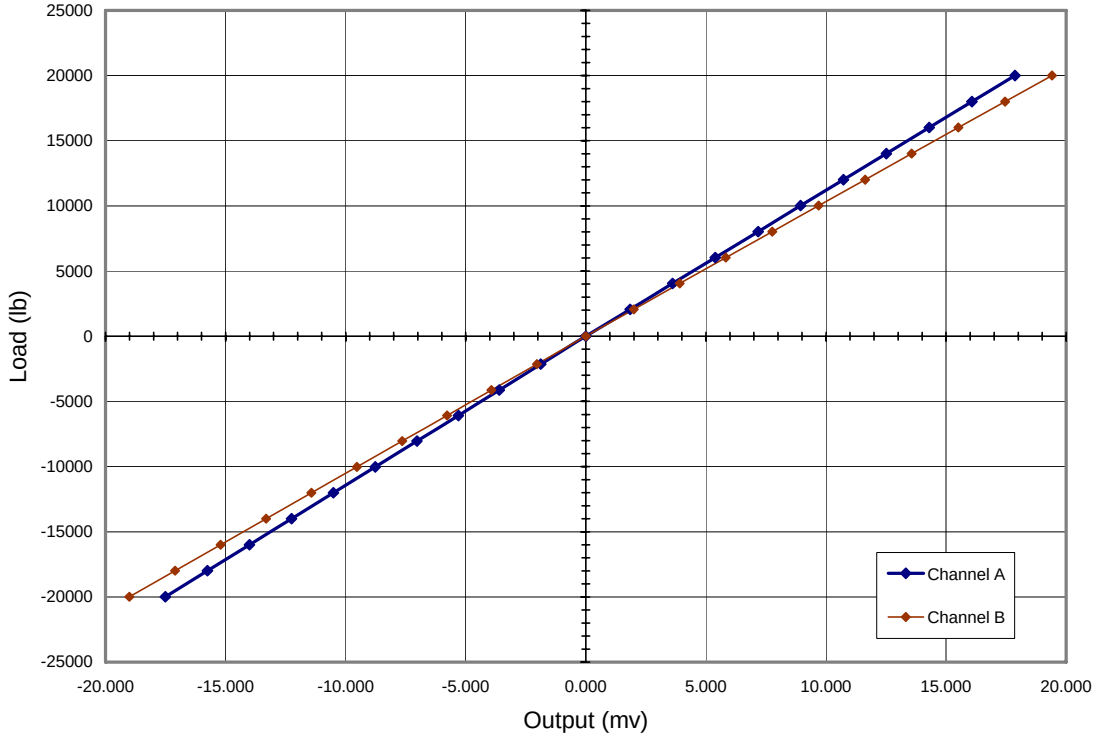

FIGURE A-9. OUTSIDE WING FITTING, RIGHT REAR

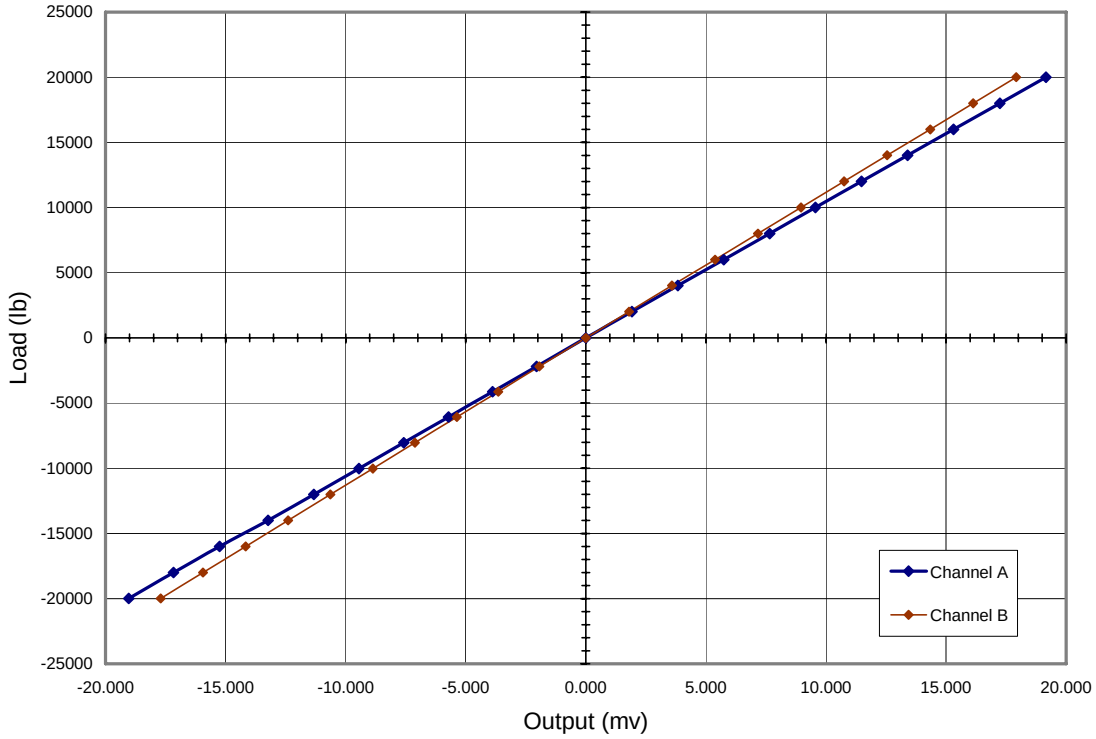

FIGURE A-10. OUTSIDE WING FITTING, LEFT REAR

TABLE A-1. OUTSIDE WING FITTING SENSITIVITY COEFFICIENTS

Support	Sensitivity Coefficient z direction y = mx +b Tension and Compression		Nonlinearity Typical	Hysteresis Typical
	m (lb/mv)	b (lb)	% FS	% FS
Outside fitting right front A	1148.55	0.0	<1	<1
Outside fitting right front B	1263.95	0.0	<1	<1
Outside fitting left front A	1178.35	0.0	<1	<1
Outside fitting left front B	1289.05	0.0	<1	<1
Outside fitting right rear A	1131.15	0.0	<1	<1
Outside fitting right rear B	1041.90	0.0	<1	<1
Outside fitting left rear A	1051.90	0.0	<1	<1
Outside fitting left rear B	1123.15	0.0	<1	<1

TABLE A-2. INSIDE WING FITTING SENSITIVITY COEFFICIENTS

Support	Sensitivity Coefficient z direction y = mx +b Tension		Nonlinearity Typical	Hysteresis Typical
	m (lb/mv)	b (lb)	% FS	% FS
Inside fitting right front A	4386.5	0.0	<1	<1
Inside fitting right front B	4414.4	0.0	<1	<1
Inside fitting left front A	4439.6	0.0	<1	<1
Inside fitting left front B	4277.0	0.0	<1	<1
Inside fitting right rear A	8077.0	0.0	<1	<2
Inside fitting right rear B	8213.0	0.0	<1	<2
Inside fitting left rear A	8763.2	0.0	<2	<2
Inside fitting left rear B	8959.5	0.0	<1	<2
Support	Sensitivity Coefficient z direction $y = C1(x^2) + C2(x)$ Compression		Nonlinearity Typical	Hysteresis Typical
	C1 (lb/mv)	C2 (lb/mv)	% FS	% FS
Inside fitting right front A	1.214	4829.9	<1	<1
Inside fitting right front B	0.605	4631.5	<1	<1
Inside fitting left front A	1.006	4801.3	<1	<1
Inside fitting left front B	0.393	4422.4	<1	<1
Inside fitting right rear A	-14.434	5432.2	<4	<4
Inside fitting right rear B	-13.692	5736.8	<4	<4
Inside fitting left rear A	-13.729	6420.5	<4	<4
Inside fitting left rear B	-18.412	5921.9	<5	<4

APPENDIX B—TEST DATA

B.1 FUSELAGE DATA—SIDEWALL ACCELERATIONS.

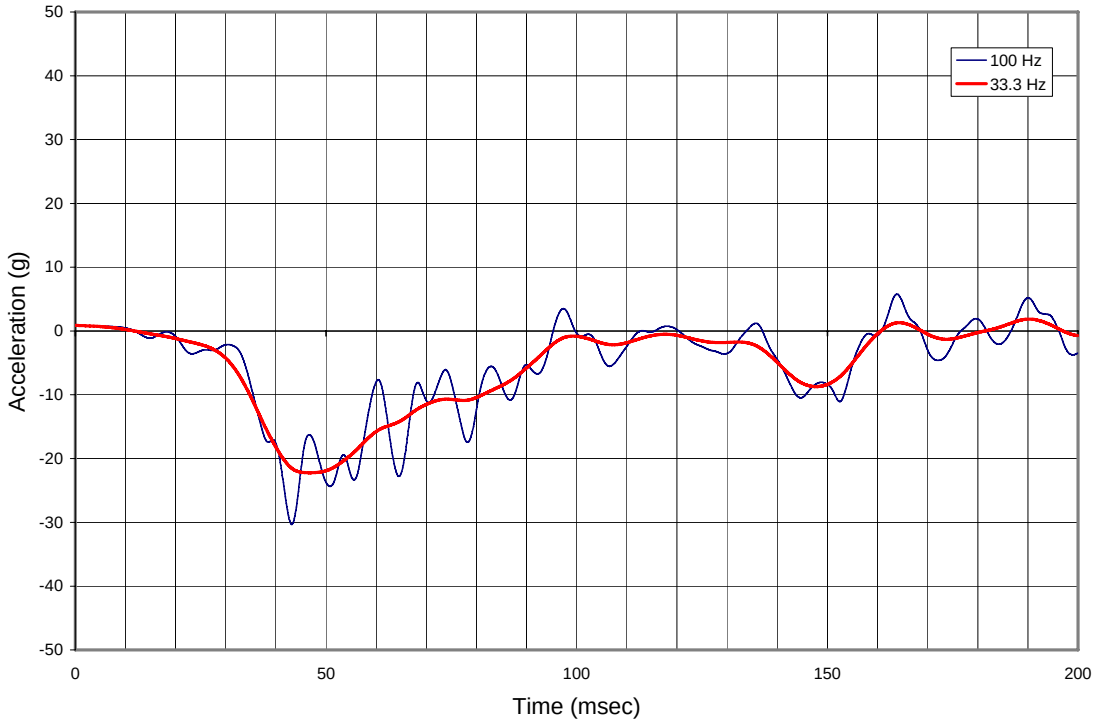

FIGURE B-1. FRAME 18, LEFT LOWER SIDEWALL ACCELERATION

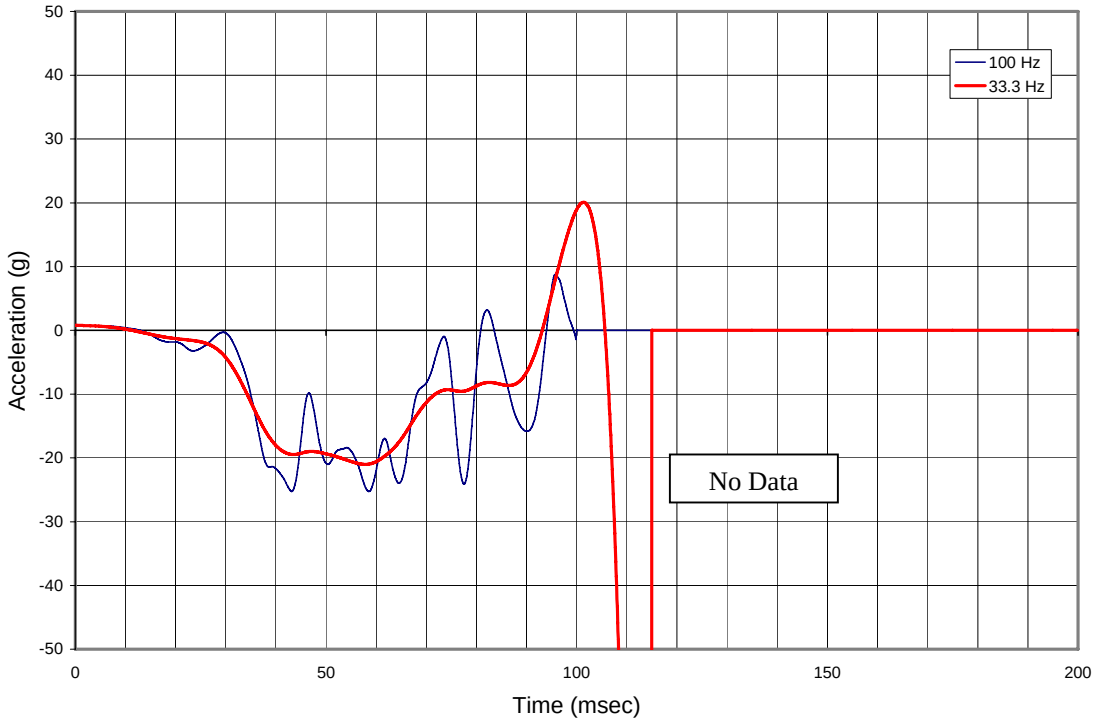

FIGURE B-2. FRAME 18, RIGHT LOWER SIDEWALL ACCELERATION

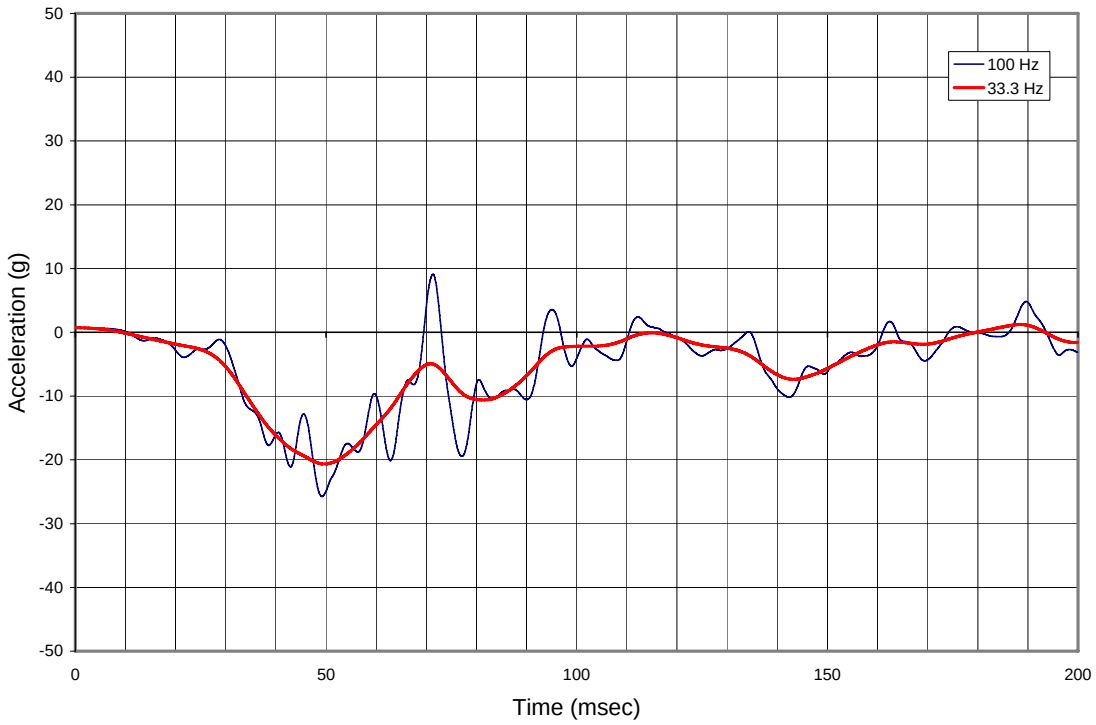

FIGURE B-3. FRAME 20, LEFT LOWER SIDEWALL ACCELERATION

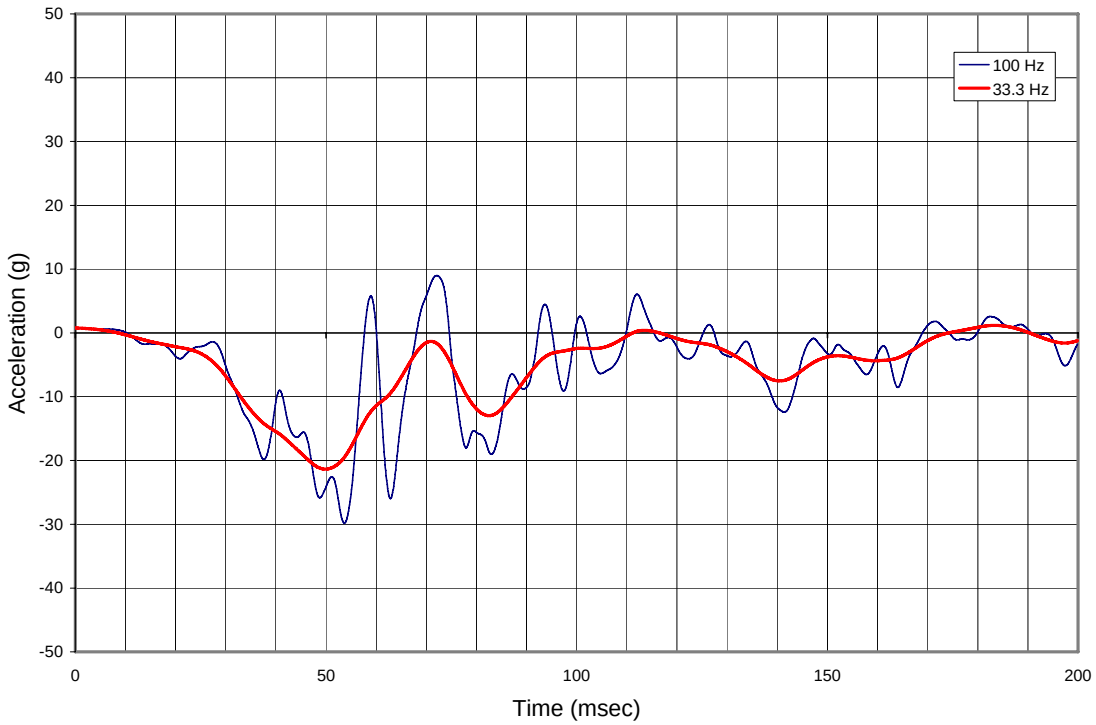

FIGURE B-4. FRAME 22, LEFT LOWER SIDEWALL ACCELERATION

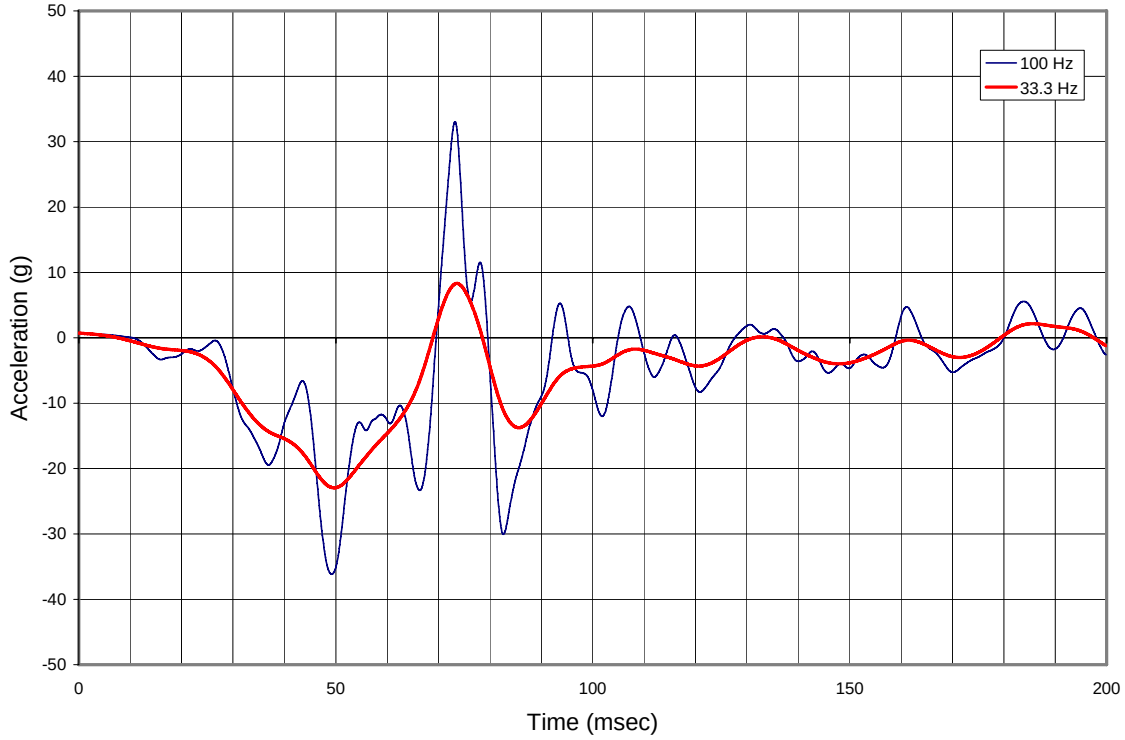

FIGURE B-5. FRAME 22, RIGHT LOWER SIDEWALL ACCELERATION

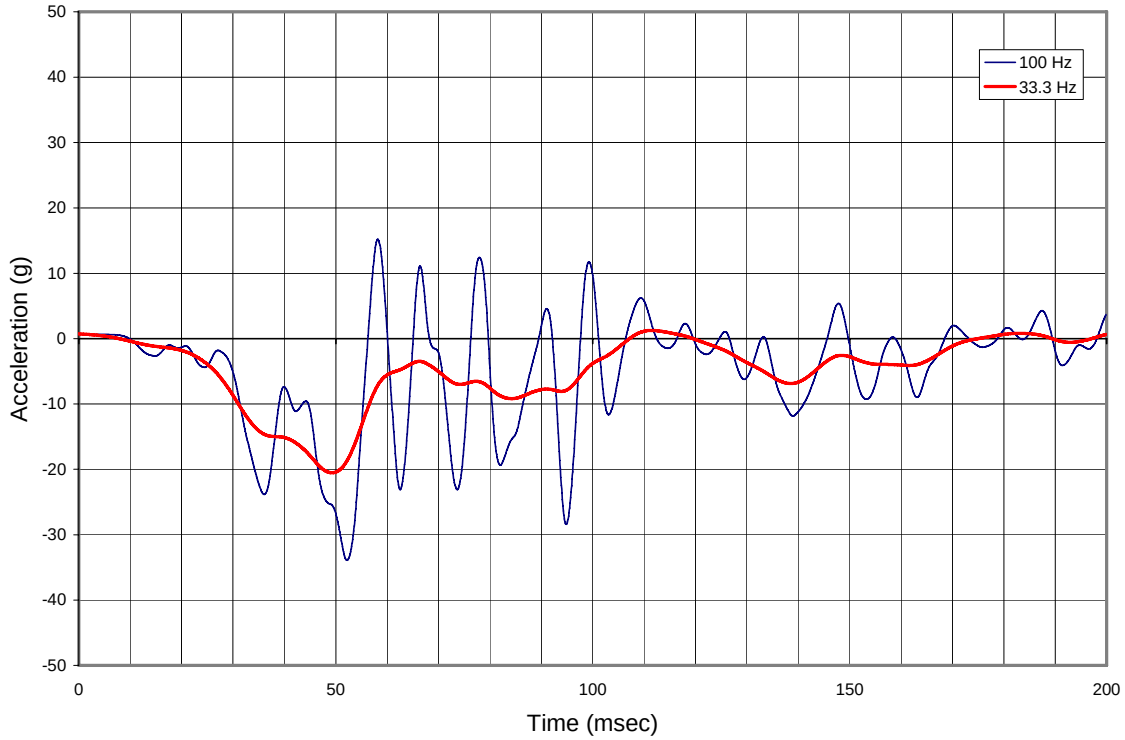

FIGURE B-6. FRAME 24, LEFT LOWER SIDEWALL ACCELERATION

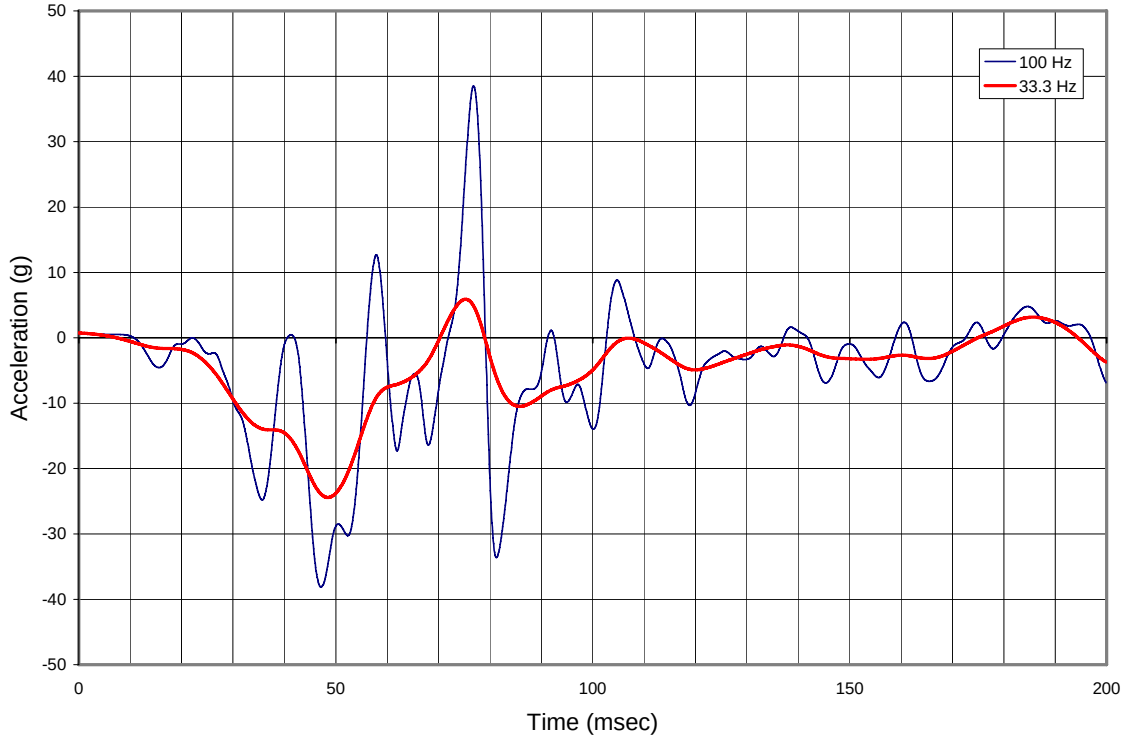

FIGURE B-7. FRAME 24, RIGHT LOWER SIDEWALL ACCELERATION

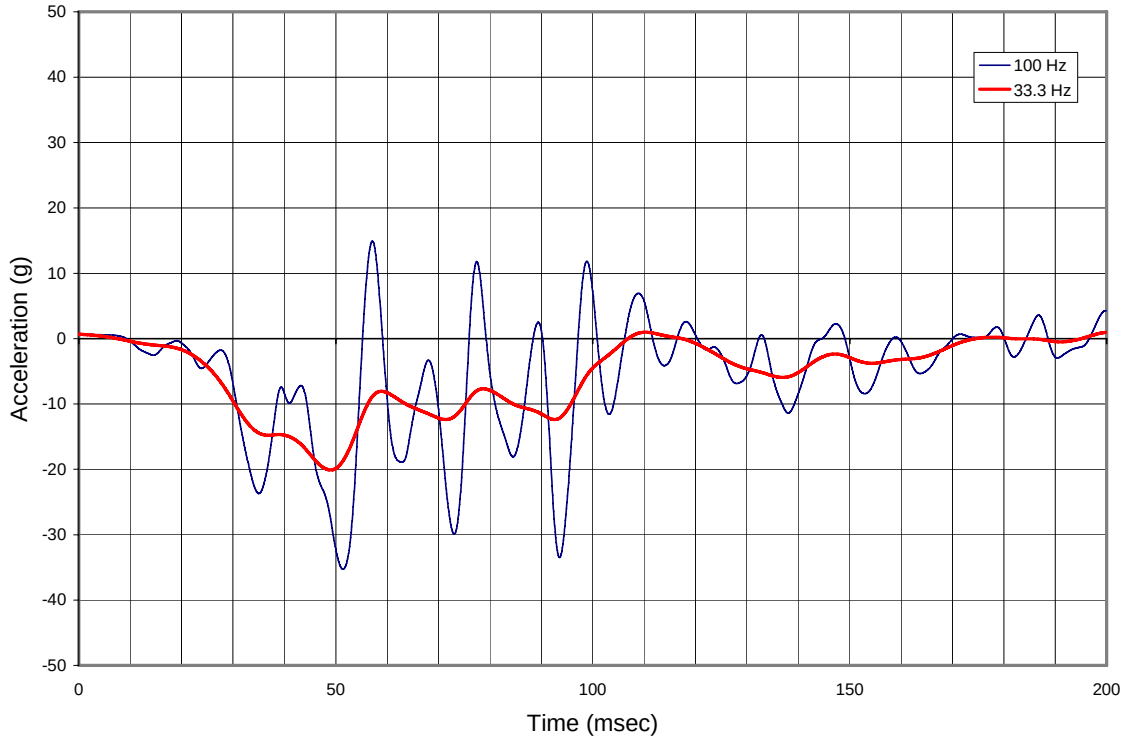

FIGURE B-8. FRAME 25, LEFT LOWER SIDEWALL ACCELERATION

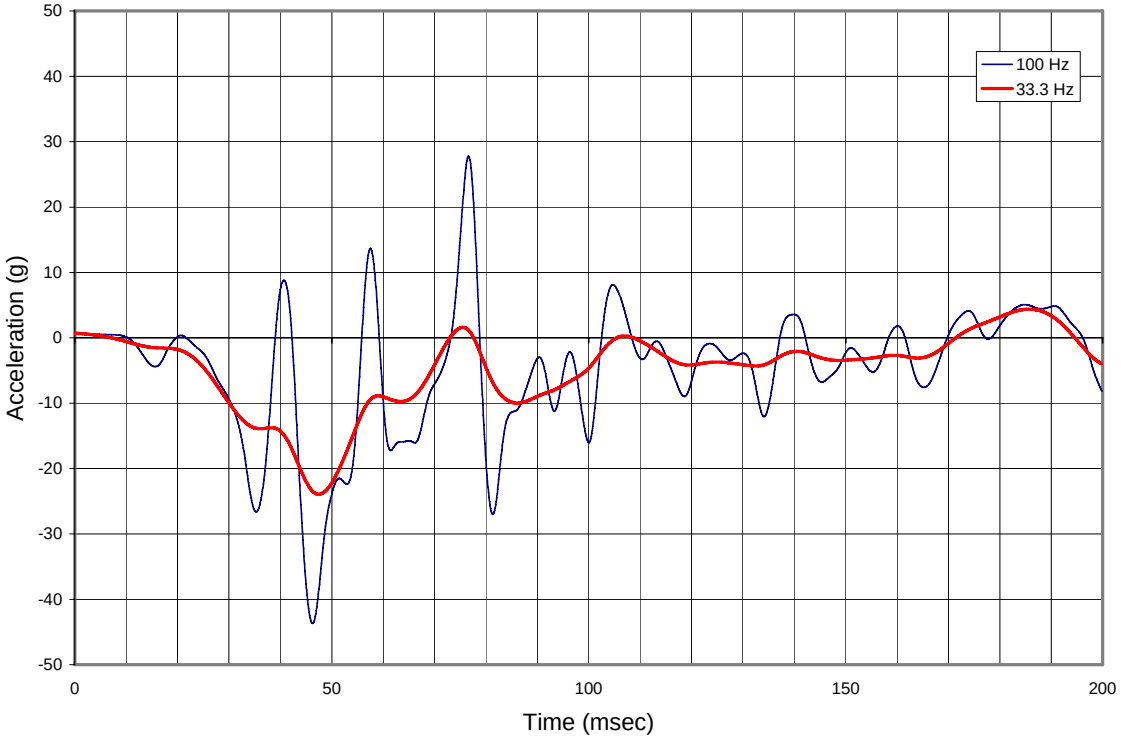

FIGURE B-9. FRAME 25, RIGHT LOWER SIDEWALL ACCELERATION

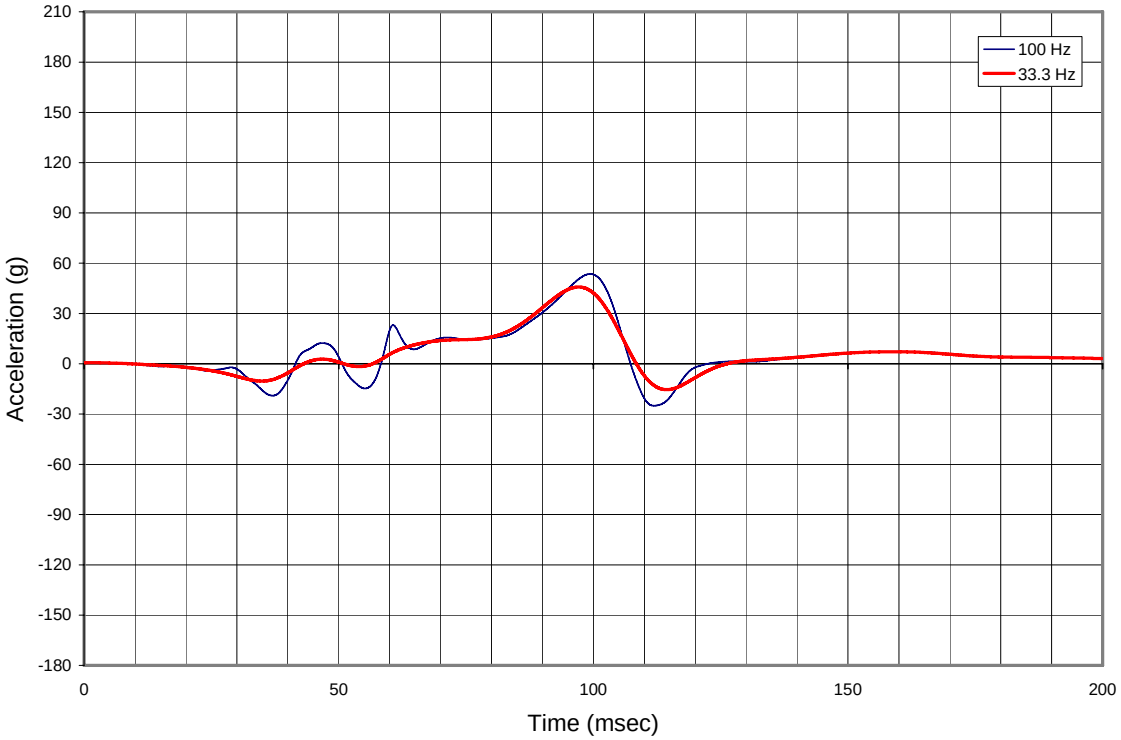

FIGURE B-10. FRAME 25, LEFT MIDDLE SIDEWALL ACCELERATION

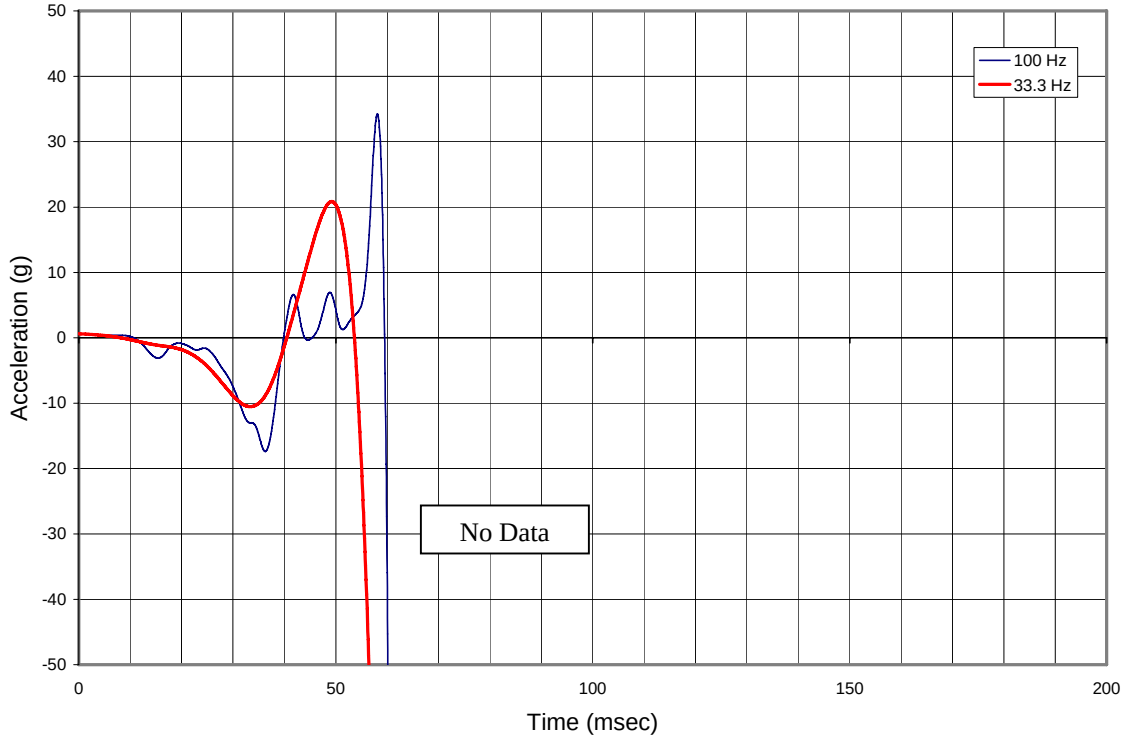

FIGURE B-11. FRAME 25, RIGHT MIDDLE SIDEWALL ACCELERATION

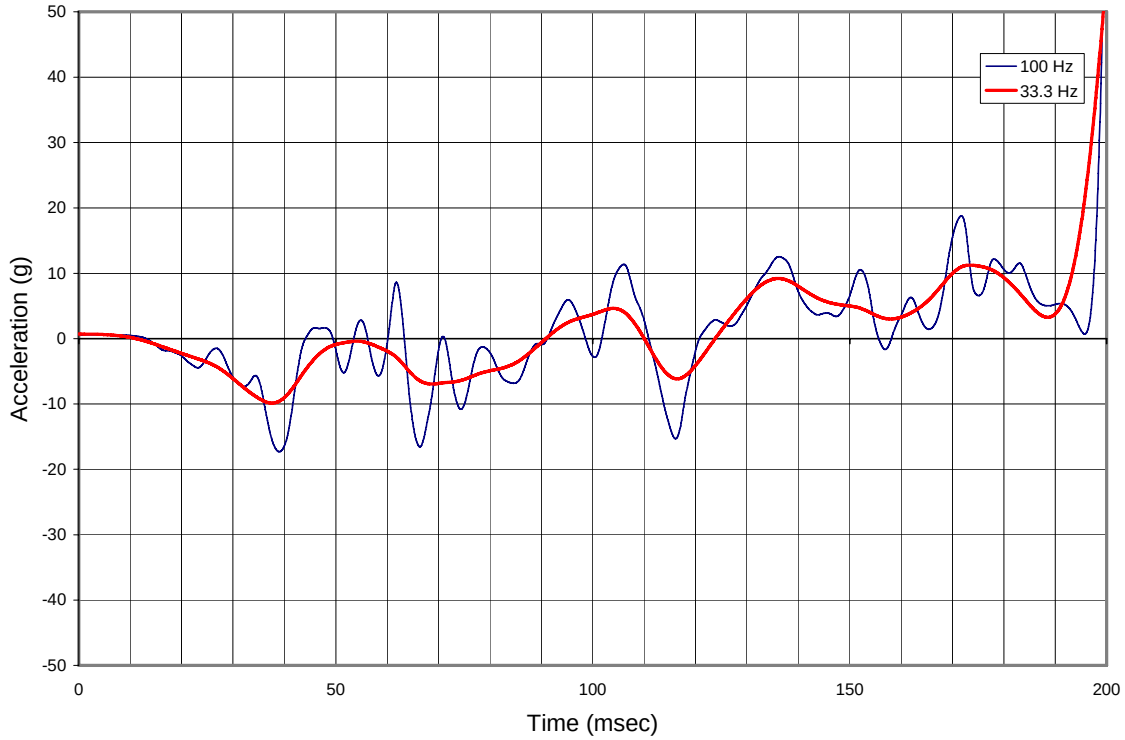

FIGURE B-12. FRAME 25, RIGHT UPPER SIDEWALL ACCELERATION

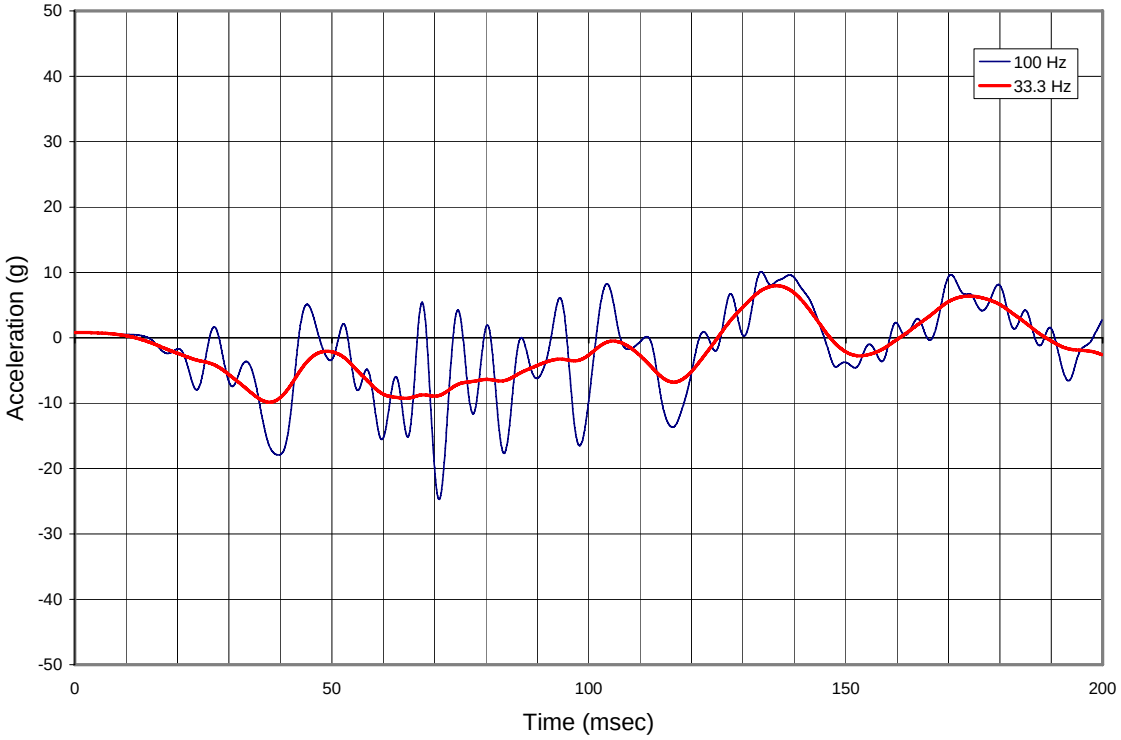

FIGURE B-13. FRAME 26, CENTER CEILING ACCELERATION

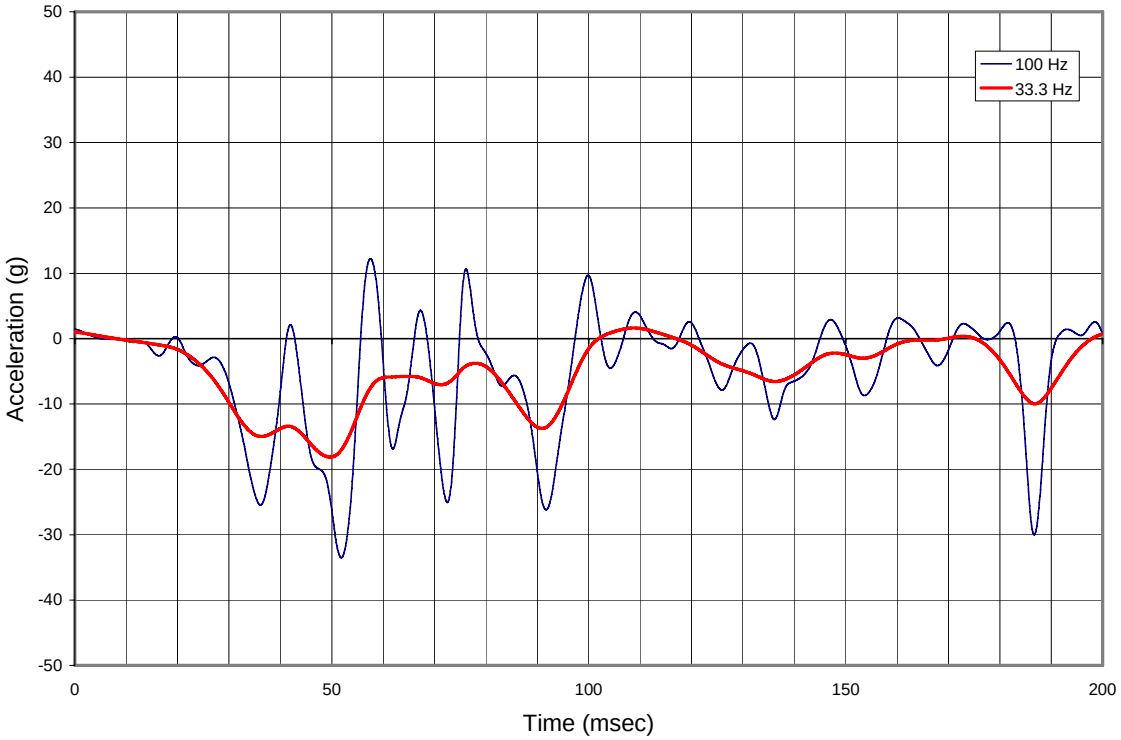

FIGURE B-14. FRAME 27, LEFT LOWER SIDEWALL ACCELERATION

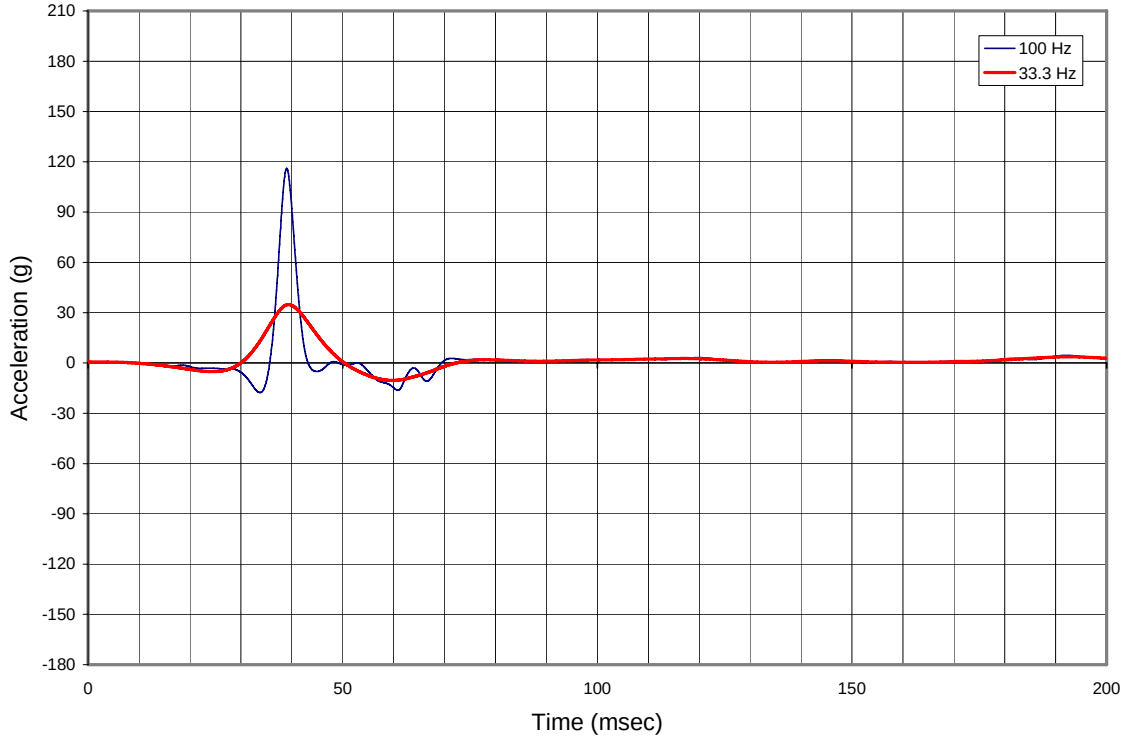

FIGURE B-15. FRAME 27, LEFT MIDDLE SIDEWALL ACCELERATION

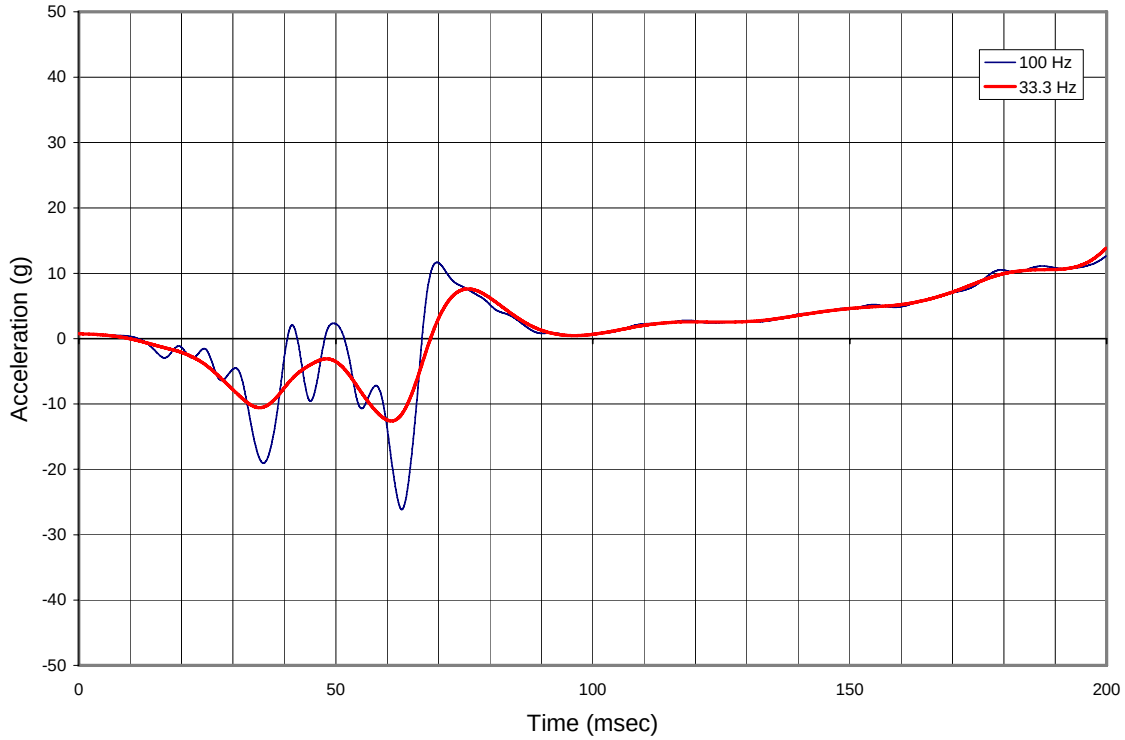

FIGURE B-16. FRAME 27, RIGHT MIDDLE SIDEWALL ACCELERATION

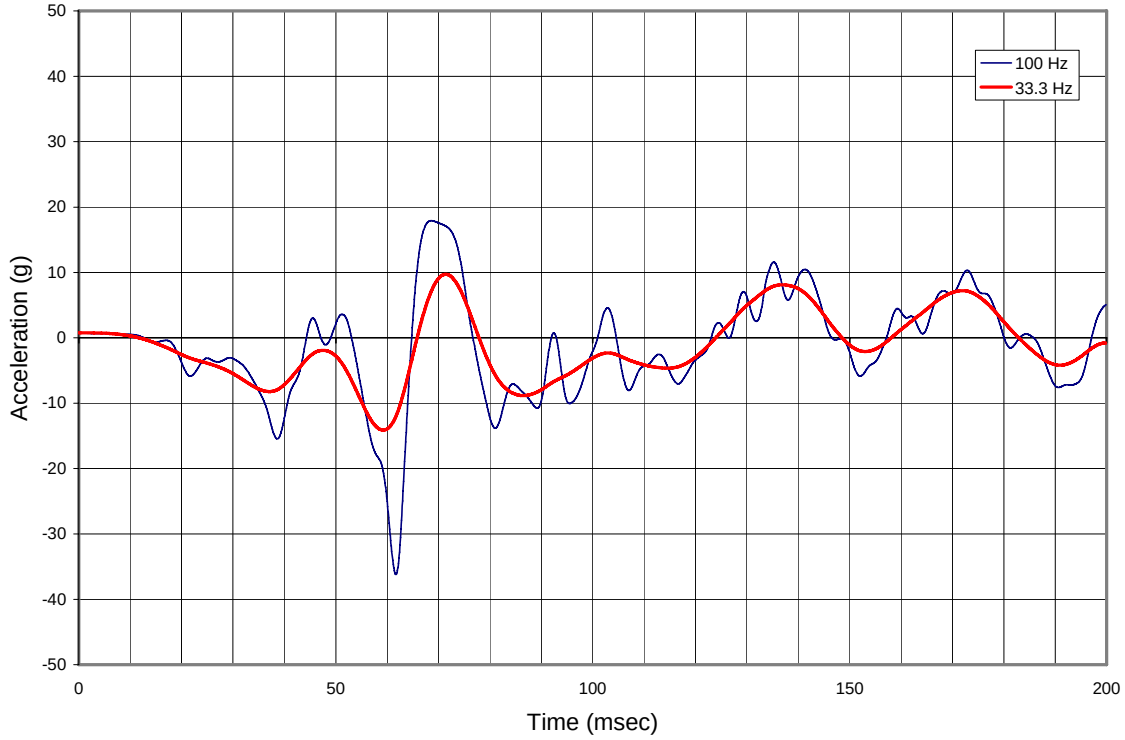

FIGURE B-17. FRAME 27, LEFT UPPER SIDEWALL ACCELERATION

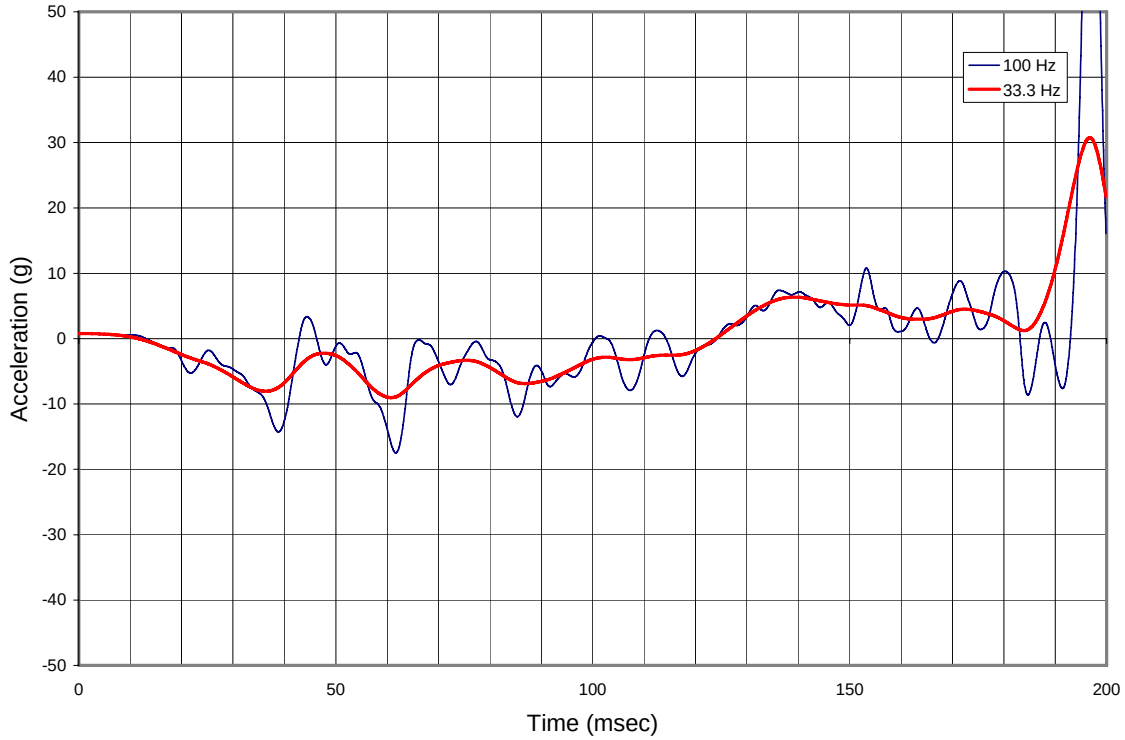

FIGURE B-18. FRAME 27, RIGHT UPPER SIDEWALL ACCELERATION

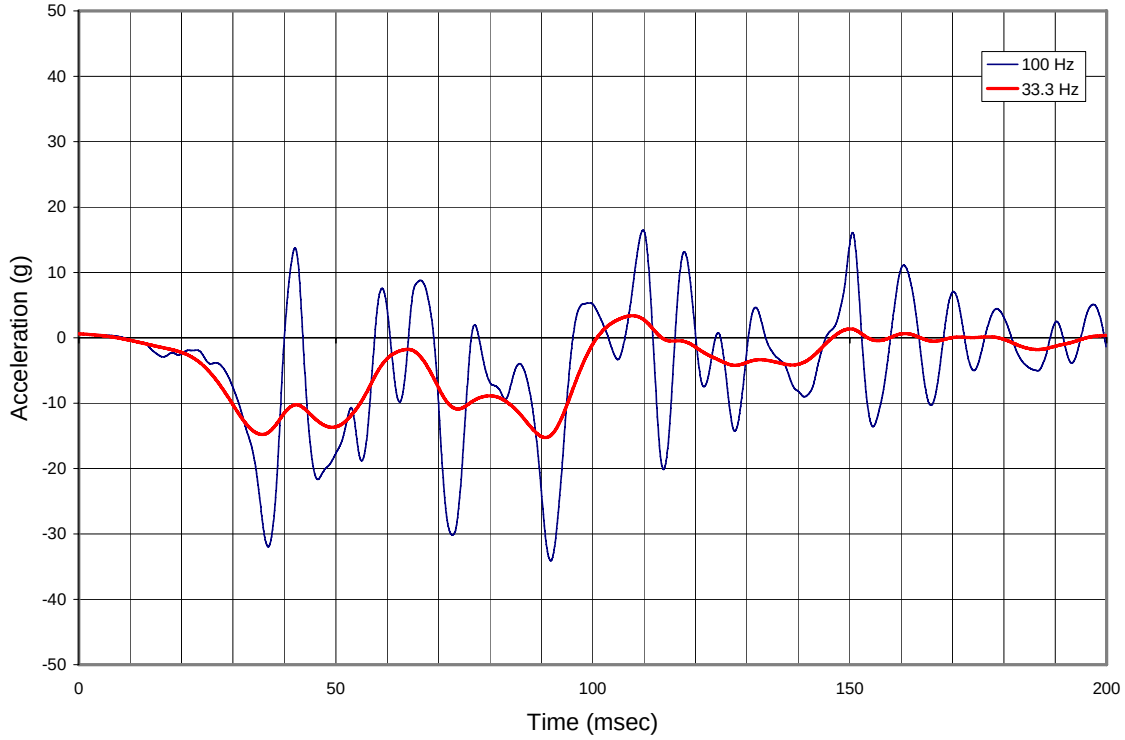

FIGURE B-19. FRAME 28, LEFT LOWER SIDEWALL ACCELERATION

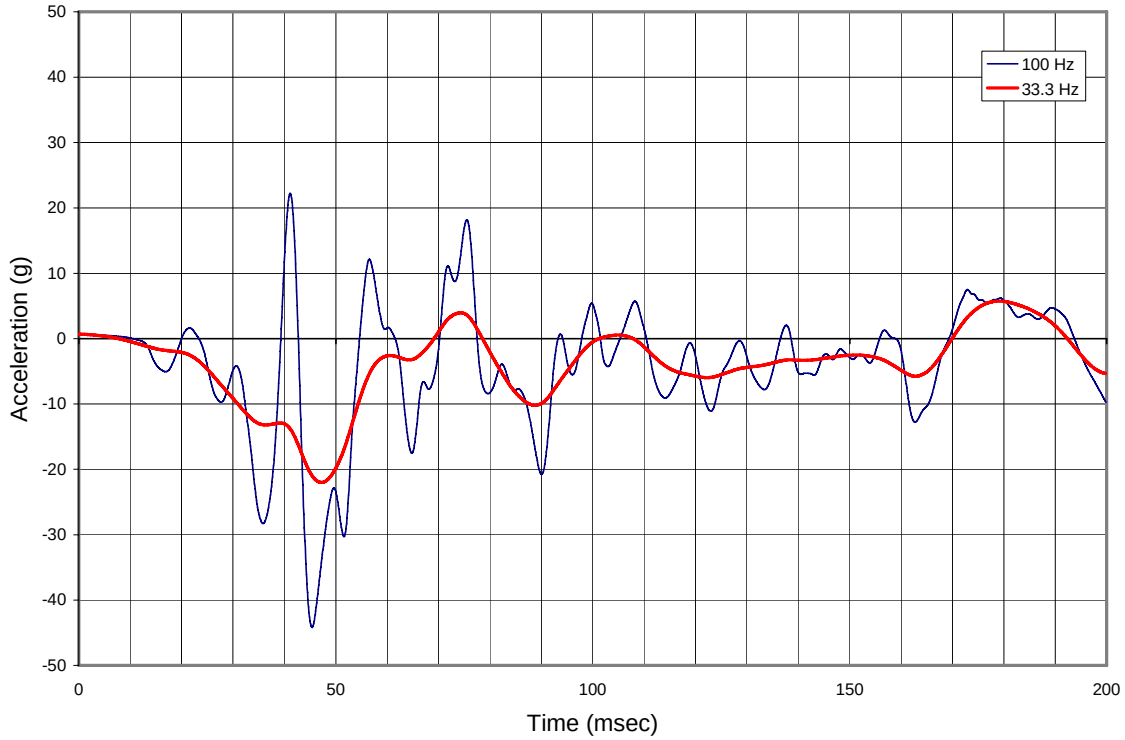

FIGURE B-20. FRAME 28, RIGHT LOWER SIDEWALL ACCELERATION

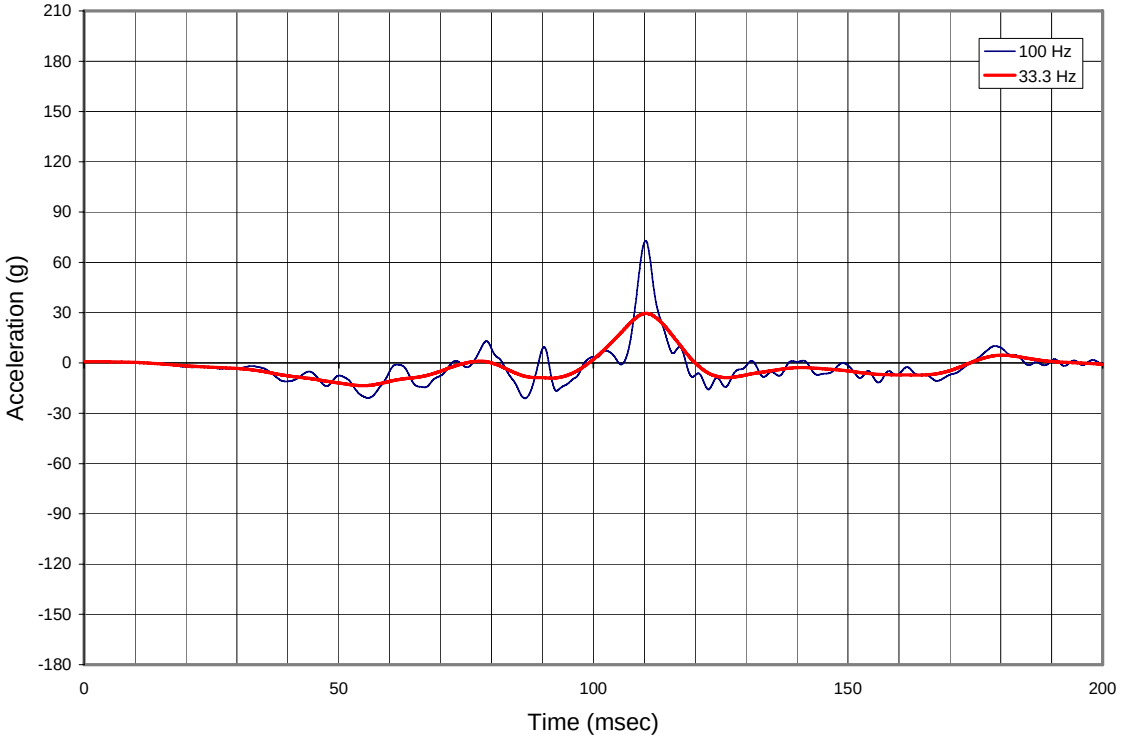

FIGURE B-21. FRAME 37, RIGHT LOWER SIDEWALL ACCELERATION

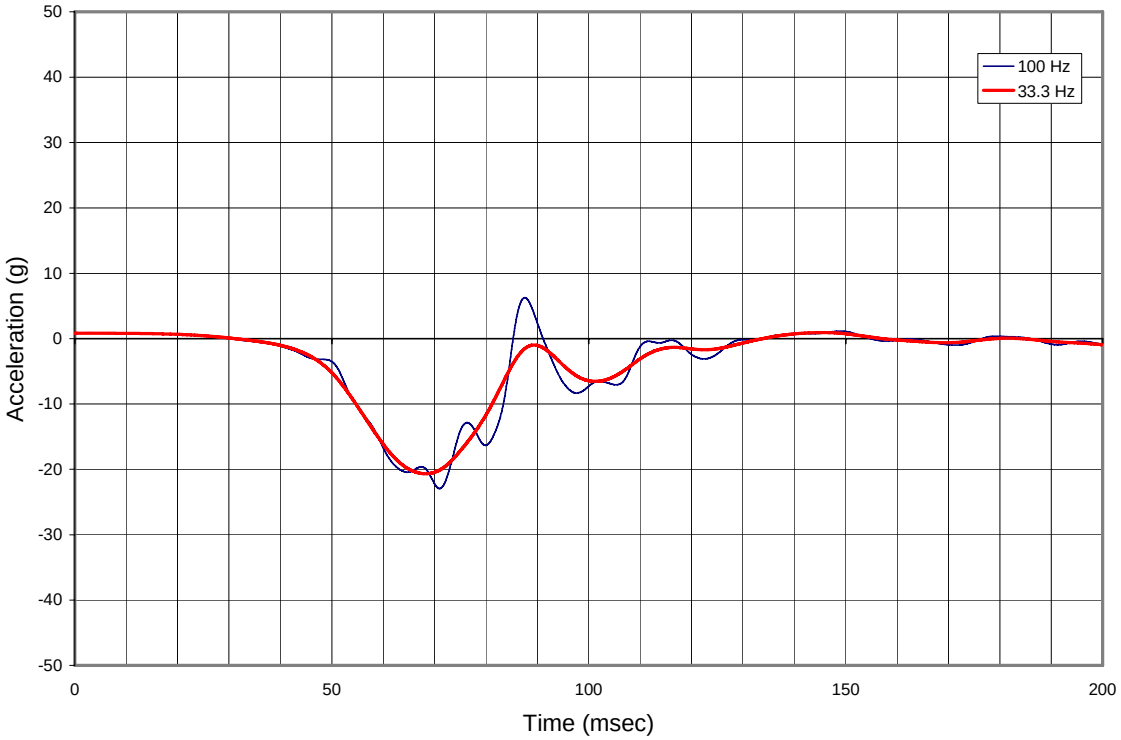

FIGURE B-22. FRAME 45, REAR CENTER ACCELERATION

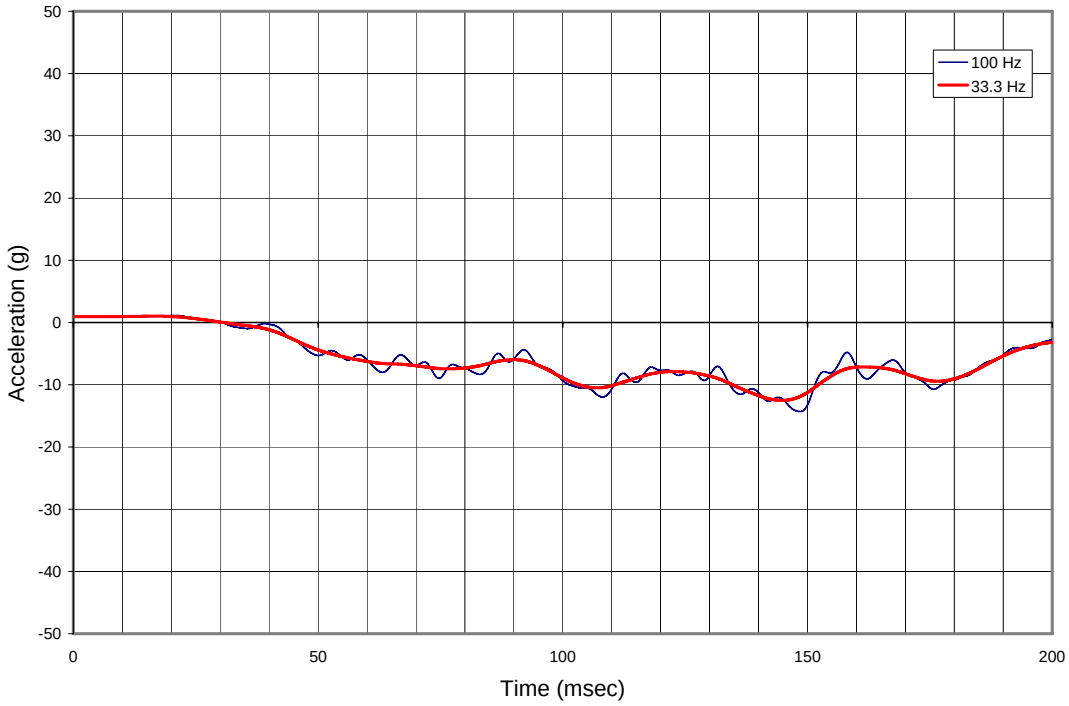

FIGURE B-23. FRAME 47, REAR CENTER ACCELERATION

B.2 FUSELAGE DATA—FLOOR ACCELERATIONS; FLOOR TRACK ACCELERATIONS.

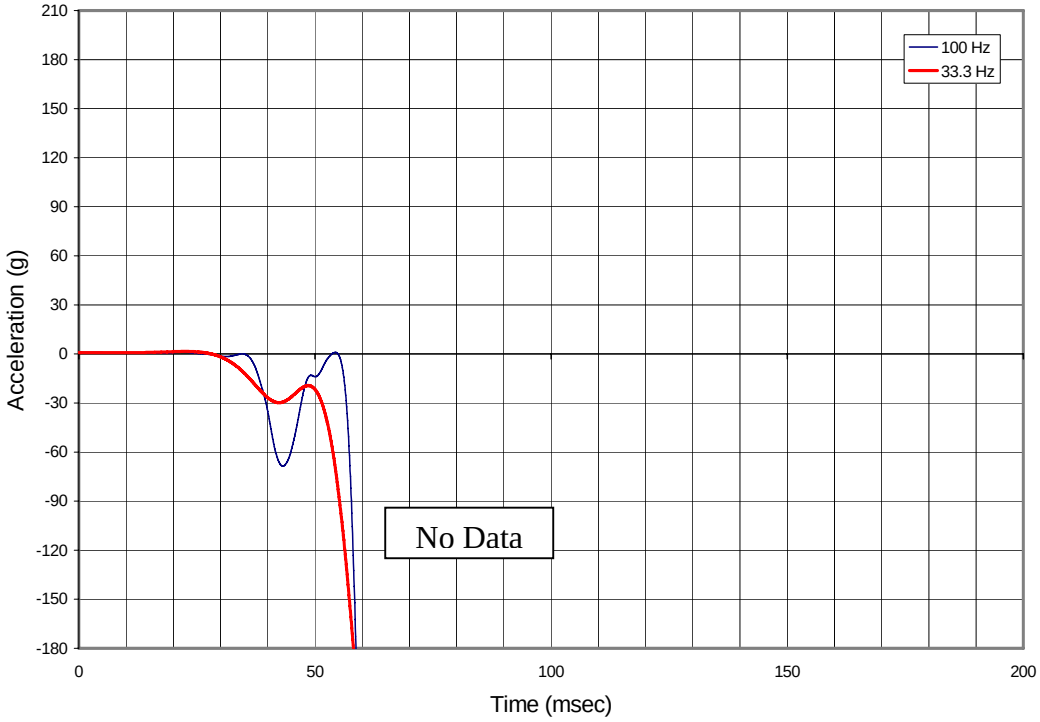

FIGURE B-24. FRAME 7, LEFT SIDE COCKPIT FLOOR ACCELERATION

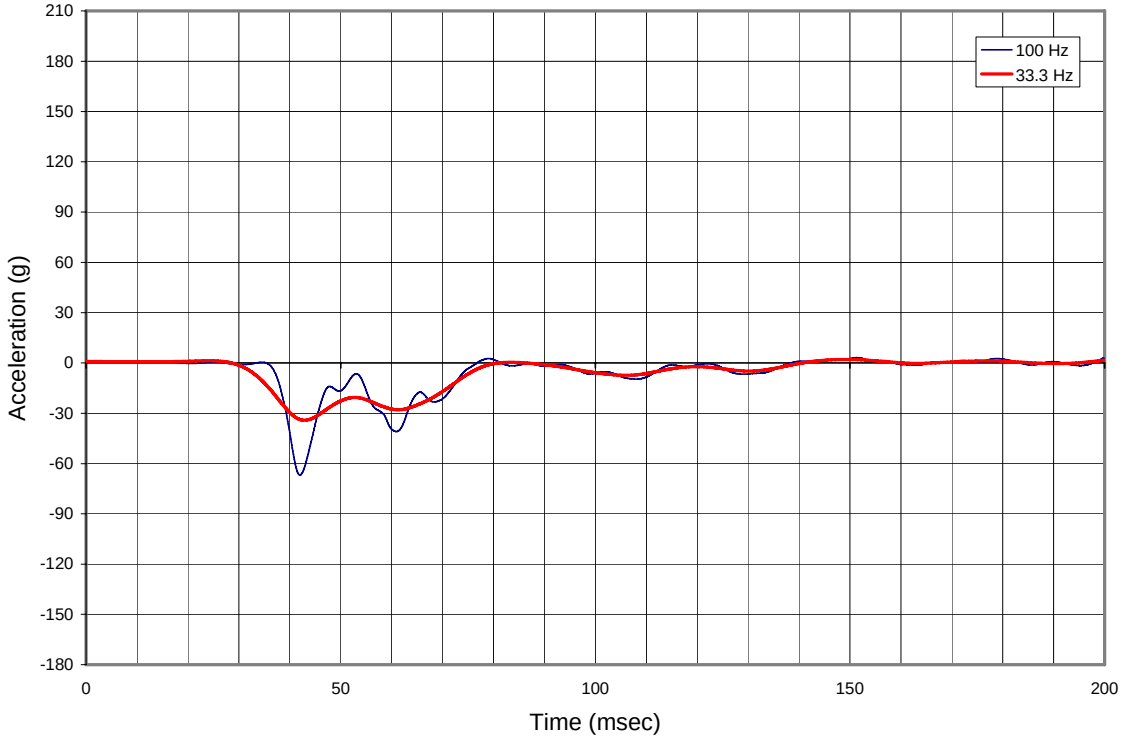

FIGURE B-25. FRAME 7, RIGHT SIDE COCKPIT FLOOR ACCELERATION

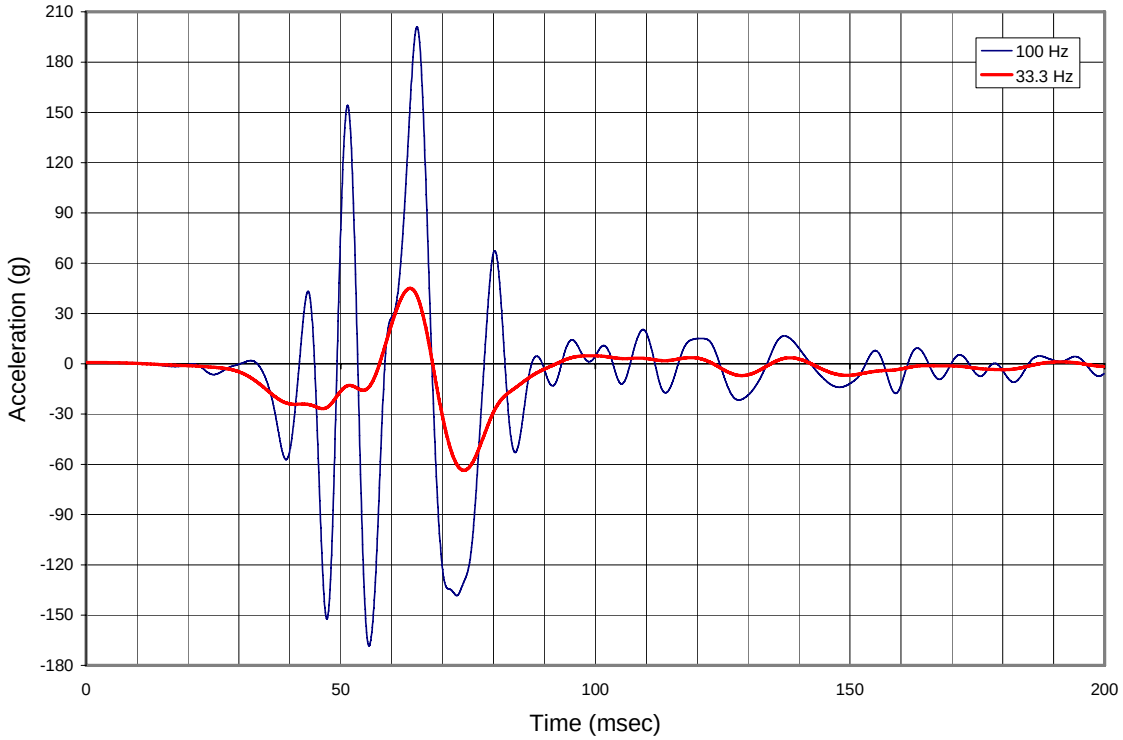

FIGURE B-26. FRAME 18, LEFT INNER FLOOR TRACK ACCELERATION

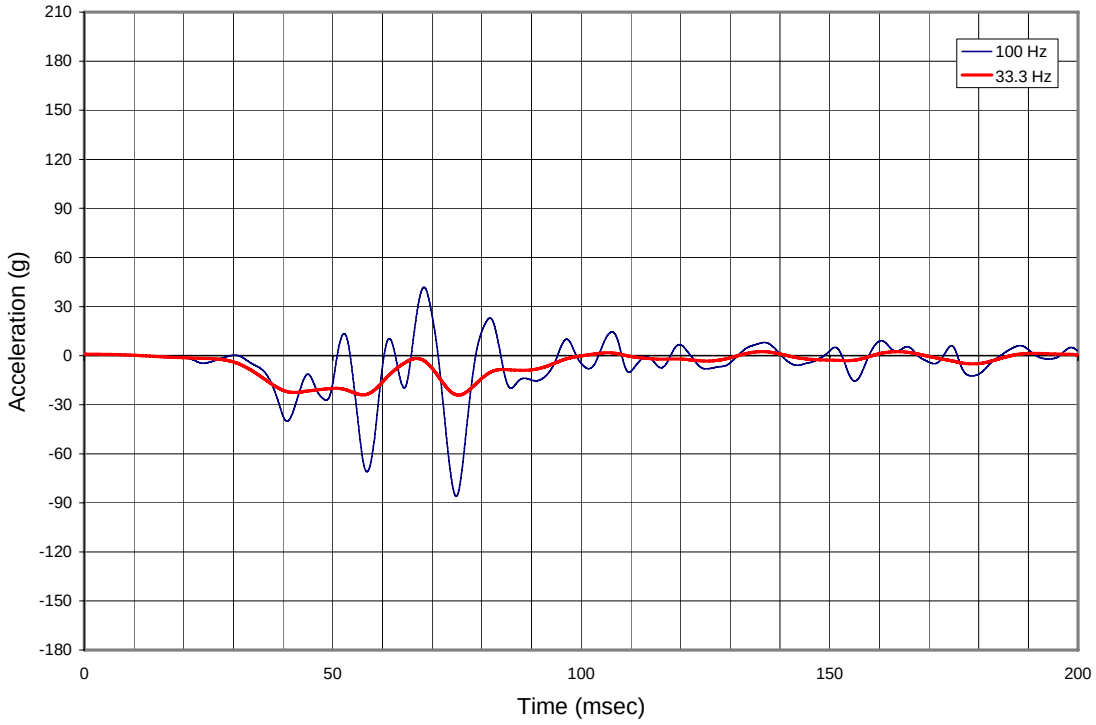

FIGURE B-27. FRAME 18, RIGHT OUTER FLOOR TRACK ACCELERATION

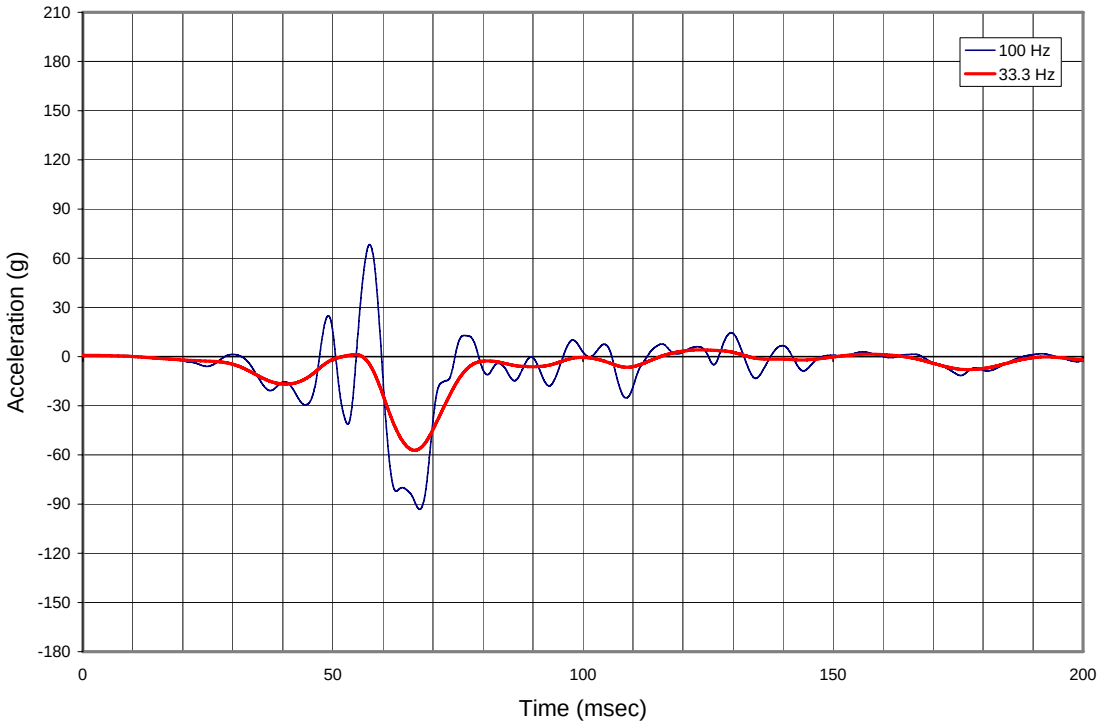

FIGURE B-28. FRAME 20, LEFT INNER FLOOR TRACK ACCELERATION

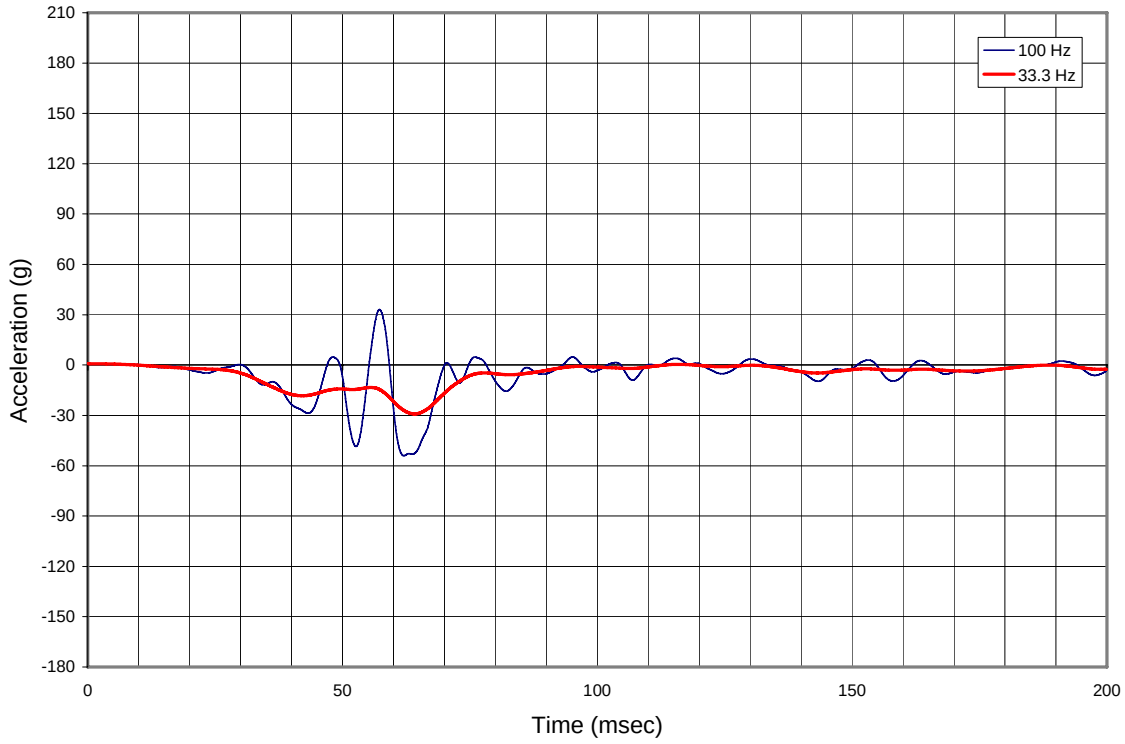

FIGURE B-29. FRAME 20, LEFT OUTER FLOOR TRACK ACCELERATION

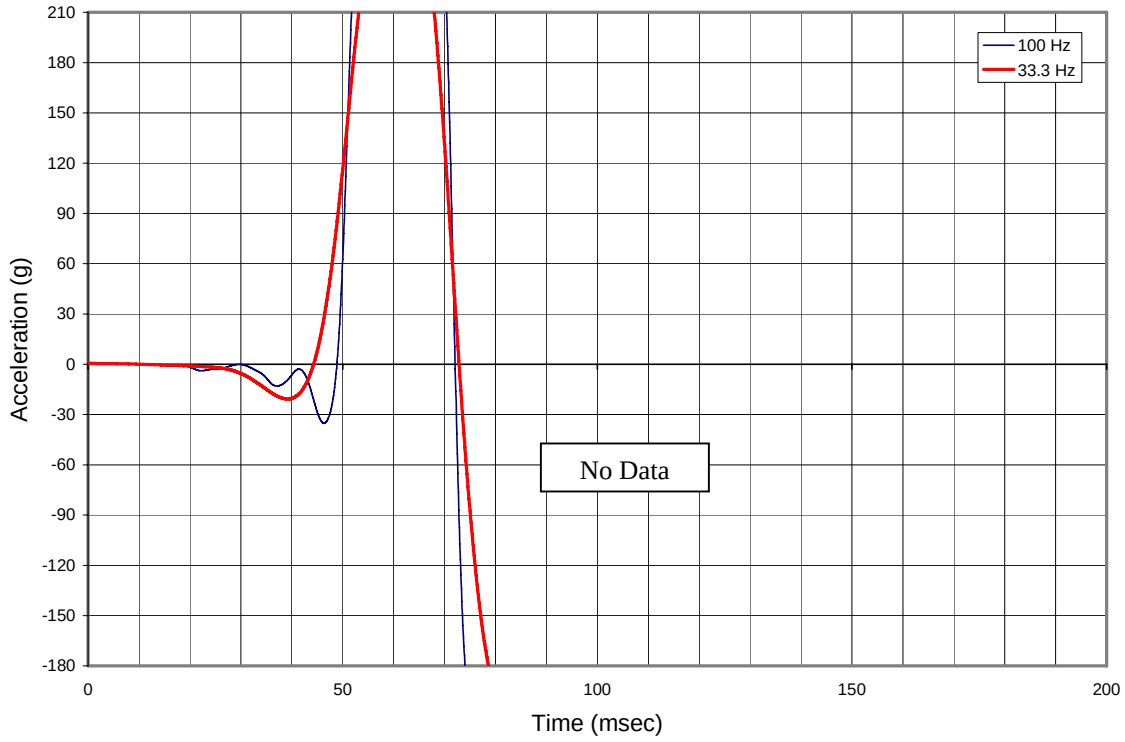

FIGURE B-30. FRAME 20, RIGHT INNER FLOOR TRACK ACCELERATION

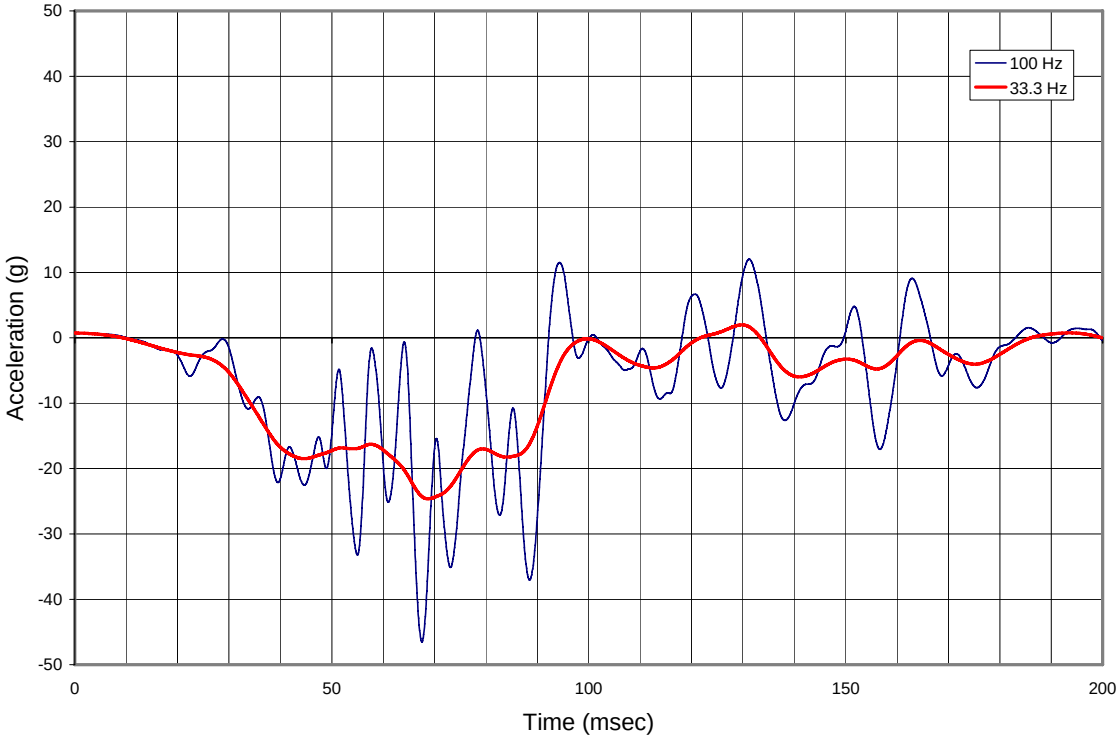

FIGURE B-31. FRAME 20, RIGHT OUTER FLOOR TRACK ACCELERATION

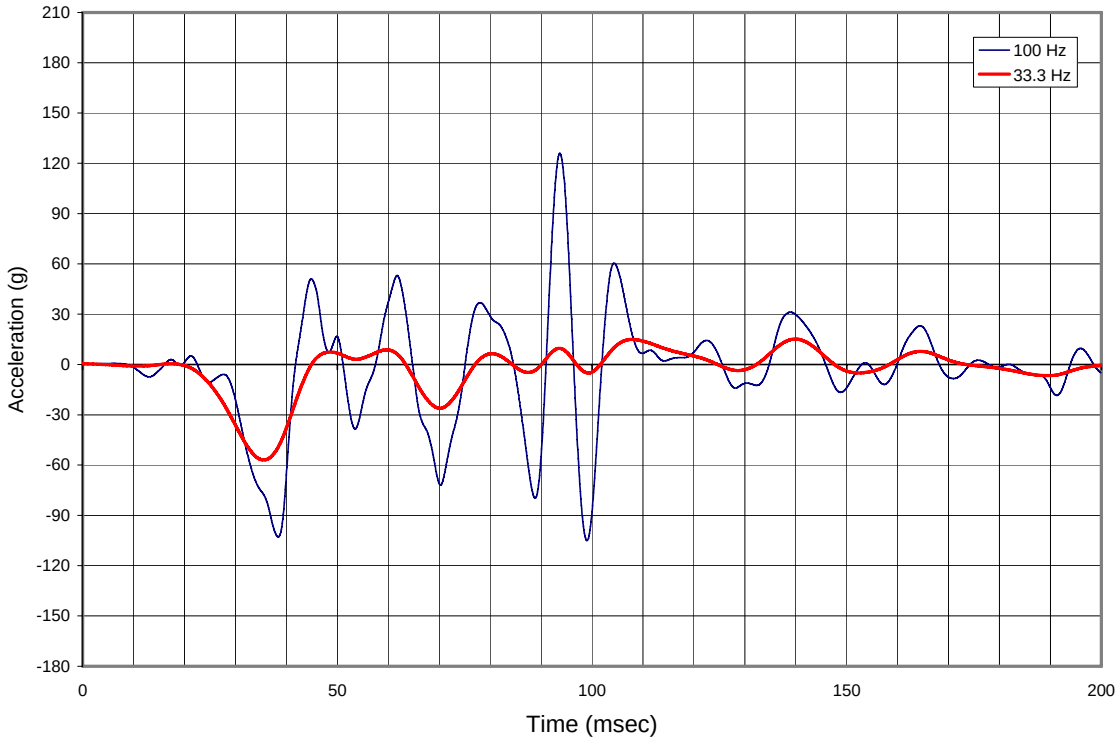

FIGURE B-32. FRAME 25, LEFT INNER FLOOR TRACK ACCELERATION

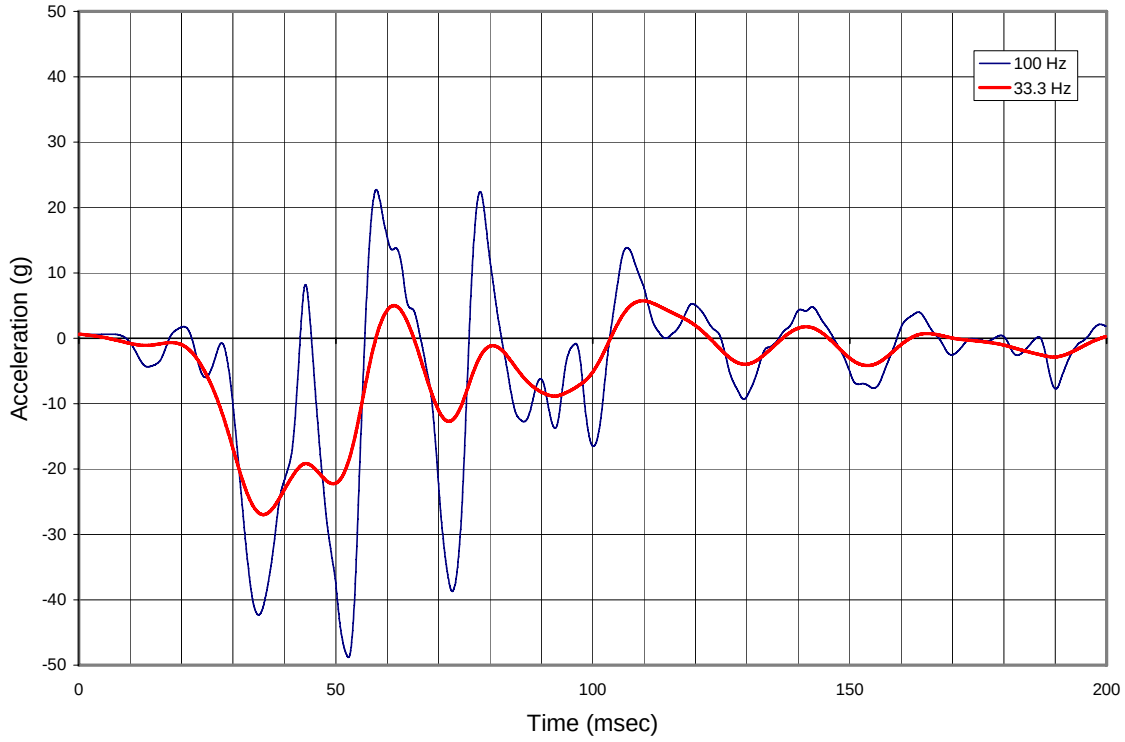

FIGURE B-33. FRAME 25, LEFT OUTER FLOOR TRACK ACCELERATION

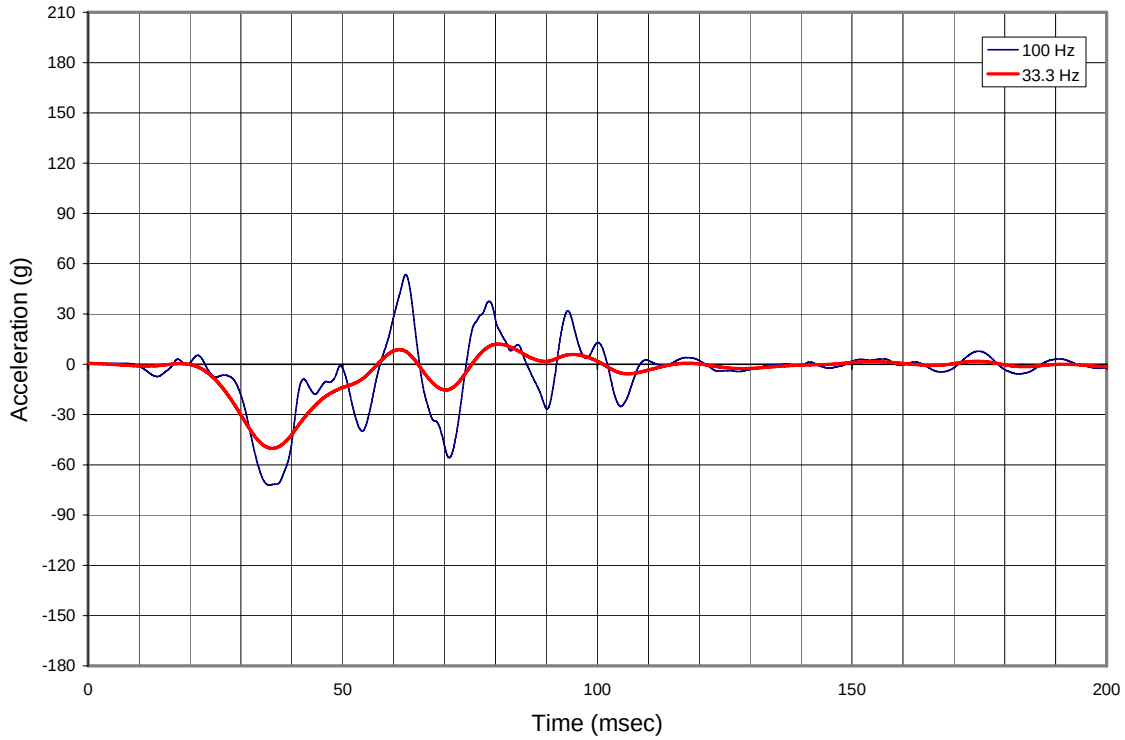

FIGURE B-34. FRAME 25, RIGHT INNER FLOOR TRACK ACCELERATION

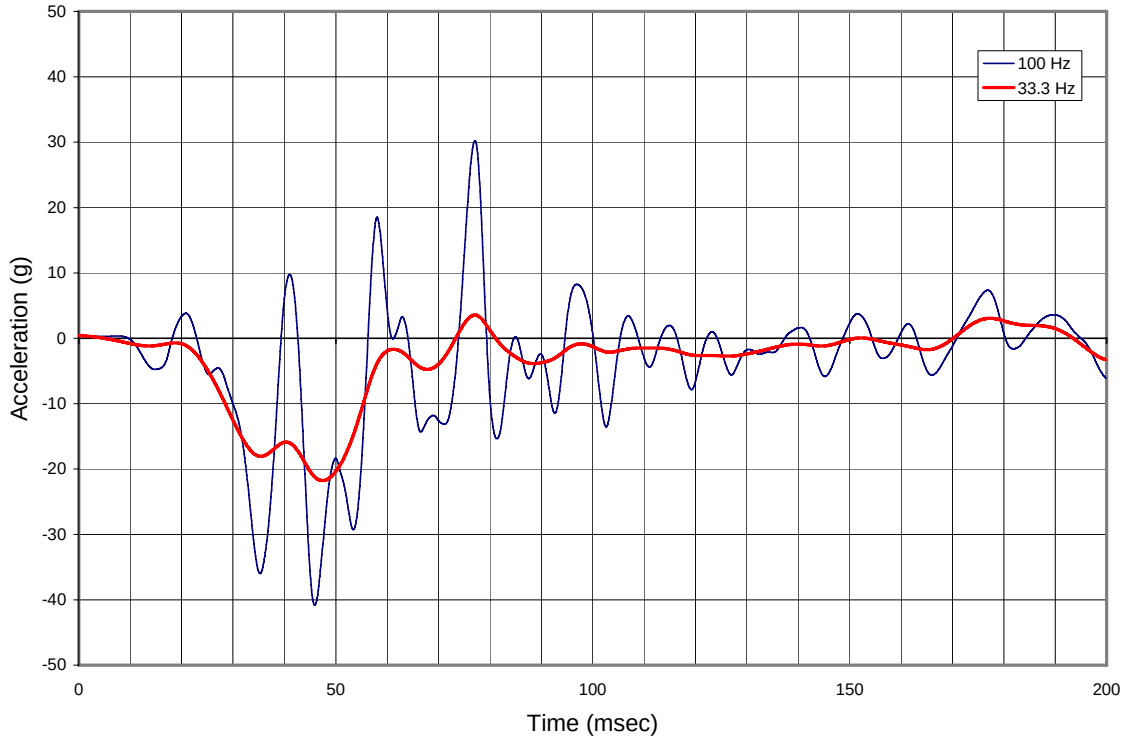

FIGURE B-35. FRAME 25, RIGHT OUTER FLOOR TRACK ACCELERATION

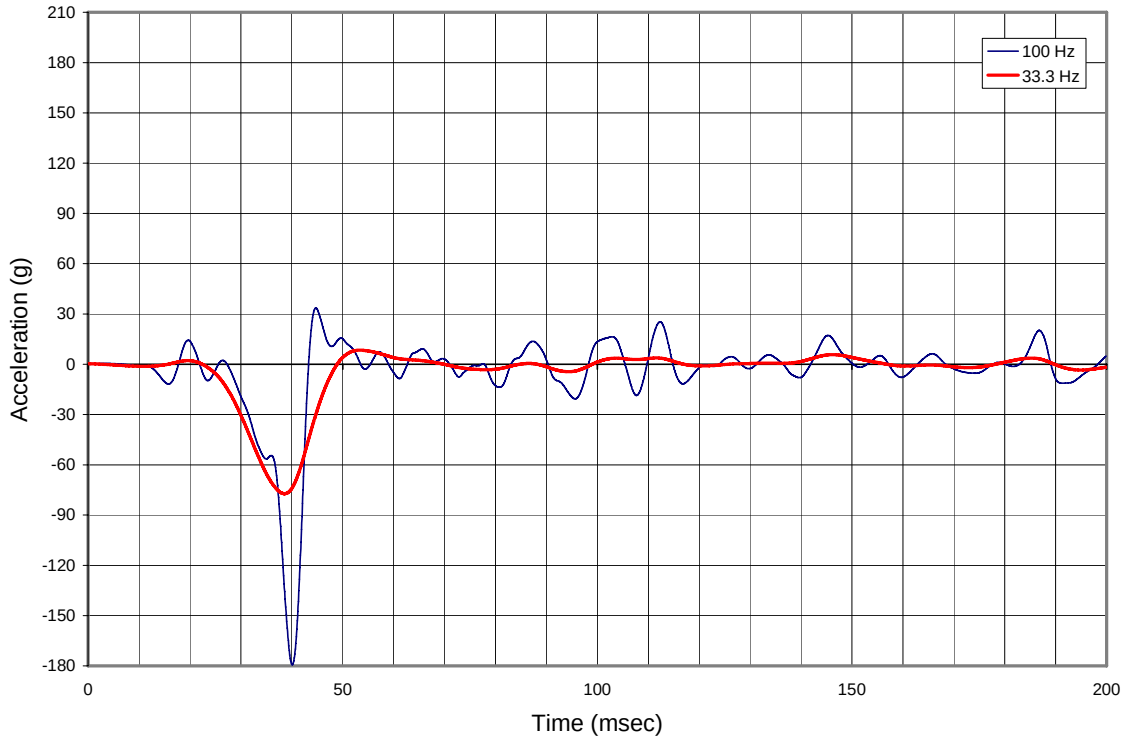

FIGURE B-36. FRAME 27, LEFT INNER FLOOR TRACK ACCELERATION

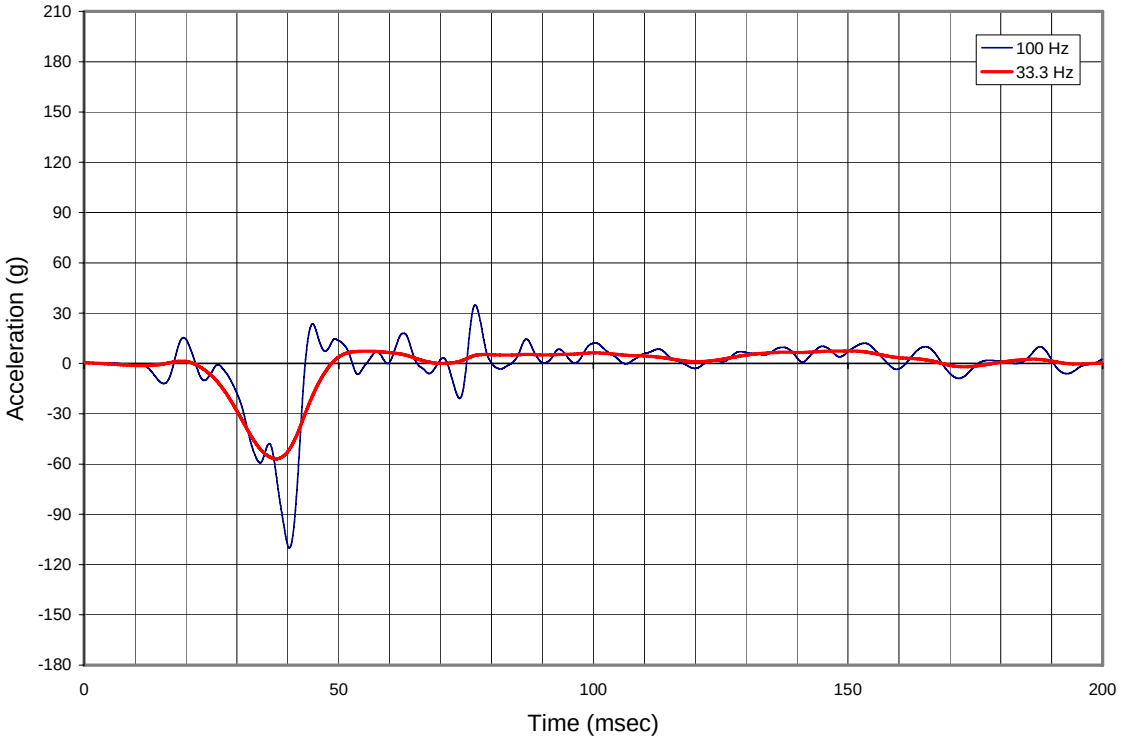

FIGURE B-37. FRAME 27, RIGHT INNER FLOOR TRACK ACCELERATION

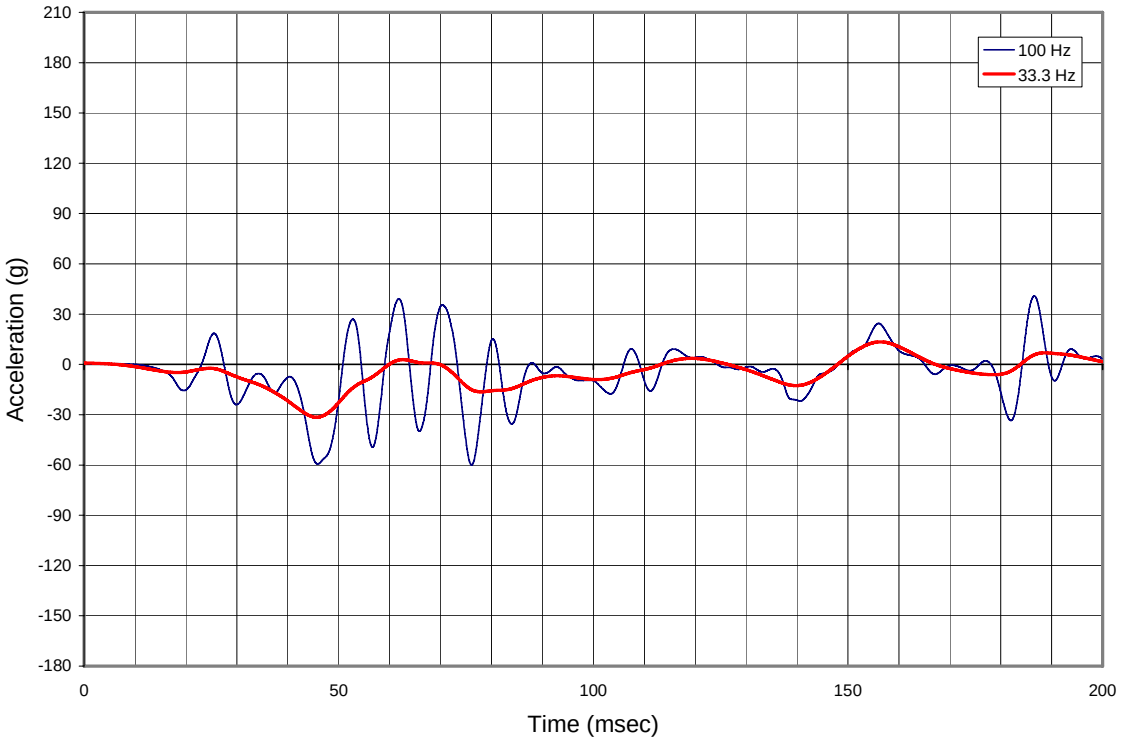

FIGURE B-38. FRAME 29, LEFT INNER FLOOR TRACK ACCELERATION

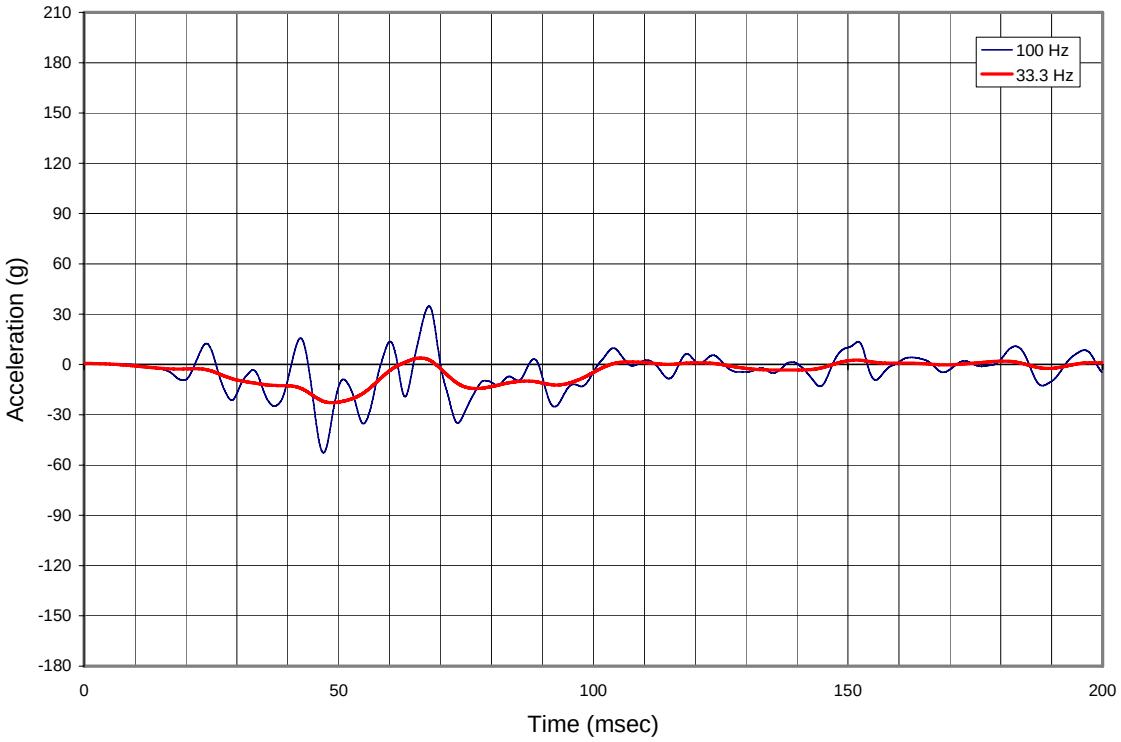

FIGURE B-39. FRAME 29, LEFT OUTER FLOOR TRACK ACCELERATION

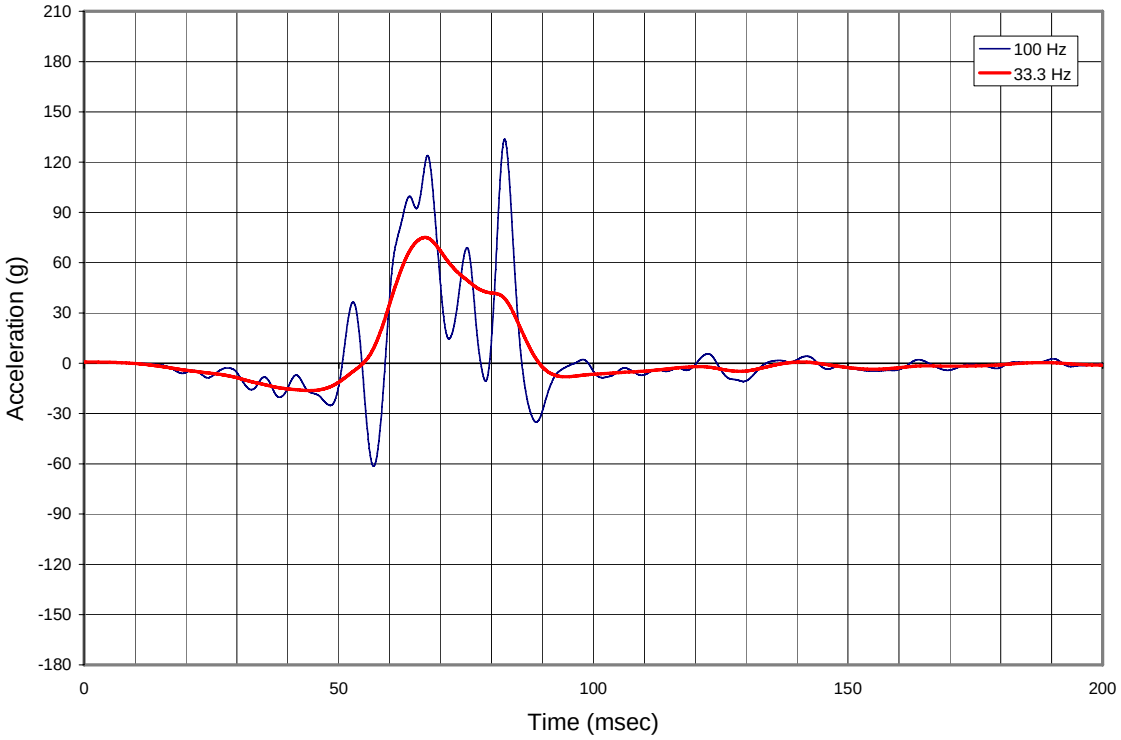

FIGURE B-40. FRAME 29, RIGHT INNER FLOOR TRACK ACCELERATION

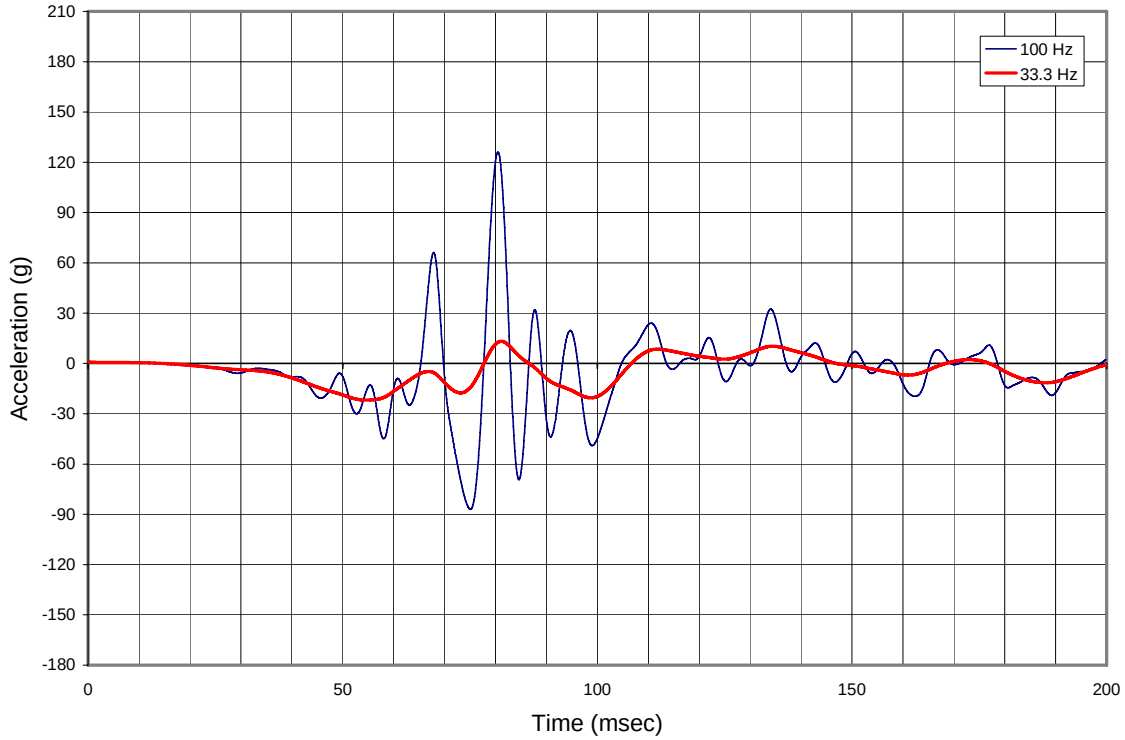

FIGURE B-41. FRAME 35, LEFT INNER FLOOR TRACK ACCELERATION

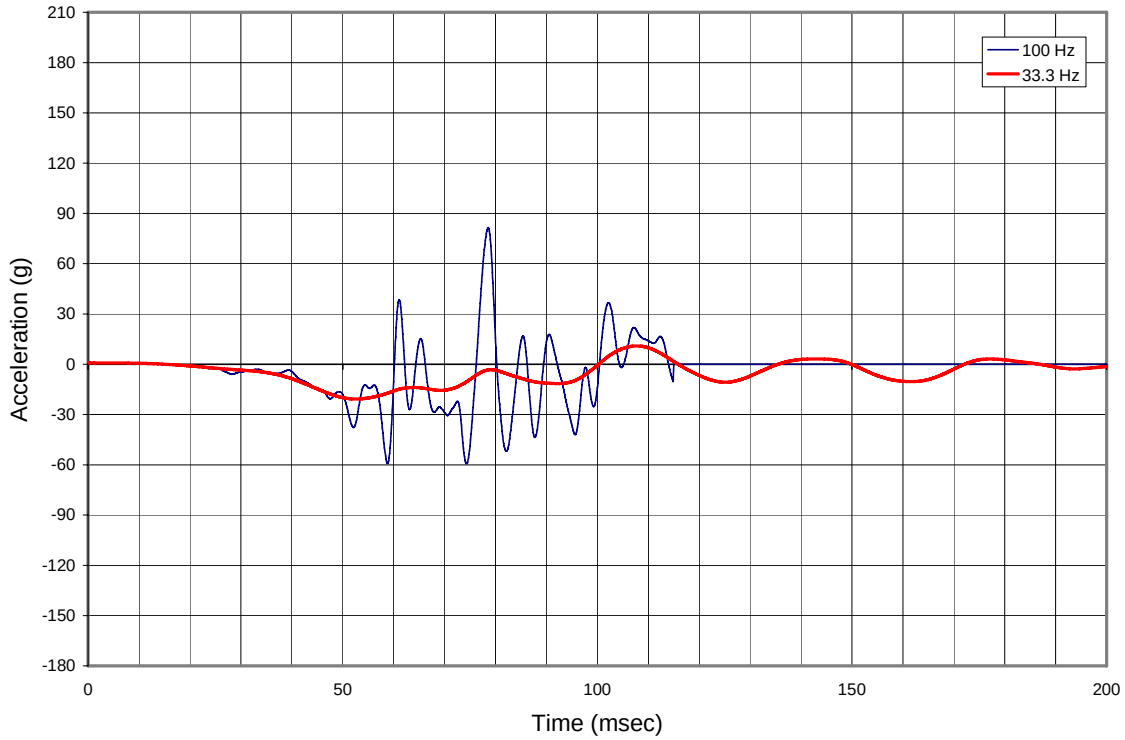

FIGURE B-42. FRAME 35, RIGHT INNER FLOOR TRACK ACCELERATION

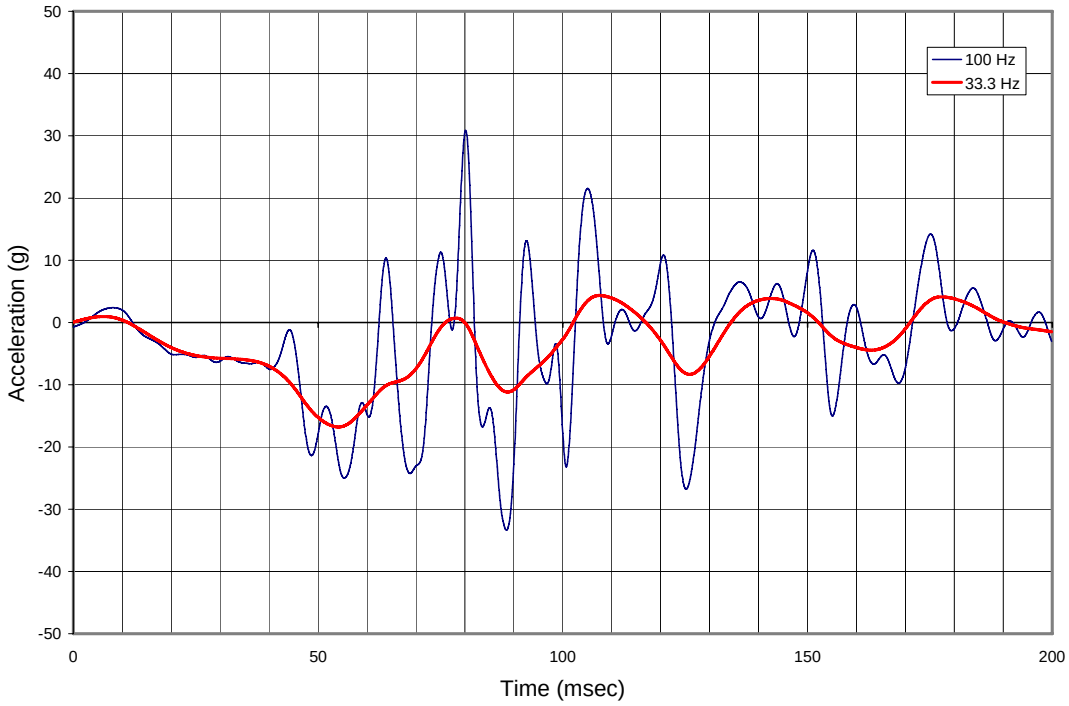

FIGURE B-43. FRAME 35, RIGHT OUTER FLOOR TRACK ACCELERATION

B.3 WING FITTING DATA—MEASURED LOADS.

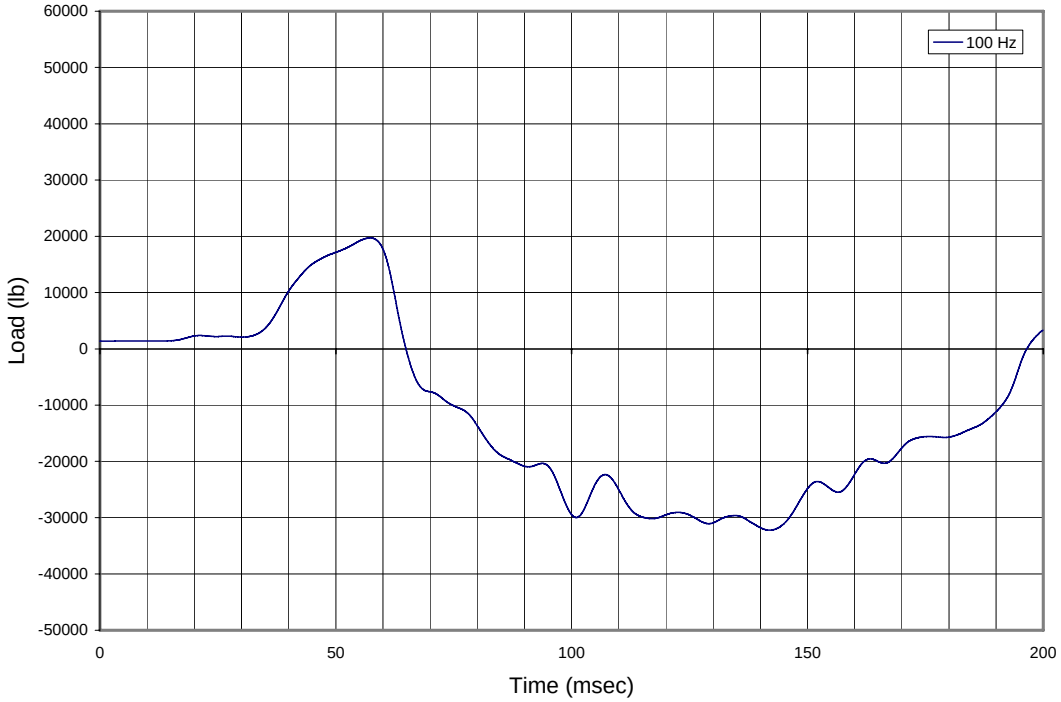

FIGURE B-44. FRAME 25, LEFT INSIDE, CHANNEL B—MEASURED LOAD

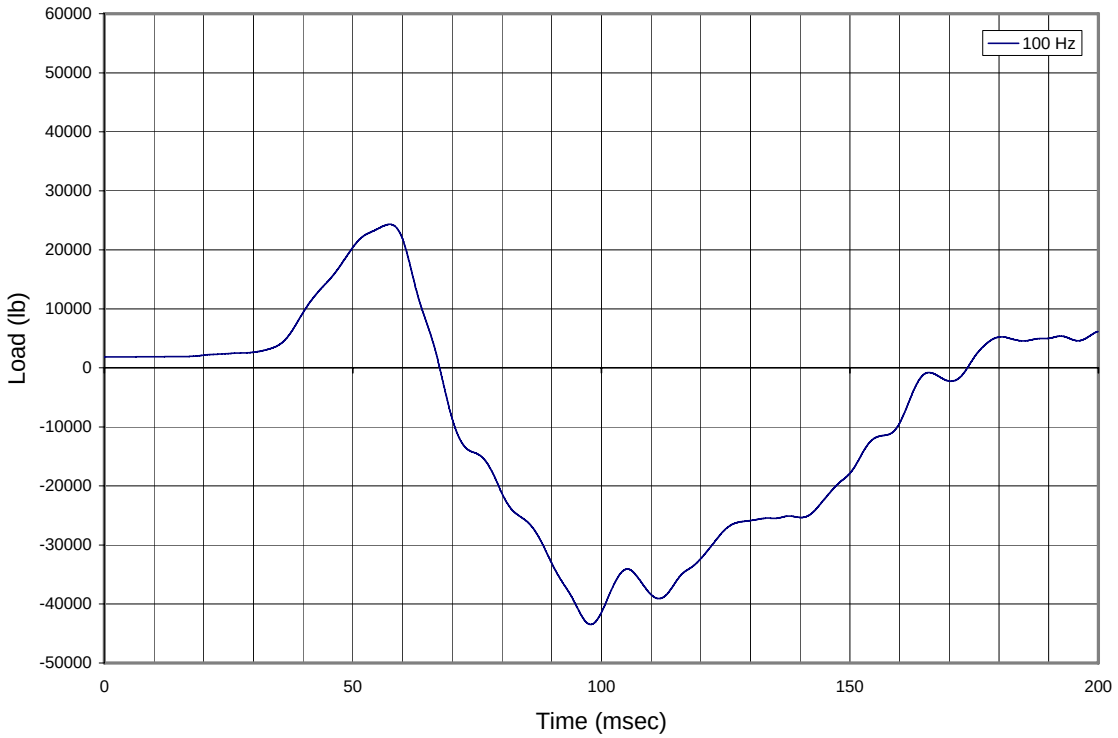

FIGURE B-45. FRAME 25, RIGHT INSIDE, CHANNEL A—MEASURED LOAD

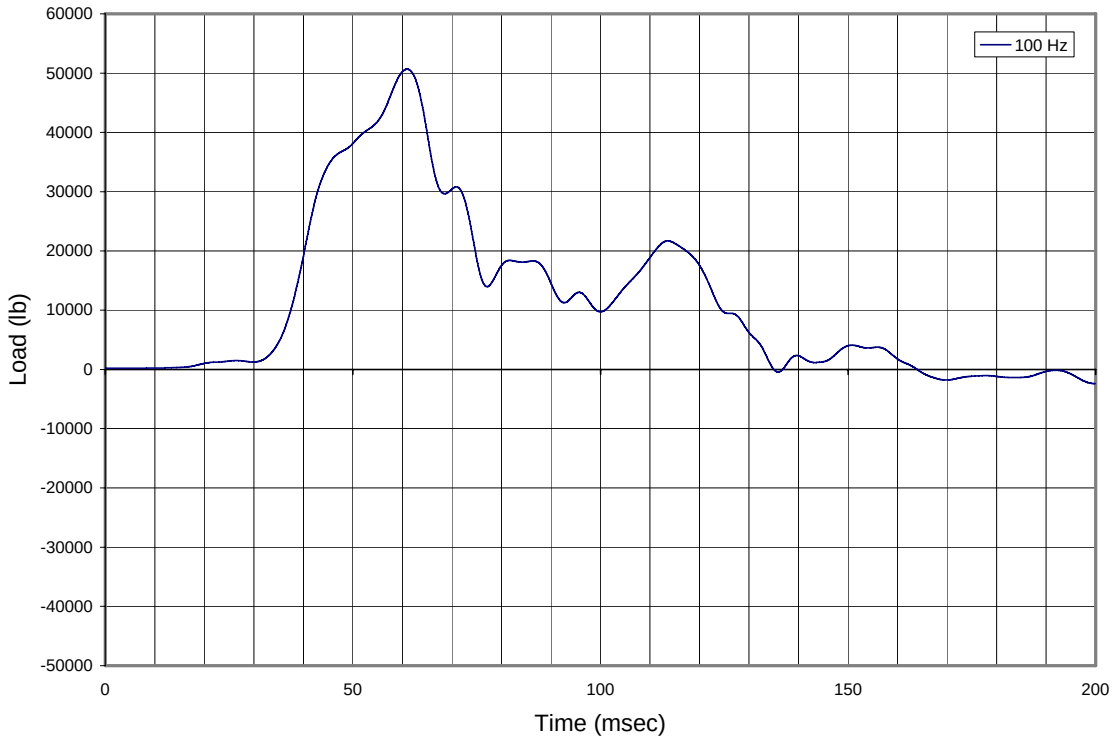

FIGURE B-46. FRAME 27, LEFT INSIDE, CHANNEL A—MEASURED LOAD

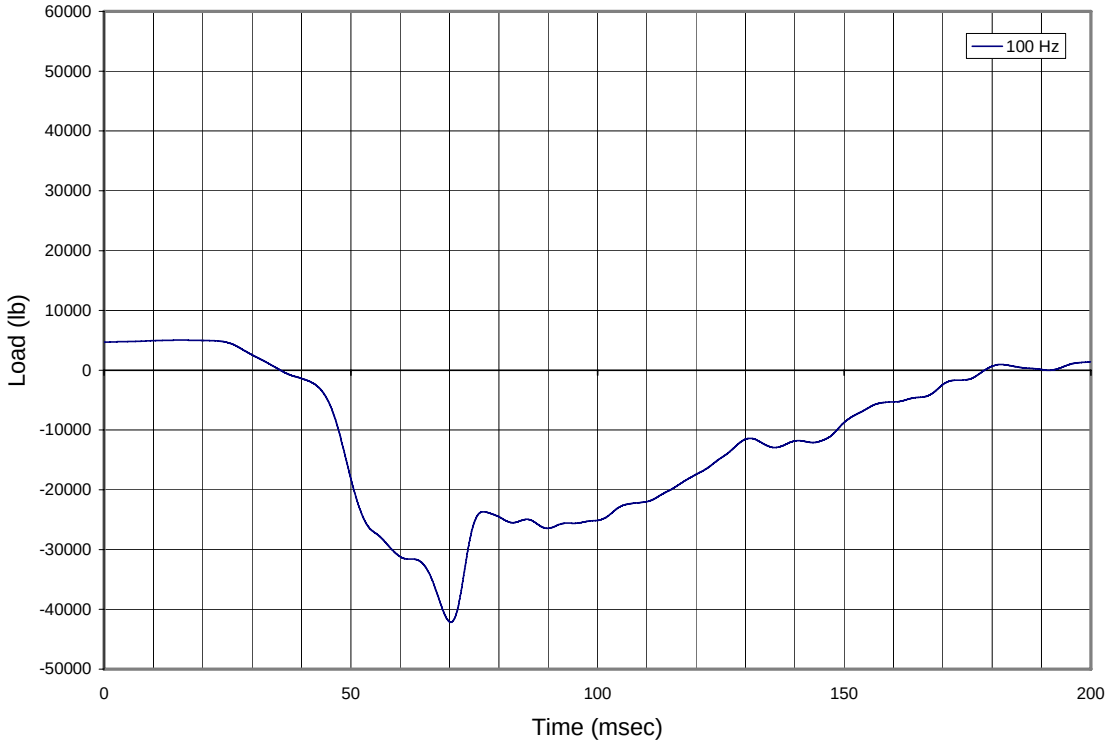

FIGURE B-47. FRAME 25, LEFT OUTSIDE, CHANNEL B—MEASURED LOAD

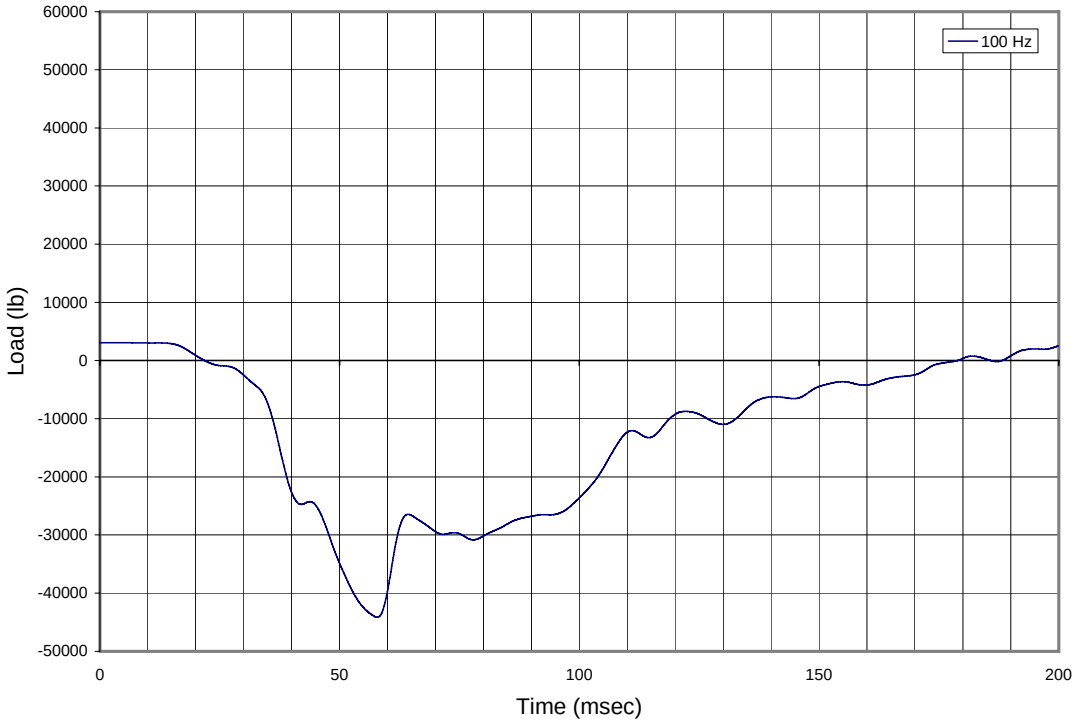

FIGURE B-48. FRAME 25, RIGHT OUTSIDE, CHANNEL B—MEASURED LOAD

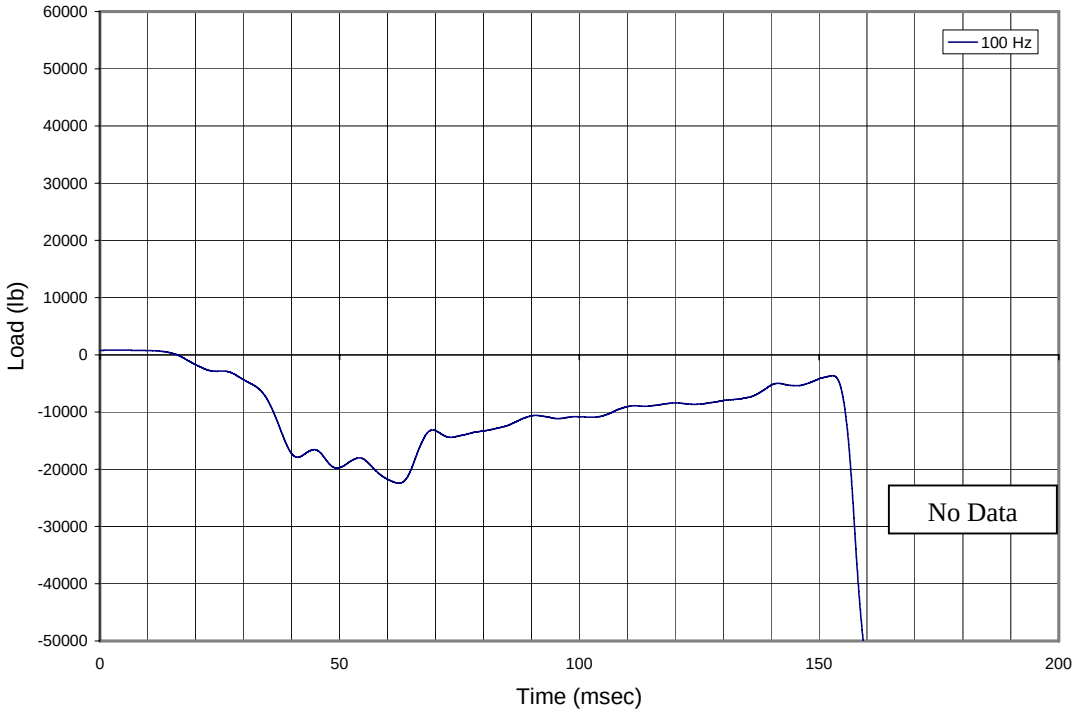

FIGURE B-49. FRAME 27, RIGHT OUTSIDE, CHANNEL B—MEASURED LOAD

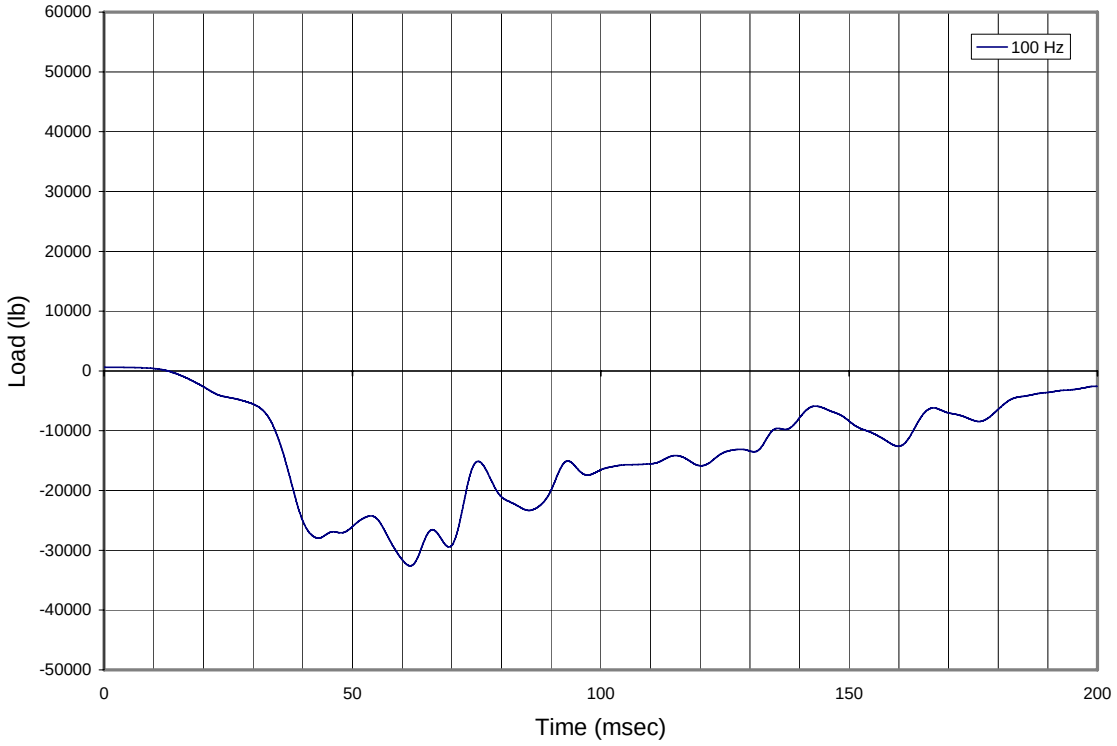

FIGURE B-50. FRAME 27, LEFT OUTSIDE, CHANNEL A—MEASURED LOAD

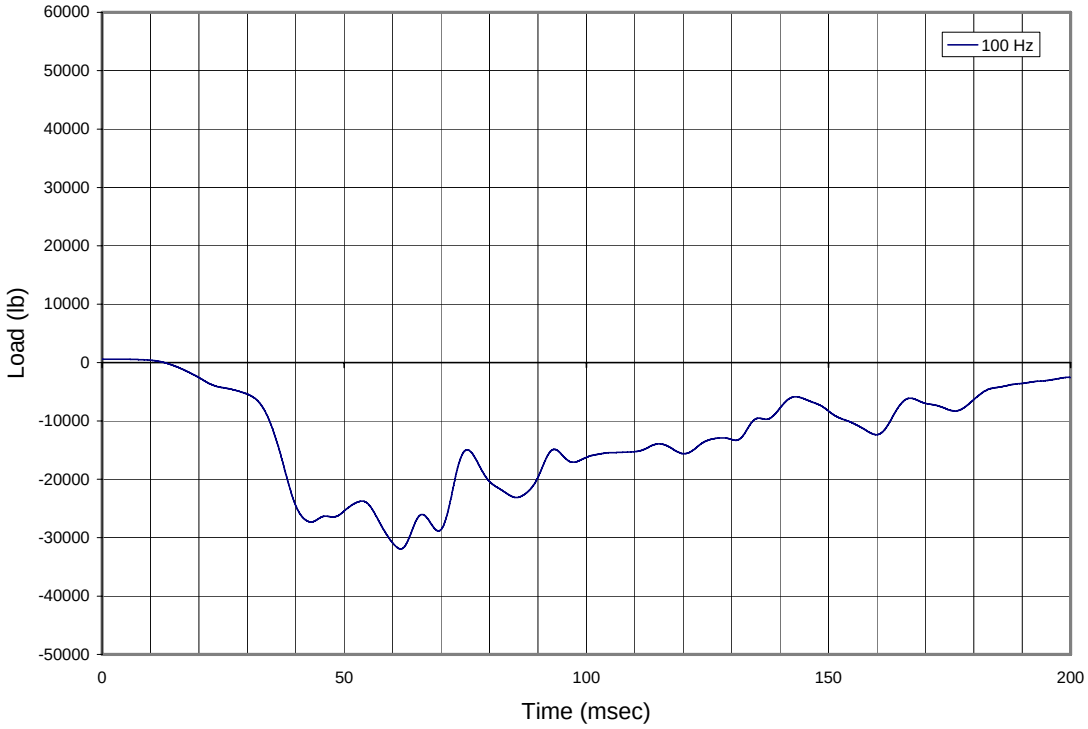

FIGURE B-51. FRAME 27, LEFT OUTSIDE, CHANNEL B—MEASURED LOAD

B.4 OVERHEAD STOWAGE BIN DATA—ACCELERATIONS.

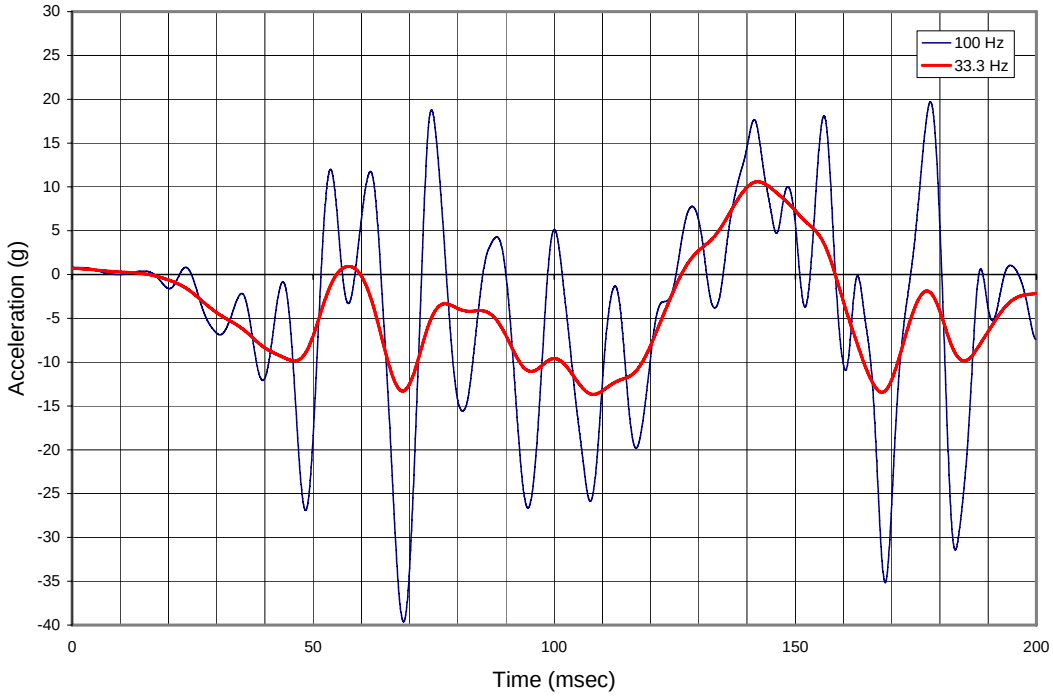

FIGURE B-52. FRAME 31, LEFT BIN—FORWARD LOCATION—ACCELERATION

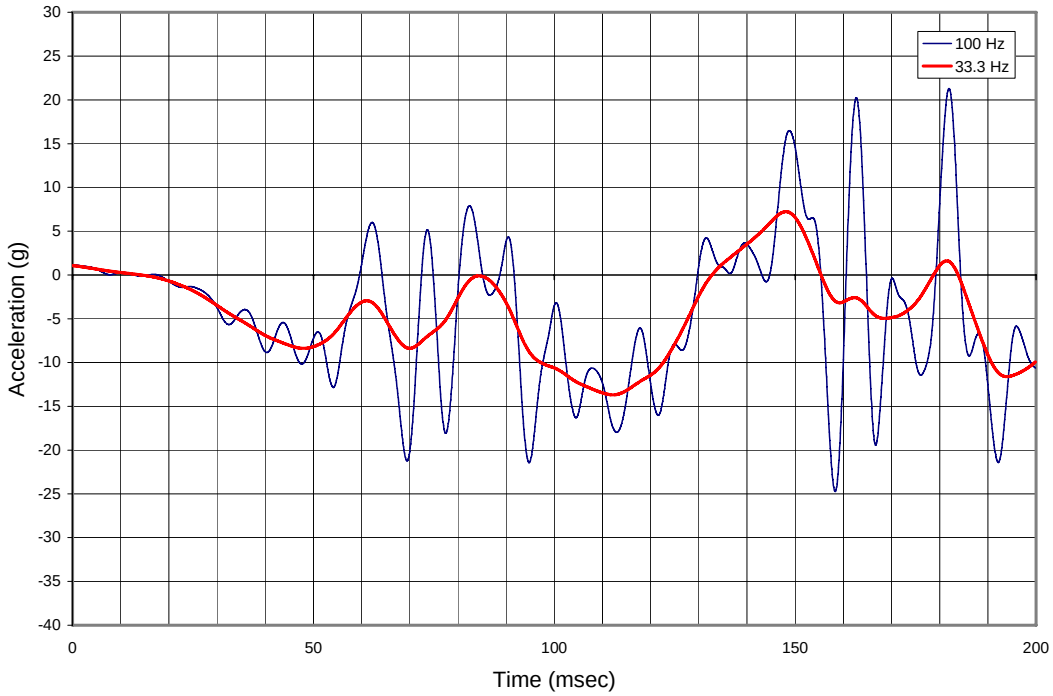

FIGURE B-53. FRAME 34, LEFT BIN—AFT LOCATION—ACCELERATION

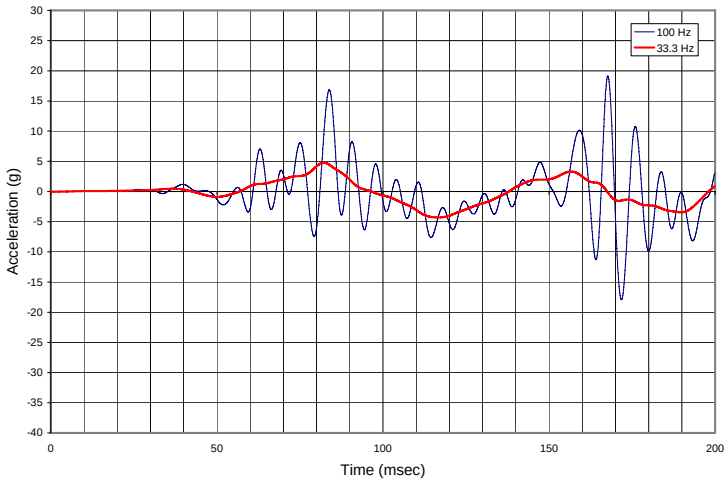

FIGURE B-54. FRAME 32, LEFT BIN—MIDDLE LOCATION—X AXIS ACCELERATION

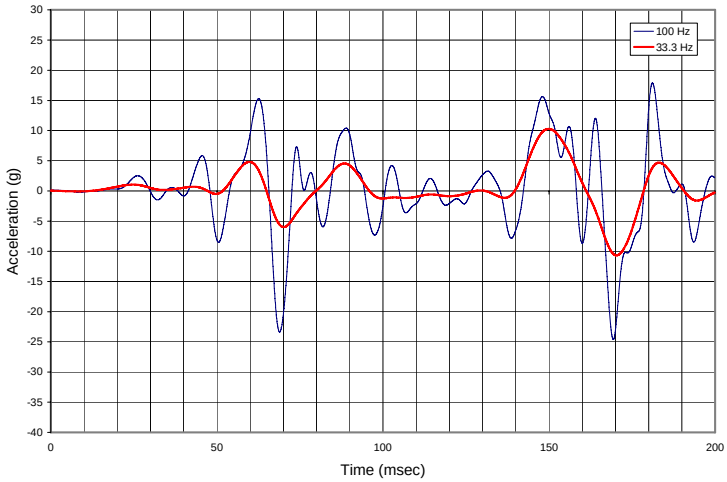

FIGURE B-55. FRAME 32, LEFT BIN—MIDDLE LOCATION—Y AXIS ACCELERATION

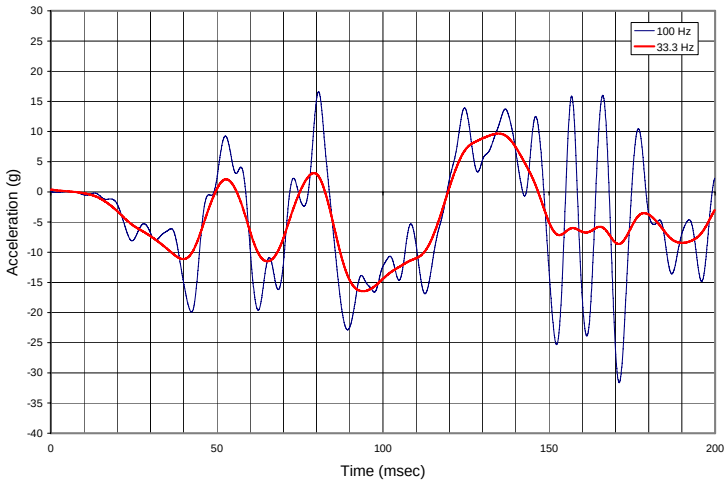

FIGURE B-56. FRAME 32, LEFT BIN—MIDDLE LOCATION—Z AXIS ACCELERATION

B.5 WING AND ENGINE DATA—ACCELERATIONS.

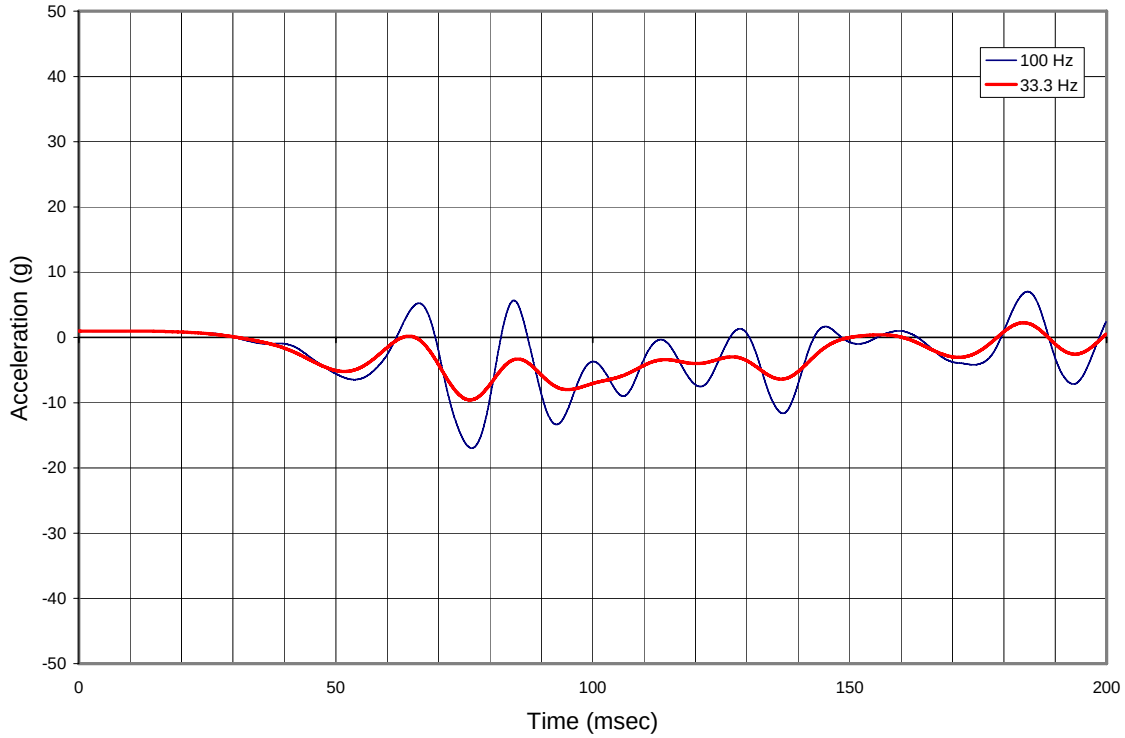

FIGURE B-57. LEFT ENGINE ACCELERATION

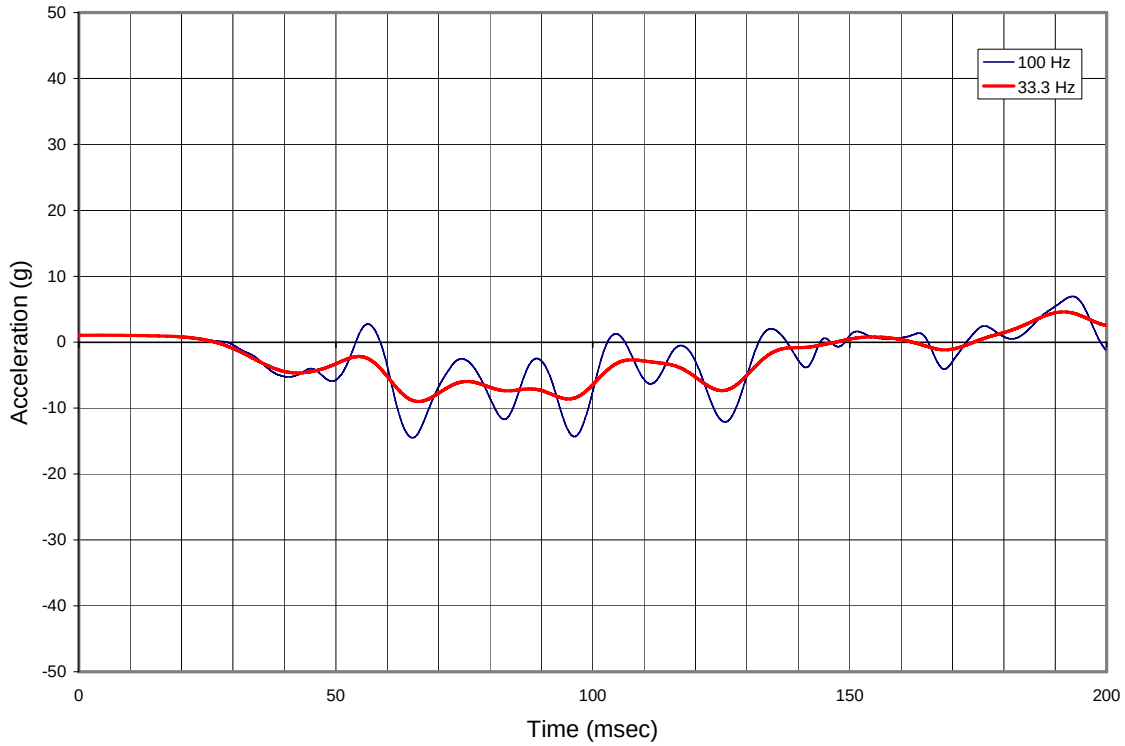

FIGURE B-58. RIGHT ENGINE ACCELERATION

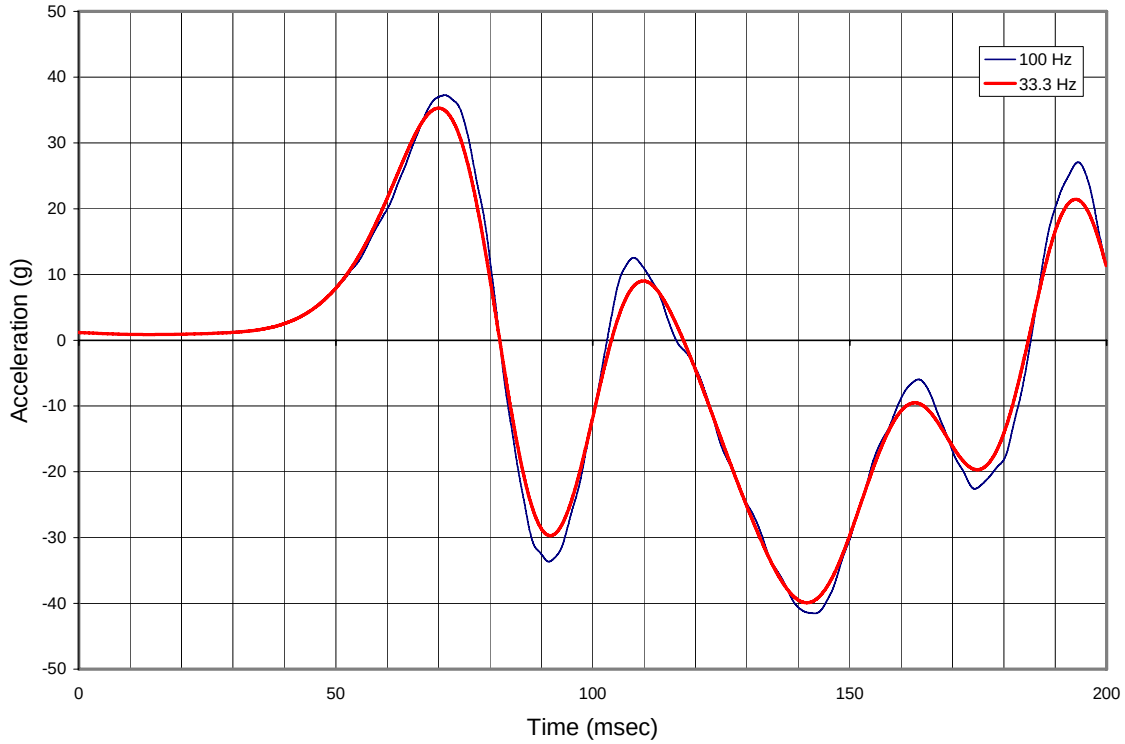

FIGURE B-59. LEFT WING TIP ACCELERATION

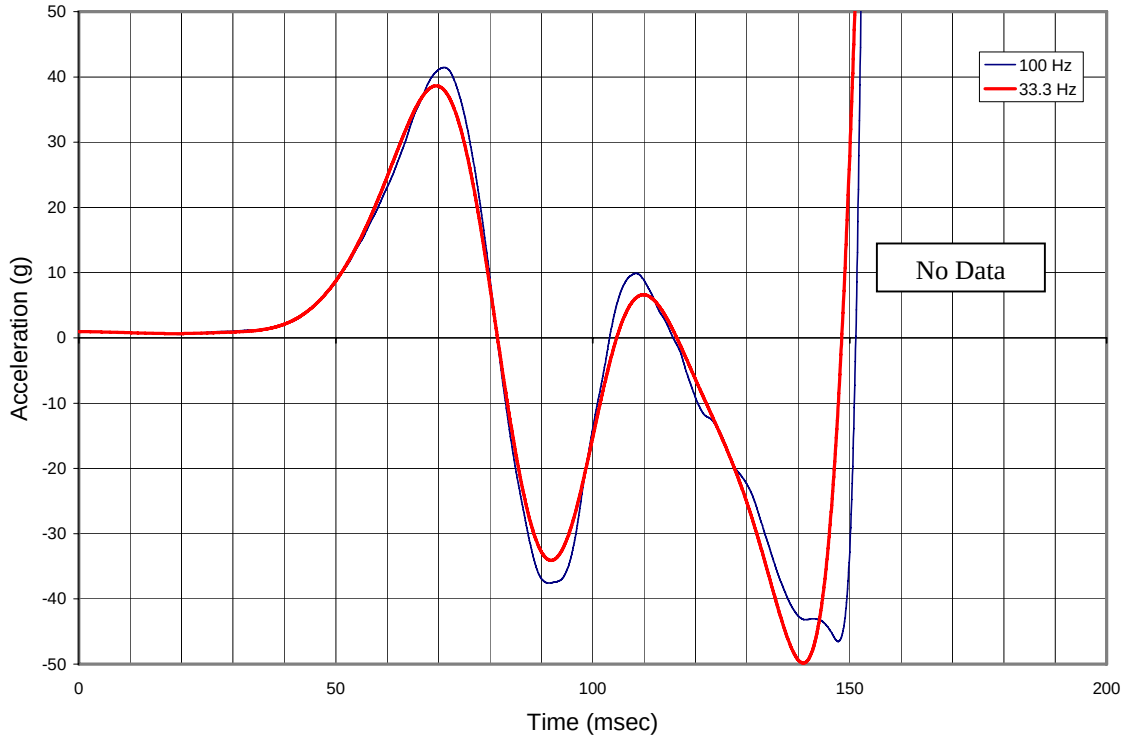

FIGURE B-60. RIGHT WING TIP ACCELERATION

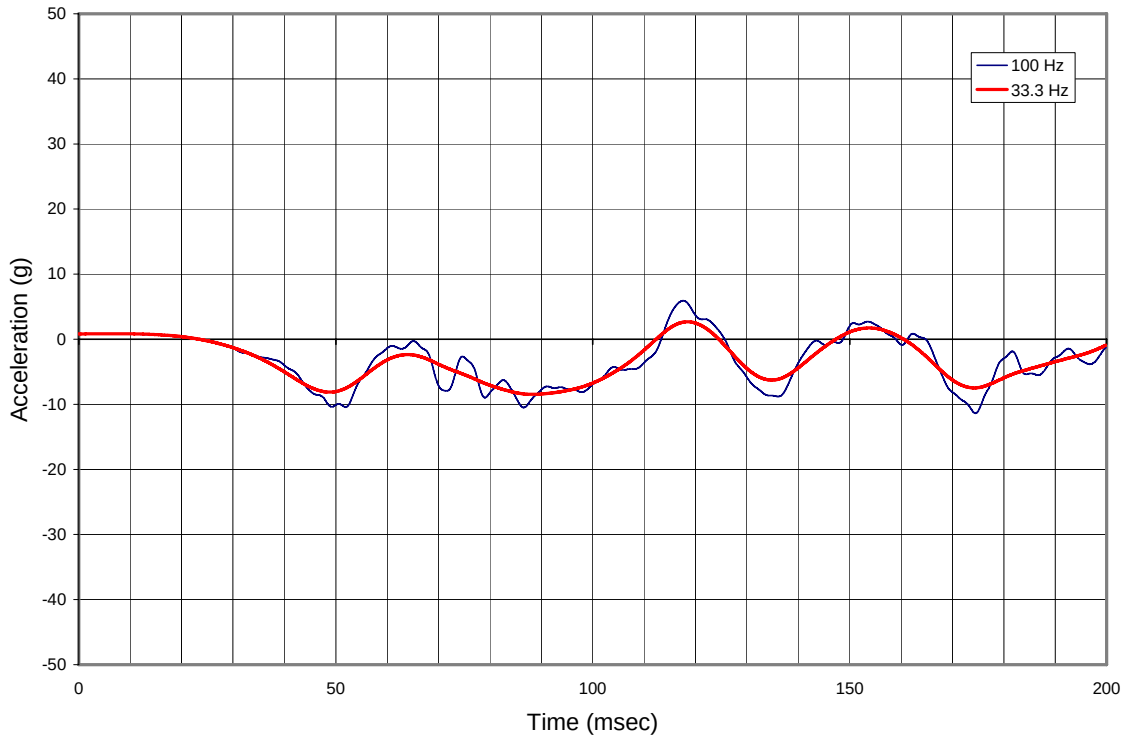

FIGURE B-61. LEFT WING, TRAILING-EDGE (BEHIND ENGINE) ACCELERATION

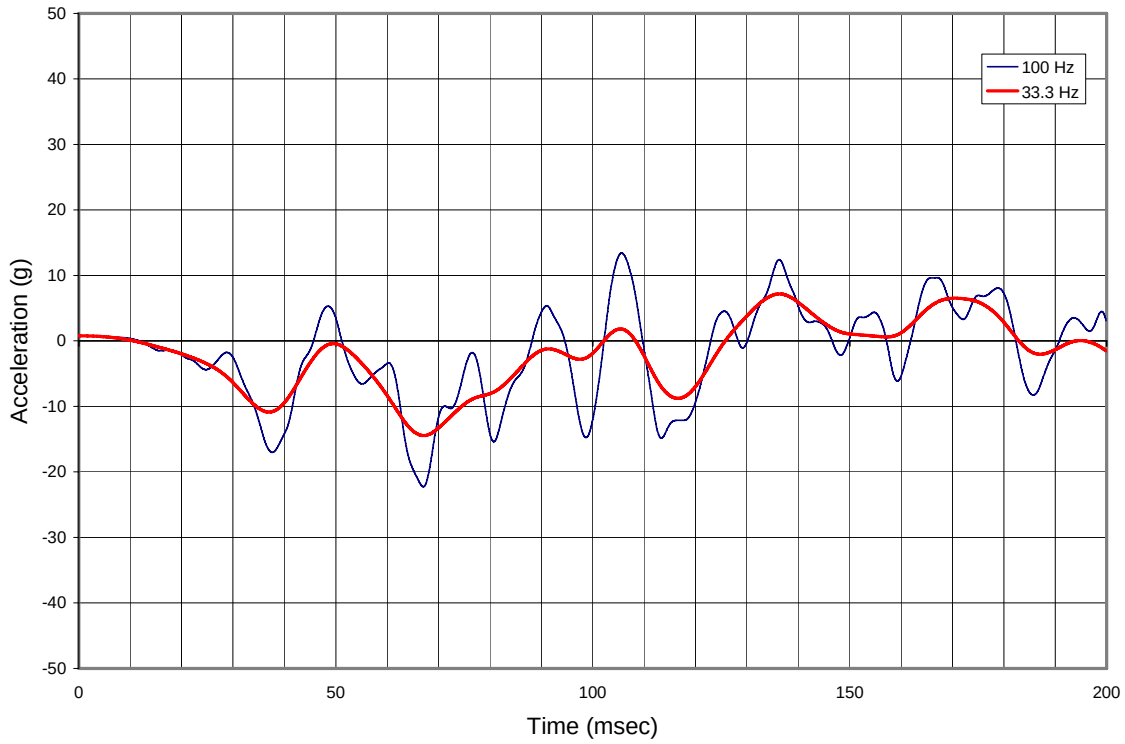

FIGURE B-62. LEFT WING, INNER LEADING-EDGE ACCELERATION

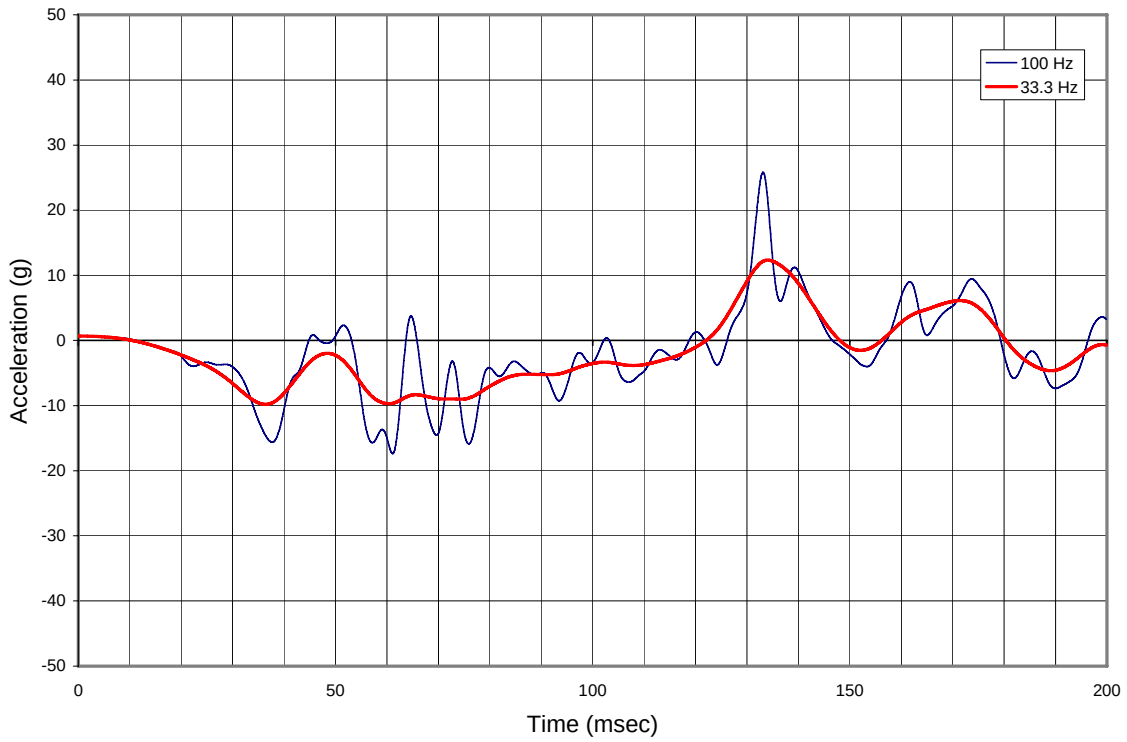

FIGURE B-63. LEFT WING, INNER TRAILING-EDGE ACCELERATION

B.6 ANTHROPOMORPHIC TEST DUMMY DATA.

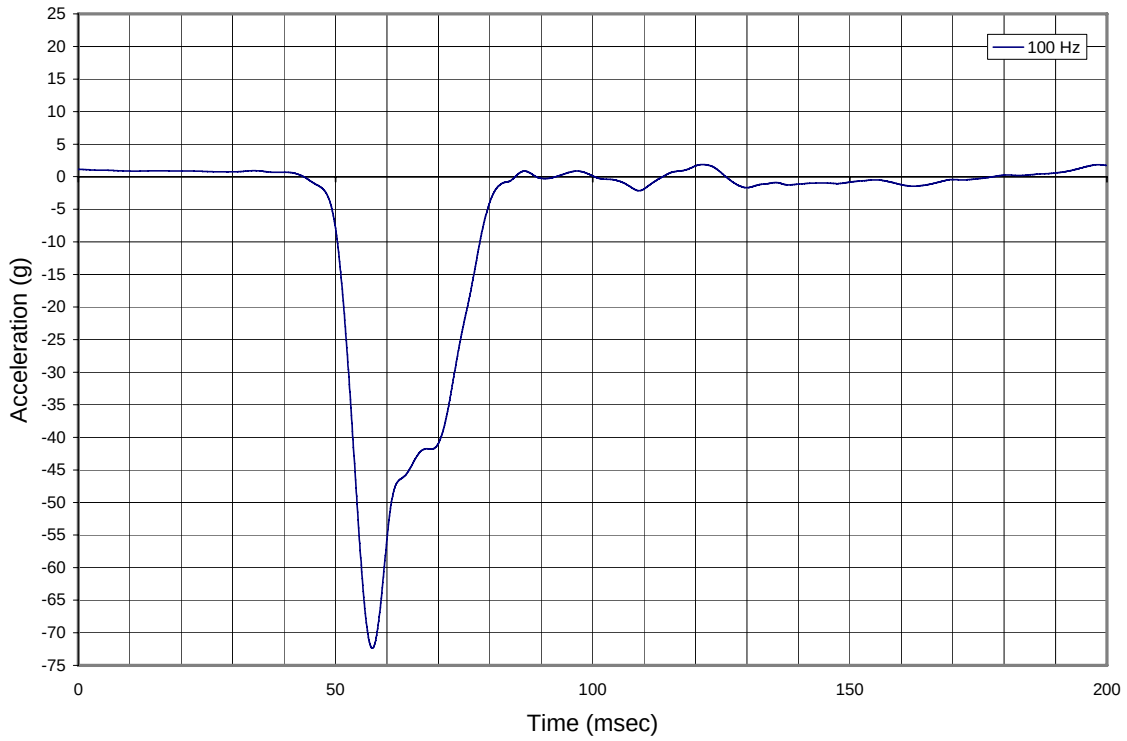

FIGURE B-64. FRAME 9, ATD 1, LEFT SIDE COCKPIT, PELVIC ACCELERATION

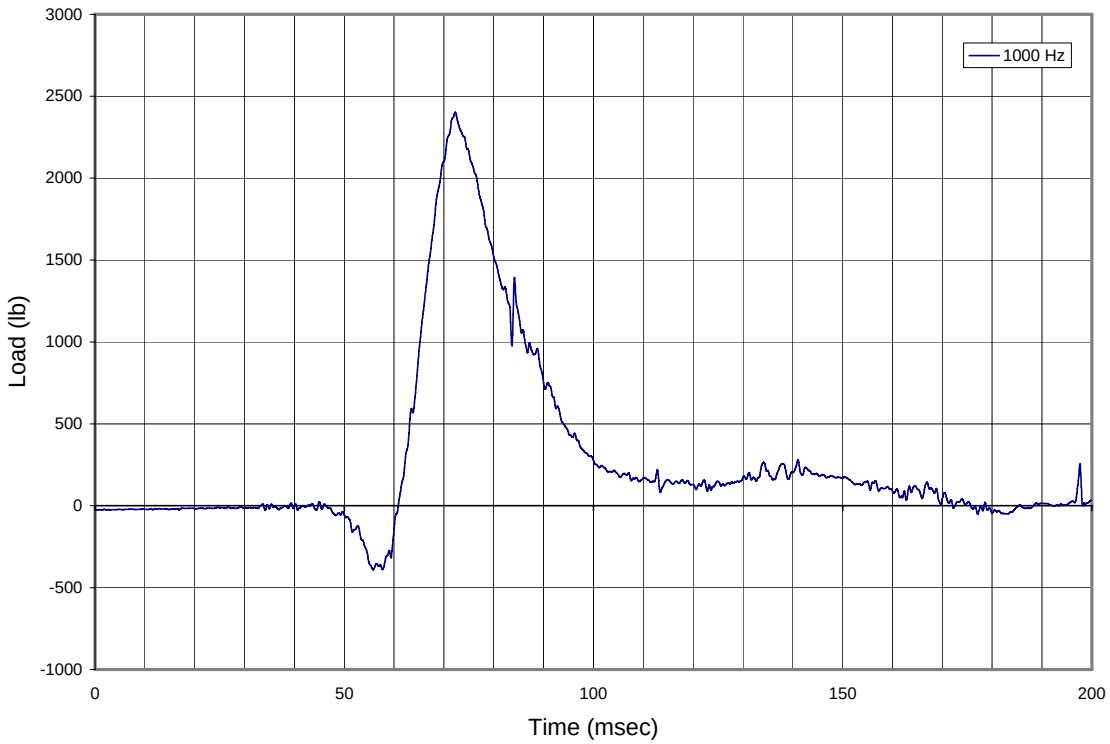

FIGURE B-65. FRAME 9, ATD 1, LEFT SIDE COCKPIT, LUMBAR LOAD

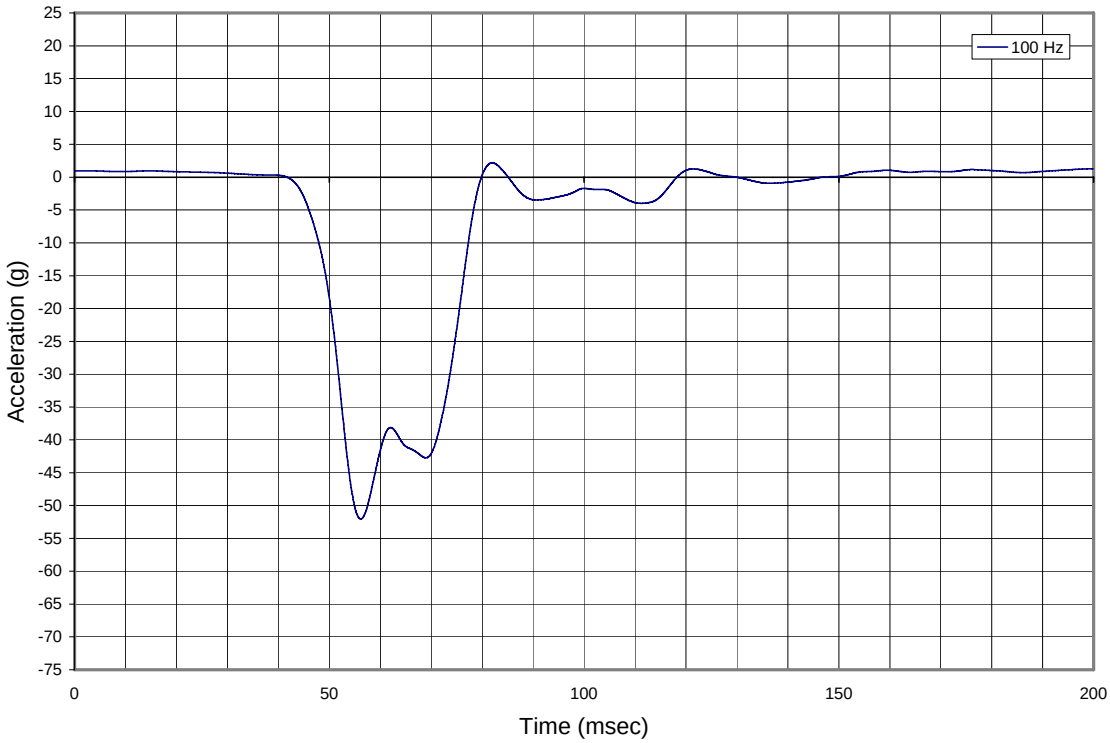

FIGURE B-66. FRAME 9, ATD 2, RIGHT SIDE COCKPIT, PELVIC ACCELERATION

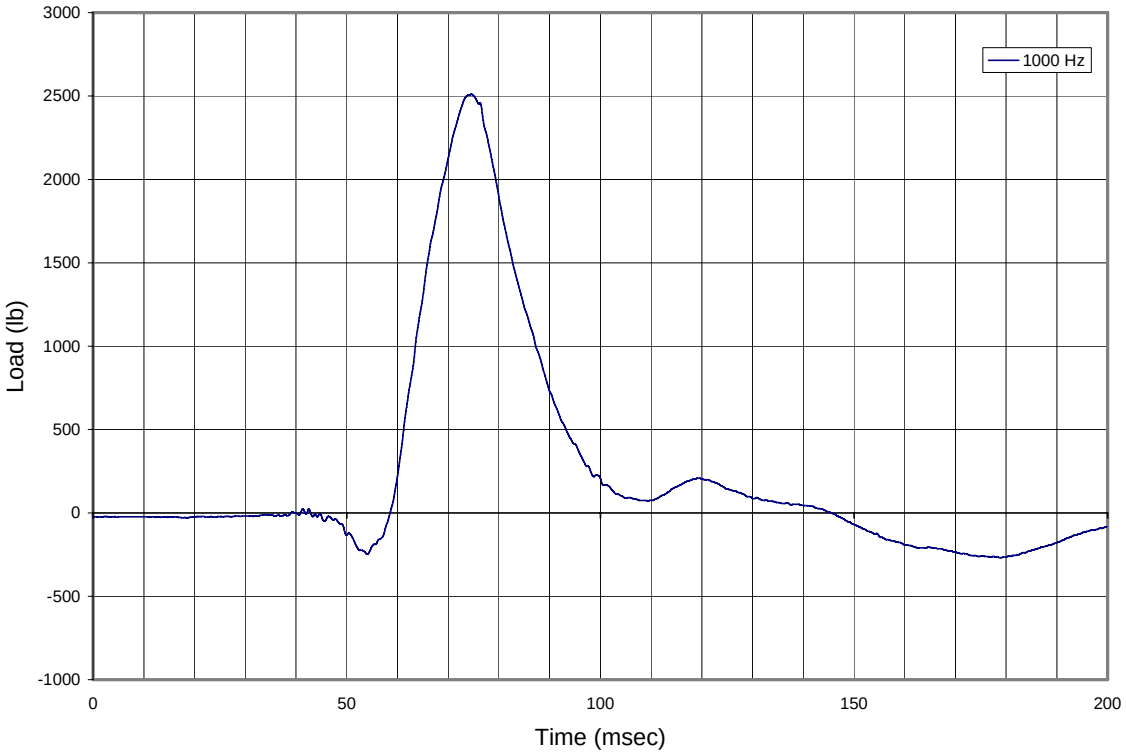

FIGURE B-67. FRAME 9, ATD 2, RIGHT SIDE COCKPIT, LUMBAR LOAD

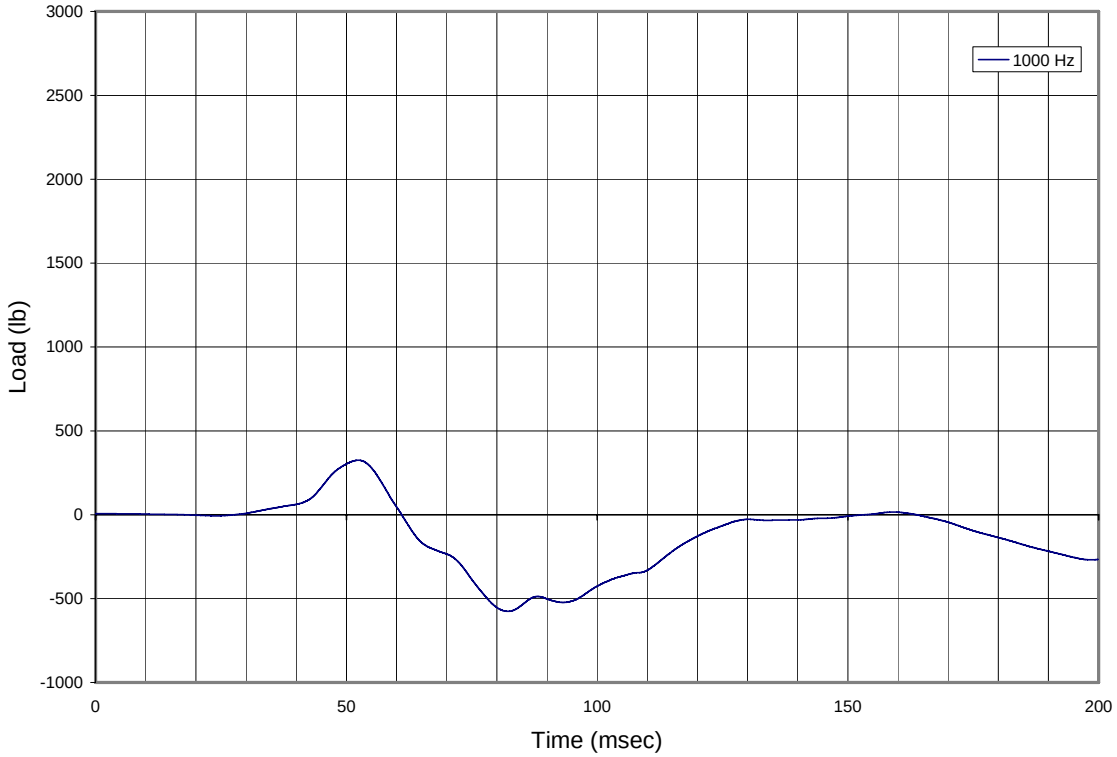

FIGURE B-68. FRAME 19, ATD 3, ROW 1 SEAT C, LUMBAR LOAD

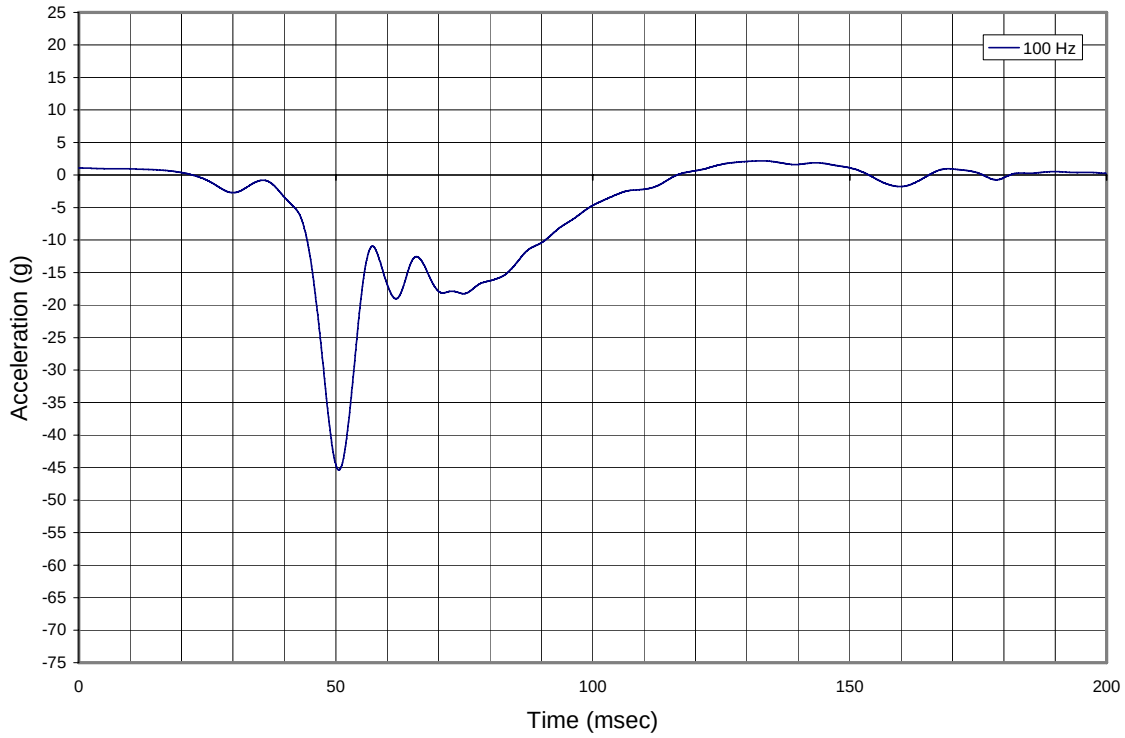

FIGURE B-69. FRAME 28, ATD 4, ROW 7 SEAT C, PELVIC ACCELERATION

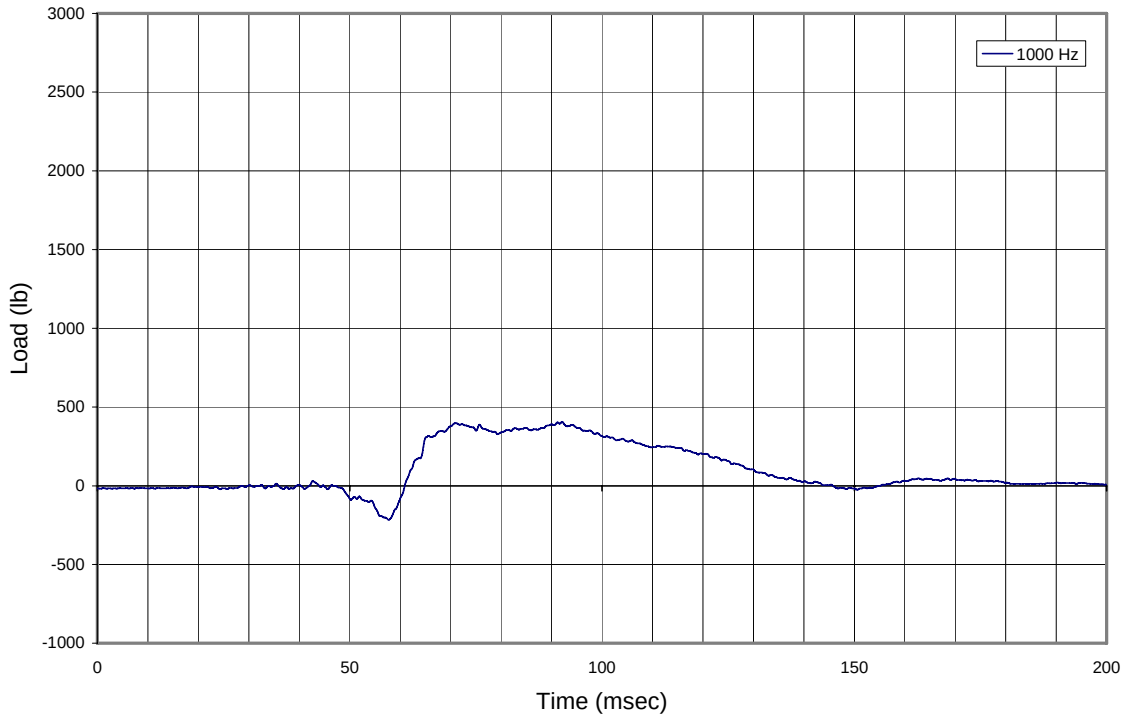

FIGURE B-70. FRAME 28, ATD 4, ROW 7 SEAT C, LUMBAR LOAD

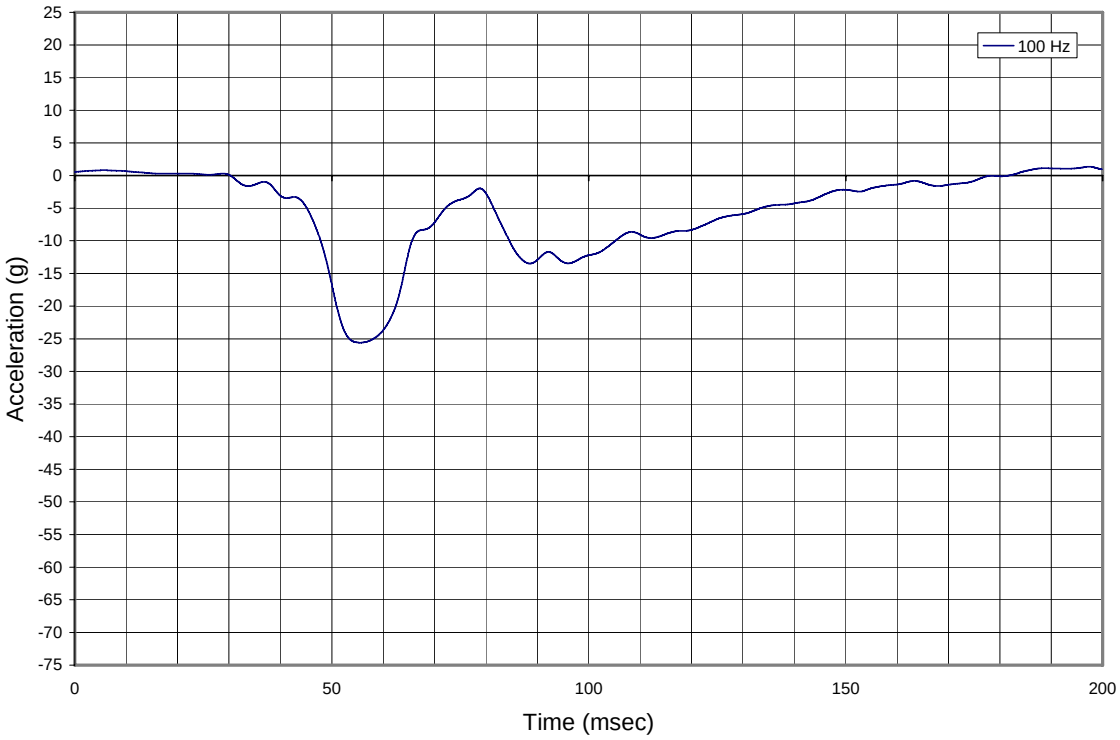

FIGURE B-71. FRAME 29, ATD 5, ROW 8 SEAT C, PELVIC ACCELERATION

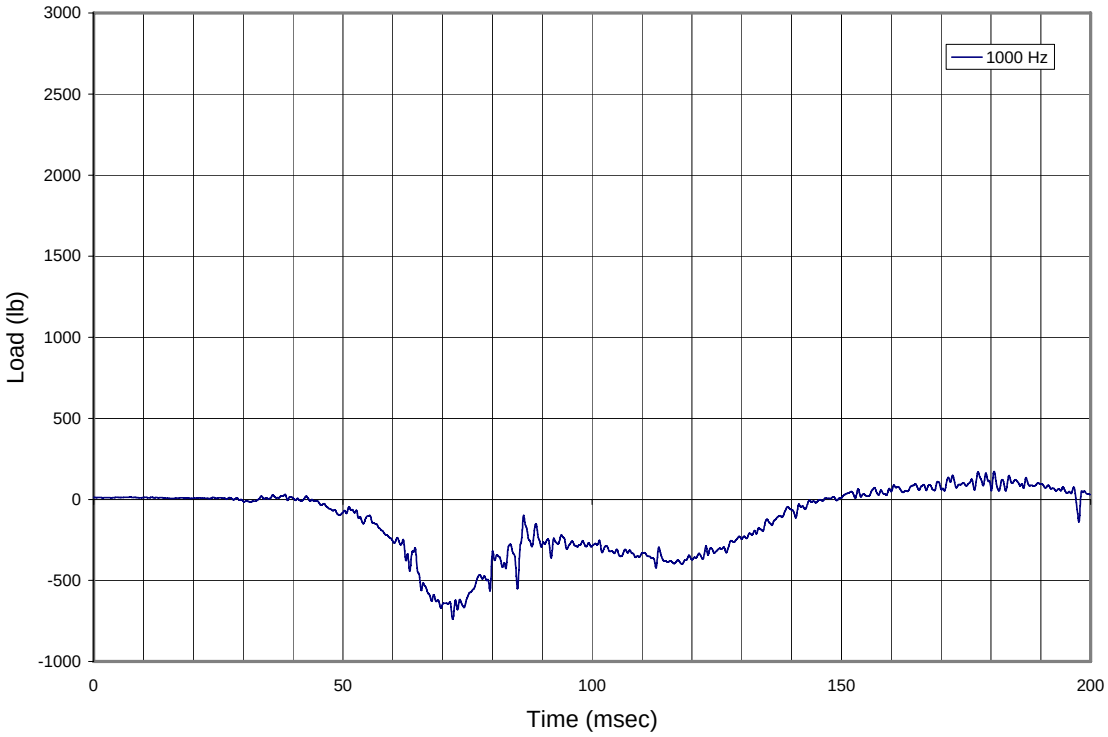

FIGURE B-72. FRAME 29, ATD 5, ROW 8 SEAT C, LUMBAR LOAD

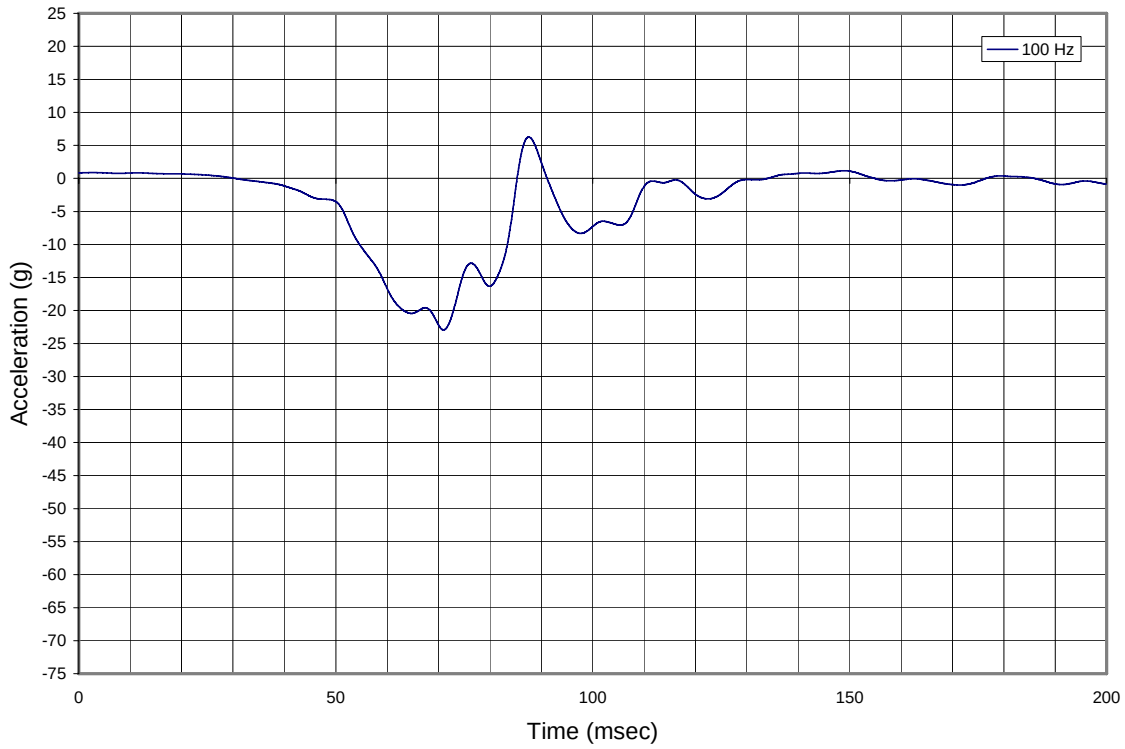

FIGURE B-73. FRAME 34, ATD 6, ROW 11 SEAT C, PELVIC ACCELERATION

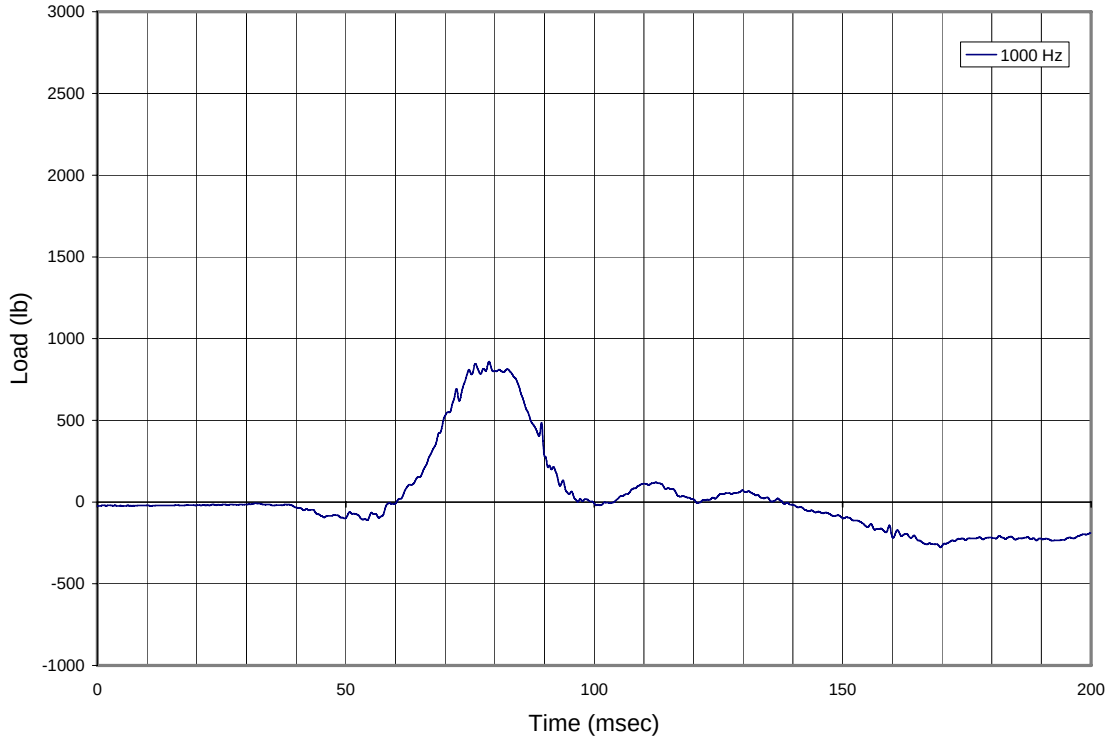

FIGURE B-74. FRAME 34, ATD 6, ROW 11 SEAT C, LUMBAR LOAD

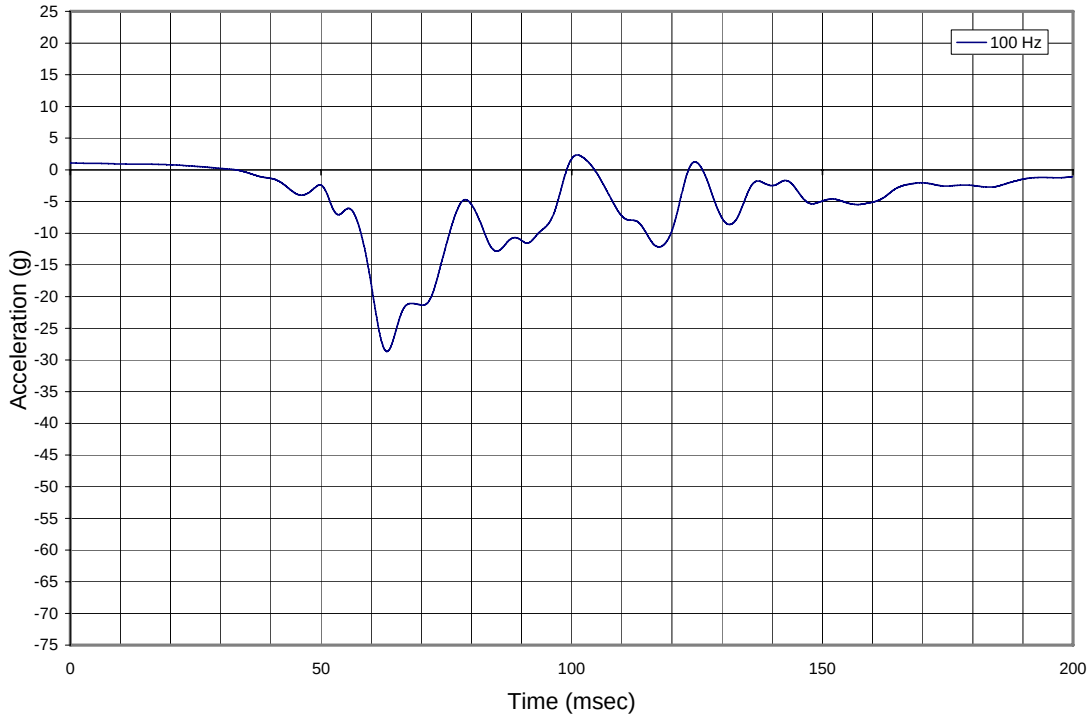

FIGURE B-75. FRAME 39, ATD 7, FLIGHT ATTENDANT SEAT, PELVIC ACCELERATION

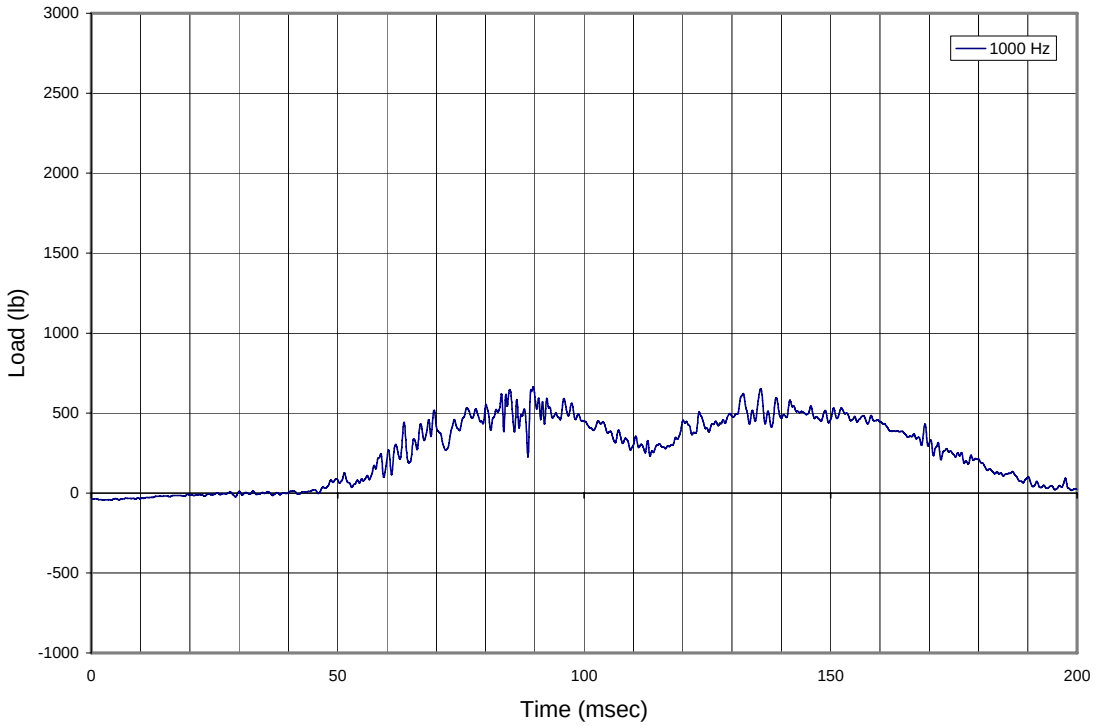

FIGURE B-76. FRAME 39, ATD 7, FLIGHT ATTENDANT SEAT, LUMBAR LOAD

APPENDIX C—PHOTORGAPHIC DOCUMENTATION

C.1 PRETEST PHOTOGRAPHS—ATR 42-300—EXTERIOR.

FIGURE C-1. ATR 42-300—TOP VIEW

FIGURE C-2. ATR 42-300—FRONT VIEW

FIGURE C-3. ATR 42-300—FRONT RIGHT QUARTER

FIGURE C-4. ATR 42-300—RIGHT SIDE

FIGURE C-5. ATR 42-300—REAR RIGHT QUARTER

FIGURE C-6. ATR 42-300—REAR LEFT QUARTER

FIGURE C-7. ATR 42-300—LEFT SIDE

FIGURE C-8. ATR 42-300—FRONT LEFT QUARTER

FIGURE C-9. LANDING GEAR HOUSING—RIGHT SIDE

FIGURE C-10. LANDING GEAR HOUSING—LEFT SIDE

FIGURE C-11. LANDING GEAR HOUSING—CLOSE-UP—LEFT SIDE

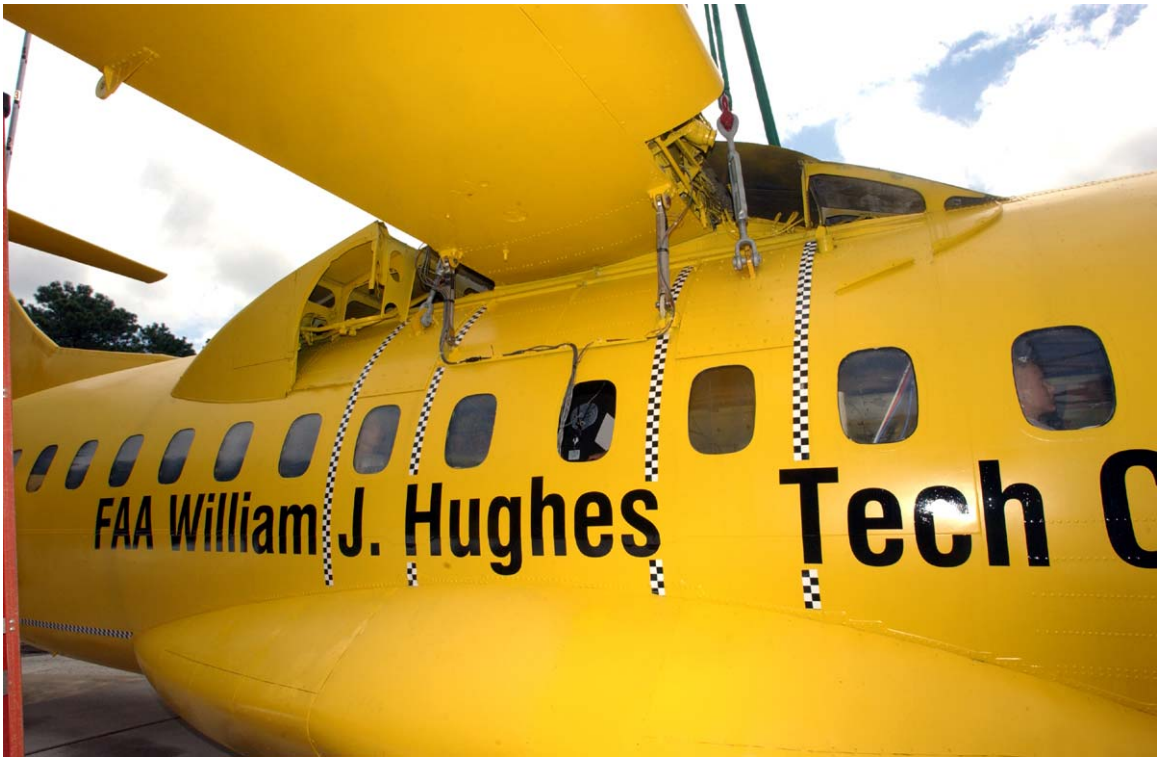

FIGURE C-12. WING ATTACHMENTS—RIGHT SIDE

FIGURE C-13. WING ATTACHMENTS—RIGHT SIDE CLOSE-UP

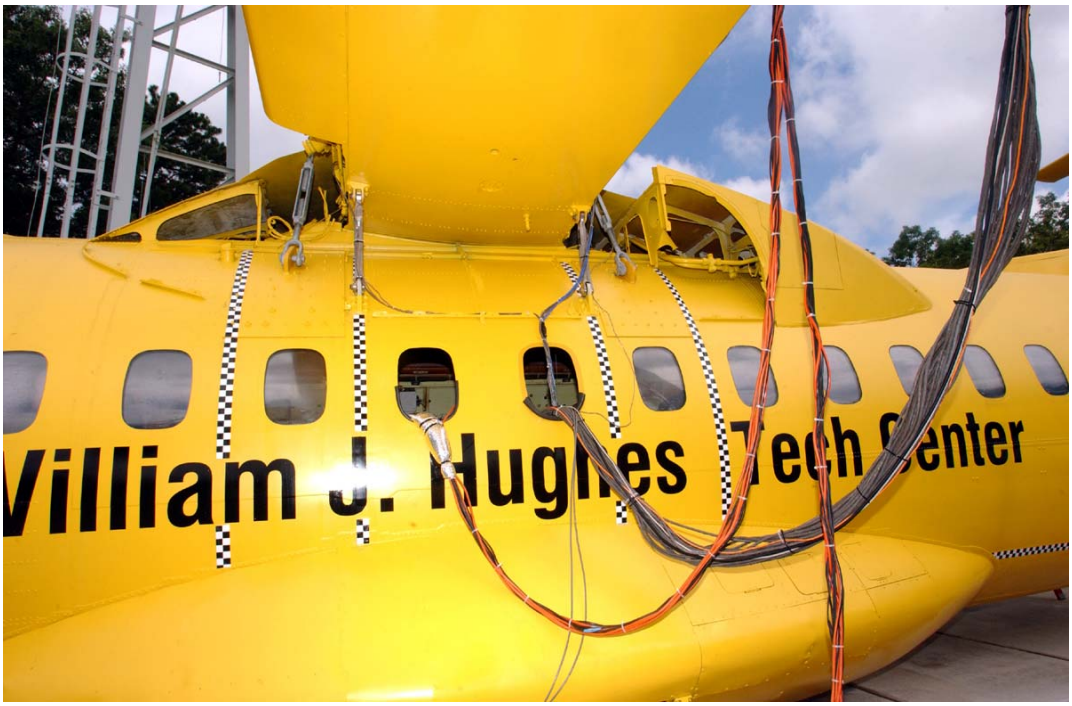

FIGURE C-14. WING ATTACHMENTS—LEFT SIDE

FIGURE C-15. WING ATTACHMENTS—LEFT SIDE CLOSE-UP

FIGURE C-16. CARGO DOOR

FIGURE C-17. SIMULATED ENGINE—RIGHT SIDE

FIGURE C-18. REAR BULKHEAD—CLOSE-UP

FIGURE C-19. CABLES AND TURNBUCKLES

C.2 PRETEST PHOTOGRAPHS—ATR 42-300—INTERIOR.

FIGURE C-20. FLOOR TRACKS—AFT LOOKING FORWARD

FIGURE C-21. FLOOR TRACKS—FORWARD LOOKING AFT

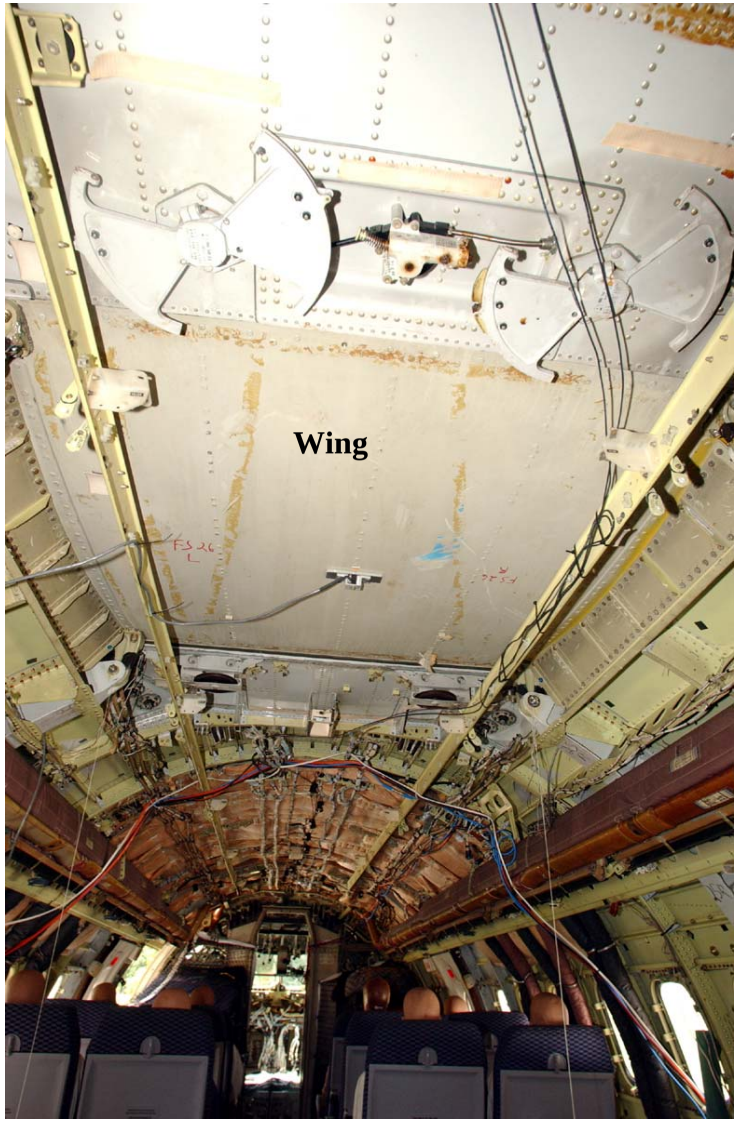

FIGURE C-22. CEILING—AFT LOOKING FORWARD

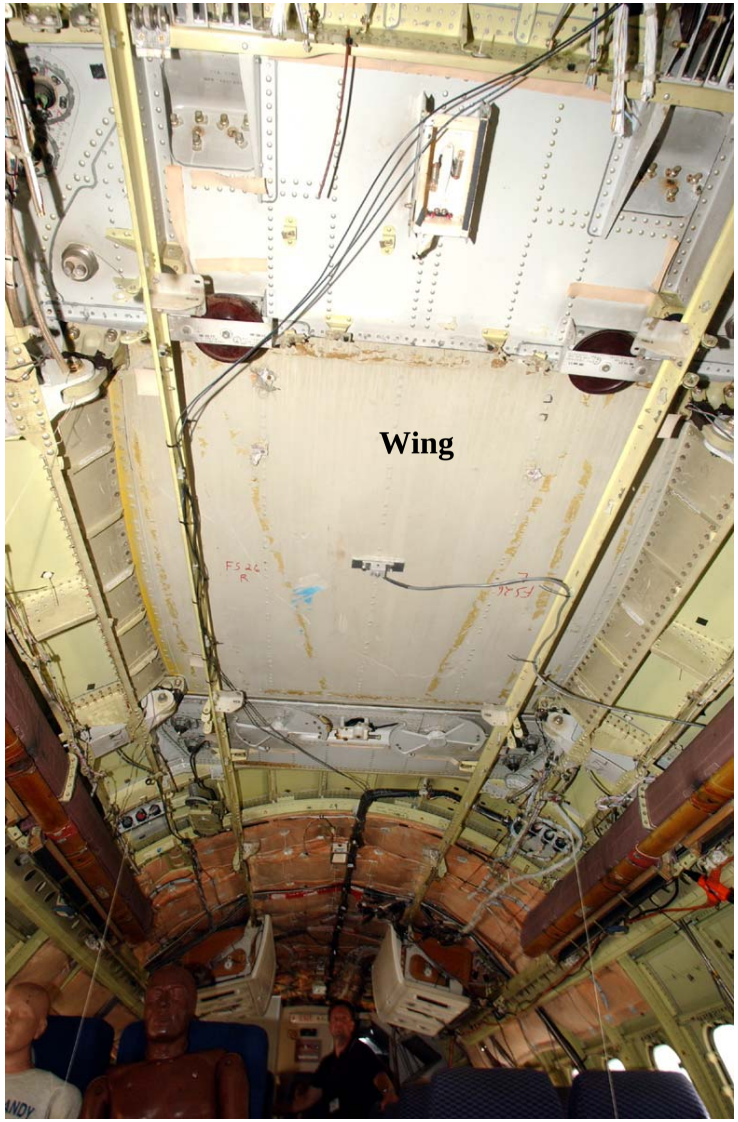

FIGURE C-23. CEILING—FORWARD LOOKING AFT

FIGURE C-24. OVERHEAD STOWAGE BIN—LEFT SIDE

FIGURE C-25. OVERHEAD STOWAGE BIN—RIGHT SIDE

(a) Frame 27 Wing Attachment

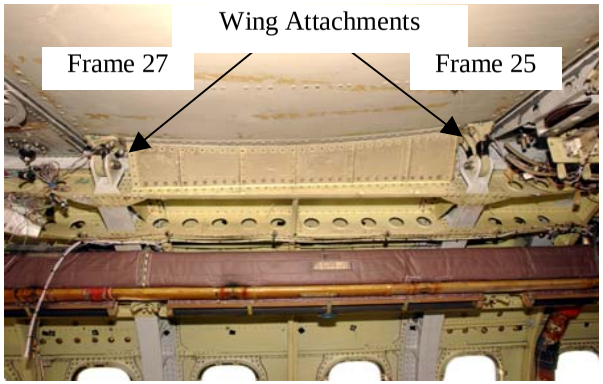

(b) Wing Attachments

Forward

(c) Frame 25 Wing Attachment

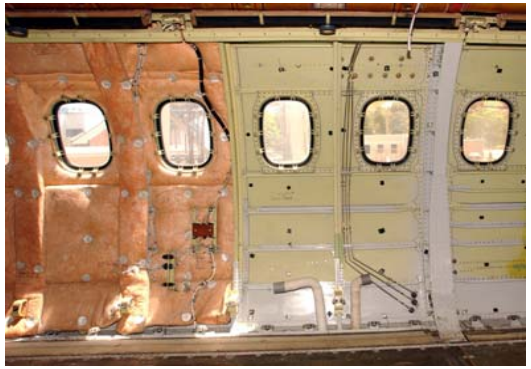

(d) Frames 31-27

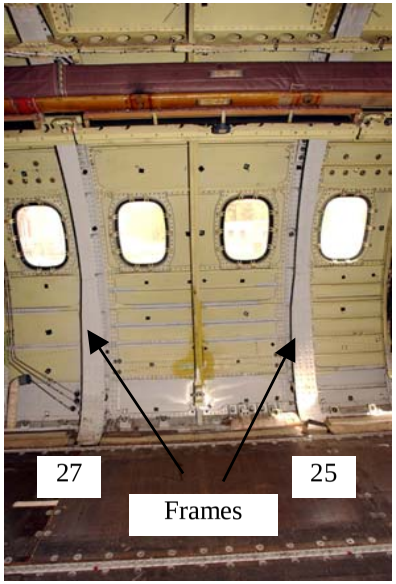

(e) Frames 27-25

(f) Frames 25-21

FIGURE C-26. INNER WING ATTACHMENTS AND SIDEWALLS—LEFT SIDE

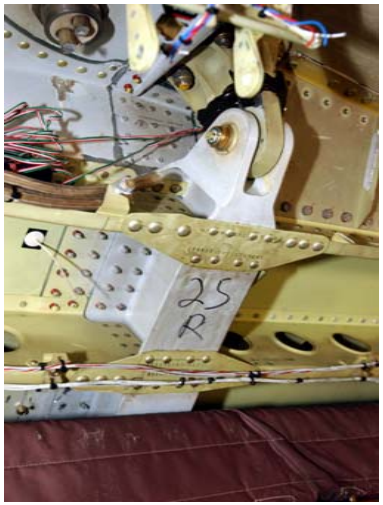

(a) Frame 25 Wing Attachment

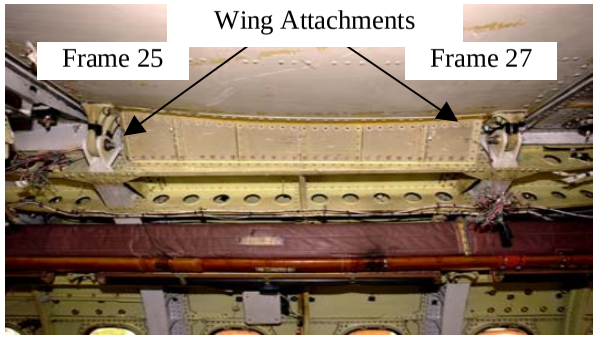

(b) Wing Attachments

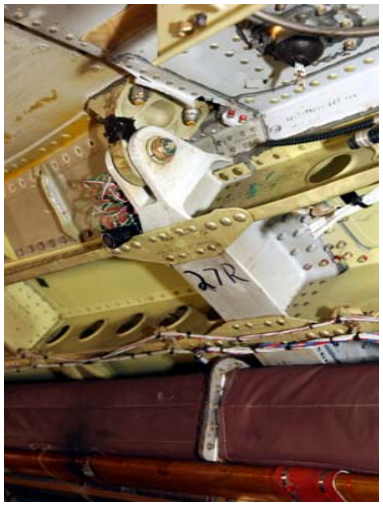

(c) Frame 27 Wing Attachment

Forward

(d) Frames 19-25

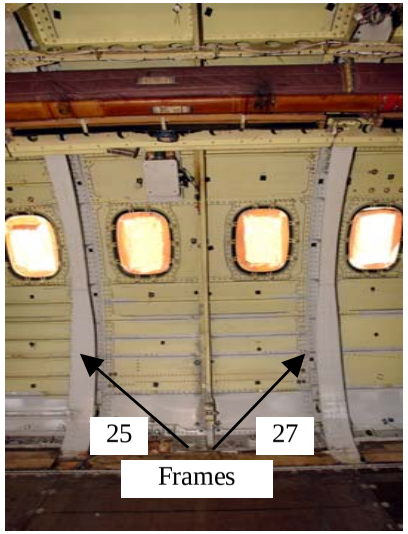

(e) Frames 25-27

(f) Frames 27-32

FIGURE C-27. INNER WING ATTACHMENTS AND SIDEWALLS—RIGHT SIDE

FIGURE C-28. FRONT CABIN

FIGURE C-29. REAR CABIN

(a) Forward Luggage—Left Side

(b) Forward Luggage—Right Side

(c) From Center of Cabin

(d) From Rear of Cabin

FIGURE C-30. CABIN—AFT LOOKING FORWARD

(e) Cockpit

(f) Pilot

(g) Copilot

(h) Forward Section of Cabin

FIGURE C-30. CABIN—AFT LOOKING FORWARD (Continued)

(a) Row 2-3 Right Side

(b) Rows 2-3 Left Side

(c) Row 2

(d) From Cockpit—Row 1

FIGURE C-31. CABIN—FORWARD LOOKING AFT

(e) From Center of Cabin

(f) Row 7 Right Side

(g) Row 7 Left Side

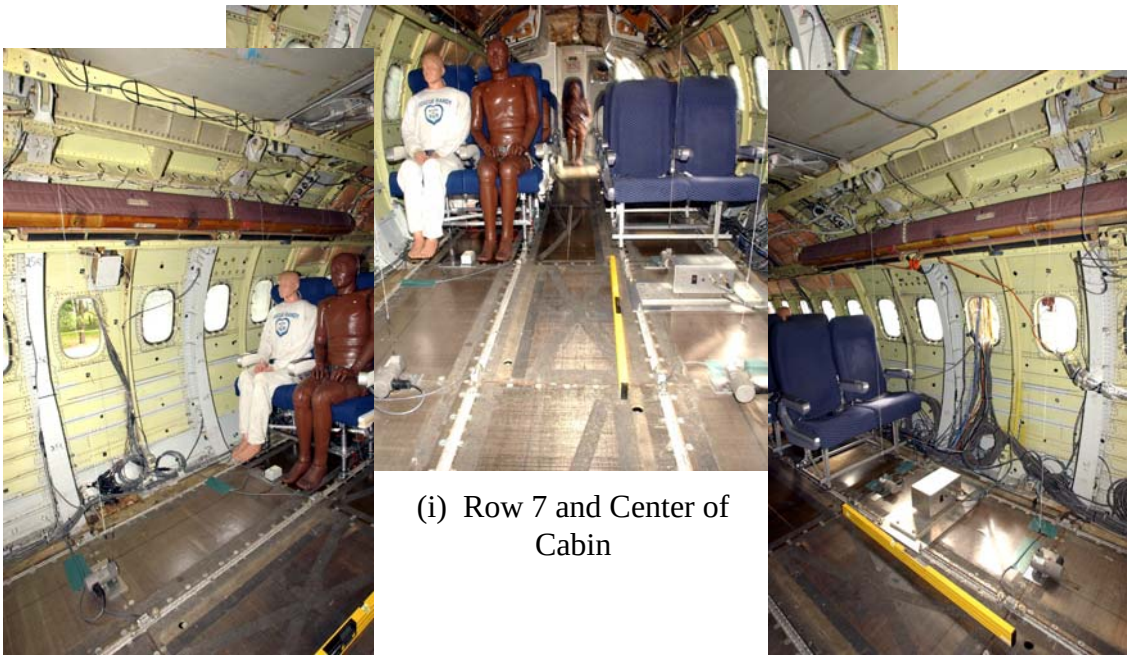

(i) Row 7 and Center of Cabin

(h) Frames 25-27 Right Side

(j) Frames 25-27 Left Side

FIGURE C-31. CABIN—FORWARD LOOKING AFT (Continued)

(k) Flight Attendant Seat

(l) Rows 9-11 Right Side

(m) Rows 9-11 Left Side

(n) Rows 8-11 Right Side

(o) Rows 8-11 Left Side

FIGURE C-31. CABIN—FORWARD LOOKING AFT (Continued)

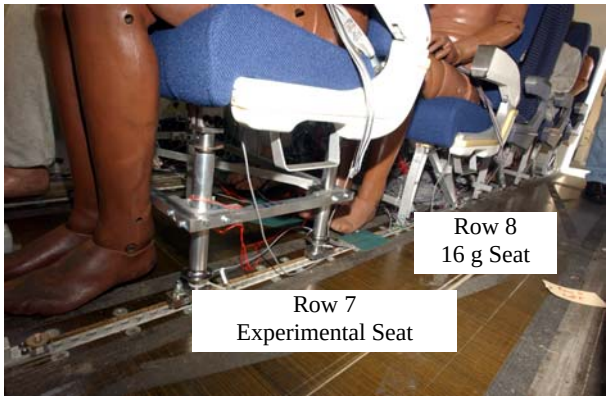

(a) Rows 7 and 8 Right Side

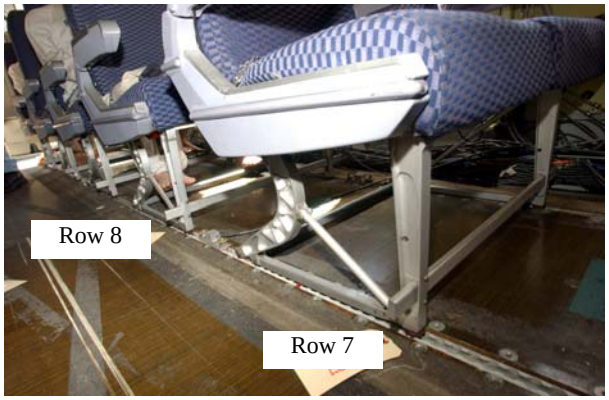

(b) Rows 7 and 8 Left Side

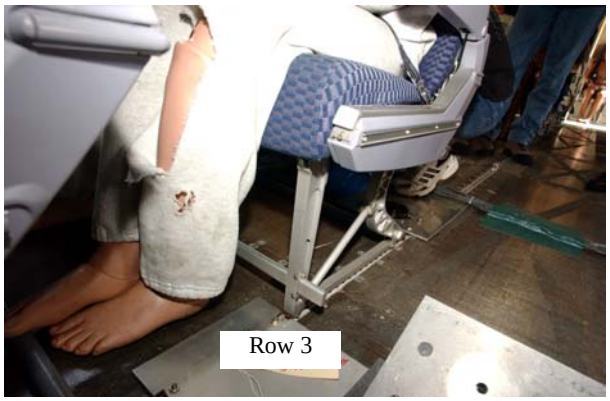

(c) Row 3 Right Side

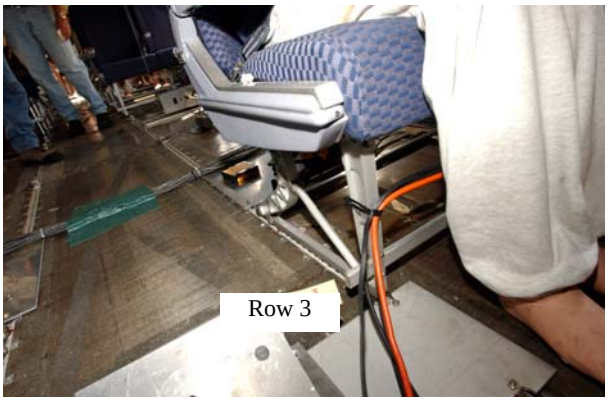

(d) Row 3 Left Side

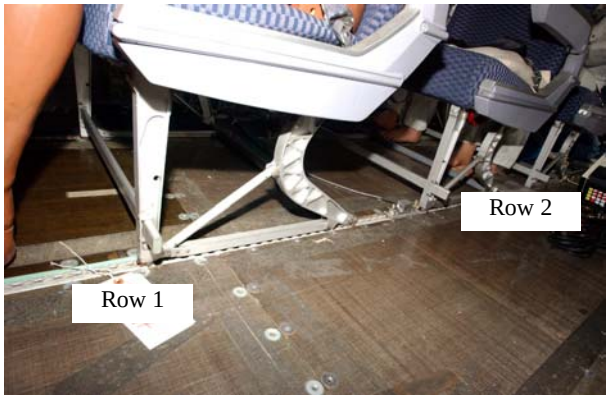

(e) Rows 1 and 2 Right Side

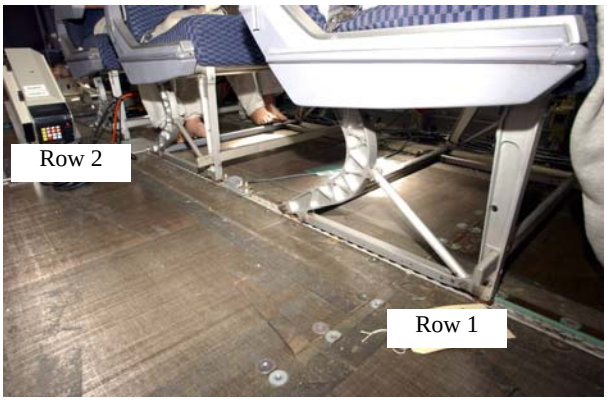

(f) Rows 1 and 2 Left Side

FIGURE C-32. SEAT DETAILS

(g) Flight Attendant Seat

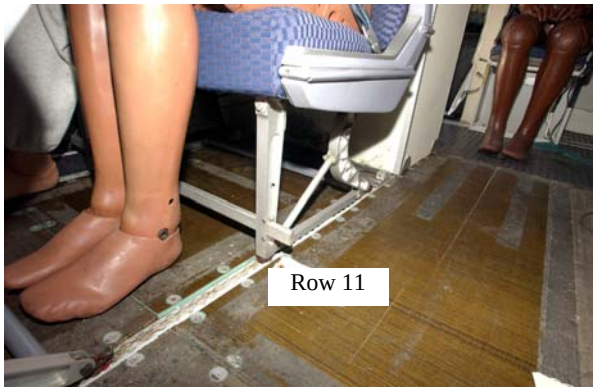

(h) Row 11 Right Side

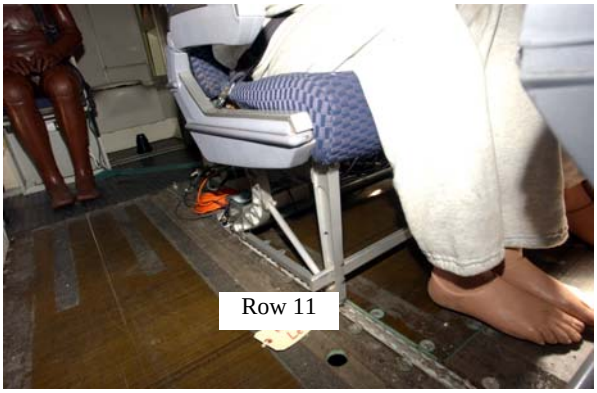

(i) Row 11 Left Side

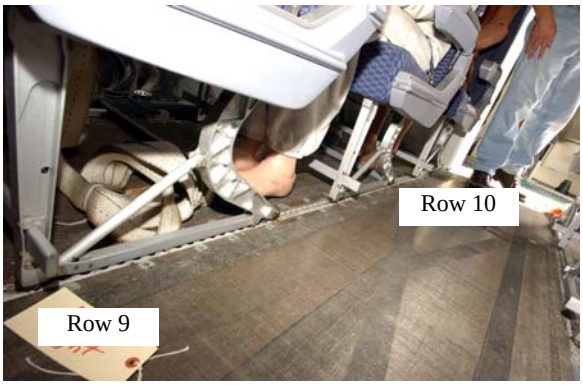

(j) Rows 9 and 10 Right Side

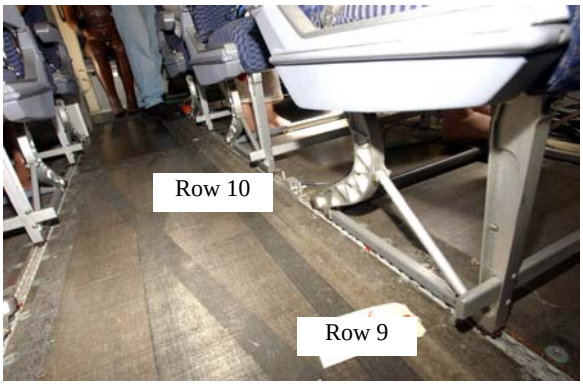

(k) Rows 9 and 10 Left Side

FIGURE C-32. SEAT DETAILS (Continued)

(l) Tenryu Modified 16 g Seat

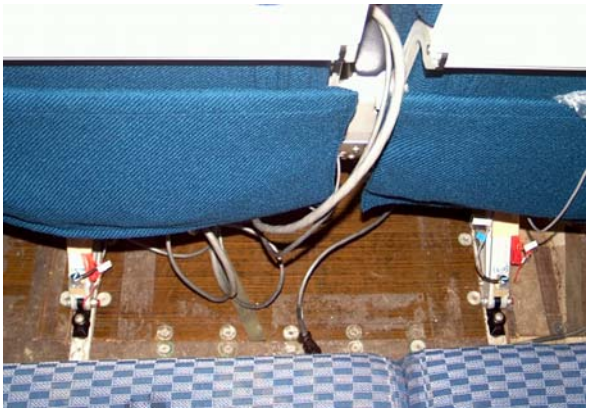

(m) Tenryu Modified 16-G Seat Legs

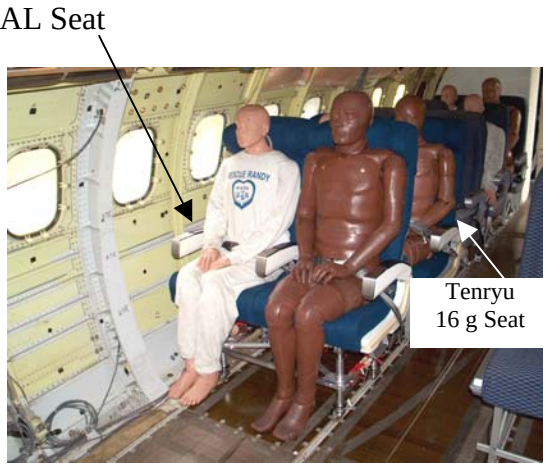

(n) NAL Experimental Seat
Tenryu Modified 16 g Seat

(o) Data Acquisition System for
NAL-Tenryu Seats

(p) NAL Experimental Seat

FIGURE C-32. SEAT DETAILS (Continued)

C.3 PRETEST PHOTOGRAPHS—EXIT DOORS.

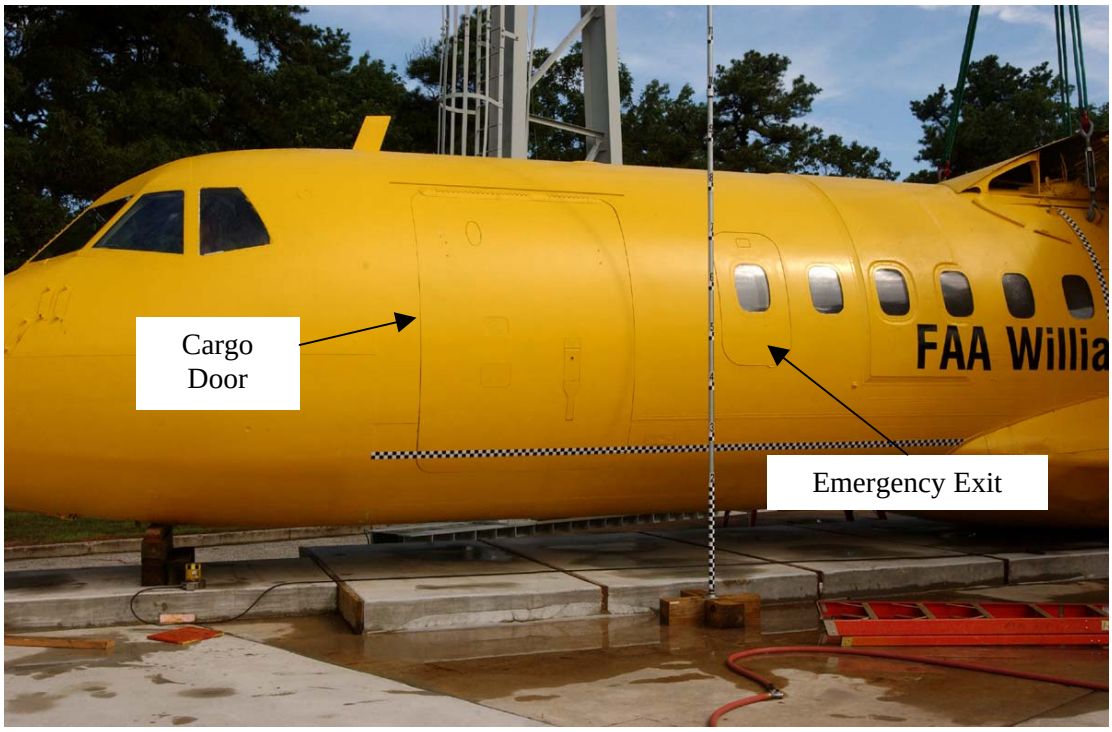

FIGURE C-33. EMERGENCY EXIT AND CARGO DOOR—LEFT FRONT EXTERIOR

FIGURE C-34. EMERGENCY EXIT AND CARGO DOOR—LEFT FRONT INTERIOR

FIGURE C-35. EMERGENCY EXIT—RIGHT FRONT EXTERIOR

FIGURE C-36. EMERGENCY EXIT—RIGHT FRONT INTERIOR

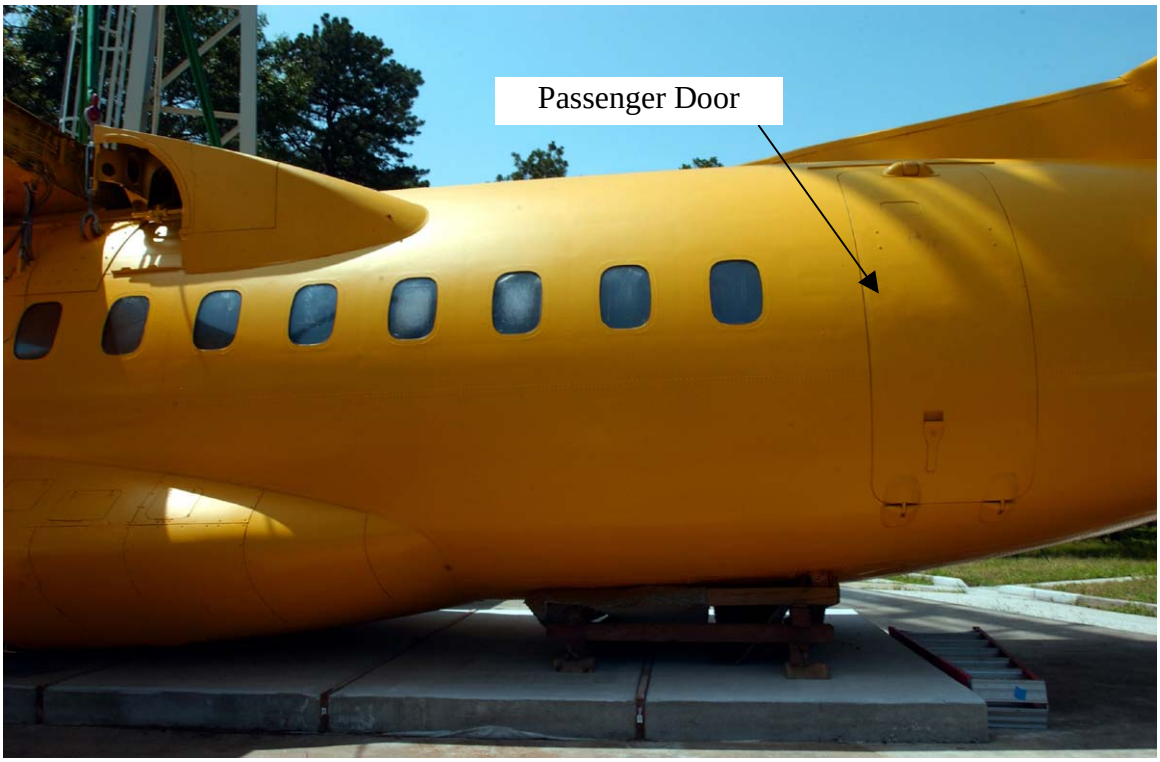

FIGURE C-37. MAIN PASSENGER DOOR—LEFT SIDE EXTERIOR

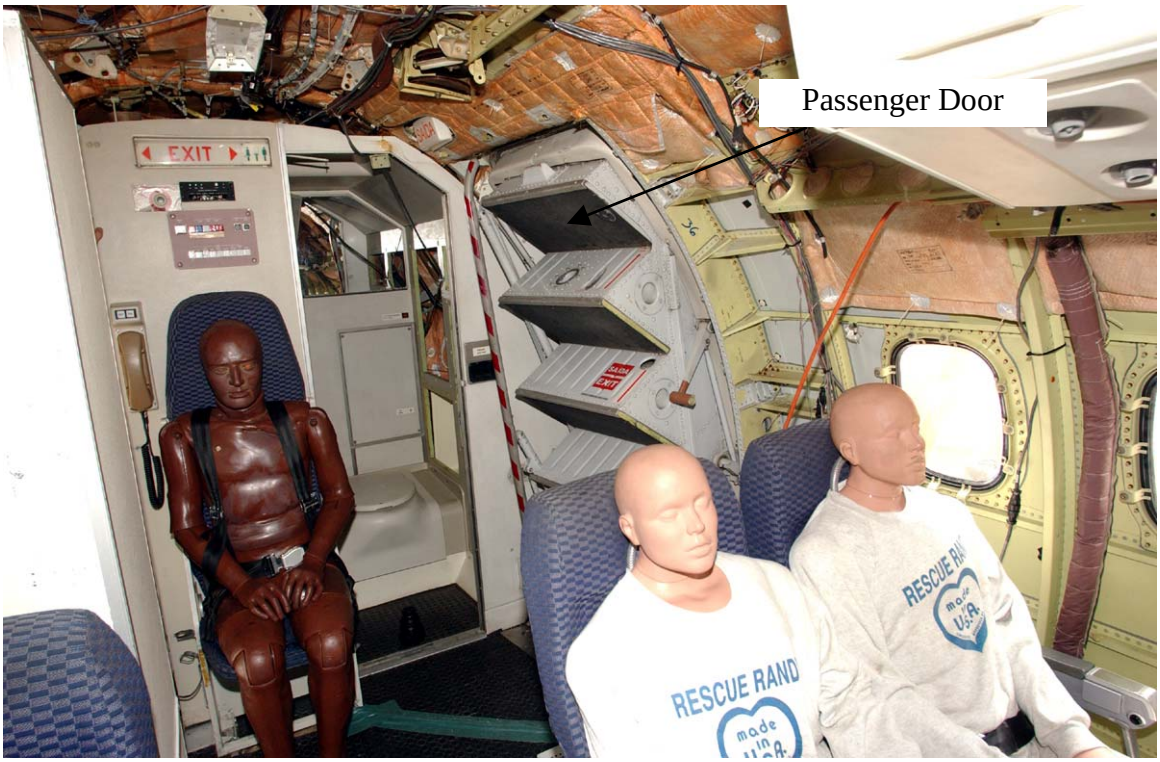

FIGURE C-38. MAIN PASSENGER DOOR—LEFT SIDE INTERIOR

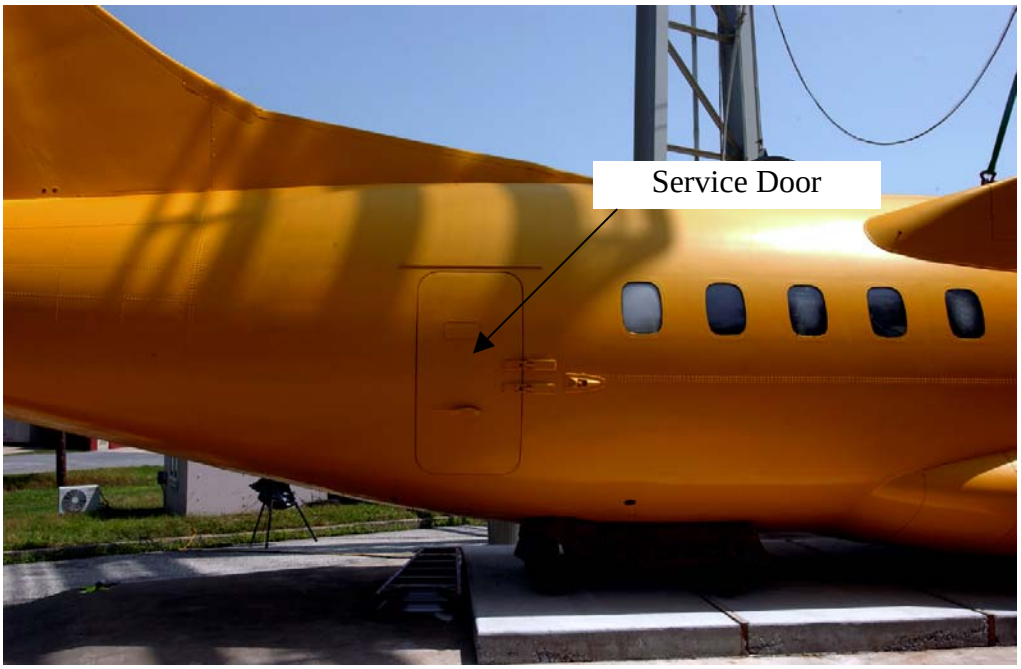

FIGURE C-39. SERVICE DOOR—RIGHT SIDE EXTERIOR

FIGURE C-40. SERVICE DOOR—RIGHT SIDE INTERIOR

C.4 POSTTEST PHOTOGRAPHS—ATR 42-300—EXTERIOR.

FIGURE C-41. RIGHT SIDE—FRONT

FIGURE C-42. RIGHT SIDE—REAR

FIGURE C-43. RIGHT SIDE—FORWARD LOOKING AFT VIEW 1

FIGURE C-44. RIGHT SIDE—FORWARD LOOKING AFT VIEW 2

FIGURE C-45. RIGHT SIDE—FORWARD LOOKING AFT VIEW 3

FIGURE C-46. RIGHT SIDE—FORWARD LOOKING AFT VIEW 4

FIGURE C-47. RIGHT SIDE

FIGURE C-48. RIGHT SIDE—AFT LOOKING FORWARD

FIGURE C-49. RIGHT SIDE, CLOSE-UP

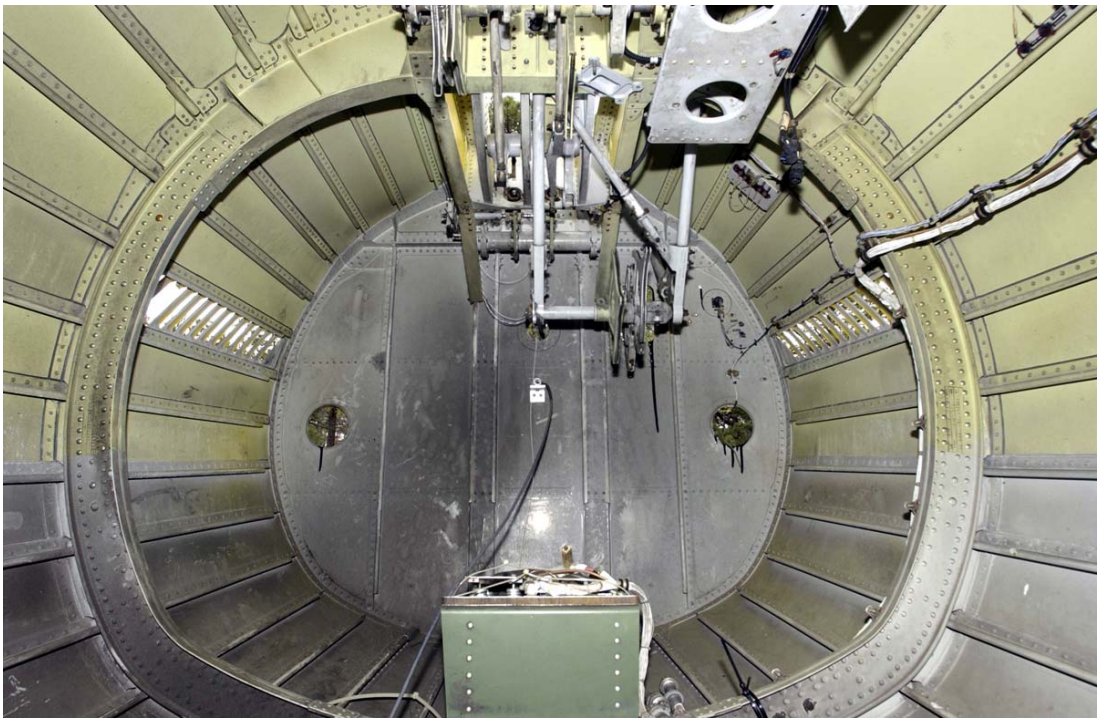

FIGURE C-50. AFT PRESSURE BULKHEAD LOOKING FORWARD

FIGURE C-51. RIGHT SIDE FUSELAGE—AFT LOOKING FORWARD

FIGURE C-52. RIGHT SIDE FUSELAGE—AFT LOOKING FORWARD, CLOSE-UP

FIGURE C-53. RIGHT SIDE WING—AFT LOOKING FORWARD VIEW 1

FIGURE C-54. RIGHT SIDE WING—AFT LOOKING FORWARD VIEW 2

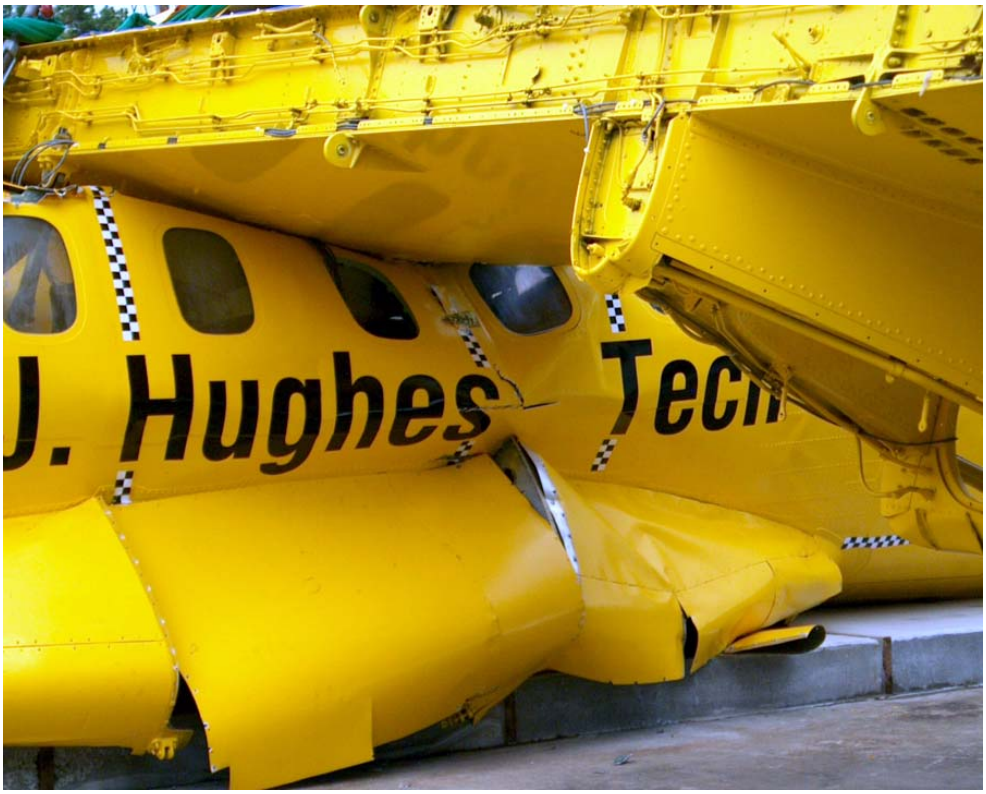

FIGURE C-55. RIGHT SIDE WING—AFT LOOKING FORWARD VIEW 3

FIGURE C-56. RIGHT SIDE WING—AFT LOOKING FORWARD VIEW 4

FIGURE C-57. RIGHT SIDE—TOP VIEW

FIGURE C-58. RIGHT SIDE—WING REMOVED TOP VIEW 1

FIGURE C-59. FRONT RIGHT QUARTER VIEW—WING REMOVED TOP VIEW 2

FIGURE C-60. FRONT RIGHT QUARTER VIEW—WING REMOVED

FIGURE C-61. RIGHT SIDE—WING REMOVED

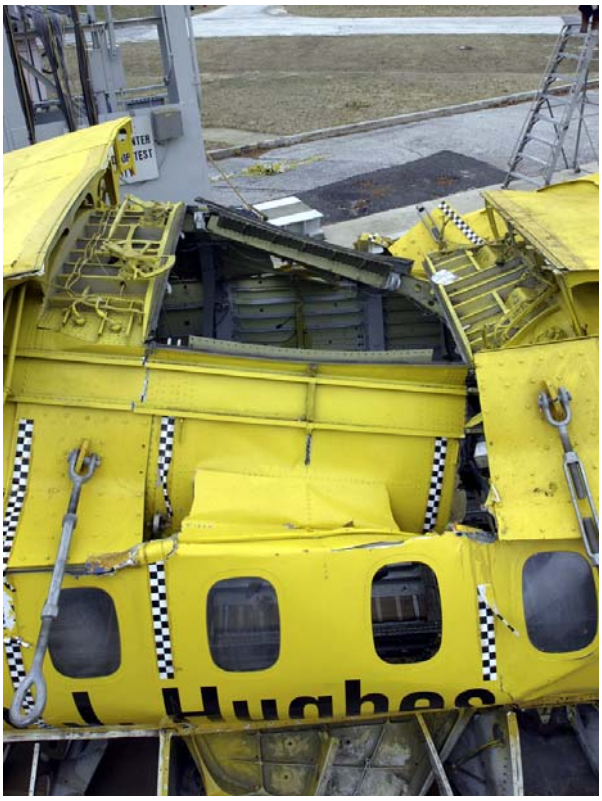

FIGURE C-62. RIGHT SIDE—WING REMOVED, CLOSE-UP

(a) Overall

(b) Close-Up

(c) Aft

(d) Forward

FIGURE C-63. LANDING GEAR HOUSING—RIGHT SIDE

FIGURE C-64. LEFT SIDE—FRONT

FIGURE C-65. LEFT SIDE—REAR

FIGURE C-66. FRONT LEFT QUARTER

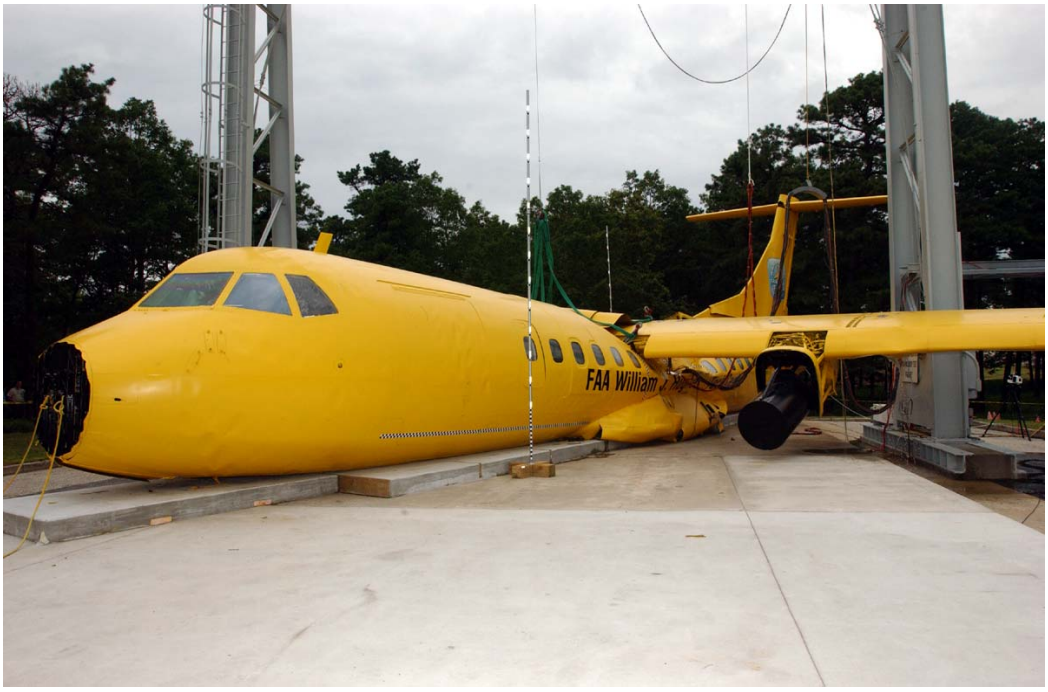

FIGURE C-67. FRONT LEFT QUARTER, CLOSE-UP

FIGURE C-68. LEFT SIDE—FORWARD LOOKING AFT

FIGURE C-69. FUEL TANK LEAK—LEFT SIDE

FIGURE C-70. LEFT SIDE FUSELAGE—FORWARD LOOKING AFT

FIGURE C-71. LEFT SIDE—FORWARD LOOKING AFT, WING REMOVED

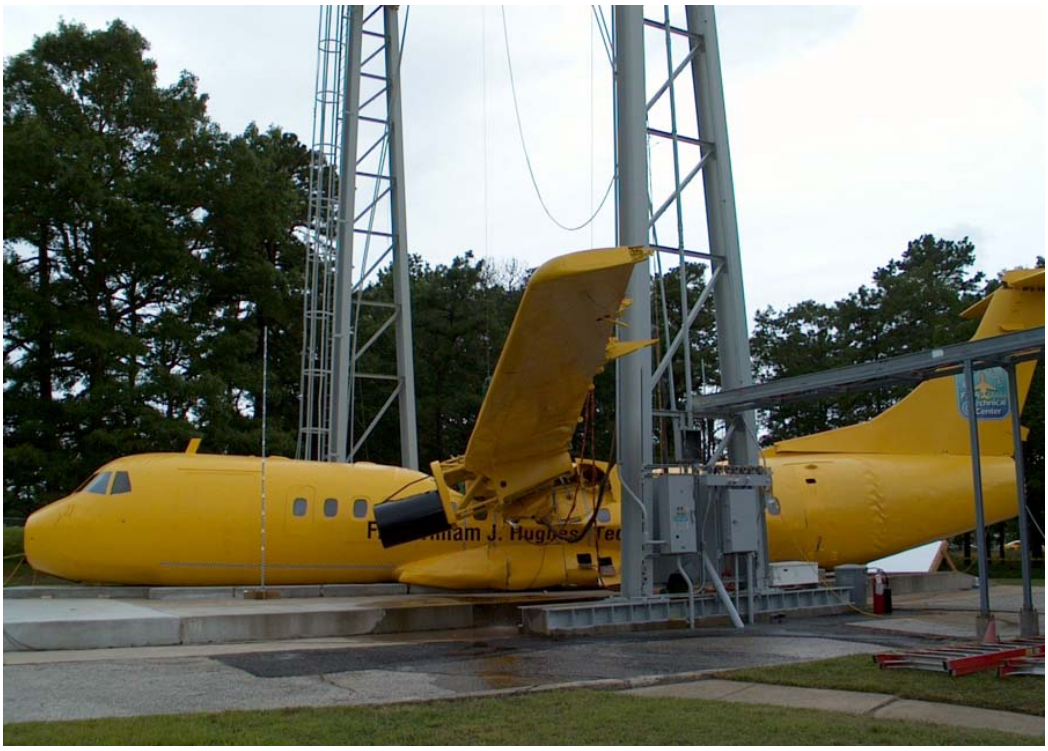

FIGURE C-72. LEFT SIDE VIEW 1

FIGURE C-73. LEFT SIDE VIEW 2

FIGURE C-74. LEFT SIDE VIEW 3

FIGURE C-75. LEFT SIDE—FUEL TANK LEAK

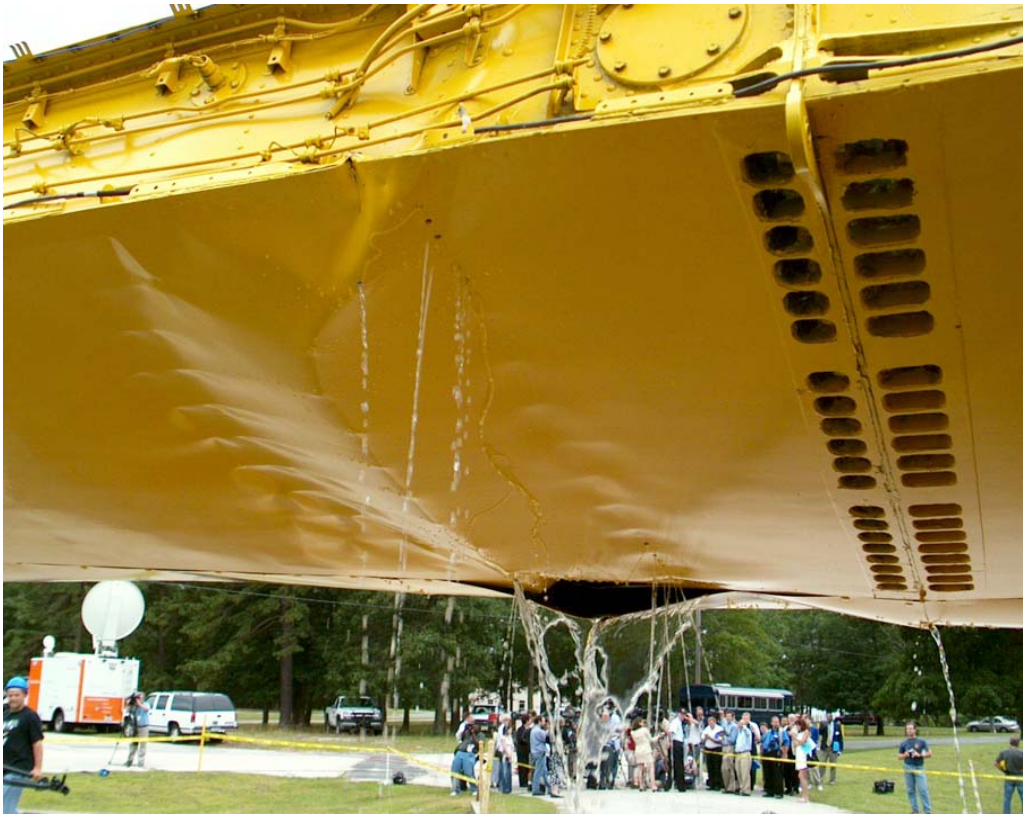

FIGURE C-76. LEFT SIDE FUEL TANK LEAK—AFT LOOKING FORWARD

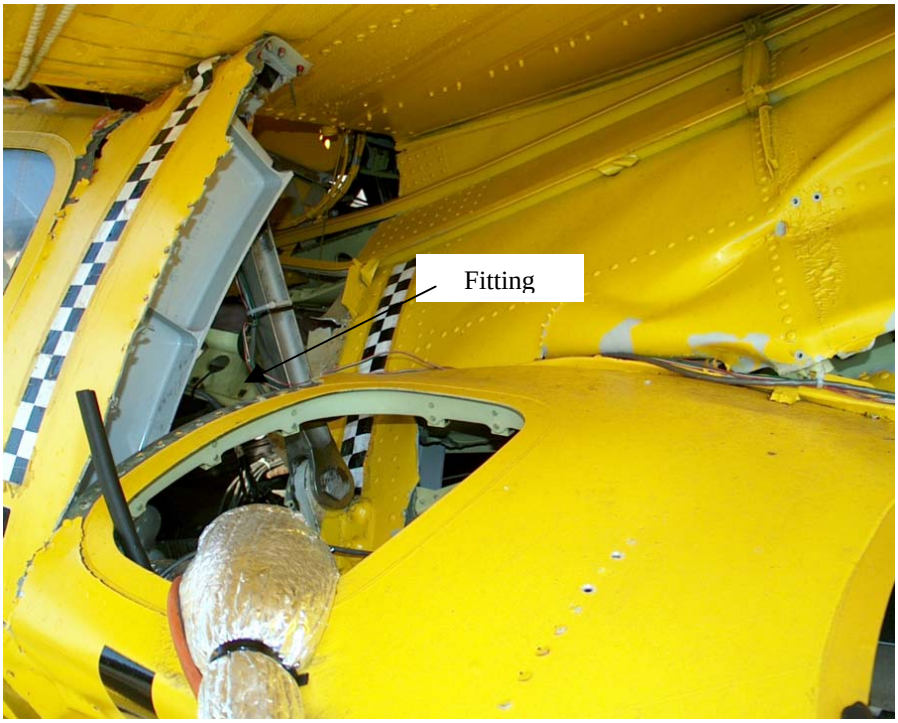

FIGURE C-77. LEFT SIDE—FORWARD WING FITTING

FIGURE C-78. LEFT SIDE—AFT LOOKING FORWARD VIEW 1

FIGURE C-79. LEFT SIDE—AFT LOOKING FORWARD VIEW 2

FIGURE C-80. LEFT SIDE—AFT LOOKING FORWARD VIEW 3

FIGURE C-81. LEFT SIDE—AFT LOOKING FORWARD VIEW 4

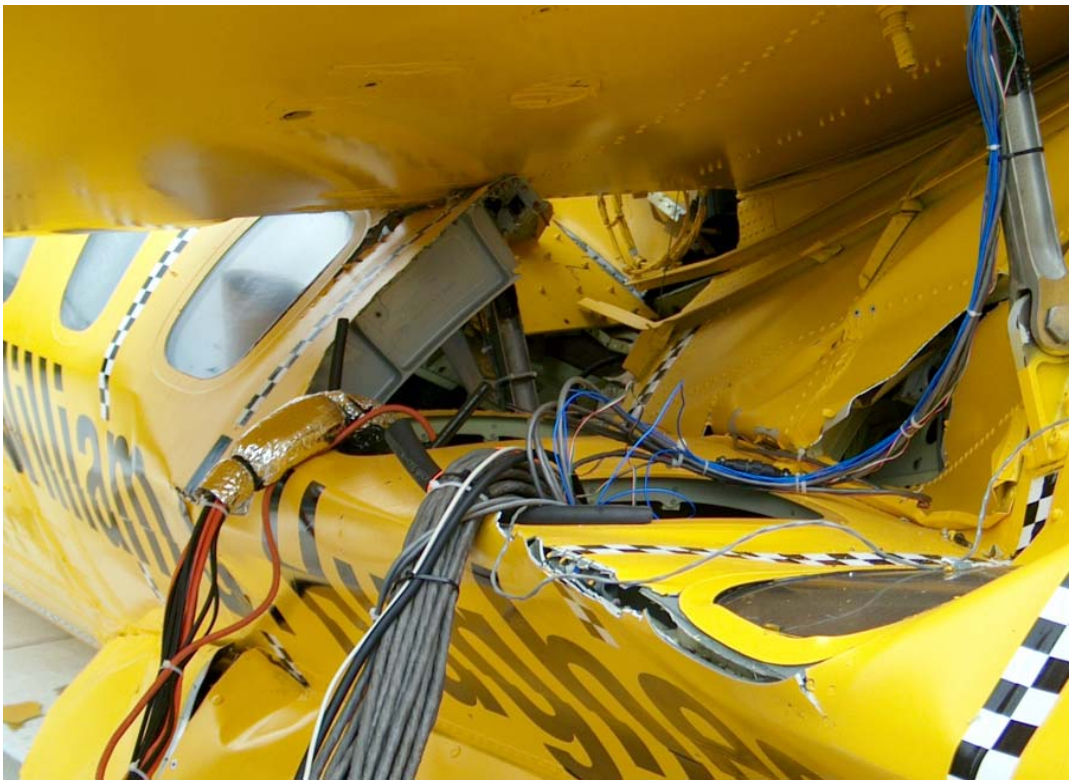

FIGURE C-82. LEFT SIDE—AFT LOOKING FORWARD VIEW 5

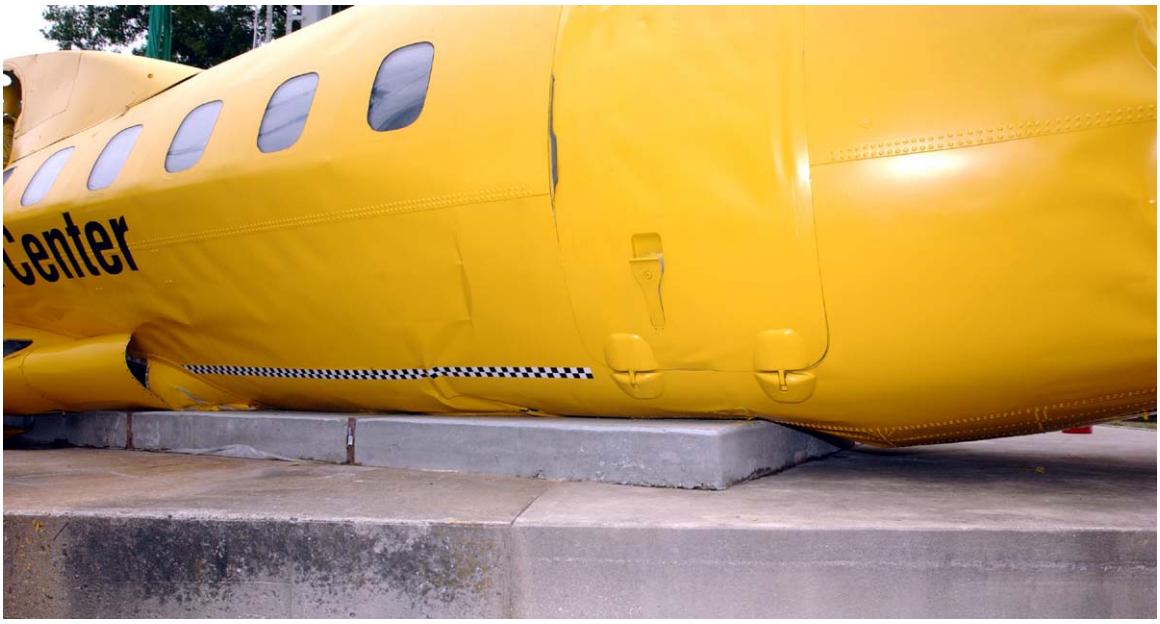

FIGURE C-83. LEFT SIDE—AFT LOOKING FORWARD VIEW 6

FIGURE C-84. LEFT SIDE—REAR, PASSENGER DOOR

FIGURE C-85. LEFT SIDE—REAR, PASSENGER DOOR CLOSE-UP

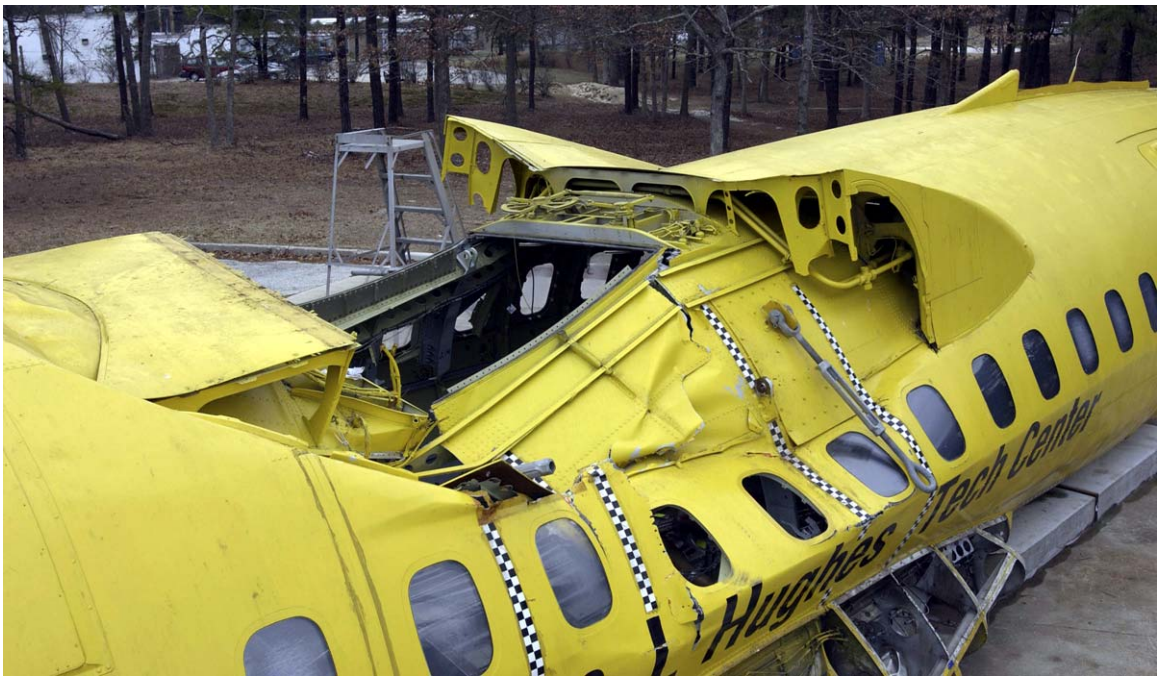

FIGURE C-86. LEFT SIDE—WING REMOVED, TOP VIEW 1

FIGURE C-87. LEFT SIDE—WING REMOVED, TOP VIEW 2

a. Overall

b. Close-Up

c. Forward

d. Aft

FIGURE C-88. LANDING GEAR HOUSING—LEFT SIDE

C.5 POSTTEST PHOTOGRAPHS—ATR 42-300 FLOOR AND FLOOR TRACKS.

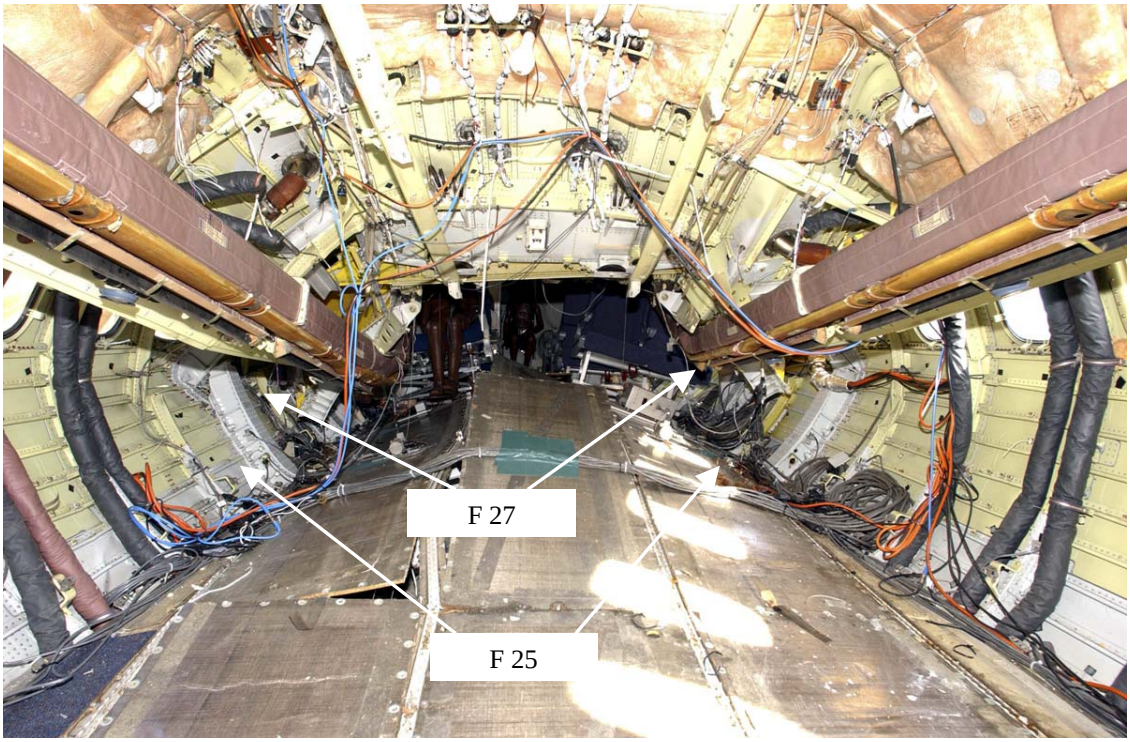

FIGURE C-89. FLOOR TRACKS—FORWARD LOOKING AFT

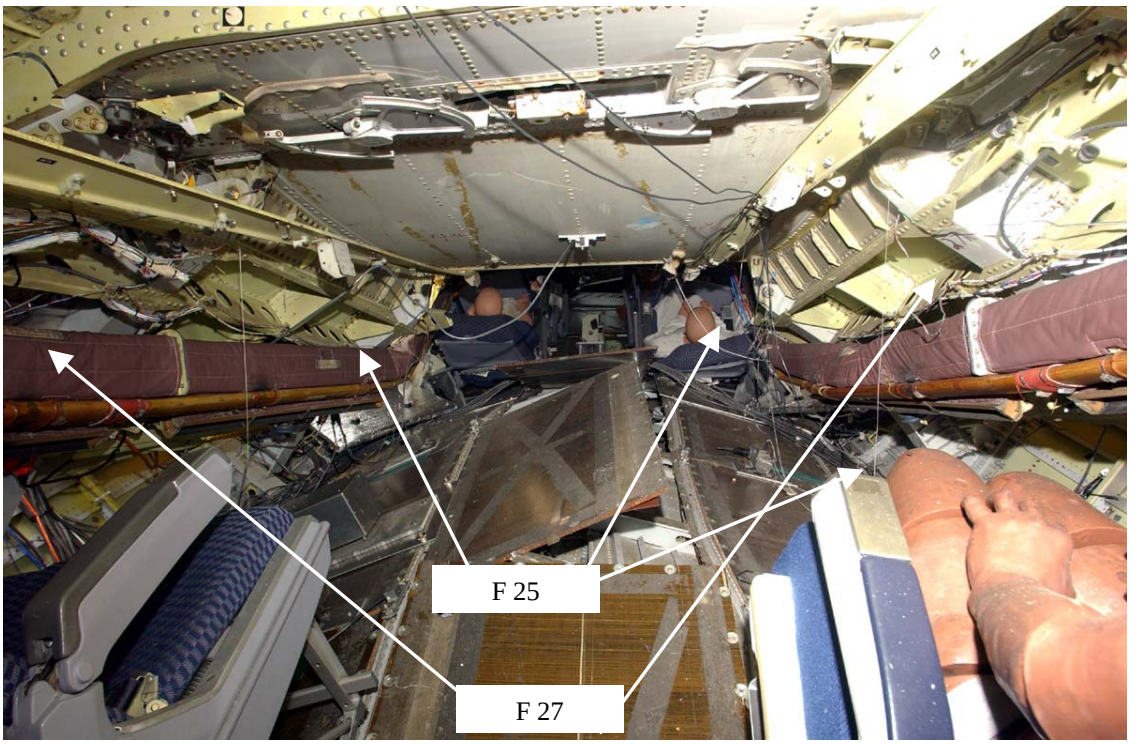

FIGURE C-90. FLOOR TRACKS—AFT LOOKING FORWARD

FIGURE C-91. FLOOR TRACKS, WING REMOVED—
FORWARD LOOKING AFT

FIGURE C-92. FLOOR TRACKS, WING REMOVED—
AFT LOOKING FORWARD

FIGURE C-93. FLOOR TRACKS, PANALS REMOVED—FORWARD LOOKING AFT

FIGURE C-94. FLOOR TRACKS, PANALS REMOVED—AFT LOOKING FORWARD

(a) Floor Tracks—Front Cabin

(b) Floor Beam Fractures at Frames 20-22—Right Side

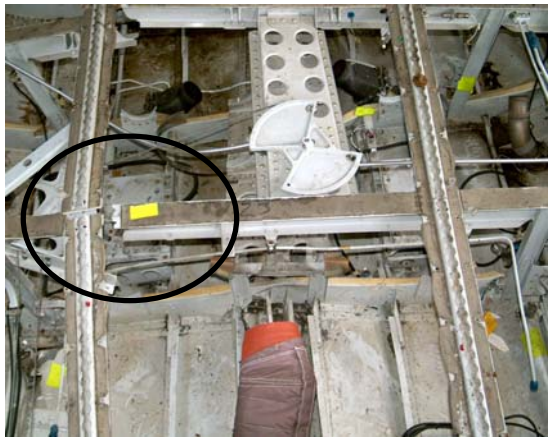

(c) Floor Track Distortion at Frame 23—Center

FIGURE C-95. FLOOR TRACKS AND FLOOR BEAMS, FORWARD CABIN

(a) Floor Tracks at Frames 27-29—Right Side

(b) Landing Gearbox Fractures

(c) Floor Tracks at Frames 30-32—Right Side

(d) Floor Racks—Cabin Rear

FIGURE C-96. FLOOR TRACKS AND FLOOR BEAMS, AFT CABIN

(a) Floor Tracks—Frame 20 Right

(b) Floor Tracks—Frame 20 Left

(c) Floor Tracks—Frame 19 Right

(d) Floor Tracks—Frame 19 Left

(e) Floor Tracks—Frame 18 Right

(f) Floor Tracks—Frame 18 Left

FIGURE C-97. FLOOR TRACKS—FORWARD LOOKING AFT

(g) Floor Tracks—Frame 22 Right

(h) Floor Tracks—Frame 22 Left

(i) Floor Tracks—Frame 21 Right

(j) Floor Tracks—Frame 21 Left

FIGURE C-97. FLOOR TRACKS—FORWARD LOOKING AFT (Continued)

(k) Floor Tracks—Frame 24 Right

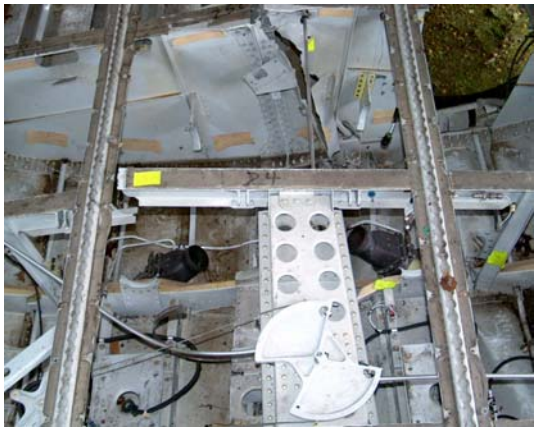

(l) Floor Tracks—Frame 24 Center

(m) Floor Tracks—Frame 24 Left

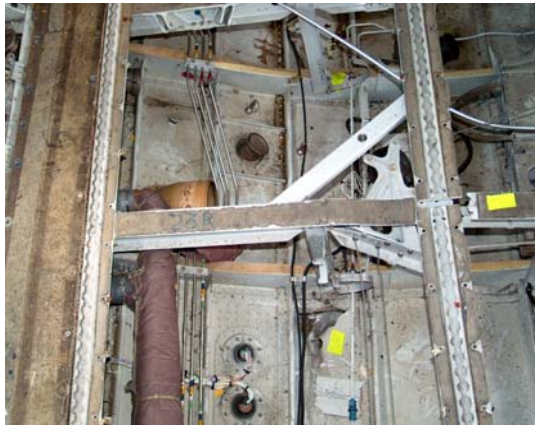

(n) Floor Tracks—Frame 23 Right

(o) Floor Tracks—Frame 23 Center

(p) Floor Tracks—Frame 23 Left

FIGURE C-97. FLOOR TRACKS—FORWARD LOOKING AFT (Continued)

(q) Floor Tracks—Frame 26 Right

(r) Floor Tracks—Frame 26 Center

(s) Floor Tracks—Frame 26 Left

(t) Floor Tracks—Frame 25 Right

(u) Floor Tracks—Frame 25 Center

(v) Floor Tracks—Frame 25 Left

FIGURE C-97. FLOOR TRACKS—FORWARD LOOKING AFT (Continued)

(w) Floor Tracks—Frame 27 Right

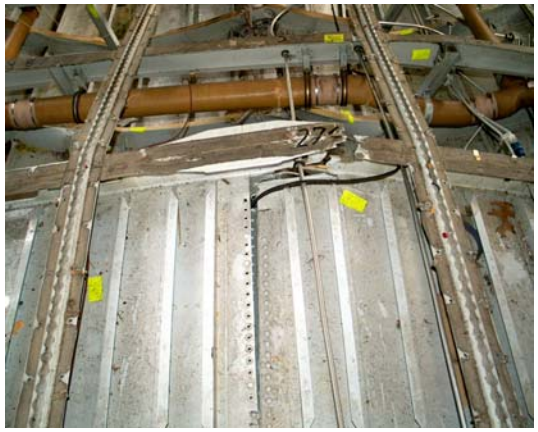

(x) Floor Tracks—Frame 27 Center

(y) Floor Tracks—Frame 27 Left

FIGURE C-97. FLOOR TRACKS—FORWARD LOOKING AFT (Continued)

(a) Floor Tracks—Frame 28 Right

(b) Floor Tracks—Frame 28 Center

(c) Floor Tracks—Frame 28 Left

(d) Floor Tracks—Frame 29 Left

(e) Floor Tracks—Frame 29 Center

(f) Floor Tracks—Frame 29 Right

FIGURE C-98. FLOOR TRACKS—AFT LOOKING FORWARD

(g) Floor Tracks—Frame 30 Left

(h) Floor Tracks—Frame 30 Right

(i) Floor Tracks—Frame 31 Left

(j) Floor Tracks—Frame 31 Right

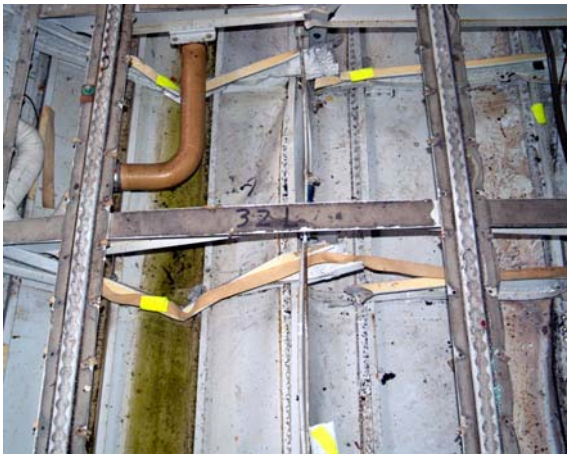

(k) Floor Tracks—Frame 32 Left

(l) Floor Tracks—Frame 32 Right

FIGURE C-98. FLOOR TRACKS—AFT LOOKING FORWARD (Continued)

(m) Floor Tracks—Frame 33 Left

(n) Floor Tracks—Frame 33 Right

(o) Floor Tracks—Frame 34 Left

(p) Floor Tracks—Frame 34 Right

(q) Floor Tracks—Frames 37-35 Left

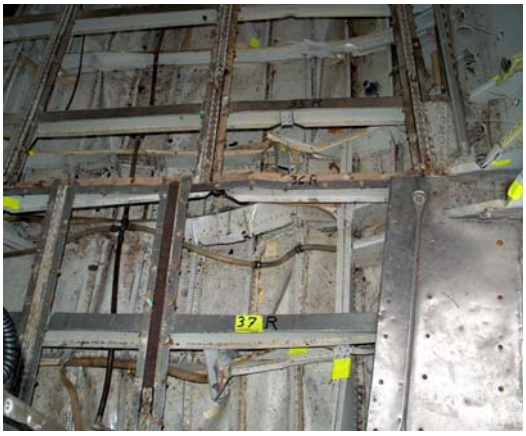

(r) Floor Tracks—Frames 37-35 Right

FIGURE C-98. FLOOR TRACKS—AFT LOOKING FORWARD (Continued)

C.6 POSTTEST PHOTOGRAPHS—ATR 42-300 CEILING.

FIGURE C-99. CEILING—FORWARD LOOKING AFT

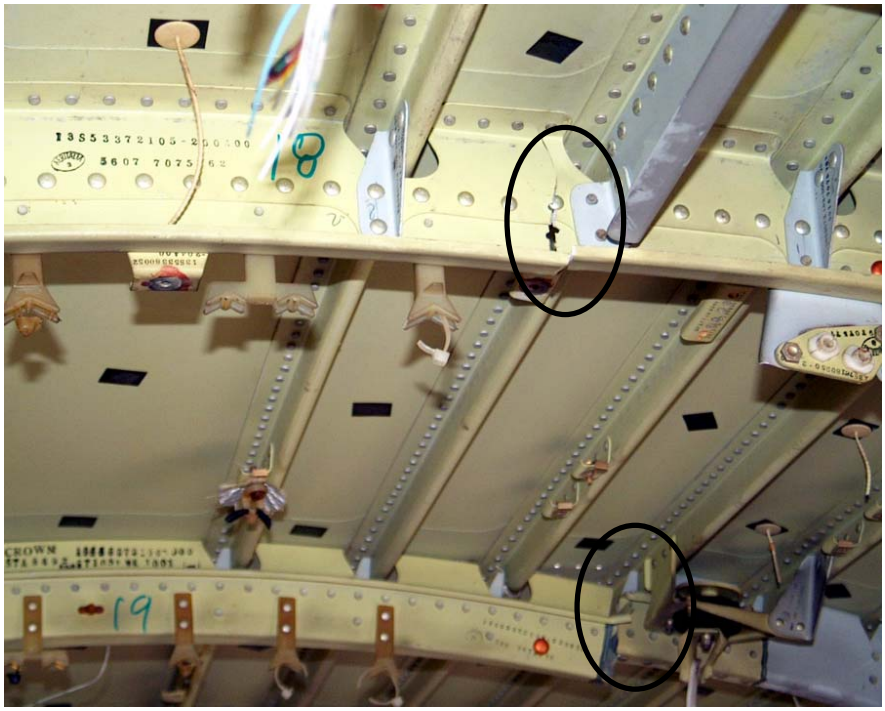

FIGURE C-100. CEILING—FRAMES 18 AND 19

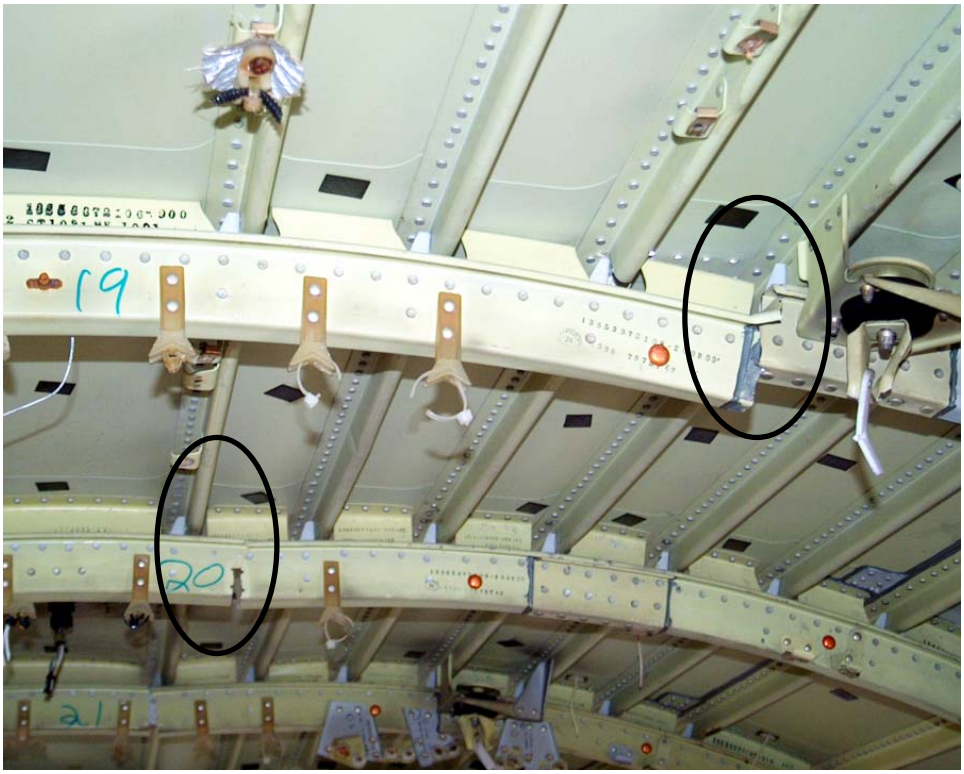

FIGURE C-101. CEILING—FRAMES 19 AND 20

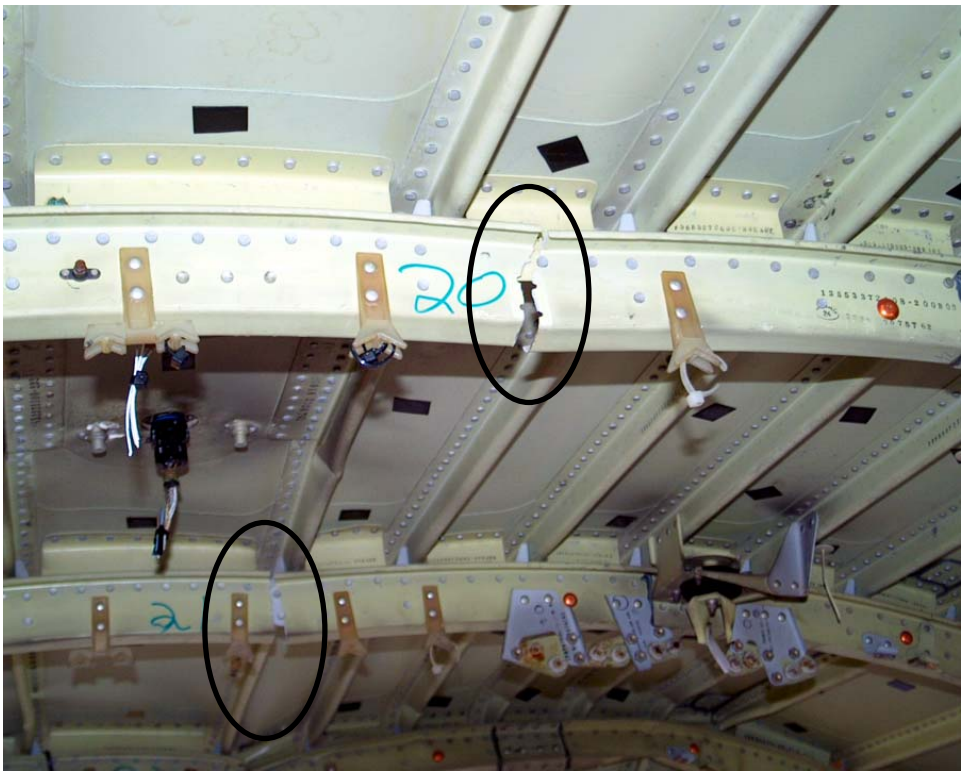

FIGURE C-102. CEILING—FRAMES 20 AND 21

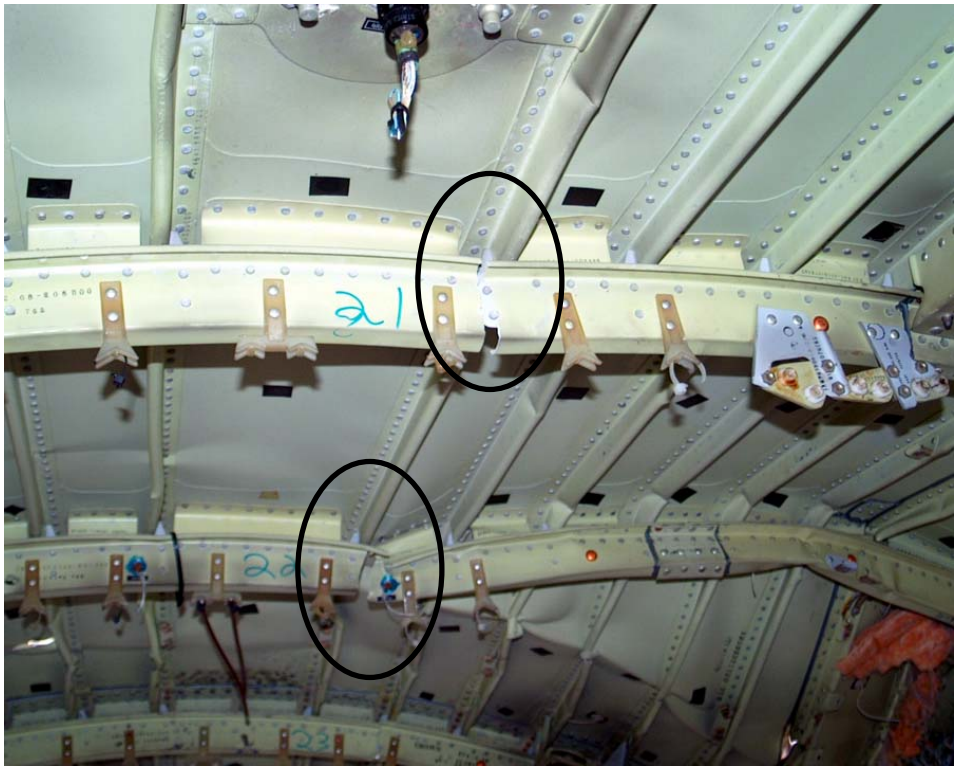

FIGURE C-103. CEILING—FRAMES 21 AND 22

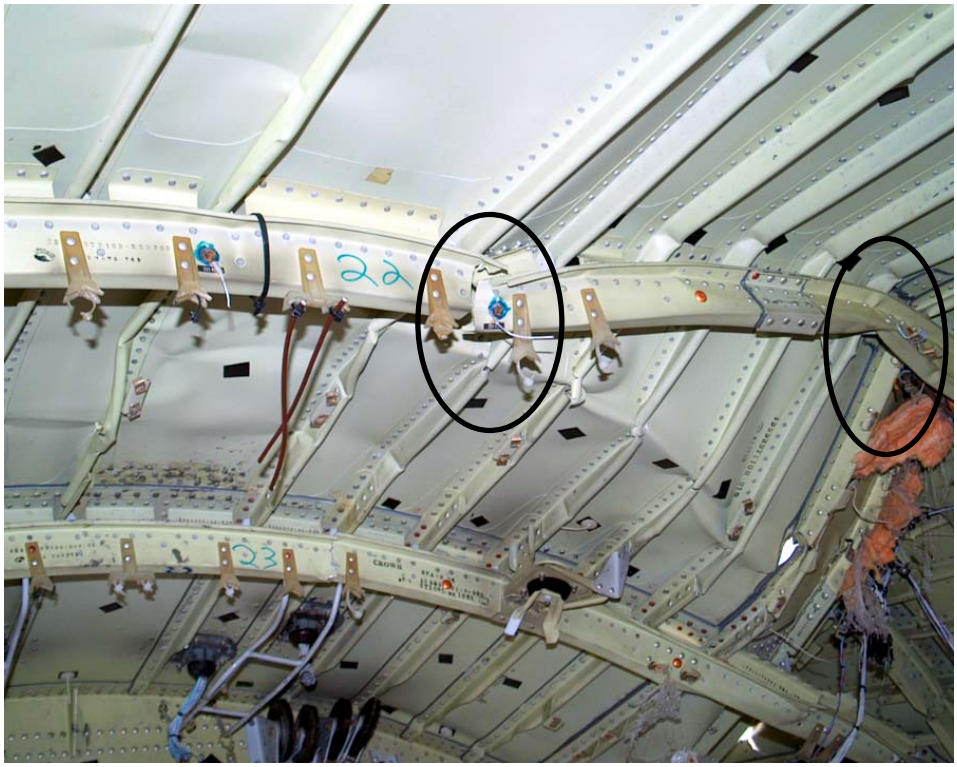

FIGURE C-104. CEILING—FRAMES 22 AND 23

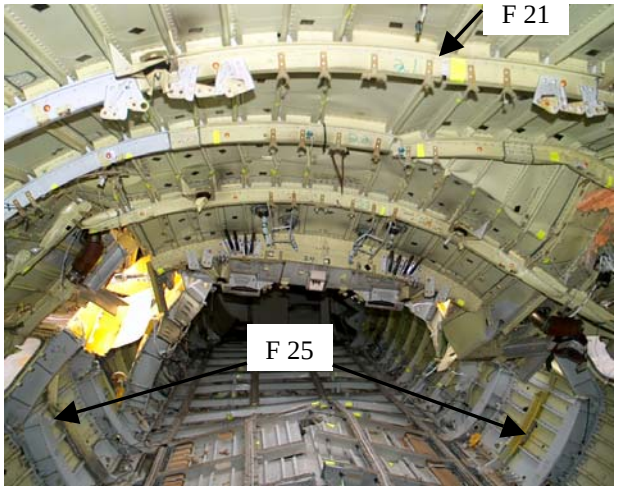

(a) Forward Looking Aft—Frames 21 to 25 (Wing)

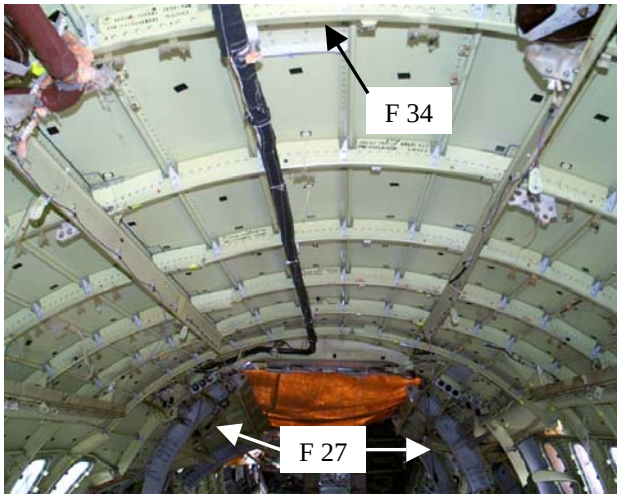

(b) Aft Looking Forward—Frames 34 to 27 (Wing)

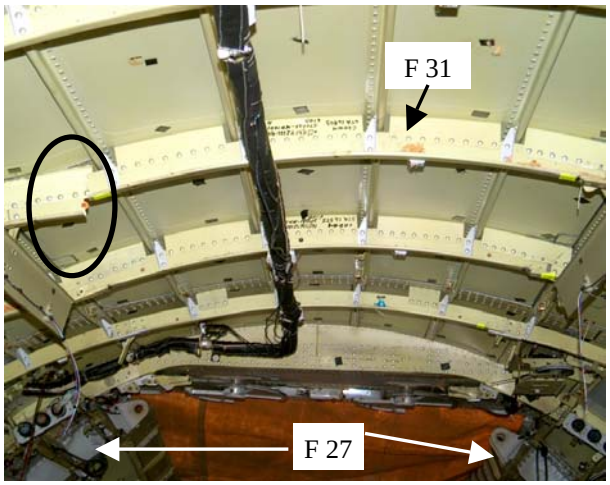

(c) Aft Looking Forward—Frames 31 to 27 (Wing)

FIGURE C-105. CEILING

C.7 POSTTEST PHOTOGRAPHS—ATR 42-300 BINS.

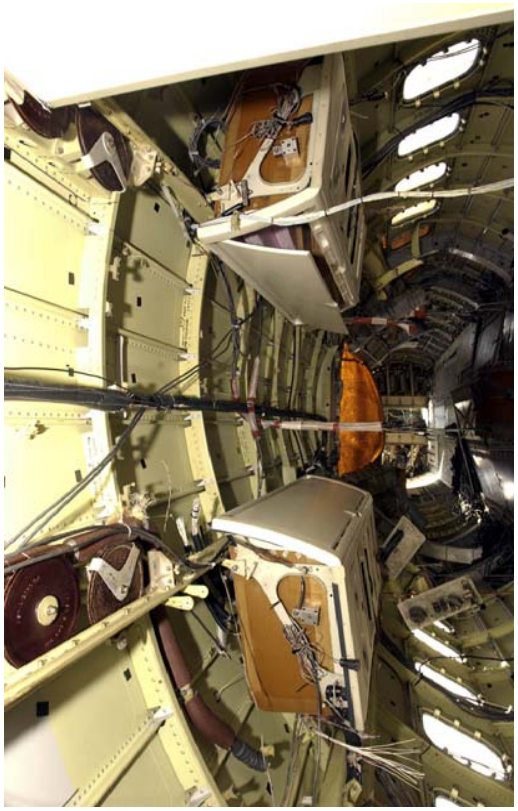

(a) Aft Looking Forward

(b) Left Stowage Bin—Aft Looking Forward

(c) Right Stowage Bin—Aft Looking Forward

FIGURE C-106. OVERHEAD STOWAGE BINS

C.8 POSTTEST PHOTOGRAPHS—ATR 42-300 SIDEWALLS.

FIGURE C-107. FRAMES 17-22, EMERGENCY EXIT, CARGO DOOR LEFT SIDE

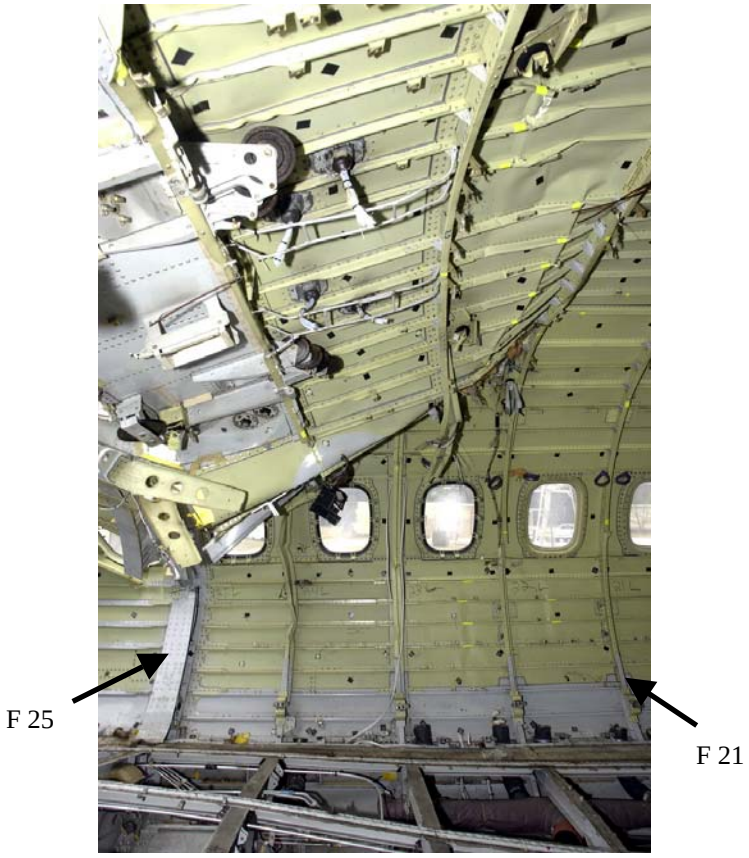

FIGURE C-108. FRAMES 21-25 LEFT SIDE

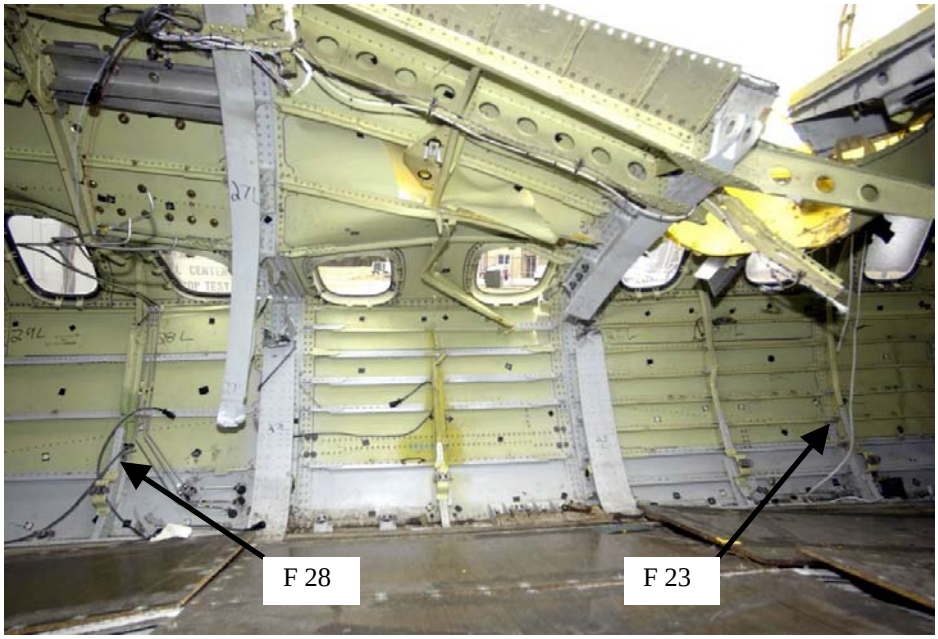

FIGURE C-109. FRAMES 23-28 LEFT SIDE

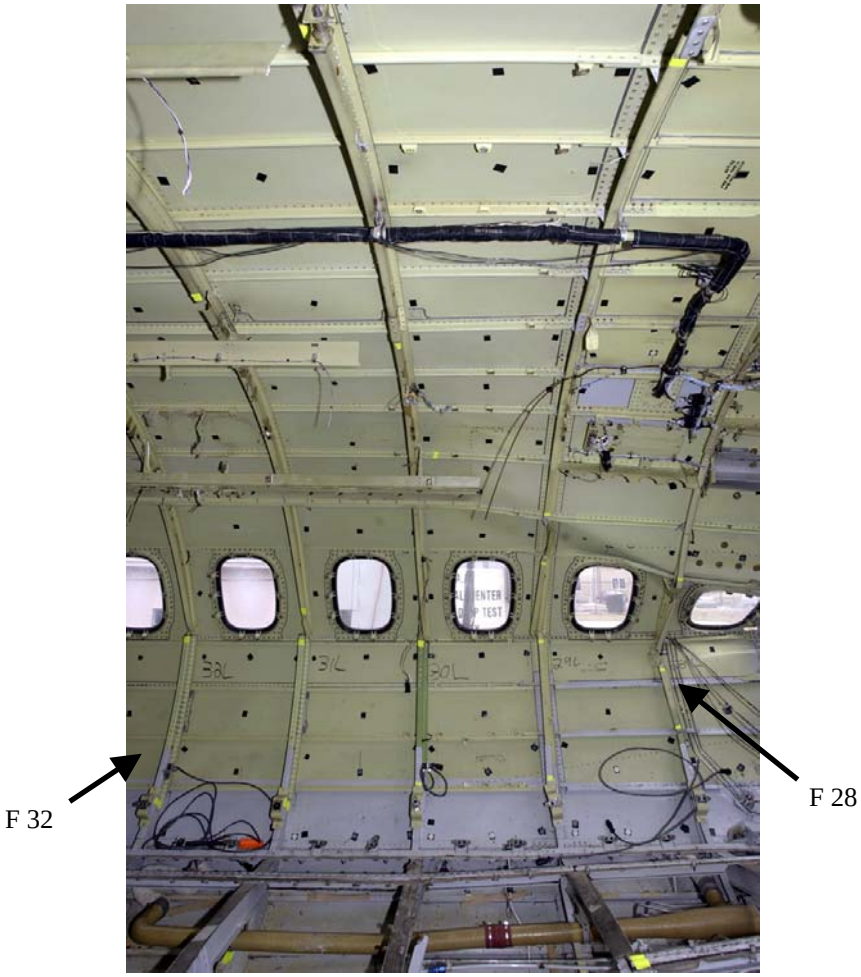

FIGURE C-110. FRAMES 28-32 LEFT SIDE

FIGURE C-111. FRAMES 31-36 LEFT SIDE

FIGURE C-112. FRAMES 19-21, EMERGENCY EXIT LEFT SIDE

FIGURE C-113. FRAMES 20-22 LEFT SIDE

FIGURE C-114. FRAMES 21-23 LEFT SIDE

FIGURE C-115. FRAMES 23-25 LEFT SIDE

FIGURE C-116. FRAMES 27-30 LEFT SIDE

FIGURE C-117. FRAMES 30-33 LEFT SIDE

FIGURE C-118. FRAMES 33-36 LEFT SIDE

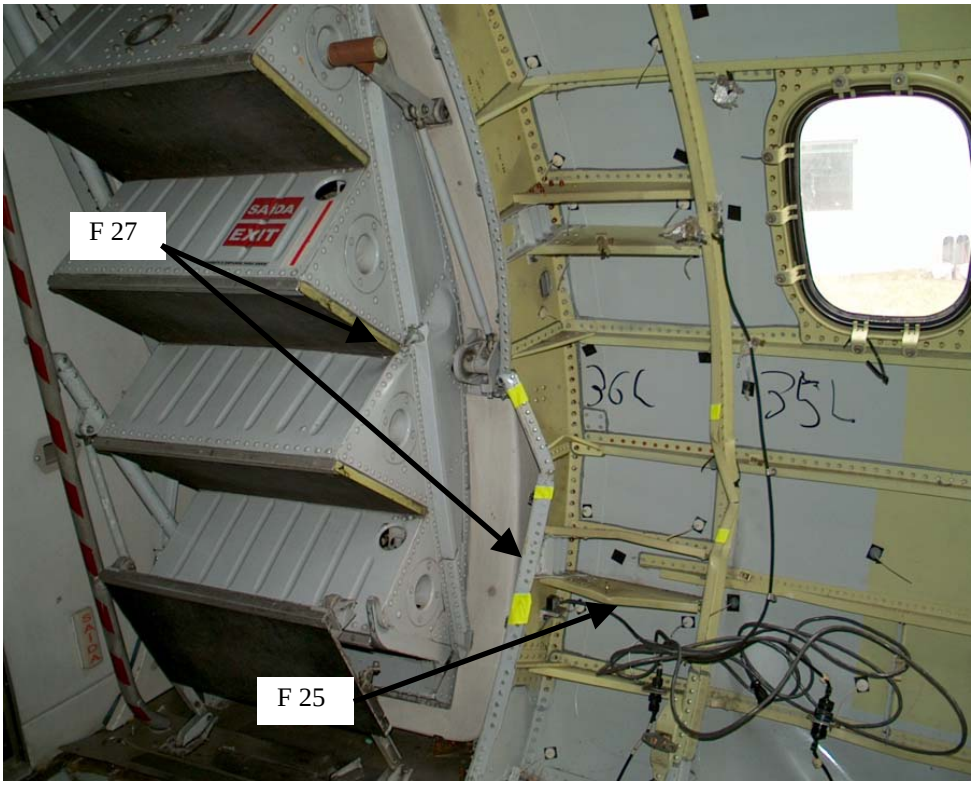

FIGURE C-119. FRAMES 35 AND 36, MAIN PASSENGER DOOR LEFT SIDE

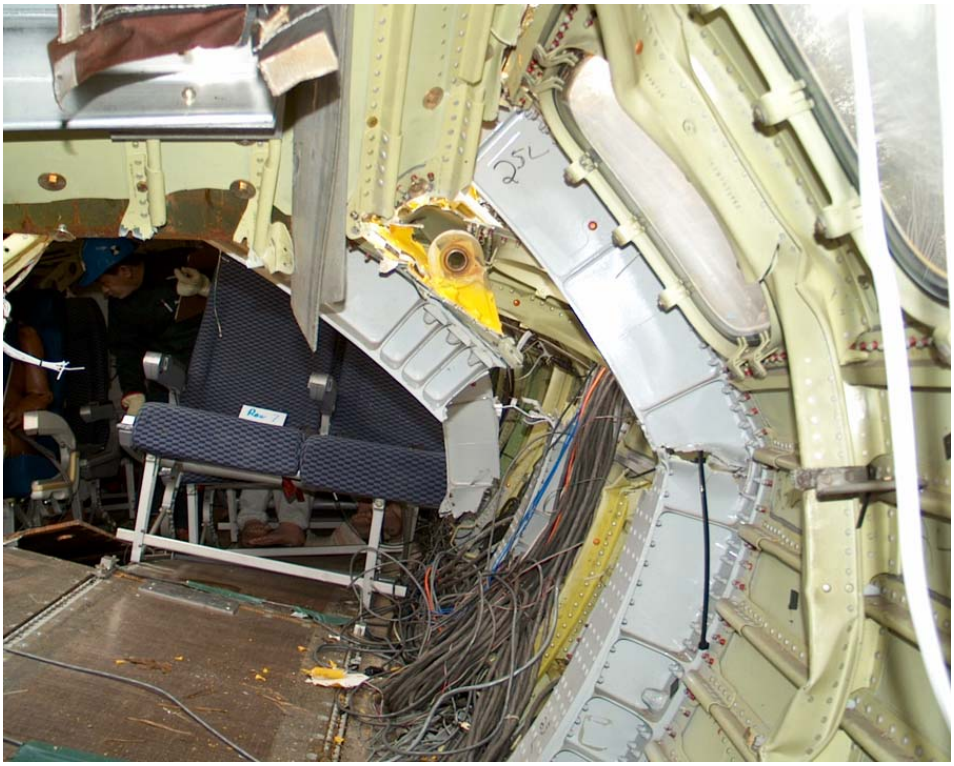

FIGURE C-120. FRAMES 25 AND 27 LEFT SIDE

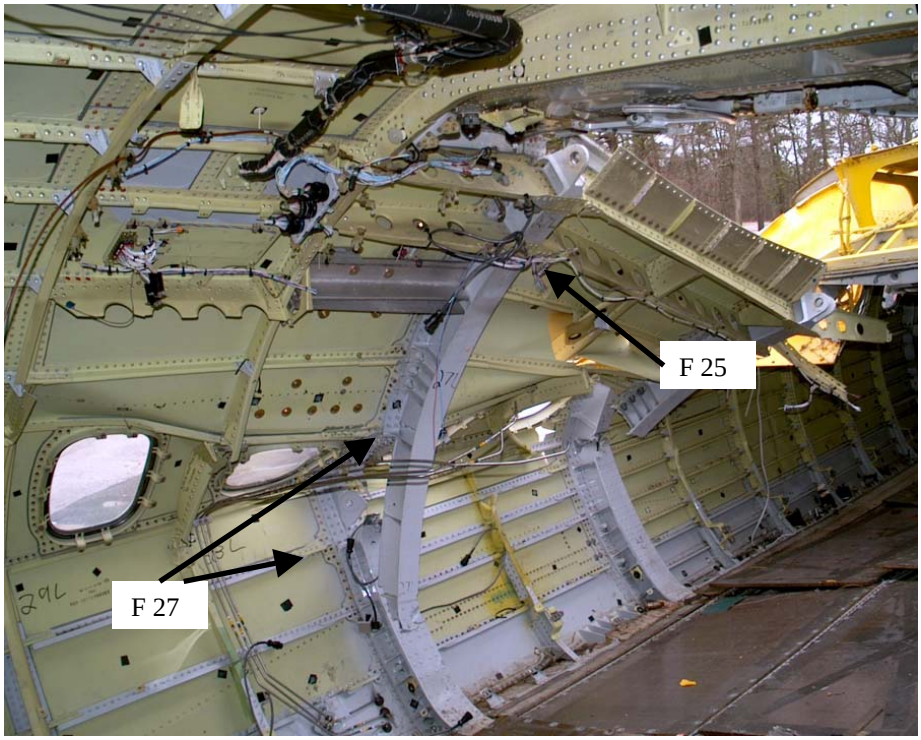

FIGURE C-121. FRAMES 27 AND 25 LEFT SIDE VIEW 1

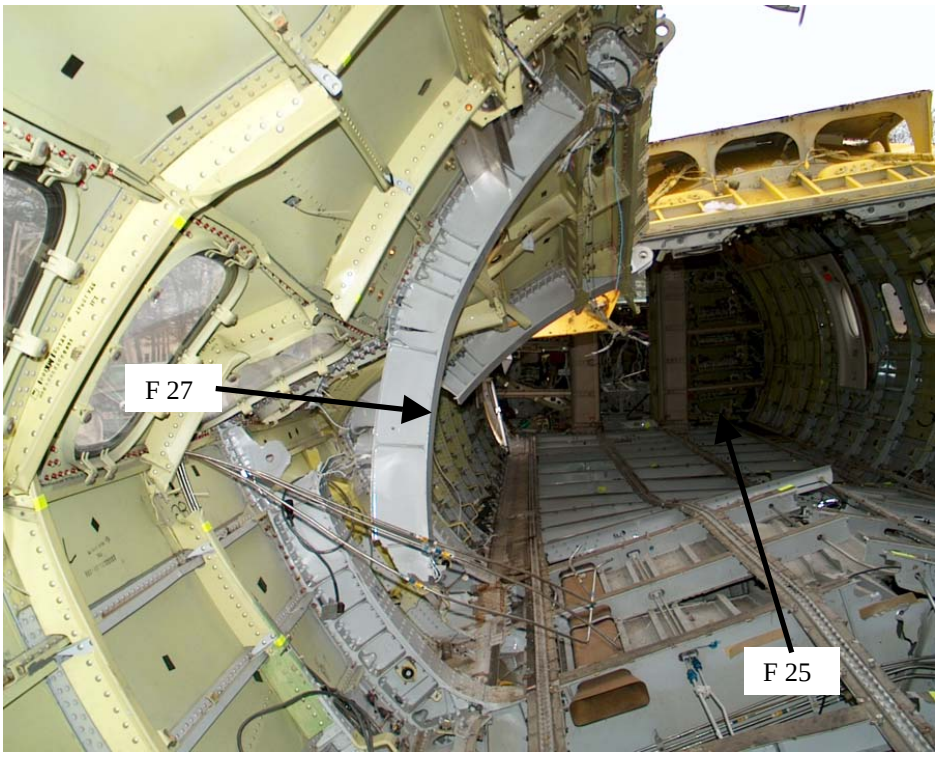

FIGURE C-122. FRAMES 27 AND 25 LEFT SIDE VIEW 2

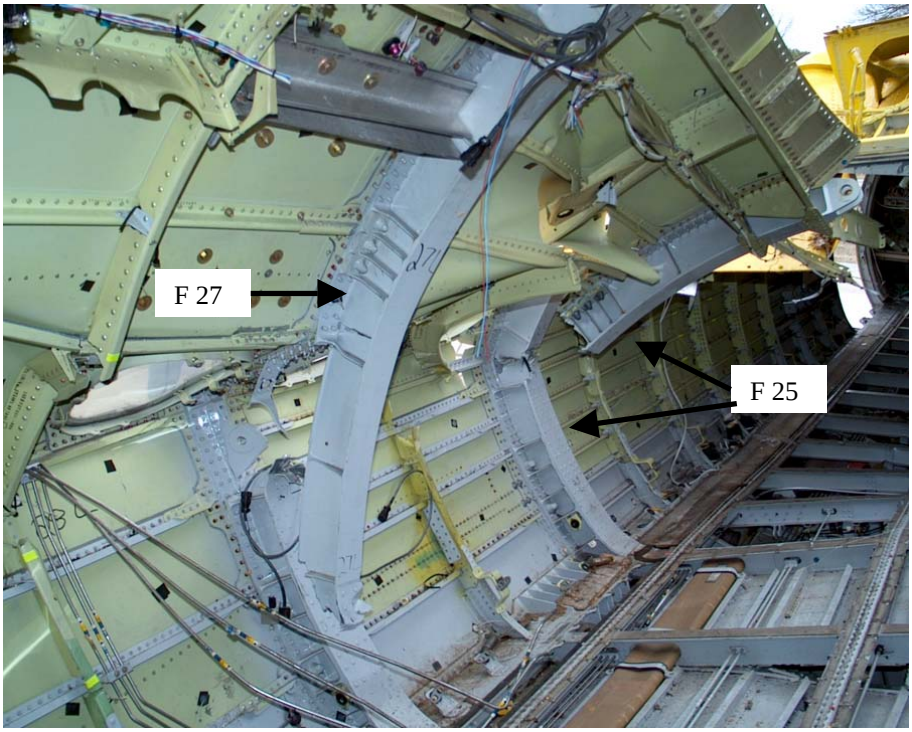

FIGURE C-123. FRAMES 27 AND 25 LEFT SIDE VIEW 3

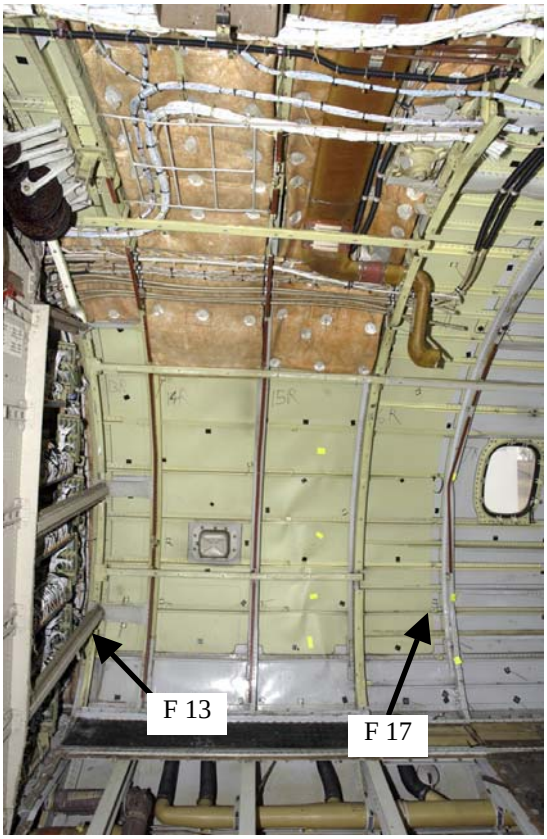

FIGURE C-124. FRAMES 13-17 RIGHT SIDE

FIGURE C-125. FRAMES 17-22, EMERGENCY EXIT RIGHT SIDE

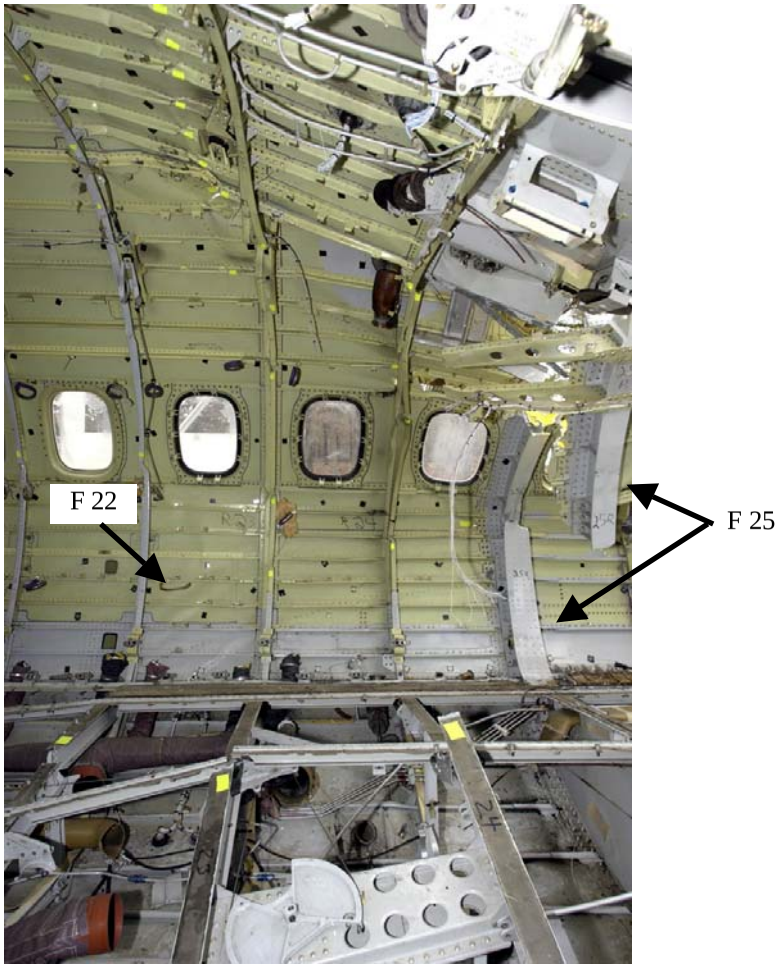

FIGURE C-126. FRAMES 22-25 RIGHT SIDE

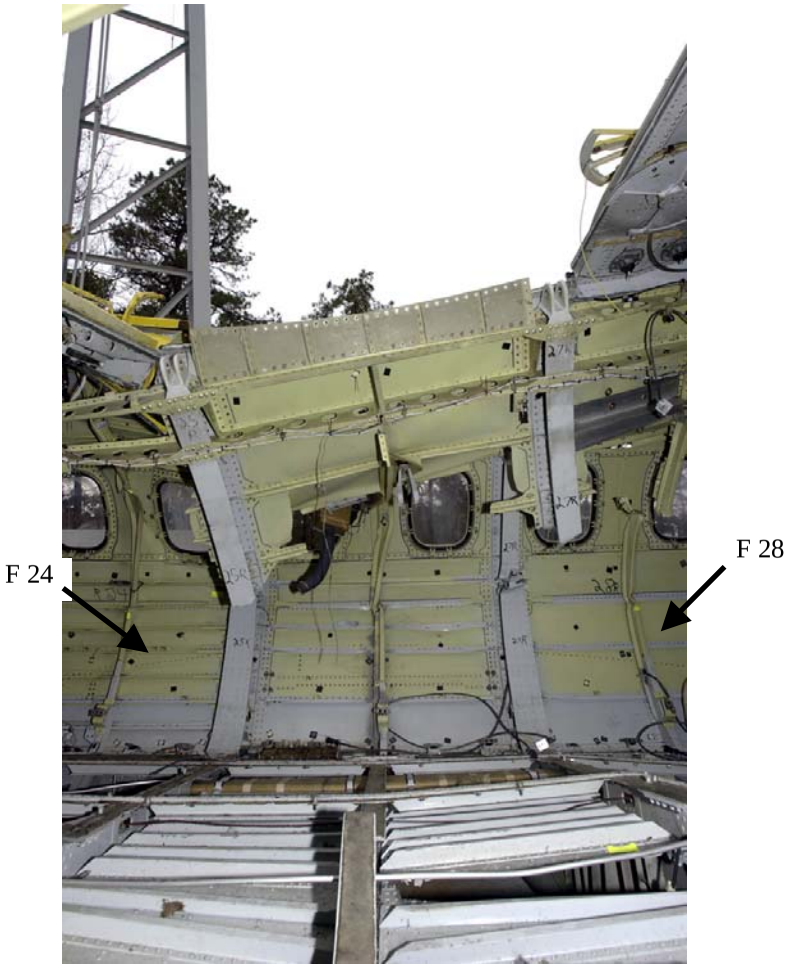

FIGURE C-127. FRAMES 24-28 RIGHT SIDE

FIGURE C-128. FRAMES 28-33 RIGHT SIDE

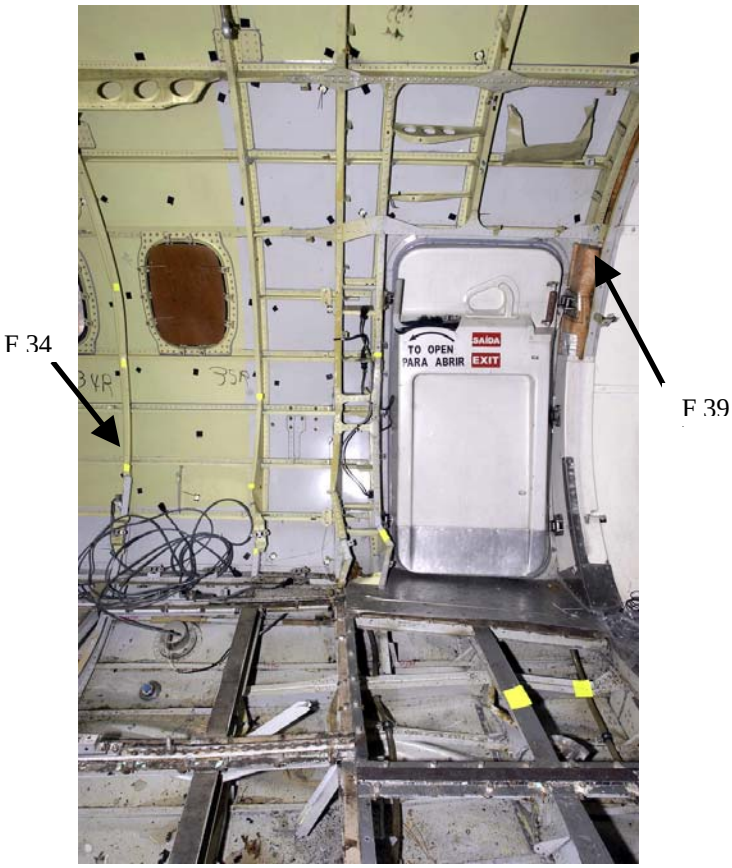

FIGURE C-129. FRAMES 34-39, SERVICE DOOR RIGHT SIDE

FIGURE C-130. FRAMES 13-16 RIGHT SIDE

FIGURE C-131. FRAMES 16-18 RIGHT SIDE

FIGURE C-132. FRAMES 19-21 RIGHT SIDE

FIGURE C-133. FRAMES 21 AND 22 RIGHT SIDE

FIGURE C-134. FRAMES 22 AND 23 RIGHT SIDE

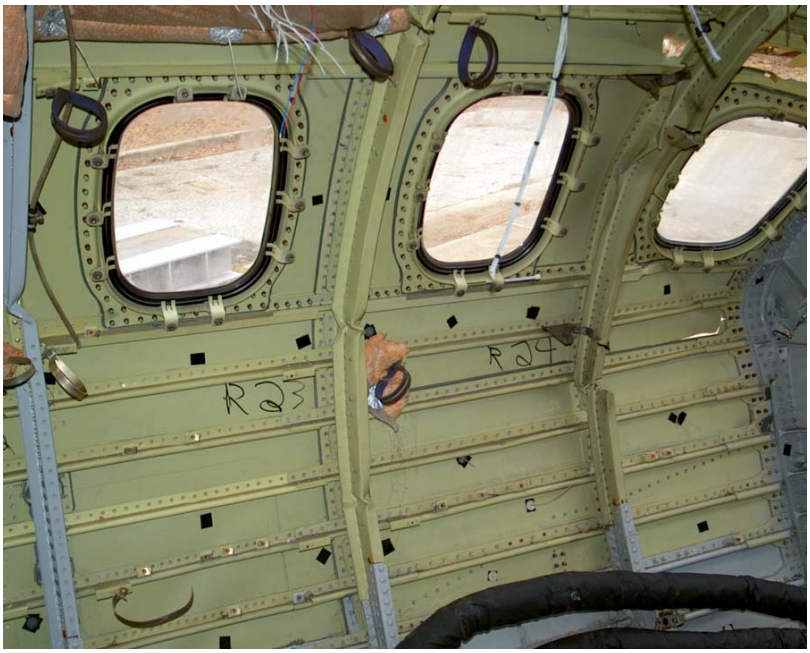

FIGURE C-135. FRAMES 23 AND 24 RIGHT SIDE

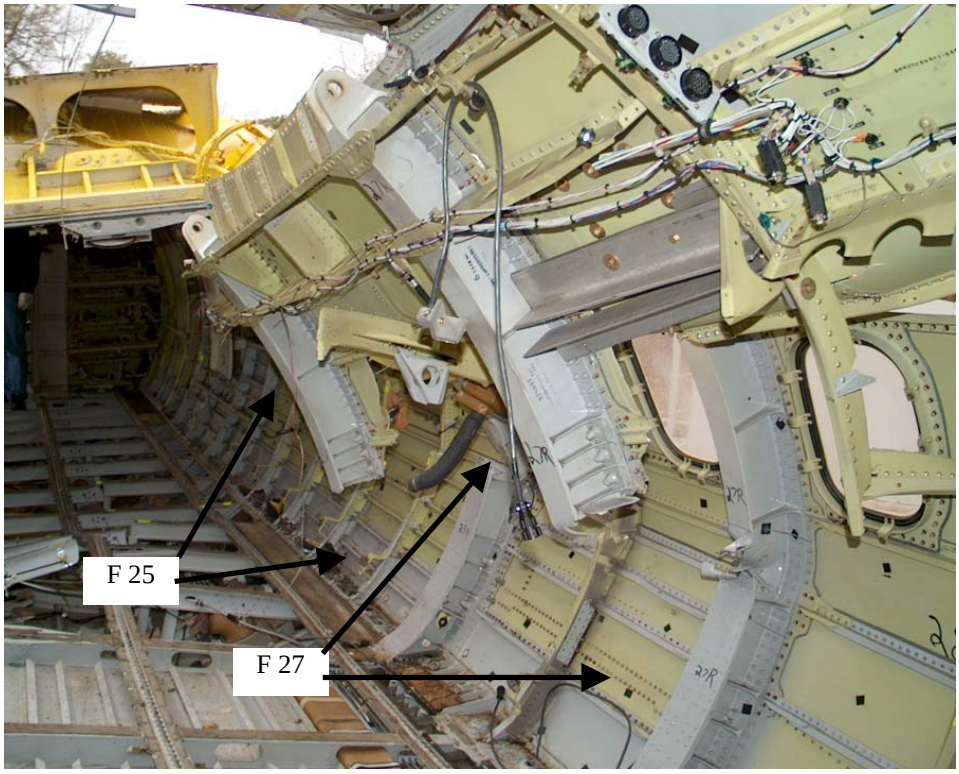

FIGURE C-136. FRAMES 27 AND 25 RIGHT SIDE VIEW 1

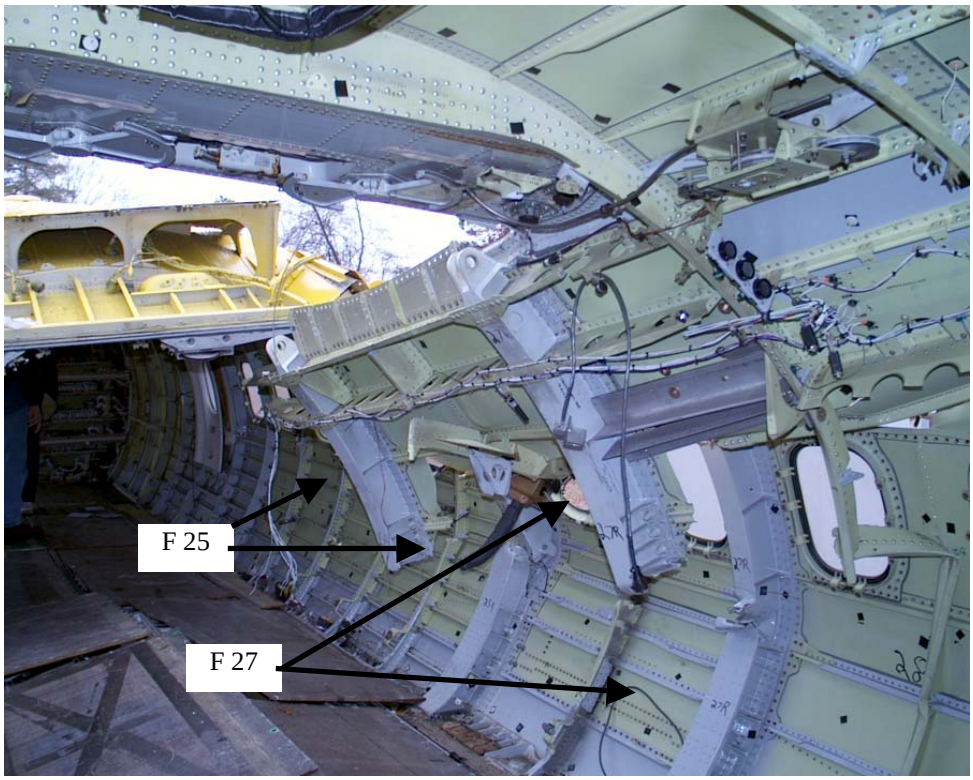

FIGURE C-137. FRAMES 27 AND 25 RIGHT SIDE VIEW 2

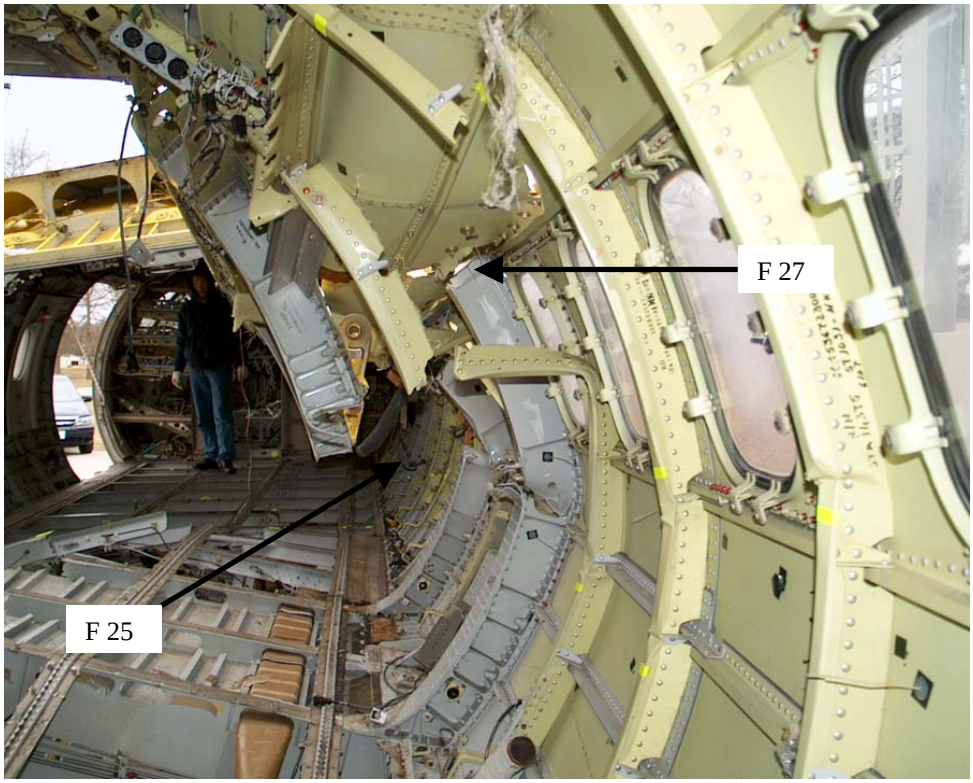

FIGURE C-138. FRAMES 27 AND 25 RIGHT SIDE VIEW 3

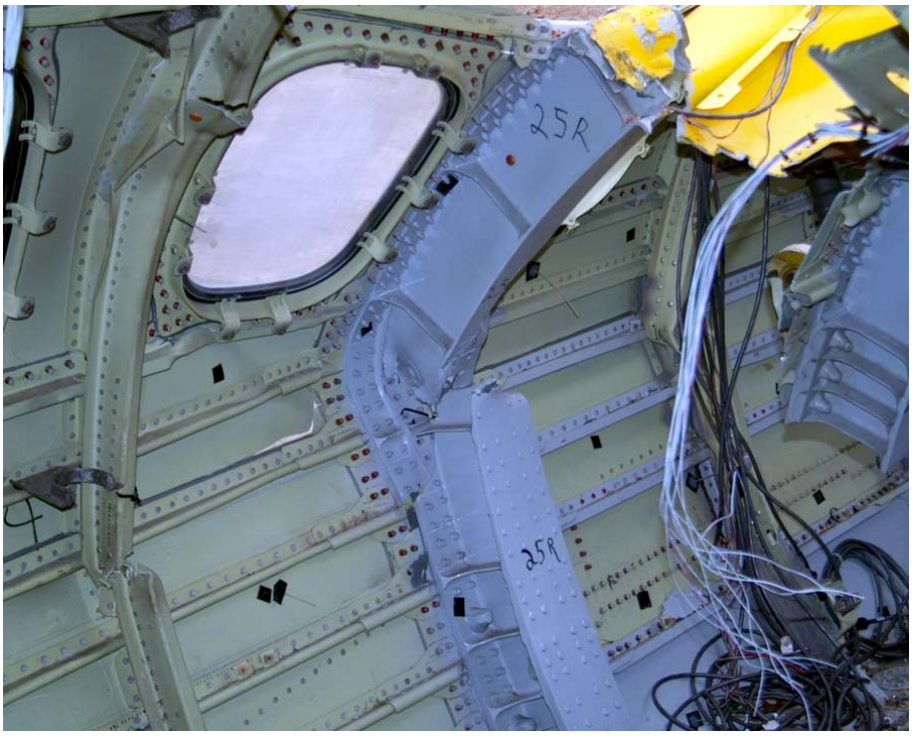

FIGURE C-139. FRAME 25 RIGHT SIDE

C.9 POSTTEST PHOTOGRAPHS—SEATS.

FIGURE C-140. ROW 1 SEATS WITH DUMMIES

FIGURE C-141. ROW 1 SEATS

FIGURE C-142. ROW 1 SEATS D AND C

FIGURE C-143. ROW 1 SEATS B AND A

FIGURE C-144. ROW 2 SEATS

FIGURE C-145. ROW 2 SEATS D AND C, VIEW 1

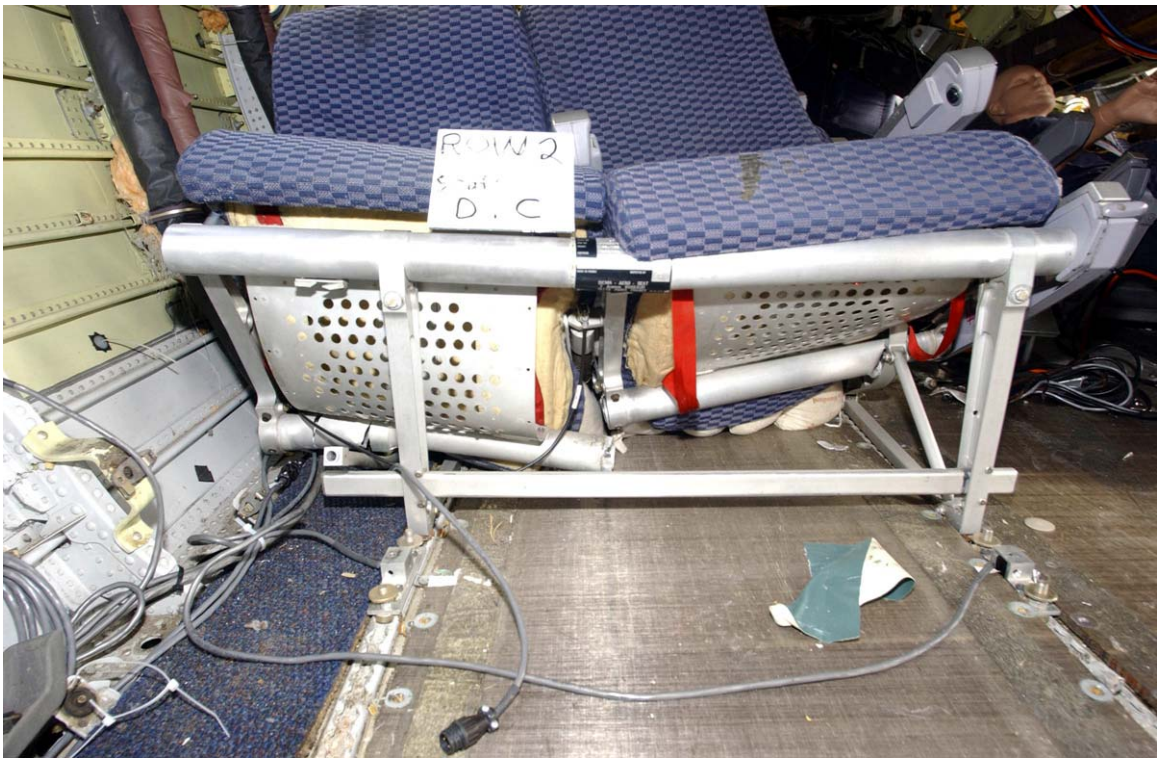

FIGURE C-146. ROW 2 SEATS D AND C, VIEW 2

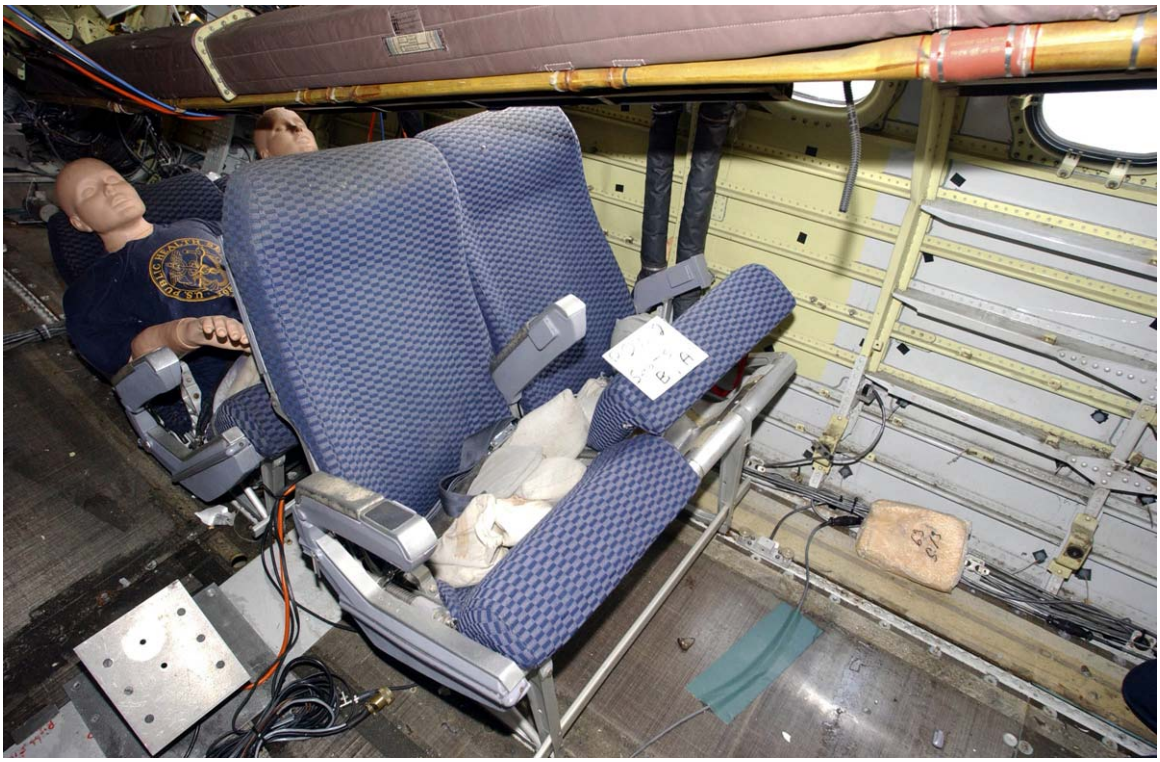

FIGURE C-147. ROW 2 SEATS B AND A, VIEW 1

FIGURE C-148. ROW 2 SEATS B AND A, VIEW 2

FIGURE C-149. ROW 3 SEATS WITH DUMMIES

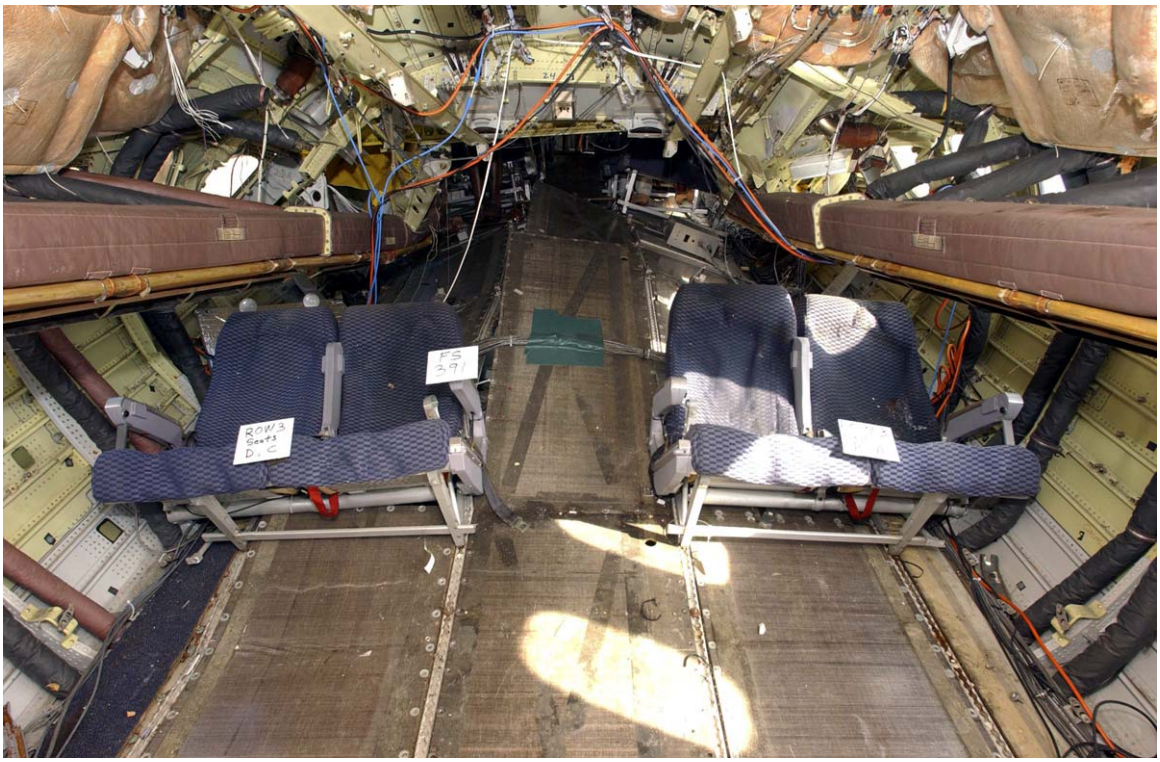

FIGURE C-150. ROW 3 SEATS

FIGURE C-151. ROW 3 SEATS D AND C

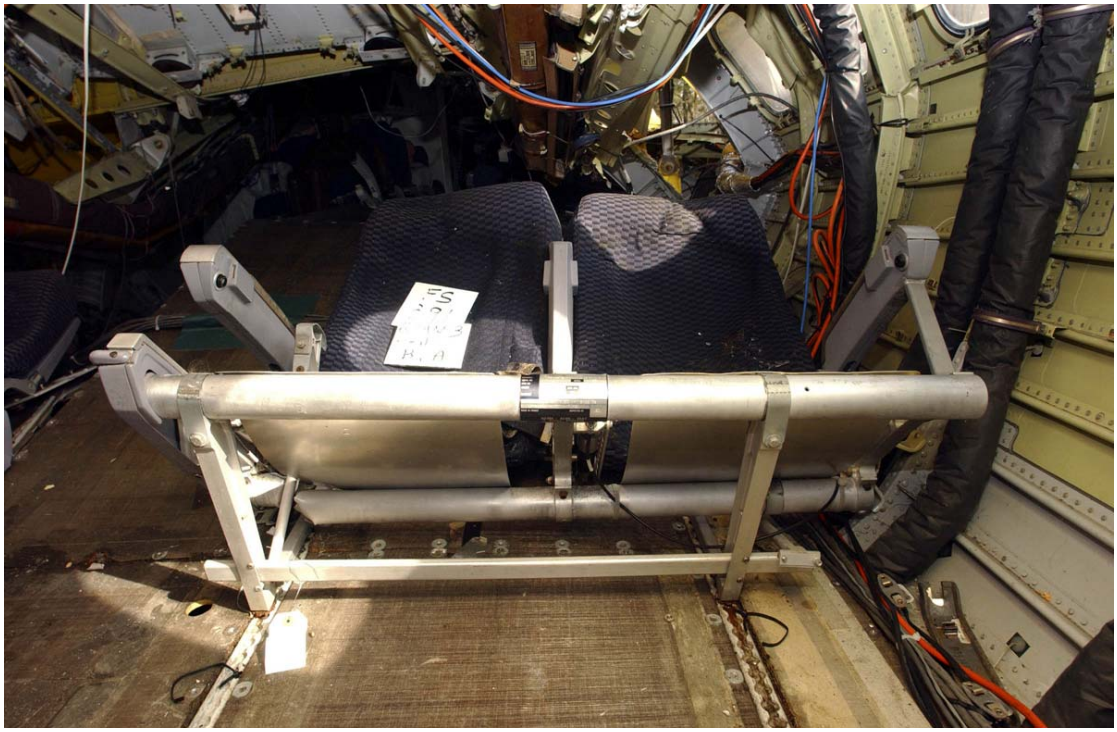

FIGURE C-152. ROW 3 SEATS B AND A

FIGURE C-153. ROW 7 NAL EXPERIMENTAL SEATS D AND C, FRONT VIEW

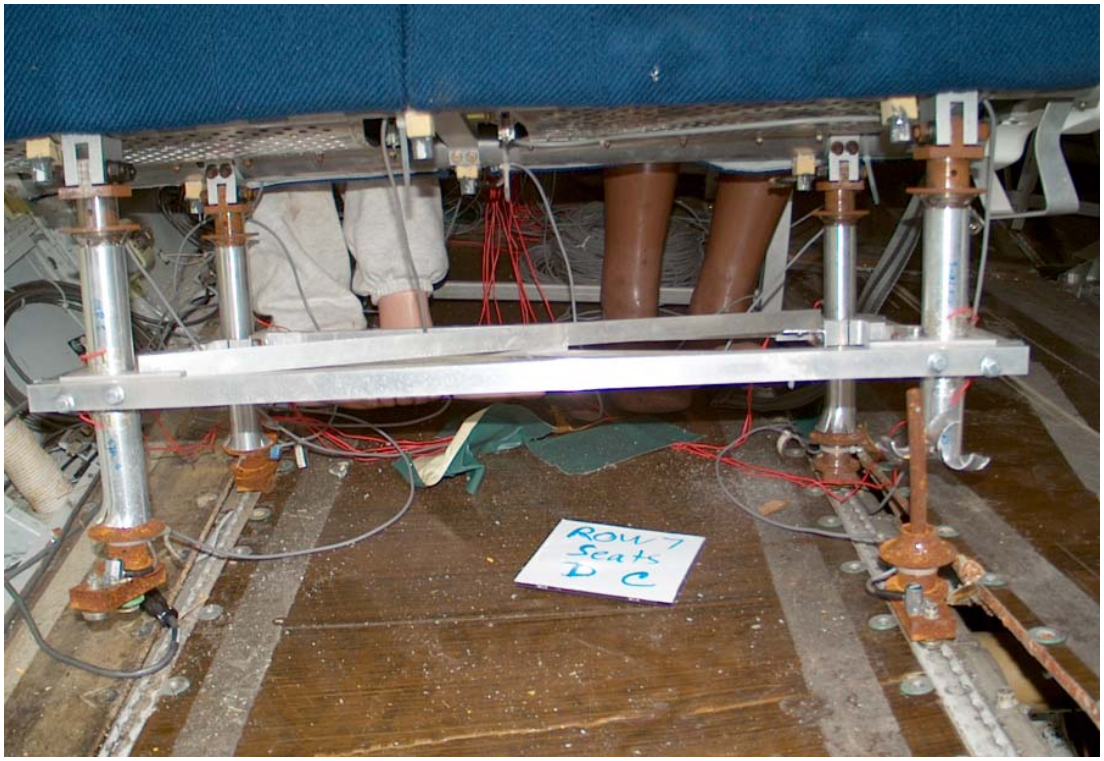

FIGURE C-154. ROW 7 NAL EXPERIMENTAL SEATS D AND C, REAR VIEW

FIGURE C-155. ROW 7 SEATS B AND A, VIEW 1

FIGURE C-156. ROW 7 SEATS B AND A, VIEW 2

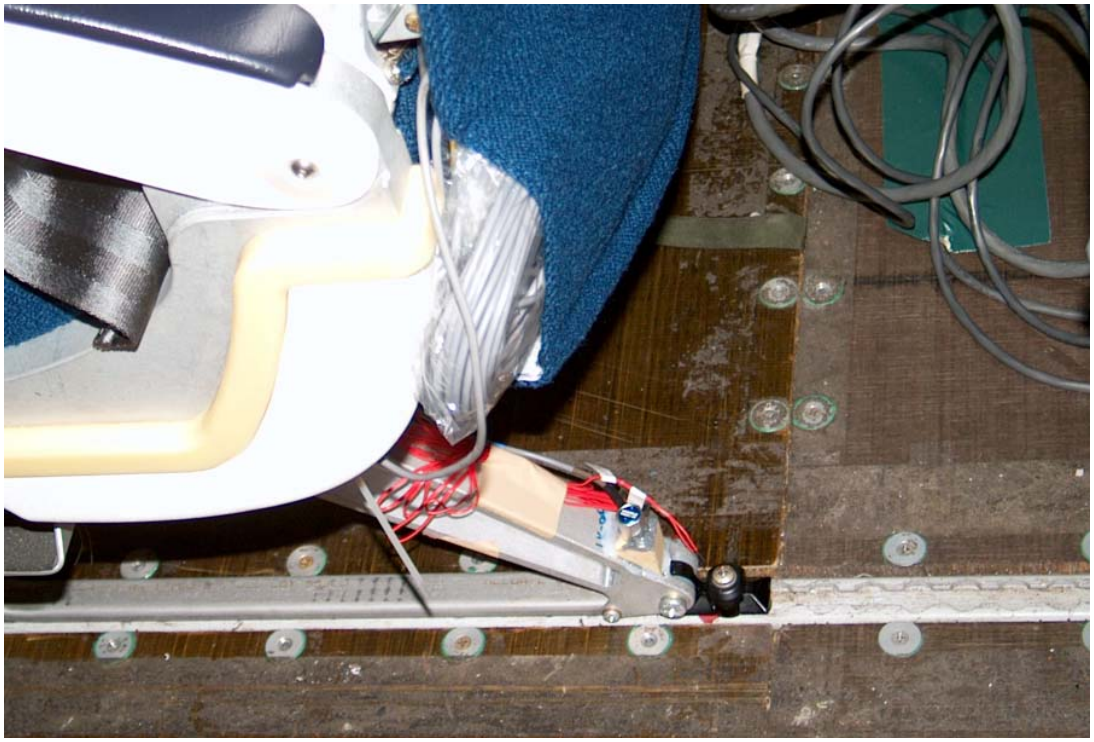

FIGURE C-157. ROW 8 TENRYU MODIFIED 16-g SEAT ISLE LEG

FIGURE C-158. ROW 8 TENRYU MODIFIED 16-g SEATS D AND C

FIGURE C-159. ROW 8 TENRYU MODIFIED 16-g SEAT C

FIGURE C-160. ROW 8 SEATS B AND A

FIGURE C-161. ROW 10 SEATS D AND C, VIEW 1

FIGURE C-162. ROW 10 SEATS D AND C, VIEW 2

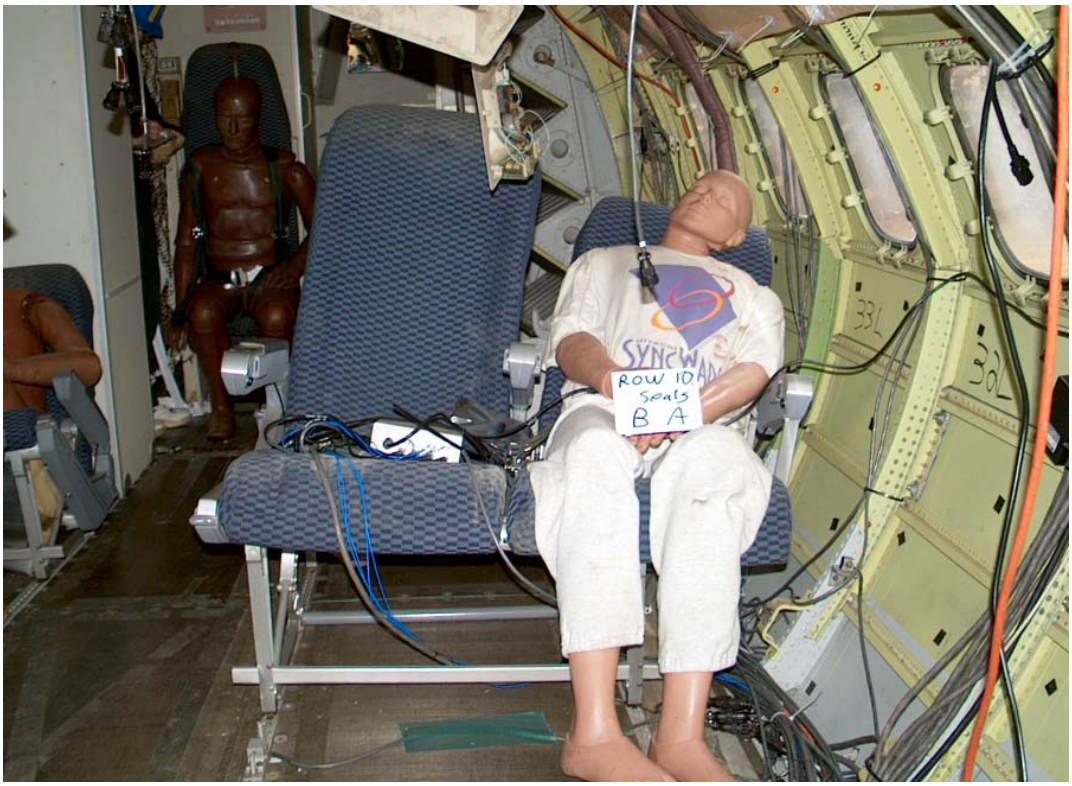

FIGURE C-163. ROW 10 SEATS B AND A, VIEW 1

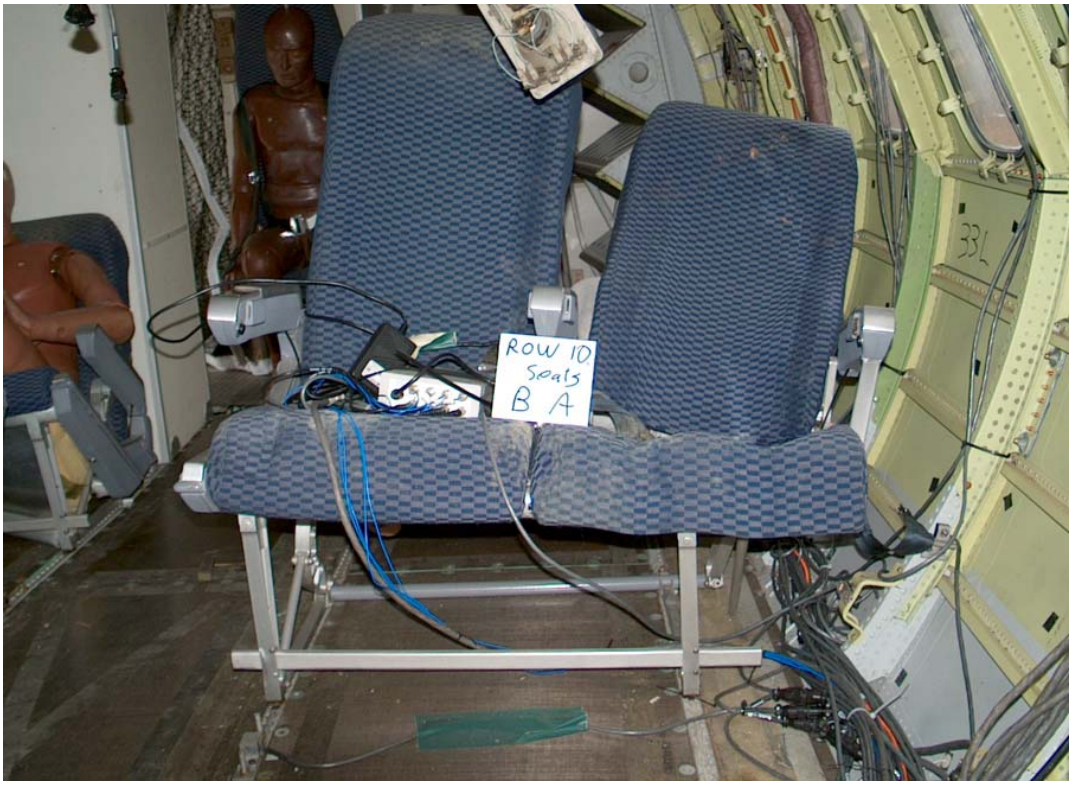

FIGURE C-164. ROW 10 SEATS B AND A, VIEW 2

FIGURE C-165. ROW 10 SEATS B AND A, VIEW 3

FIGURE C-166. ROW 11 SEATS B AND A, VIEW 1

FIGURE C-167. ROW 11 SEATS B AND A, VIEW 2

FIGURE C-168. ROW 11 SEATS B AND A, VIEW 3

FIGURE C-169. ROW 11 SEATS B AND A, VIEW 4

FIGURE C-170. ROW 11 SEATS D AND C, VIEW 1

FIGURE C-171. ROW 11 SEATS D AND C, VIEW 2

FIGURE C-172. ROW 11 SEATS D AND C, VIEW 3

FIGURE C-173. FLIGHT ATTENDANT SEAT, FRONT VIEW

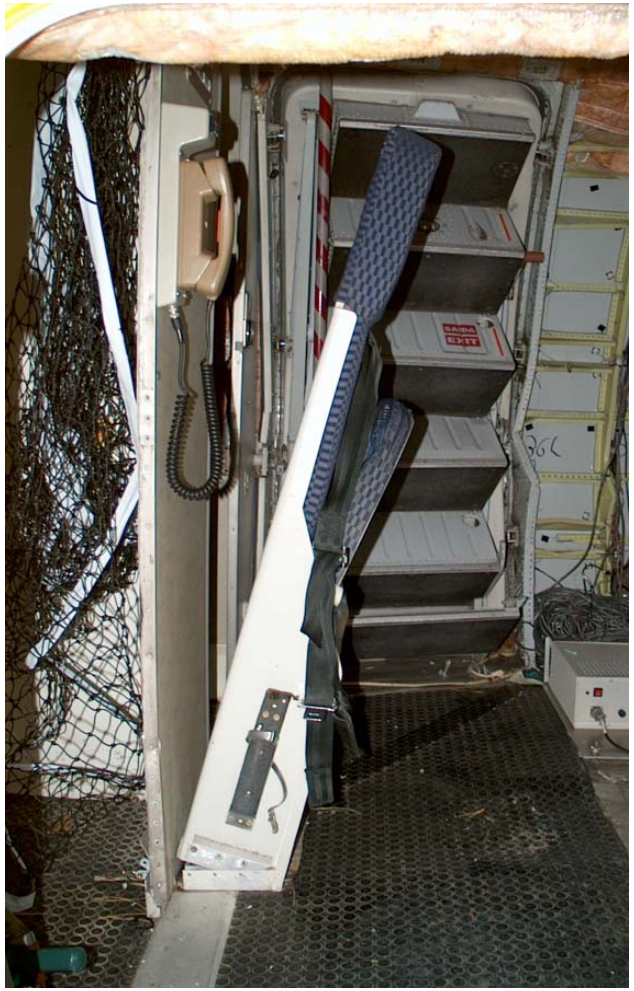

FIGURE C-174. FLIGHT ATTENDANT SEAT, RIGHT SIDE VIEW

FIGURE C-175. ROW 1 SEATS D, C, B, AND A, VIEW 1

FIGURE C-176. ROW 1 SEATS D, C, B, AND A, VIEW 2

FIGURE C-177. ROW 1 SEATS A, B, C, AND D

FIGURE C-178. ROW 2 SEATS D, C, B, AND A

FIGURE C-179. ROW 2 SEATS D AND C

FIGURE C-180. ROW 2 SEATS B AND A

FIGURE C-181. ROW 2 SEATS A AND B TOP VIEW

FIGURE C-182. ROW 2 SEATS C AND D TOP VIEW

FIGURE C-183. ROW 2 SEATS A AND B BOTTOM VIEW

FIGURE C-184. ROW 2 SEATS C AND D BOTTOM VIEW

FIGURE C-185. ROW 3 SEATS D, C, B, AND A

FIGURE C-186. ROW 3 SEATS A, B, C, AND D, TOP VIEW

FIGURE C-187. ROW 3 SEATS A, B, C, AND D, BOTTOM VIEW

FIGURE C-188. ROW 7 SEATS B AND A, TOP VIEW

FIGURE C-189. ROW 7 SEATS B AND A, BOTTOM VIEW

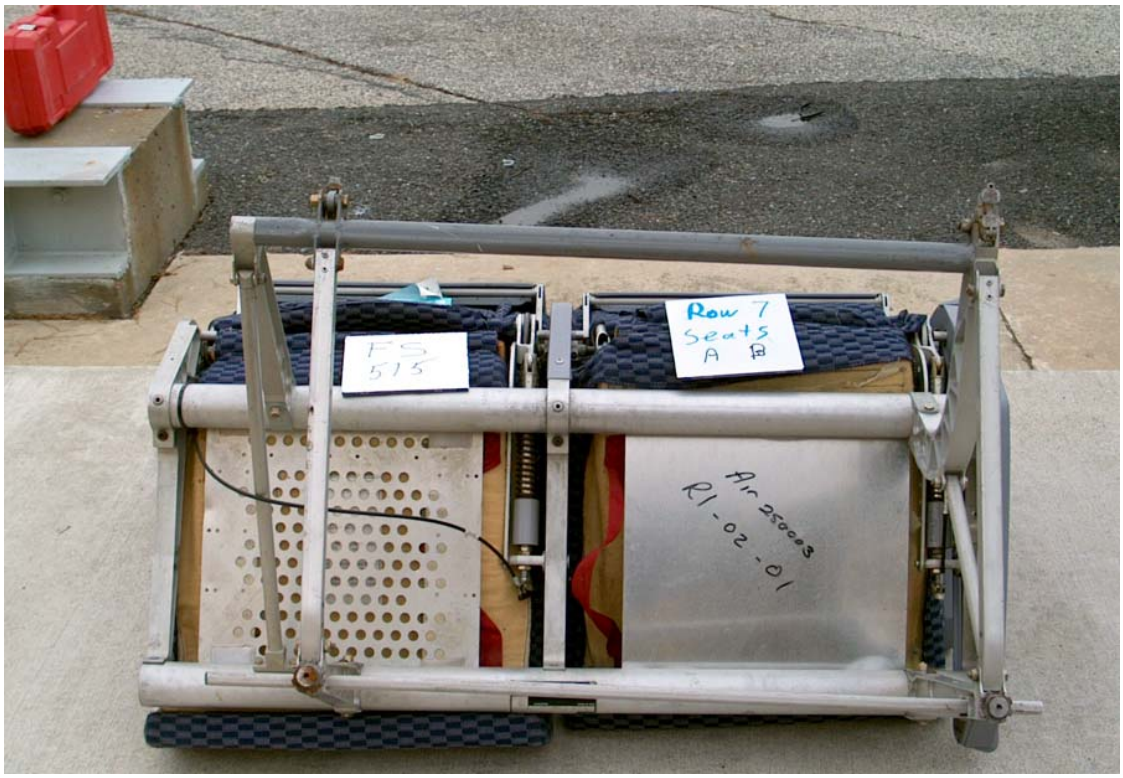

FIGURE C-190. ROW 7 SEATS A AND B

FIGURE C-191. ROW 7 NAL EXPERIMENTAL SEATS D AND C, VIEW 1

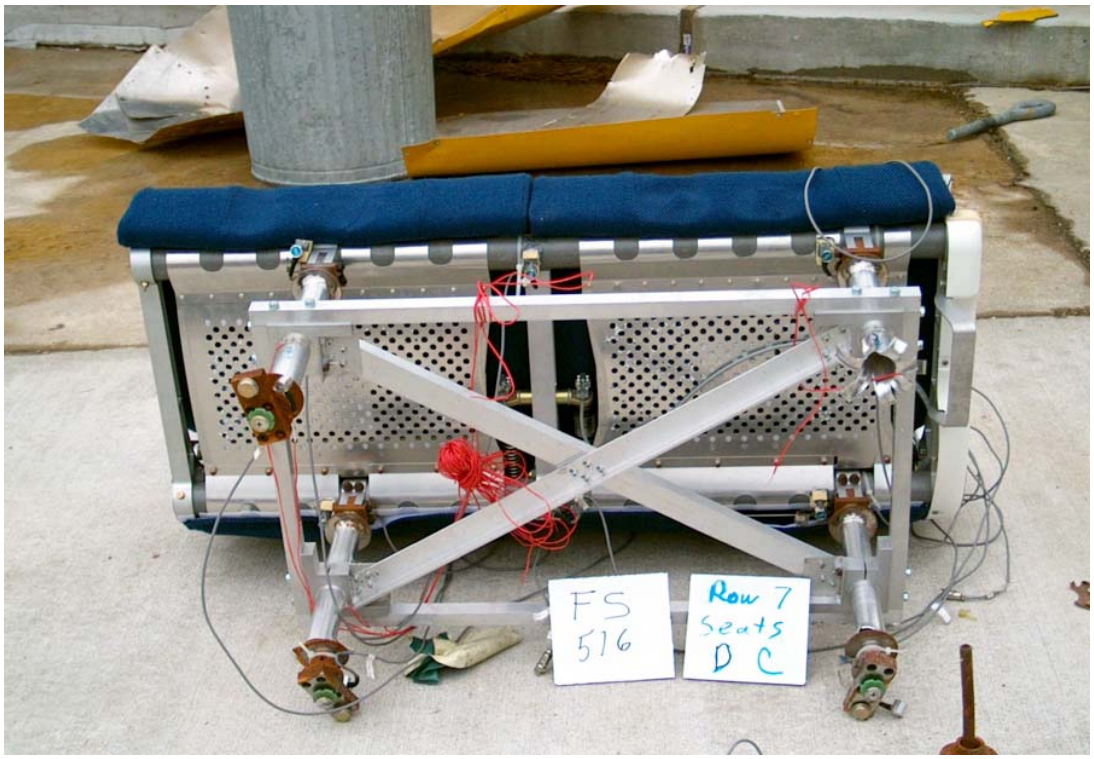

FIGURE C-192. ROW 7 NAL EXPERIMENTAL SEATS D AND C, VIEW 2

FIGURE C-193. ROW 7 NAL EXPERIMENTAL SEAT, SEATS C AND D, VIEW 1

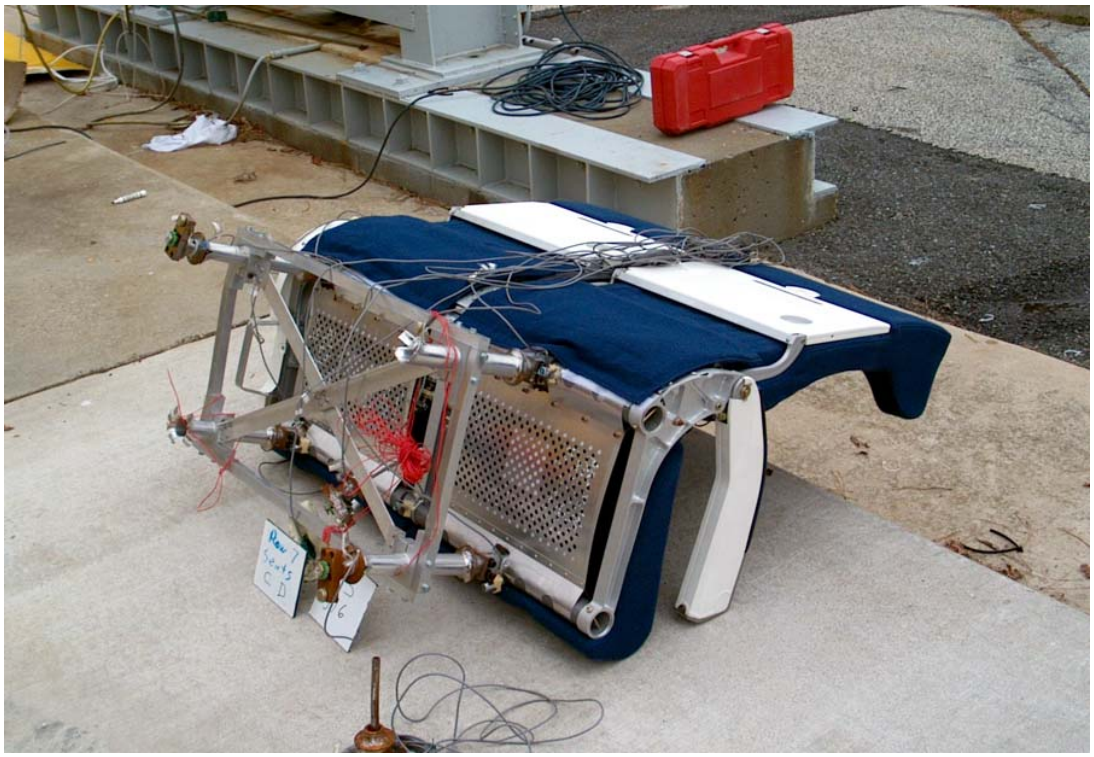

FIGURE C-194. ROW 7 NAL EXPERIMENTAL SEAT, SEATS C AND D, VIEW 2

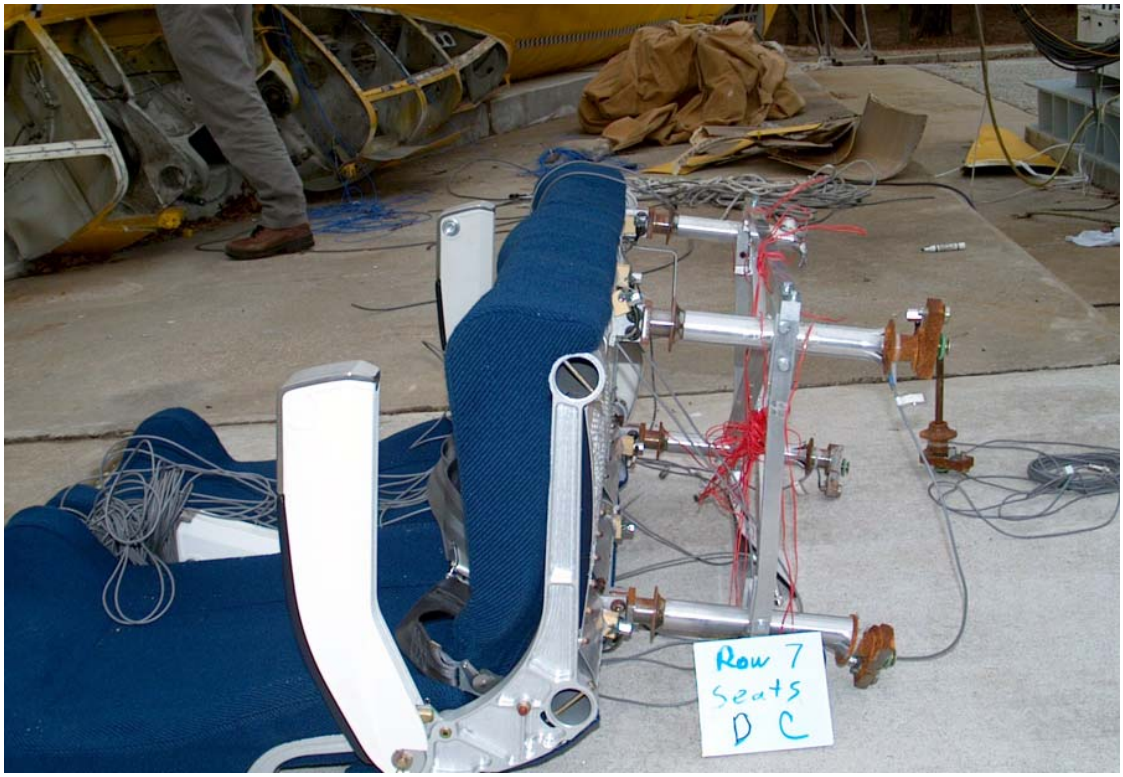

FIGURE C-195. ROW 7 NAL EXPERIMENTAL SEATS D AND C

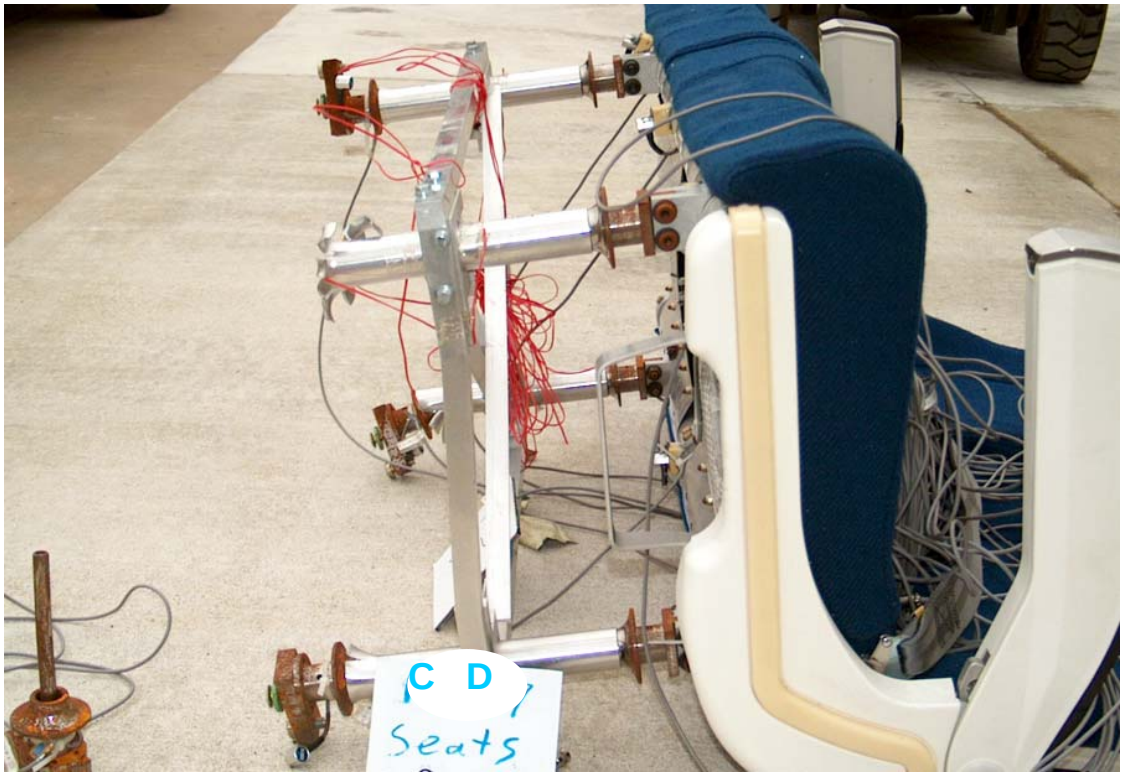

FIGURE C-196. ROW 7 NAL EXPERIMENTAL SEATS C AND D

FIGURE C-197. ROW 8 TENRYU MODIFIED 16-g SEATS D AND C, VIEW 1

FIGURE C-198. ROW 8 TENRYU MODIFIED 16-g SEATS D AND C, VIEW 2

FIGURE C-199. ROW 8 TENRYU MODIFIED 16-g SEATS D AND C, VIEW 3

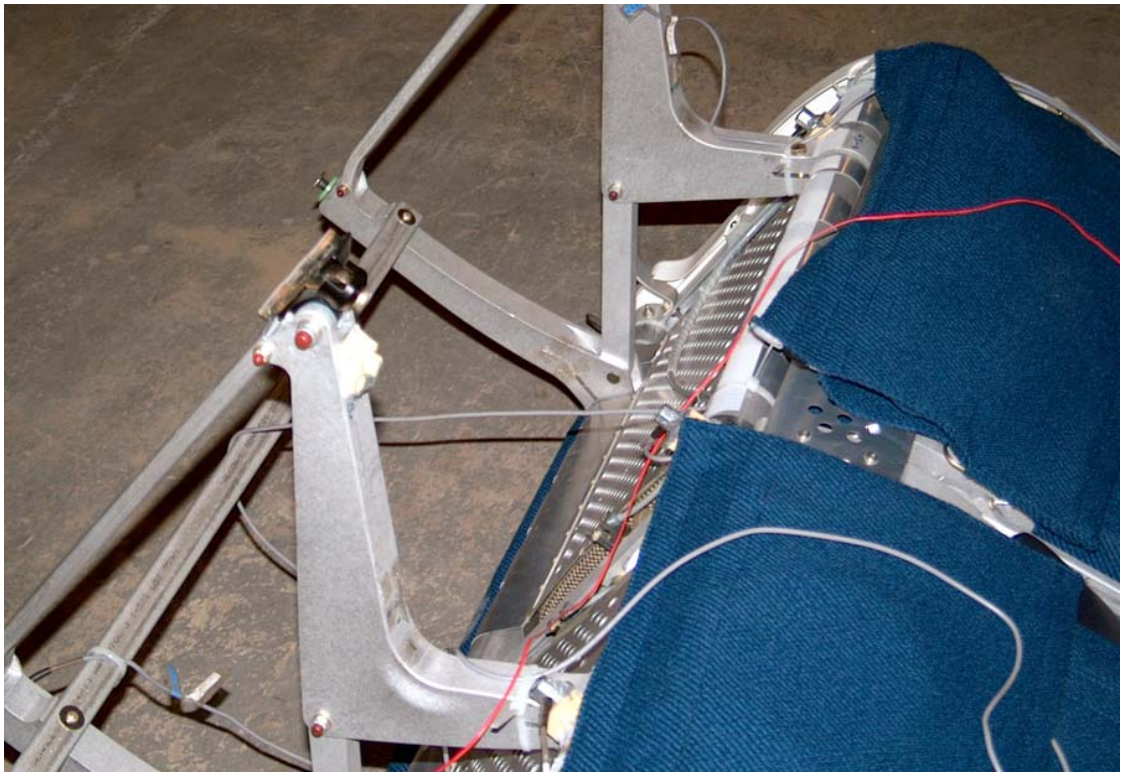

FIGURE C-200. ROW 8 TENRYU MODIFIED 16-g SEATS D AND C, VIEW 4

FIGURE C-201. ROW 8 TENRYU MODIFIED 16-g SEATS C AND D

FIGURE C-202. ROW 9 SEATS B AND A

FIGURE C-203. ROW 9 SEATS D AND C, TOP VIEW

FIGURE C-204. ROW 9 SEATS A AND B

FIGURE C-205. ROW 9 SEATS D AND C, BOTTOM VIEW

FIGURE C-206. ROW 9 SEATS B AND A, BOTTOM VIEW

FIGURE C-207. ROW 9 SEATS C AND D

FIGURE C-208. ROW 10 SEATS B AND A

FIGURE C-209. ROW 10 SEATS D AND C, FRONT VIEW

FIGURE C-210. ROW 10 SEATS A AND B, VIEW 1

FIGURE C-211. ROW 10 SEATS A AND B, VIEW 2

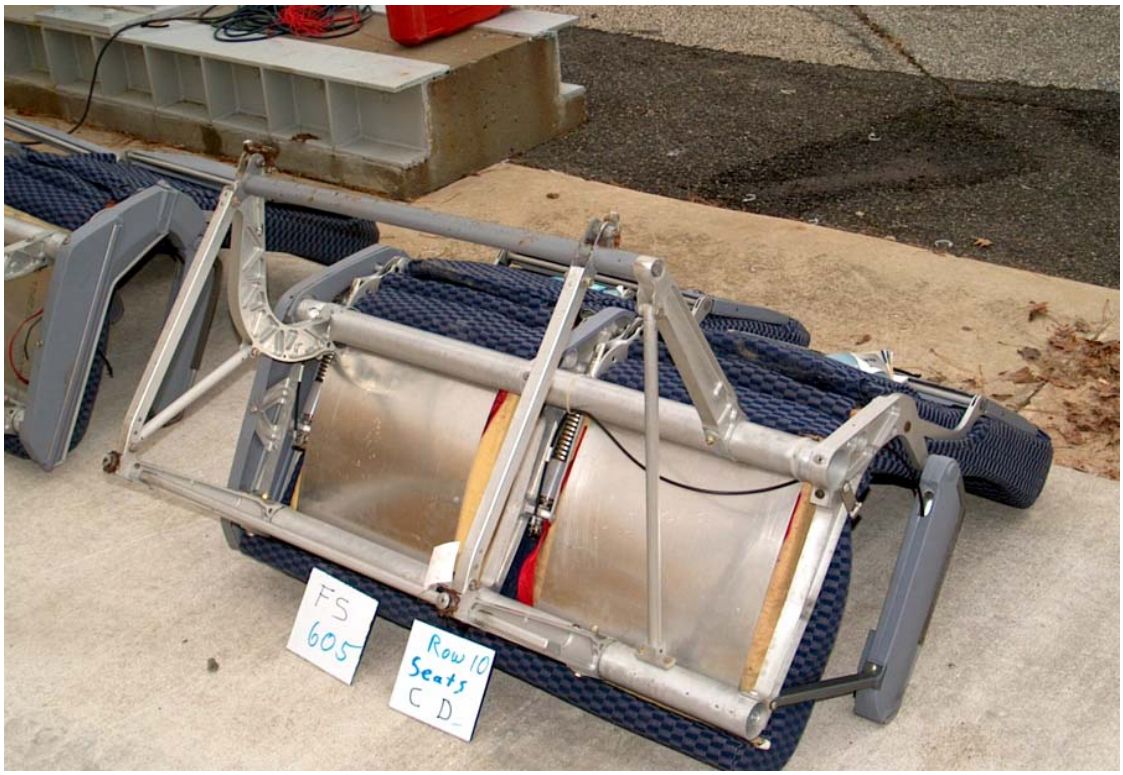

FIGURE C-212. ROW 10 SEATS C AND D

FIGURE C-213. ROW 10 SEATS D AND C, BOTTOM VIEW

FIGURE C-214. ROW 11 SEATS B AND A

FIGURE C-215. ROW 11 SEATS D AND C

FIGURE C-216. ROW 11 SEATS A AND B, VIEW 1

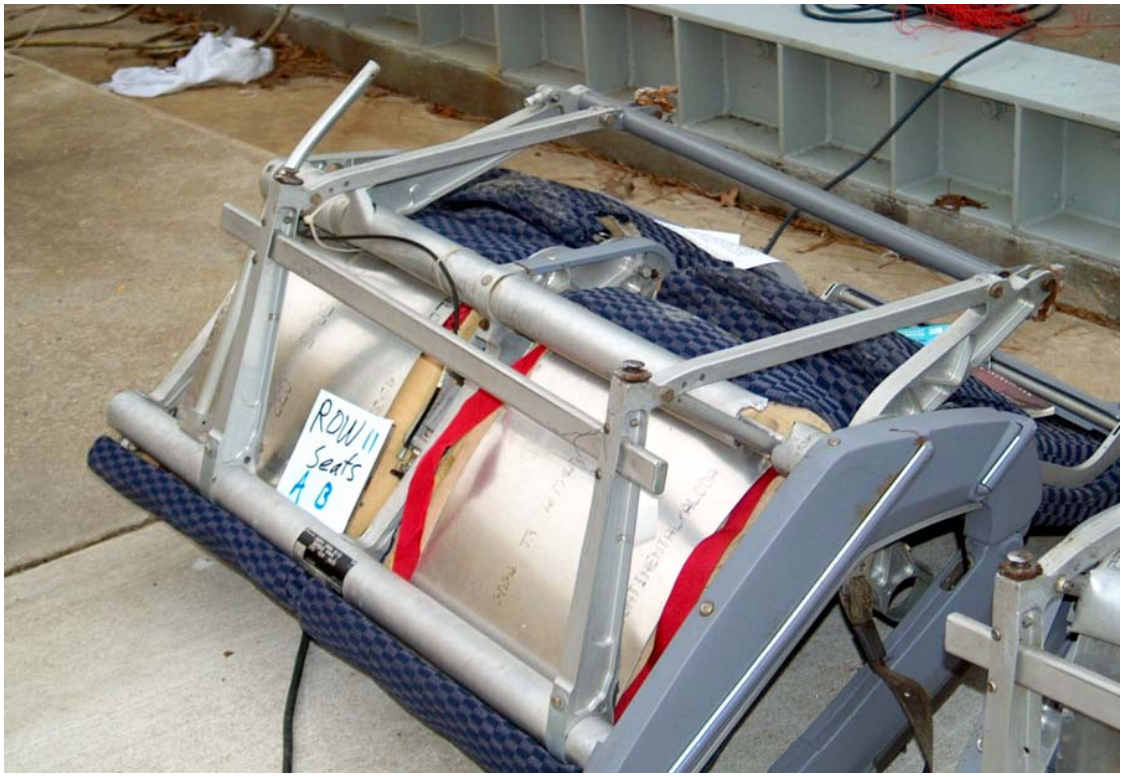

FIGURE C-217. ROW 11 SEATS A AND B, VIEW 2

FIGURE C-218. ROW 11 SEATS C AND D, VIEW 1

FIGURE C-219. ROW 11 SEATS C AND D, VIEW 2